Applications of Acidic Lithium Bromide Trihydrate in Lignocellulose Biorefining

By

NING LI

A dissertation submitted in partial fulfillment of

the requirements for the degree of

Doctor of Philosophy

(Biological Systems Engineering)

at

UNIVERSITY OF WISCONSIN-MADISON

2018

Date of final oral examination: May 3rd, 2018

The dissertation is approved by the following members of the Final Oral Committee:

Xuejun Pan, Professor, Biological Systems Engineering

John Ralph, Professor, Biochemistry and Biological Systems Engineering

Troy Runge, Associate professor, Biological Systems Engineering

George Huber, Professor, Chemical and Biological Engineering

John Grabber, Research Agronomist, US Dairy Forage Research Center

ABSTRCT

Acidic lithium bromide trihydrate (ALBTH, an inorganic ionic liquid solution) is an excellent solvent for swelling, dissolving, and controlled hydrolyzing recalcitrant cellulose, and fractionating lignocellulose. The objectives of this thesis are to exploit ALBTH in pursuit of more competitive lignocellulose biorefining, including lignin quantitation, fractionation and saccharification of lignocellulose, oligosaccharide synthesis, and preparation of cellulose nanocrystals.

Lignin quantitation of lignocellulosic biomass is an essential and routine assay in the areas of plant chemistry, forage, biomass conversion, and pulp & paper. In Chapter 2, a facile and quick method was developed to quantitate lignin in lignocellulosic biomass by using ALBTH as a reaction medium. Cellulose and hemicelluloses in the biomass were quickly and completely dissolved and hydrolyzed, leaving insoluble residue (major) for gravimetric quantitation and soluble lignin (minor) determined by UV spectrophotometry. The recommended conditions for the ALBTH method were 60 wt% LiBr solution containing 40 mM HCl, 110 °C, and 30 min. The ALBTH method gave comparable lignin (both insoluble and soluble lignin) quantity with the Klason method for varied biomass species including hardwood, softwood, and grasses. The ALBTH method followed a one-step procedure in shorter quantitation time (~30 min) than the Klason method (>3 h) and avoided the potential hazards of utilizing concentrated sulfuric acid.

Following Chapter 2, the lignin fractions isolated from lignocellulose by dissolution and hydrolysis of cellulose and hemicelluloses were characterized in order to investigate the chemical fate of native lignin in the ALBTH system. Abundant uncondensed moieties (i.e., Hibbert's ketones and benzodioxanes) and partial depolymerization of native lignin were discovered in the

isolated ALBTH lignin. Reactions using lignin model compounds (LMCs, guaiacylglycerol-β-guaiacyl ether and various aromatic monomers) confirmed the formation of the uncondensed moieties and revealed the synergy between LiBr and acid in cleaving the β–*O*–4 aryl ether bonds. Unlike in the LMC reactions, the condensation of the real lignin in biomass under ALBTH conditions was greatly diminished, possibly due to the limited solvation of the insoluble lignin in ALBTH. This research (Chapter 3) provides a new approach to effectively isolate depolymerized lignin from lignocellulose in a less condensed form for boosting its downstream valorization.

In a practical fractionation and saccharification process (Chapter 4), poplar at high biomass loading (30%-80%, w/v) was treated in ALBTH to produce mono- and oligosaccharides under milder conditions (110 °C and 0.02-0.24 M HCl), while lignin as insoluble residue was isolated with negligible condensation. The maximum soluble mono- and oligosaccharides from glucan (91.0%, oligomer to monomer ratio=1.10) and xylan (90.7%, oligomer to monomer ratio=0.63) were produced at 60% (w/v) biomass loading. Characterization of the oligosaccharide fractions from both poplar and cellulose as a model compound, revealed a top-down process to yield oligosaccharides from polysaccharides through both controlled hydrolysis and simultaneous glycosylation.

Inspired by the occurrence of glycosylation in ALBTH, Chapter 5 demonstrated a novel process for high-single pass yield (up to 75%) and high-selectivity (~99%) synthesis of glucooligosaccharides (GlOS) from glucose via non-enzymatic glycosylation reaction in ALBTH. The synthesized GlOS were composed of 2-9 anhydrous glucose units, which were linked predominantly via α/β–1,6 glycosidic bonds (69%), followed by α/β–1,3, α/β–1,2, α/β–1,1, and α–1,4 glycosidic bonds. The enhanced glycosylation in ALBTH was attributed to the unique properties of the ALBTH system including the low water concentration, the high capacity of

dissolving glucose, and the enhanced acid dissociation in the system. Preliminary *in vitro* fermentation tests with select probiotic strains verified the prebiotic potential of the synthesized GlOS.

In the last part (Chapter 6), the severity of the ALBTH treatment was further attenuated so that hydrolysis of cellulose occurred under swelling conditions with 2.5 mM H_2SO_4 (denoted as MALBTH). This system contributed to a facile method to prepare cellulose II nanocrystal (CNC) directly from commercially available cellulose I feedstock (bleached kraft pulp, BKP) via simultaneous polymorph transformation and hydrolysis in MALBTH. Under mild oxidation conditions by ammonium persulfate (APS, 0.1-0.6 M), the oxidized CNC (ox-CNC) was released with ultra-high crystallinity (above 90%), flexible surface carboxyl group (0.3-1.2 mmol/$g_{cellulose}$) and excellent colloidal stability (up to -59 mV zeta potential). Varying the MALBTH hydrolysis and the APS oxidation severities, resulted in ox-CNC with a tunable length (10-200 nm) and relative constant lateral dimensions (8-10 nm). This study contributed to expanding the portfolio of versatile CNC with flexible aspect ratios and improved colloidal properties.

ACKNOWLEDGMENTS

I would first like to acknowledge my advisor, Prof. Xuejun Pan, for his guidance in becoming a researcher and his encouragement in completing this research project. He gave me extraordinary freedom to pursue my academic growth with broad research interest and was always ready to help me overcome my setbacks. His mentorship will be one of the most treasured memories in my life.

I am deeply indebted to my parents. “Hard work pays off” is what they have passed down to me. They encouraged me to go abroad and allowed me (as their only child) to stay 6600 miles away from them for 5 years. I would not be able to finish this project without their unconditional love.

A number of other students/postdocs in the Pan’s group and on campus are responsible for part of the data in this project including Jane Alexander (who assisted me in the lignin quantitation experiment of Chapter 2), Yanding Li (who did GC-MS analysis for lignin GG models in Chapter 3), Joseph Kraft (who helped me in poplar saccharification experiment in Chapter 4), Zening Wang and Dr. Jeehwan OH (who conducted the *in vitro* fermentation of Chapter 5), Tianjiao Qu (who was partially involved in the secondary hydrolysis experiment of Chapter 5), and Huiyang Bian (who did the AFM observation in Chapter 6). Dr. Junyong Zhu in USDA Forest Products Laboratory kindly allowed me to use their instruments for cellulose nanocrystal analysis and provided constructive suggestions. In addition, I would appreciate the technical training and support by Dr. Alexander Kvit, Dr. Richard Noll, Dr. Donald Savage, and Dr. Anna Kiyanova in the Material Science Center, Dr. Charlie Fry and Dr. Lingchao Zhu in the Department of Chemistry, Dr. Greg Sabat in the Biotechnology Center for part of the instruments used in this project.

I was fortunate to work with all my labmates who built exciting and cheering environment for doing research. In particular, I would like to thank Dr. Chang Geun Yoo and Dr. Qiang Yang for their generous help to get me started when I first joined the lab. I would also like to express my gratitude to Dr. Hongdan Zhang, Dr. Xiaohui Yang, and Dr. Chang Geun Yoo for the collaborative projects (shown in the Appendix).

It has been a privilege to have Prof. John Ralph, Dr. John Grabber, Prof. George Huber, and Prof. Troy Runge as my dissertation committee members. It is their assistance and useful comments on my research that helped me conceive my idea and improve my research work.

TABLE OF CONTENTS

LIST OF TABLES

Chapter 1

Chapter 2

Chapter 3

Chapter 4

Chapter 5

Chapter 6

LIST OF FIGURES

Chapter 1

Chapter 2

Chapter 3

Chapter 4

Chapter 5

Chapter 6

Chapter 7

Chapter 1 Introduction to biorefining

1.1 Introduction to lignocellulosic biomass

Biomass is the most abundant bio-resource on Earth. Utilization of biomass as energy sources and tools can date back 10000 years.[1] The techniques of harnessing biomass had evolved in parallel with the development of the human civilization until the industrial revolution (at the start of the 19th century). With the further development of the industrial revolution, usage of petroleum resources for energy and chemical production became predominant chemicals production, fading decreasing the demand for biomass resources.[2] However, the tremendous amounts of fossil fuel consumption inevitably resulted in severe environmental and political issues. Greenhouse gas emission induced global warming and energy security concerns emerged due to the limited and uneven distribution of fossil fuel reserves in the world. Since the early 20th century, these increasingly critical problems have triggered academia, industry and government to revisit the potential of renewable biomass feedstock for producing bulky fuels, chemicals and materials.[3-7]

Biomass, by definition, is the organic materials derived from living or recent living organisms. It is produced directly or indirectly by biological photosynthesis using atmospheric CO_2 and H_2O with sunlight as an energy source (sunlight).[8] For biofuel and biochemicals production, the biomass utilized is generally confined to lignocellulosic biomass (lignocellulose) which involves the energy corps grown in marginal land, plant residues from agricultural harvest, woody biomass from the forest, etc.[9] As one of the most abundant renewable resources, lignocellulose ensures sustainable supplies of feedstocks (1.4 trillion ton/year in the United States) at a relatively low price.[10] Derived from different sources than edible feedstocks, utilization of lignocellulose will not

result in competition with feedstocks used for food supplies and even promote and improve rural economies.

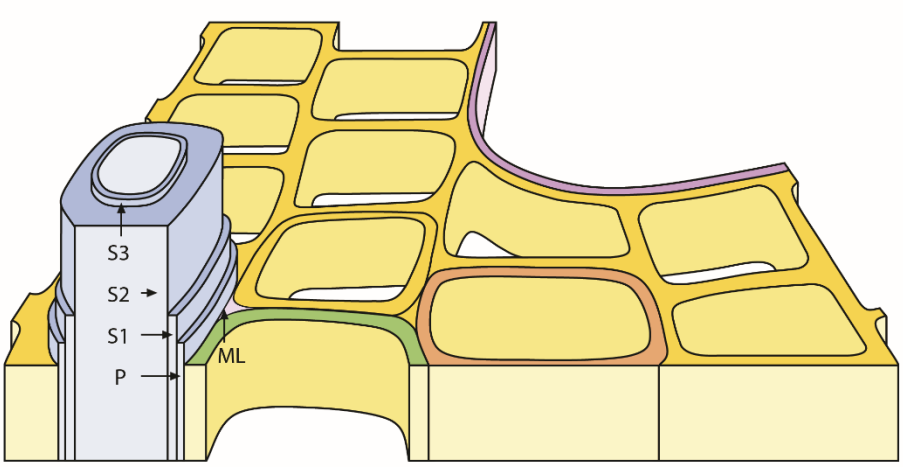

Figure 1.1 Schematic illustration of the hierarchical plant cell wall. (Adapted from the reference[11])

Lignocellulosic biomass, (primarily the cell walls of dry plants), is known for its hierarchical structure (Figure 1.1). The rigid cell walls encompass multiple layers, including middle lamella (ML), primary layer (P), and secondary layer (containing S1, S2, and S3 sublayers).[12] This hierarchical structure plays a crucial role in providing the mechanical strength to withstand natural stresses and aids in maintaining cell shape necessary for the metabolic activity of plants.[13] The cell wall chemically resembles "reinforced concrete" material in which the cellulose microfibrils "steel rods" with high tensile strength are imbedded in a matrix of lignin and hemicellulose "concrete".[14] Cellulose, hemicelluloses, and lignin are the three major components in the chemical makeup of lignocellulose (over 90%) as illustrated in Figure 1.2. Minor components include extractives, pectin, ash, and protein and their contents vary depending on the species and harvest conditions.

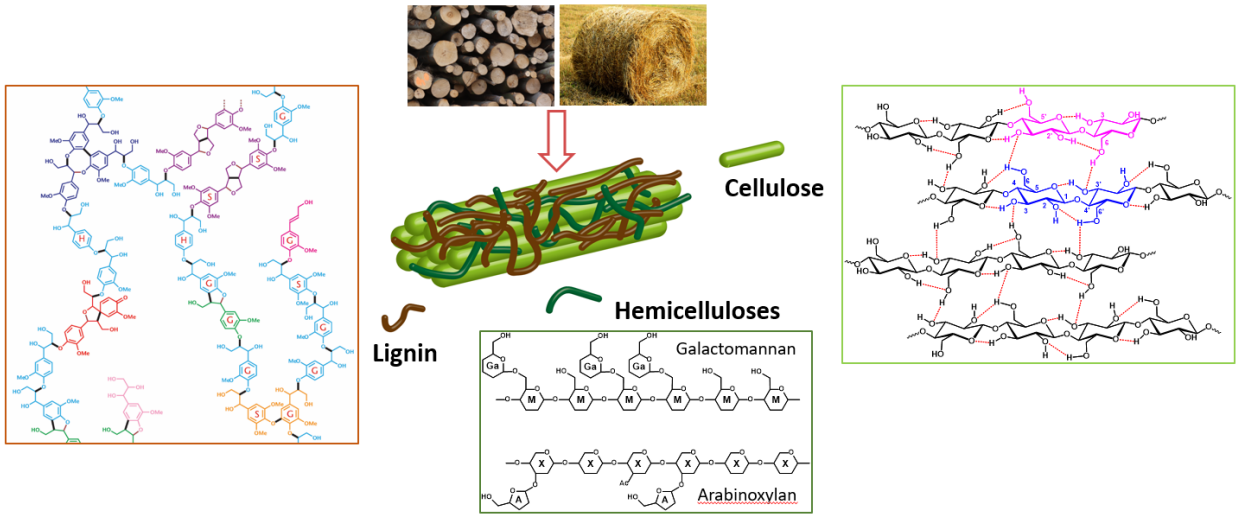

Figure 1.2 Three major components in lignocellulosic biomass. (Adapted from the references[13,15,16])

Cellulose, is the most abundant portion of lignocellulosic biomass, accounting for 35-50 wt% of the total mass. It is a linear polymer of anhydrous D-glucopyranose units uniformly linked by β–1,4 glycosidic linkages. The number of anhydrous units (degree of polymerization, *DP*) can reach 2000-6000 and 2000-10000 in primary and secondary layers, respectively.[13] In the plant cell wall, multiple parallel cellulose chains, are synthesized simultaneously by cellulose synthases. It results in a microfibril containing both amorphous and crystalline regions. Although the number of cellulose chains in one microfibril is still debatable, an assembly of 18-24 chains is the most accepted number.[17] At the molecular level, the hydroxyl groups at C2, C3, and C6 positions of the glucopyranose units form intra-hydrogen bonds with the adjunct hydroxyl groups on the same cellulose chain and inter-hydrogen bonds with the hydroxyl groups on the neighbor chains. The well-organized intra-chain and inter-chain hydrogen bonds contribute to the rigid crystalline structures of cellulose. The natural cellulose crystallites in lignocellulose (such as wood, grass, cotton) is of cellulose Iβ polymorph in which the monoclinic unit cell ($P2_1$) has two adjacent

parallel chains with a two-fold screw axis.[18,19] This crystalline structure differs slightly from the cellulose Iα structure found in bacterial and algae cells and which is not discussed in this dissertation. The cellulose Iβ crystallite can be artificially transformed to the cellulose II crystallite by mercerization treatments or dissolution/regeneration processes. The monoclinic unit cell in cellulose II has anti-parallel cellulose chains in a P21 space group unit, and it is thermodynamically more favorable than cellulose Iβ.[18,20]

Hemicelluloses, a complex of polysaccharides, constitute 20-40 wt% of lignocellulose.[3] The side chains in hemicelluloses are generally substantial, inhibiting the formation of crystalline structures. Similar to a "glue", they can bind the microfibrils together via hydrogen bonding with cellulose. The compositional units and structures of hemicelluloses can vary greatly between different species.[21,22] In angiosperms including grasses (monocots) and hardwood trees (dicots), xylan is the prevalent hemicellulose in which the β–1,4 linked backbone of D-xylopyranose units contains side chains consisting of L-arabinose, D-glucuronic acid, ferulic acid, and acetyl end groups., Hemicelluloses found in the cell walls of softwood (gymnosperms) are predominately composed of galactomannans and galactoglucomannans, which involve β–1,4 linked backbones of mannose and glucose with side chains consisting of α–1,6 linked galactose and acetyl end groups.[13]

Lignin, generally makes up 15-30 wt% of biomass. It is known as a heterogeneous mixture of aromatic polymers and serves as a "plasticizer" to render strength, hydrophobicity, and acts as a protective barrier for lignocellulosic material.[17] In lignin biosynthesis, there are three primary precursors (*p*-coumaryl, coniferyl, and sinapyl alcohols) which vary in methoxyl substitution at 3,5 position of the aromatic ring. Free radicals are formed by enzymatic dehydrogenation/oxidation of the monolignols and contribute to radical polymerization which

forms lignin. The corresponding aromatic units in lignin are *p*-hydroxyphenyl (**H**), guaiacyl (**G**), and syringyl (**S**), respectively. The occurrence of **H**, **G**, and **S** varies among different biomass species. Softwood lignin is comprised primarily of **G**, while hardwood lignincontains both **G** and **S**. The presence of **H** units (4-15%) together with **G** and **S** units is characteristic of grass lignin.[23] Small amounts of other aromatic units such as flavonoid and tricin, are also found in the lignin fraction of grasses.[24] As opposed to cellulose and hemicelluloses which have uniform chemical structures, the chemical structures of native lignin are exceedingly diverse as the radical coupling of various monomers occurs at multiple active sites. This inherently results from the delocalized radicals on the conjugated lignin monomers and oligomers during the polymerization.[25] A further complication is the number of lignin stereoisomers increases exponentially with the number of chiral centers. As a result, complete elucidation of the native lignin structures is not practical. Fortunately, most of the linkages in lignin have been unveiled due to the advent of NMR technologies and traditional chemical degradation methods. It is primarily connected by C–*O*–C ether linkages and C–C linkages.[15] The arylglycerol–β–aryl ether (β–*O*–4) linkage is the most abundant (50-80%) in native lignin. Other ether linkages include arylglycerol-α-aryl ether (α–*O*–4) linkage, diaryl ether (5–*O*–4) linkage, and resinol ether (α–*O*–γ) linkage. The primary C–C linkages in lignin are phenylcoumaran (β–5), biphenyl (5–5), 1,2-diarylpropane (β–1), and resinol (β–β).[25] In addition, lignin is not a stand-alone polymer, and can form linkages/interactions with polysaccharides (known as lignin-carbohydrate complex, LCC).[11]

1.2 Hydrolysis of lignocellulose

Biorefining of lignocellulose, by definition, involved an integrated process to convert the major components (cellulose, hemicelluloses and lignin) to valuable products, such as liquid fuels,

commodity chemicals and industrial materials.[26] Chemically, cellulose and hemicelluloses are polysaccharides, comprised of hydrophilic pentoses (arabinose, xylose) and hexoses (galactose, glucose, and mannose) units. These monomeric sugars can be released after hydrolysis and are recognized as well-accepted platform intermediates showing a wide range of applications in biofuels and biochemical production (Figure 1.3).[7,27] These fermentable sugars can be biologically transformed to alcohols and long-chain alkyl esters as fossil fuel alternatives, or organic acids as important precursors to produce biodegradable polymers. Monosaccharides and oligosaccharides are also highly viable for chemical catalysis for the production of a wide variety of platform chemicals such as polyols, furans, organic acids and their derivatives. In addition, the polysaccharides, under controlled hydrolysis, can be selectively tailored to oligosaccharides as potential prebiotics[28] and cellulose nanocrystals with numerous applications in biomedical engineering, environmental treatment, energy harvesting/storage, food packaging, etc.[29-31].

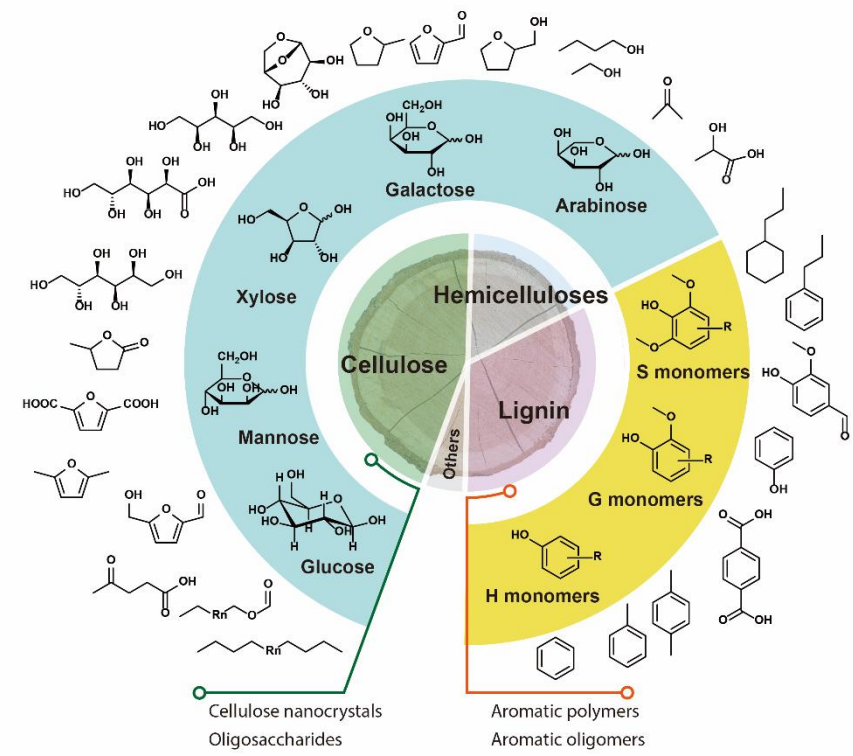

Figure 1.3 Promising intermediates and products for biofuel, biochemical and functional material production from lignocellulose. (Adapted from the references[16,32])

Hydrolysis, as an entry point to lignocellulose biorefining, is routinely performed to cleave the β–1,4 glycosidic bonds in the carbohydrate fractions (in particular cellulose). In this process, the original cellulose structures are partially deconstructed in order to release insoluble nanocrystals and soluble oligo- and monosaccharides. Both enzymes and acids have been extensively studied for catalytic depolymerization of cellulose.

1.2.1 Enzymatic hydrolysis

In nature, various fungi and bacteria can decompose and digest cellulose. This mainly involves the synergy of three major cellulases: endoglucanases (EG, cleaving the glycosidic bonds randomly along the cellulose chains primarily in amorphous regions), cellobiohydrolases (CBH 1 and CBH 2, cutting a cellobiose molecule off the cellulose chains from the reducing end and from the non-

reducing end, respectively), and β-glucosidases (converting cellobiose to glucose), as shown in Figure 1.4.[33] In the late 19th century, generation of cellobiose and glucose was reported from hydrolysis of amorphous cellulose, thought the hydrolysis efficiency was significantly reduced in the case of microcrystalline cellulose and lignocellulose as substrates.[34] Since then, tremendous efforts have been exerted to improve the enzymatic hydrolysis of cellulose from recalcitrant natural biomass and various limiting factors to enzymatic hydrolysis have been characterized and comprehensively reviewed.[35,36]

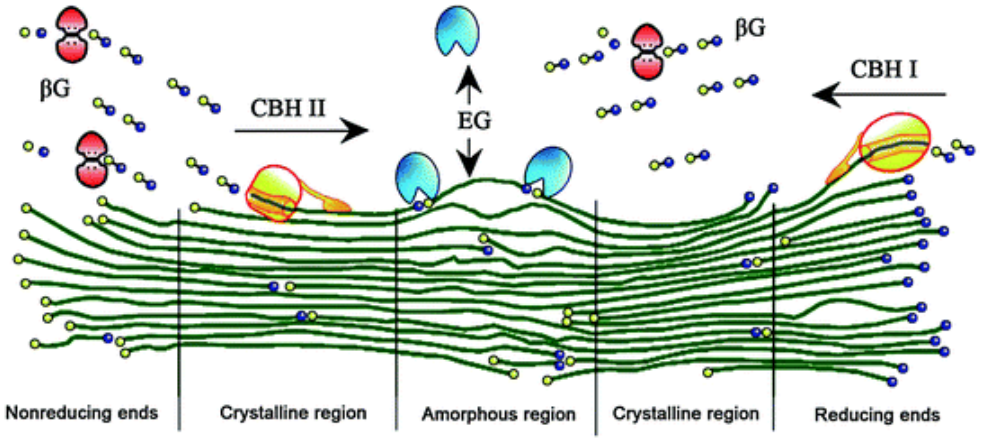

Figure 1.4 Synergy of endoglucanase (EG), cellobiohydrolase (CBH I and CBH II), β-glucosidase for cellulose hydrolysis.[33]

Ultra-structures of cellulose

The inherent ultra-structures of cellulose could impede the efficiency of cellulase hydrolysis depending on the molecular weight and crystallinity of the cellulose substrates. Cellulose contains both amorphous and crystalline regions. Crystalline cellulose, was believed to be more resistant to enzymatic hydrolysis than amorphous cellulose. Experimental observations have challenged this assumption since a direct correlation between the crystallinity and hydrolysis efficiency was not observed from the hydrolysis of several lignocellulosic substrates using ammonia fiber expansion treatment.[37] It is known that not all the cellulases are capable of hydrolyzing crystalline cellulose.

The presence of CBH is a prerequisite for crystalline cellulose hydrolysis, since it can form tight bonding with the microfibrils and disrupt the rigid crystalline structure of cellulose by synergistically cooperating with other cellulases, while both EG and CBH are capable of hydrolyzing amorphous cellulose independently. In the presence of sufficient cellulases, especially CBH, differences in hydrolysis efficiency between amorphous and crystalline regions become insignificant.[35] The *DP* of cellulose represents the initial length of cellulose to be cleaved by cellulases. The decrease in *DP* mainly relies on EG which is capable of cutting cellulose randomly along the chain. There is a point where the decrease in DP levels off.[35,38,39] This is mainly due to the fact that EG tends to selectively cleave cellulose in the amorphous region, leaving the recalcitrant crystalline cellulose.

Contents of hemicelluloses and lignin

The presence of hemicelluloses and lignin in lignocellulose poses a significant impediment to the accessibility of cellulose to cellulases. As mentioned in Section 1.1, cellulose in native lignocellulose is surrounded by hemicelluloses and lignin. They, as glues and plasticizers, act as a physical barrier, limiting enzymatic access to surface areas of cellulose which would allow for hydrolysis to take place.[40] In addition, lignin could compete with cellulose in cellulase binding. The hydrophobic groups and the phenolic hydroxyl groups in lignin are believed to have inhibitory effects on cellulase activity in biomass hydrolysis. [41]

Physical structure of substrates (particle size and pore size)

Lignocellulose is known for its heterogeneous structures. Reduction of particle size from decimeter or centimeter level to millimeter level is preferred to increase the specific surface area and homogeneity of substrates, resulting in high enzymatic accessibility.[40] The inner pore size in lignocellulosic substrates is an importantvariable in cellulase hydrolysis. In general, cellulases

have an ellipsoid core shape with a diameter of 4-6.5 nm and a length of 18-21.5 nm.[42] Diffusion of cellulases requires a minimum width of the substrate inner pores to be more than 40-60 nm. Increasing the pore size of cellulosic substrates enables cellulases to work both inside and around the crack pores and thus increasing available catalytic sites.

1.2.2 Acidic hydrolysis

In the process of chemical catalysis, various types of acids can be utilized to cleave the β–glycosidic bonds, including liquid mineral acids, liquid organic acids, and solid acids.[43-45] Hydrolysis of cellulose by acids generally follows a proton catalyzed pathway, as illustrated in Figure 1.5 using cellobiose as a model compound. The initial step of the hydrolysis involves the reversible protonation of the β–1,4 glycosidic bond on the O1 site. It is a fast and equilibrium-controlled process. The C1-O1 bond is subsequently cleaved, resulting in a free glucose molecular and an oxocarbonium ion. This is considered as the rate-determining step for cleaving the β–1,4 glycosylic bond.[46,47] The oxocarbenium ion is then promptly reacts with H_2O, yielding a glucose molecule together with the catalytic proton for further hydrolysis.[48]

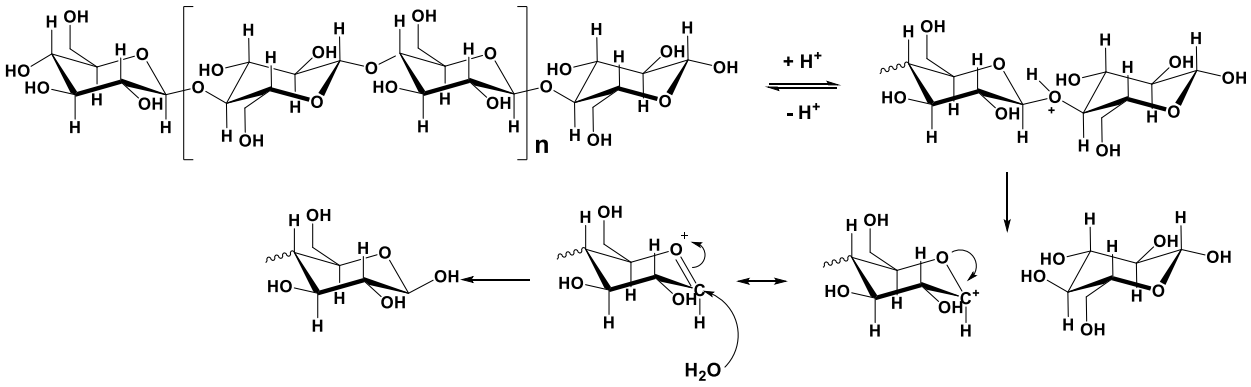

Figure 1.5 The mechanism of acid catalyzed hydrolysis of the β–1,4 glycosidic bond.

Liquid mineral acids

Utilization of mineral acids for cellulose hydrolysis to produce fermentable sugars has been recorded since the early 20th century, such as the American process, Scholler/Madison process, and Bergius process.[45,49] It is one of the most convenient and facile approaches to yield sugars from cellulose and lignocellulose. Sulfuric acid (H_2SO_4), hydrochloric acid (HCl), and phosphoric acids (H_3PO_4) are the acids most frequently used. In the dilute acid media, the temperature requirement for depolymerization of hemicelluloses and cellulose varies. Hydrolysis at low temperatures favors conversion of hemicelluloses to monosaccharides while the majority of the cellulose fraction remains insoluble because of its rigid crystalline structures which require much higher temperatures to activate the hydrolysis reactions. For example, hydrolysis of palm oil empty fruit bunch fiber in dilute H_2SO_4 (6 wt%) yielded 29.4 g/L of xylose and 2.3 g/L of glucose at 120 °C for 15 min,[50] whereas up to 40-60 g/L of glucose was released at 220-240 °C in 1% H_2SO_4.[49] Concentrated acids could serve as a more effective type of catalysts for high yield production of sugars (especially glucose). A 70:30 mixture of H_3PO_4 (~85%) and H_2SO_4 (~98%) was reported to swell and depolymerize corncob at ambient temperature (below 30 °C) for 16 h and up to 90% yields of glucose and xylose were achieved after water dilution and subsequent hydrolysis at 80 °C for 4 h with negligible degradation by-products. This process was also compatible with other types of lignocelluloses such as switchgrass and bagasse, producing monosaccharides with 75-90% yields.[51]

Organic acids

Catalytic depolymerization of lignocellulose was reported using organic acids, such as oxalic acid, formic acid, aryl sulfonic acids, etc..[44] Aryl sulfonic acids (e.g., p-toluenesulfonic acid, 2-naphthalenesulfonic acid, and 4- biphenylsulfonic acid), have comparable acidity to strong mineral acids. Using the identical acid strengths (0.0321 mol H^+ ion/L), the aryl sulfonic acids tended to

produce 4-9% more total reducing sugars compared to sulfuric acid at 140-190 °C.[52] Formic acid (5-20%) was utilized as an effective acid as well as an organic solvent for hydrolysis of wheat pulp and microcrystalline cellulose at 180-220 °C.[53] The maximum yields of glucose and xylose were ~40% and 60%, respectively with a certain amount of furfural and HMF. Since lignin could be partially dissolved in formic acid, partial delignification occurred together with carbohydrate hydrolysis. In addition, as formic acid itself was derived from glucose dehydration, it was recognized as a renewable organic acid for biomass biorefining. For cellulose hydrolysis using dicarboxylic acids (such as oxalic and maleic acids), high reaction temperature was essential due to the low acidity. In an approach developed by Stein V., et al.(2010), inexpensive NaCl (30%) was added to reduce the hydrolysis temperature to 100-125 °C and the improved depolymerization was ascribed to the salt/dicarboxylic acid mixture which could disrupt the hydrogen bonds in cellulose network.[54]

Solid acids

In the processes of lignocellulose hydrolysis, it is challenging to recycle the liquid acid catalysts. Neutralization of the resultant hydrolysates also leads to accumulation of solid wastes, especially when using concentrated acids.[45] The solid acids are designed to facilitate the product/catalyst separation and the subsequent catalyst recycling. Solid acid catalysts can provide large surface areas containing surface functionalized groups (catalytic sites) and high substrate absorption abilities (physical supports). In the cellulose hydrolysis catalyzed by solid acids, either Lewis acid sites or Brønsted acid sites are responsible for the catalytic cleavage of the glycosidic bonds.

Solid metal oxides contain abundant Lewis acid sites with a high specific surface and porous structure, providing the cellulosic substrates sufficient contact with the acid sites. Domen's group developed various metal oxide catalysts including mesoporous Nb-W oxide, layered $HNbMoO_6$,

and exfoliated nanosheet $HTiNbO_5$ for cellulose hydrolysis.[55,56] They found that increasing the W content could enhance the acid strength of the catalysts and the highest hydrolysis rates were achieved using Nb_3W_7 oxide. While the Nb-W oxides generally lacked strong Brønsted acid sites for cellobiose and cellulose hydrolysis, the layered HNbMoO6 catalyst was capable of hydrolyzing cellobiose and sucrose, possibly due the high acidity, water tolerance and sugar intercalation ability. However, hydrolysis of cellulose was still hard to achieve without further increases of the acid site density and surface areas. A nano Zn-Ca-Fe oxide catalyst was reported to hydrolyze cellulose with up to 43% of cellulose conversion at 160 °C for 20h. In addition, separation of the reaction mixture from the catalyst using magnetic filtration was facilitated by the presence of paramagnetic Fe oxides.[57]

The solid acid catalysts bearing the Brønsted acid site (-SO_3H) are effective for cellulose hydrolysis.[43] Most of the Brønsted acid sites were grafted on the surface of porous solid supports such as polymers and carbonaceous solids. Various commercially available PS-DVB catalysts (Amberlyst series) were investigated for cellulose hydrolysis in ionic liquid [BMIM]Cl.[58] The sulfonated resins with a large pore size were found to be suitable for depolymerization of cellulose, yielding over 10% of reducing sugars at 100 °C. Increasing the concentration of the Amberlyst 15Dry catalyst greatly minimized the induction time making it comparable to strong acids. In order to optimize the catalytic performance, a cellulase-mimetic catalyst containing both a cellulose binding domain (-Cl group) and a catalytic domain (-SO_3H) was prepared from the chloromethyl polystyrene resin by –SO_3H functionalization (CP-SO_3H).[59] Under mild conditions (120 °C), both the cellobiose and microcrystalline cellulose could be hydrolyzed with over 93% of glucose yield. The activation energies for hydrolysis of cellobiose and cellulose with CP-SO_3H were ~78 and 83 kJ/mol, respectively, which were significantly lower than those using sulfuric acid (~170 kJ/mol).

This was potentially due to its ability to interrupt the hydrogen bonding within cellulose crystallites by adsorbing/attracting cellobiose and cellulose on the surface of the cellulase-mimetic catalyst.

The sulfonated carbonaceous solid acid is another type of solid catalyst used with high substrate adsorption and catalyst reusability in the production of sugars .[43] An amorphous carbon based catalyst was prepared from cellulose by fuming sulfuric acid, and contained -SO_3H, -COOH, and -OH functional groups.[60] The subsequent hydrolysis of 3% cellulose in water at 100 °C resulted in 68% cellulose conversion with 4% glucose yield. The carbonaceous carbon also showed significantly lower apparent activation energy for hydrolyzing cellulose to glucose (110 kJ/mol), when compared to the strong sulfuric acids. After complete dissolution of cellulose, the recovered catalyst preserved over 99% catalytic activity with negligible decrease even after 25 runs. The sulfonated biomass chars from bamboo, cotton and starch were also subjected to cellulose hydrolysis in water solution along with microwave irradiation, at 90 °C, resulting in maximum yields of 20% glucose and 8% oligosaccharides.[61]

Solid acid catalysts for cellulose hydrolysis rely on their porous surfaces which tend to adsorb cellulose chains on the catalytic sites, resulting in low activation energy and high turnover numbers. The primary drawback is when lignocellulose is used as the feedstock, the lignin fraction is negligibly soluble and mix with the solid acid after hydrolysis completion, complicating the recycling of solid catalysts after lignocellulose saccharification.

1.2.3 Solvent systems for hydrolysis

The enzymes utilized for hydrolysis, are sensitive to the catalytic environment which determines their bio-reactivity. As a result, enzymatic hydrolysis of cellulose generally requires a buffered water solvent (pH 4.8) at confined temperature ranges (40-50 °C). Cellulases are touted for the high product selectivity, however they remain active only under limited conditions so it is difficult

to modify the solvent environment for improved hydrolysis. In order to tackle with the recalcitrance of lignocellulose, extra physical and/or chemically pretreatments are necessary. When compared to enzymatic catalysts, acid catalysts are compatible with various solvent systems (both aqueous and organic solvents) allowing for more options in the cellulose hydrolysis process.

Hydrolysis in water

Water is the cheapest and the most universal solvent in nature with low toxicity and environmental friendliness. Metabolic activities of living organisms are exclusively conducted in the presence of water. For cellulose hydrolysis, addition of water is required during the cleavage of cellulose chains to form mono- and oligosaccharides. However, hydrolysis of cellulose generally occurrs at high temperatures (over 220 °C) with significant amounts of catalysts, which inevitably led to poor product selectivity from biomass.[62] Cellulose hydrolysis in aqueous dilute acid solutions exhibited the high apparent activation energy (171-189 kJ mol^{-1}) which was significantly higher than those for di- and monosaccharides degradation.[63] It was possibly due to the insoluble crystalline cellulose mandated extra energy input to break the hydrogen bonds.

Water is relatively effective at absorbing energy, and microwave irradiation can simultaneously activate and accelerate the hydrolysis of cellulose. The microwaves utilized are at a wavelength range of 1 mm-1 m, and correspond to frequency range between 0.3 and 300 GHz.[64] In order to avoid interference with other applications, the microwave frequency utilized for the heating process is 2.45 GHz. The yield of reducing sugars using microwave treatment was reported to be 3.8 fold higher than that under conventional heating.[61] Above the softening temperature of 180 °C, microwave irradiation contributed to the localized rotation of CH_2OH groups of amorphous cellulose, enhancing the microwave energy transfer to surrounding environment with disruption of crystalline cellulose structures observed at temperatures over 220 °C.[65]

As compared to conventional water, supercritical water, where the medium is heated to past the thermodynamic critical point (647 K and 22 MPa), exhibits a sharp decrease in its dielectric constant, viscosity, and density. Increasing the water temperature at 25 MPa, the self-ionization constant reached a minimum value of 11.0 at 260 °C, then drastically increased to 16.5 at 400 °C.[66] These changes in the physical properties of supercritical water improved dissolution of cellulose chains and allowed rapid cleavage of glycosidic bonds.[67] In supercritical water at 380 °C, 30 MPa, and 0.17 s, the native microcrystalline cellulose I was transformed to cellulose II, demonstrating cellulose dissolution.[68] As a result, the accessibility of the protonated water molecules to glycosidic bonds in cellulose molecules was greatly increased in supercritical water under swelling or dissolution conditions.[69] Reaction temperature and time are the most crucial parameters in cellulose hydrolysis. Over 50% water soluble cello-oligosaccharide and 12% glucose yields were produced from supercritical water treatment of cellulose at 360 °C for 0.5s with negligible insoluble residues as well as 40% gluco-oligosaccharide and 24% glucose yields obtained at 380 °C for 16s.[70] However, the extremely high temperatures inevitably decreased the selectivity of cellulose hydrolysis. Dehydration and retro-aldol reactions were also prevalent, resulting in formation of levoglucosan, HMF, erythrose, methylglyoxal, glycolaldehyde, and dihydroxyacetone from degradation of glucose and gluco-oligosaccharides.[70,71]

Hydrolysis in organic solvents

The organic solvents, based on polarity and capability of proton donation, can be categorized into three types: non-polar solvents (e.g., hexane and benzene), polar protic solvents (e.g., methanol, ethanol, and formic acid), and polar aprotic solvents [e.g., dimethyl sulfoxide (DMSO), acetone, dioxane, tetrahydrofuran (THF), and γ-valerolactone (GVL)]. Among them, the polar aprotic

solvents have been recognized to promote cellulose hydrolysis due to the preferred solvent-solvent interactions allowing for the control of reaction rates and product selectivity.[63,72]

The polar aprotic solvents can favor the destabilization of acidic protons, instead of protonated intermeditaes in the transition states, resulting in accelerated rates of acid-catalyzed reactions.[72] The rate constants for acid-catalyzed hydrolysis of cellobiose at 130 °C were 18, 22, and 9.1 M^{-1} $ks^{-1}[H_3O^+]^{-1}$ in GVL, THF and dioxane solutions, respectively (organic solvent to water, 4:1),[73] whereas the rate constant was 0.61 M^{-1} $ks^{-1}[H_3O^+]^{-1}$ in acidic water at the same conditions. The solvent effect also involves a decrease in the apparent activation energy for cleaving the glycosidic bonds. The GVL-H_2O (4:1) medium reduced the apparent activation energy from 131 to 81 kJ mol^{-1} for cellobiose hydrolysis, while keeping the apparent activation energy relatively constant (135-138 kJ mol^{-1}) for sugar degradation.[72,73] As a result, up to 70-90% of biomass could be directly extracted as aqueous soluble oligosaccharides from biomass in the GVL-H_2O (4:1) medium at 160-200 °C.[4]

Hydrolysis in solid state

Without a liquid solvent, mechanocatalysis allowed depolymerization of cellulose/biomass in a solid state using a small quantitiy of acids.[74,75] This process generally involved three steps in the conversion of polysaccharides in biomass to monomeric sugars : (1) wet-impregnation of the substrate with an acid (then eliminating the volatile solvents); (2) deep depolymerization of acid impregnated biomass by milling; (3) further saccharification of the water soluble lignocellulose to yield pentoses and hexoses.[76] The α-cellulose substrate impregnated with 0.44 mmol H_2SO_4 per gram cellulose was made fully soluble in water after 2 hours of milling treatment, and converted to glucose (91% yield) after dilution to 10 wt% solid concentration and subsequent hydrolysis at 130 °C.[74] The process was also compatible with lignocellulosic feedstocks such as wood and

grasses.[74] The critical variables involved in the release of monomeric sugars were: (1) the frequency of the collision induced energy transfer, (2) acid concentration, (3) milling time, and (4) moisture content of the substrate.[77] The electrical energy requirement is inevitably the main consideration in the upscale of this process necessary for industrial production.[62]

1.3 Biomass fractionation for full utilization

Compared to carbohydrates, lignin (a pool of aromatic phenylpropanols) has distinct chemical and physical properties (e.g., less polar, more complicated chemical structures, a higher tendency towards condensation) and had been historically (mis)viewed as waste material. Recently harnessing lignin is gaining more and more attention in production of value-added bio-products. As lignin polymers contain abundant free aliphatic and aromatic hydroxyl groups, they can be incorporated as a complete macromolecule into the synthesis of polyurethanes, polyesters, epoxide resins, and phenolic resins.[78,79] Although lignin fractions are relatively hard to get involved in microbial metabolism and biological valorization, several recent review papers have explicitly discussed the potential of producing useful aromatic/ phenolic monomers and oligomers via chemical catalysis and thermal decomposition reactions.[32,80,81] High-yield production of low molecular-mass aromatics was achieved via formic acid-induced depolymerization of lignin after oxidation treatment using stoichiometric Mn or Cr oxide.[82] Lignin isolated by the organosolv extraction has the potential to release up to 78% of aromatic monomers, in upgrading processes to remove the excess amount of oxygens by hydrogenolysis, hydrodeoxygenation, hydrogenation, etc.[83-85] Deriving extra added-value of lignin should also be taken into consideration in any future biorefining of lignocellulose.

The targeted products from lignin and carbohydrates are distinct in both chemical and physical properties. As a result, the conversion of lignocellulosic biomass can be sorted into two categories: 1) biomass as a whole is subjected to conversion disregarding the distinct chemical properties of the carbohydrates and lignin fractions, yielding products as a complex mixture for downstream processing; 2) biomass is first fractionated into carbohydrate and lignin fractions, each with similar chemical properties which then follow a dedicated conversion pathway for optimized yield and product quality.

The conversion strategies in the first category mostly involve thermochemical processes such as gasification (combustion with limited amounts of oxygen) and pyrolysis (thermal decomposition in the absence of oxygen). The whole biomass after gasification yields syngas (a mixture of CO, H_2, CO_2, and H_2O) which can be subsequently converted to hydrogen by water-gas shift reaction, diesel fuels by Fischer-Tropsch synthesis, and methanol by methanol synthesis. The most critical disadvantage of biomass gasification process is the low energy efficiency since over half of the energy in the biomass is irreversibly lost during the conversion process.[3] Pyrolysis of biomass feedstock generates bio-oils (a mixture of alcohols, aldehydes, esters, ketones, aromatics, acids, tars, and chars) which can be subsequently converted to liquid fuels by catalytic upgrading (e.g. hydrodeoxygenation and zeolite cracking)[86]. The pyrolysis process has higher process thermal efficiency (~70%) than the gasification process. The disadvantage of pyrolysis is that the bio-oils produced from lignocellulose exhibit thermal and chemical instability, deficient volatility, low heating values and poor miscibility with hydrocarbon fuels. The resulting bio-oils require subsequent upgrading processes, precluding the direct utilization of bio-oils which significantly reduce their economic competitiveness.

In biomass fractionation, the chemical distinctiveness of different components in lignocellulose allows for the maximization of utilization efficiency for each individual fraction (e.g., carbohydrates and lignin). It is of importance since current energy demand and operation costs remain the primary impediment to upscale lignocellulose biorefining processes. To improve both economic feasibility and conversion efficiency in biorefining, it is desirable to first separate the carbohydrate and lignin fractions in a fractionation process and to convert each fraction separately towards versatile value-added compounds.

A solvent tends to dissolve solutes of similar polarities. So, the success of biomass fractionation is dependent on the differences in solubility between lignocellulose components and their derivatives within in a given solvent system. For example, lignin, as an aromatic fraction, is less polar than carbohydrate fractions containing abundant hydroxyl groups. Therefore, lignin is preferentially concentrated in organic solvents with medium polarity such as THF, dioxane, GVL, and alcohols. In addition, small molecules also tend to be more soluble than their oligomers and polymers. For example, water dissolves monomeric sugars promptly, but fails to solvate oligosaccharides with *DP* up to 10. As a result, selective depolymerization of a targeted fraction to small molecules can greatly improve its solvent solubility and facilitate the separation from other inert fractions.

In practice, most solvents used for lignocellulose fractionation fall into two categories, either lignin solvents or carbohydrate (cellulose) solvents. The lignin solvents extract the lignin fraction from lignocellulosic biomass based on their preferential solvation to aromatic lignin. Carbohydrates can either be retained as insoluble fractions for a subsequent conversion or be depolymerized to sugars and sugar derivatives, depending on the fractionation conditions. The lignin fraction then can be isolated from the lignin solvent for downstream valorization by solvent

evaporation or water precipitation. The typical lignin solvents used for biomass fractionation, include GVL, THF, 2-methyltetrahydrofuran (2-MeTHF), dioxane, and acetic acid, etc. As a green solvent derived from carbohydrates, GVL was reported by Dumesic et al. to fractionate lignocellulose (from feedstocks such as corn stover, maple wood, and loblolly pine) via a deep depolymerization process.[4] The Lignin fraction was fully extracted in GVL, while carbohydrate fractions either stayed as insoluble fiber pulp or aqueous soluble sugars depending on the reaction conditions.[4,84] The Lignin fraction was isolated from soluble sugar fractions by precipitation in water, and consisted of abundant uncondensed structures which facilitated the subsequent hydrogenolysis process to produce lignin monomers with yields up to 38%.[87] Leitner et al. reported a water/2-MeTHF biphasic system the "organocat process, which enabled effective fractionation of the three major biomass components.[88] The hemicelluloses were selectively depolymerized to the aqueous soluble fraction since it was more vulnerable to the oxalic acid catalyst. The lignin fraction was mostly extracted to 2-MeTHF phase, leaving cellulose pulp suspended and readily separated from the reaction system. The cellulosic pulp fraction was vulnerable to both enzymes and acids, and able to yield fermentable sugars for biofuel and biochemical production. Similarly, THF/water co-solvent system was applied for corn stover fractionation to yield carbohydrates as solids for subsequent enzymatic hydrolysis or as released soluble sugars and their dehydration products, depending on the reaction temperature and acid loadings.[89,90] The less condensed lignin fraction was isolated after removal of THF under vacuum. The lignin powder had excellent solubility in common organic solvents and was suitable for catalytic upgrading to value-added aromatic chemicals.

Condensation/repolymerization is basically inevitable when lignin is fractionated by dissolution in organic solvents. The occurrence of condensation greatly reduces the value of the

isolated lignin especially in their suitability for upgrading to added-value chemicals, due to the formation inert carbon-carbon linkages.[91] In response, several innovative fractionation strategies have been developed and involve actively protecting/stabilizing the dissolved lignin in lignin solvents.[81,91] Their methods included protection of the extracted lignin polymers by formaldehyde or other aldehydes[92,93] and stabilization of the solvated lignin monomers by reductive catalysis[91] or acetal protection[94]. In those processes, carbohydrates (especially cellulose) remained as insoluble pulp for downstream valorization.

Alternatively, cellulose solvents can fractionate the biomass by selectively dissolving carbohydrate fractions and leaving the insoluble lignin as solid residues. It is generally accompanied by a homogeneous saccharification process to yield soluble sugars from carbohydrates since both the physical and chemical barriers to carbohydrate hydrolysis are significantly decreased under dissolution conditions.[63,72] An added benefit is that lignin fractions can be isolated in a relatively pure form for downstream upgrading. However, carbohydrates, especially cellulose, are marginally soluble in common solvents, due to their high molecular weight and rigid crystal structures.[95] So the choice of suitable solvents is crucial in efforts to interrupt the inter- and intra- hydrogen bonds within the rigid cellulose structures as well as to leave lignin fractions isolated in a relatively unmodified form.

1.4 Cellulose solvents for biomass fractionation and saccharification

Solvents know to be capable of cellulose dissolution include: ionic liquids, organic solvents/ inorganic salt complexes, inorganic molten salt hydrates, amine oxides, aqueous complex solutions, and aqueous alkali solutions.[95] Among them, ionic liquids (ILs) and inorganic molten salt hydrates

(MSHs) are feasible solvents for biomass fractionation and saccharification due to their high stability in acidic environments at high temperature and their ease of usage in process operations.

Ionic liquids are a group of organic salts which remain as liquid at ambient temperature. They possess numerous attractive properties such as low vapor pressure, high thermal stability, and good optical transparence. In 2002, the use of ILs was first reported by Rogers et al. as a cellulose solvent for dissolution and regeneration of cellulose.[96] Later, Zhao et al. exploited the potential of ILs for cellulose hydrolysis and lignocellulose fractionation.[97,98] Under mild reaction conditions (100-160 °C), carbohydrates were fully dissolved in [EMIM]Cl or [BMIM]Cl and effectively hydrolyzed by strong Brønsted acids, resulting in up to 70% glucose yield from various biomass feedstocks including corn stover, switchgrass, silvergrass and pine (Table 1).[99-103] Raine et al. demonstrated the key role which water played during IL hydrolysis of carbohydrates.[99,100] Processive addition of water prohibited the sugar dehydration reactions, such as glucose oligomerization and glucose dehydration to HMF and humins, resulting in increased sugar yields. With the processive addition of water to the [BMIM]Cl system, 81% of cellulose was converted to glucose and cellobiose[104] and the recovered lignin fraction was less modified and rich in β–*O*–4 aryl ethers.[100] Recently, acidic ionic liquids containing Brønsted acidic properties, such as [BMIM][HSO_4], [C_4SO_3HMIM][HSO_4], and [HMIM]Cl were synthesized and applied as the solvent to biomass fractionation without additional acid catalyst.[105,106] Fractionation and saccharification of corn straw in [HMIM]Cl was achieved at 70 °C for 2 h with 25% total reducing sugar yield on biomass.[106] However, the fractionation and conversion of biomass using ILs, still present several challenges. It is relatively hard to recover costly ILs in an economically feasible way, though techniques such as the ion exclusion chromatography and boronate solvent extraction were developed.[100,107] As listed in Table 1.1, the biomass loadings were limited (≤10%). Further

increasing the loading concentration led to deteriorated mass and heat transfer, and thus inhibiting the fractionation process. The inhibition is believed primarily due to the escalated viscosity of the media after dissolving carbohydrates in ILs.[26,99,104] The insufficient loading capacity for biomass fractionation and saccharification in ILs, could partially impede their suitability for further industrial scale-up and increase operational and infrastructural costs.

Table 1.1 Hydrolysis of cellulose from lignocellulose in ionic liquids

ILs	Biomass	Reaction conditions	Glucose yield (%)	Ref.
[BMIM]Cl	Cellulose	100 °C, 0.9% H_2SO_4, 8% loading, 9 h	43	97,98
[EMIM]Cl	Silvergrass	100 °C, 110 mM MsOH, 10% loading,	5	101
[BMIM]Cl	Pine	120 °C, 18 mM TFA, 5% loading, 120 min	10.5	102
[BMIM]Cl	Corn stover	105 °C, 140 mM HCl, 5% loading, 150 min	42	99
[BMIM]Cl	Switchgrass	160 °C, 140 mM HCl, 5% loading, 90 min	69.4	103
[BMIM]Cl	Corn stover	105 °C, 400 mM HCl, 5-10% loading, 120 min	42-33	100
[HMIM]Cl	Corn straw	70 °C, 83% [HMIM]Cl, 3.3% loading, 120 min	25[a]	106

a. Reducing sugar yield based on total biomass

Molten salt hydrates (also known as inorganic ionic liquids), refer to concentrated salt liquids with the water to salt ratio close to the hydrate number of the first coordination sphere of the cation.[95,108] They generally involve electrolytes with small and polarizing cations and in most cases polarizable anions.[109] The hydrated cations as well as the dissociated anions could contribute to association with the hydroxyl groups of cellulose, interrupting its original intra- and inter-chain hydrogen bonds for swelling and dissolution of cellulose.[95,110] The effects of salt cation on carbohydrate dissolution were mostly consistent with the Hofmeister series.[111] In practice, the

different assemblies (combinations) of cations and anions also affected the ability of molten salt hydrates to contribute to cellulose dissolution.[95,112] Some successful examples (Table 1.2) involve $ZnCl_2 \cdot 3\text{-}4H_2O$, $LiClO_4 \cdot 3H_2O$, $LiBr \cdot 3H_2O$, $LiI \cdot 2H_2O$, $FeCl_3 \cdot 6H_2O$, $Ca(SCN)_2 \cdot 3H_2O$ as well as salt mixtures such as (NaSCN/KSCN)-$LiSCN \cdot 2H_2O$, $LiCl/2ZnCl_2/H_2O$.[95,108-115] Similar to organic ILs, molten salt hydrates have low vapor pressures as well as high thermal stability but as compared to organic ionic liquids they are much cheaper and far less toxic.[116]

Table 1.2 Swell and dissolution of cellulose in molten salt hydrates

Group	Single Melt	Melt mixtures	Refs.
Dissolution	$ZnCl_2 \cdot 3\text{-}4H_2O$		110,113
	$LiClO_4 \cdot 3H_2O$		112
	$LiSCN \cdot 2H_2O$		109
	$LiI \cdot 2H_2O$		112
	$FeCl_3 \cdot 6H_2O$		109
	$LiBr \cdot 3\text{-}4H_2O$		114,115
	$Ca(SCN)_2 \cdot 3H_2O$		112
		$LiClO_4 \cdot 3H_2O$ with (≤ 25% $Mg(ClO_4)_2/H_2O$) or (≤ 10% $NaClO_4/H_2O$) or ($MgCl_2 \cdot 6H_2O$)	108
		NaSCN/KSCN-$LiSCN \cdot 2H_2O$	109
		$LiCl/2ZnCl_2/H_2O$	109
Swelling	$LiCl \cdot 2\text{-}5H_2O$		109
	$NaClO_4/H_2O$		109

Although the dissolution of cellulose in various molten salt hydrates has been extensively studied, it is surprising that applications of molten salt hydrates for cellulose saccharification and conversion have remained largely unexploited except in studies using $ZnCl_2 \cdot 3\text{-}4H_2O$. A complete

hydrolysis of cellulose was reported at 70 °C using 0.5 M H_2SO_4 in $ZnCl_2$ molten salt hydrates in 1995.[117] The glucose yield was highly dependent on the concentration of $ZnCl_2$ (the hydrate number of $ZnCl_2$). When a Ru/C catalyst was incorporated into the cellulose hydrolysis in 70% $ZnCl_2$, sorbitol as the hydrogenation product of glucose could be directly obtained in a one-pot reaction.[113] Using HCl as the catalyst, cellulose was reported to be fully dissolved and hydrolyzed in 63% $ZnCl_2$ at 120 °C and the resulting sugars were further dehydrated to 30.4% of HMF due to the water deficient nature of $ZnCl_2$ molten salt hydrate. Using a sulfated titania catalyst, dissolution and hydrolysis of cellulose in $ZnCl_2 \cdot 3H_2O$ led to selective production of glucose (maximum yield 51%) and levulinic acid (maximum yield 43%) at 80-100 ºC and 120-140 ºC, respectively.[118] There is little in the literature describing the fractionation and saccharification of lignocellulosic biomass in molten salt hydrates. Our group (Prof. Xuejun Pan) first patented the lignocellulose saccharification and fractionation process using LiBr molten salt hydrate.[114] Recently, a $ZnCl_2$ hydrate system was also utilized for bamboo fractionation to produce soluble sugars and insoluble lignin fractions.[119,120]

It is worth noting that inorganic molten salt hydrates, not only have a similar performance on carbohydrate dissolution, hydrolysis, and conversion compared to organic ionic liquids, but also dissolve only negligible amounts of lignin. These unique properties facilitate separation of lignin from the carbohydrate fraction. We believe exploitation of the molten salt hydrate as a promising reaction solvent could contribute to innovative lignocellulose biorefining technologies for value-added biofuels, biochemicals and biomaterials.

1.5 Outline of this thesis

This work mainly focuses on exploiting acidic lithium bromide trihydrate (ALBTH, an inorganic ionic liquid solution) for lignocellulose biorefining. Various solvent parameters and reaction conditions were tested. This unique solvent system exhibited excellent abilities in swelling, dissolving, controlled hydrolyzing of the recalcitrant cellulose, and fractionating lignin from lignocellulose as partially depolymerized but undissolved fractions. This thesis has demonstrated the viable applications of ALBTH in facile quantitation of lignin, effective fractionation and saccharification of lignocellulose, high-yield synthesis of oligosaccharides, and tailored preparation of cellulose nanocrystals.

Chapter 2 describes a facile and quick method for quantitation of lignin in lignocellulose by thorough dissolution and hydrolysis of cellulose and hemicelluloses under mild conditions leaving lignin as insoluble residue for gravimetric quantitation. Various factors influencing the lignin quantitation were investigated. Under recommended conditions, the ALBTH method gave comparable lignin (both insoluble and soluble lignin) quantities as the Klason method when various wood and grass biomass was used as feedstocks.

Chapter 3 illustrates the chemical fate of the ALBTH lignin fraction isolated from lignocellulose after dissolving and hydrolyzing the cellulose and hemicelluloses. Characterization of ALBTH lignin using GPC and HSQC NMR together with subsequent lignin model compound studies justified the isolated lignin as a partially depolymerized, but less condensed form and suitable for downstream valorization.

Chapter 4 investigates the saccharification and fractionation of lignocellulose at high biomass loading (30%-80%, v/w) for high-yield production of mono- and oligosaccharides in the ALBTH system. The formation of oligosaccharides is ascribed to a top-down process through both controlled hydrolysis of polysaccharides and simultaneous glycosylation of simple sugars. The

saccharification of cellulose further verified the homogeneous hydrolysis of the carbohydrates in lignocellulose and provided detailed chemical information for the oligosaccharide fractions.

Chapter 5 describes a process for high-single pass yield and high-selectivity synthesis of glucooligosaccharides (GlOS) from glucose via a non-enzymatic glycosylation reaction in ALBTH. The chemical structures of GlOS were characterized by MALDI-TOF MS, GPC, and HSQC NMR. The enhanced glycosylation in ALBTH was attributed to the unique properties of ALBTH including the low water concentration, high capacity of dissolving glucose, and enhanced acid dissociation in the system. Select probiotic strains were used to preliminarily evaluate the prebiotic potential of the GlOS.

Chapter 6 details a facile method to prepare cellulose II nanocrystal (CNC II) directly from a commercially available cellulose I feedstock (bleached kraft pulp) via simultaneous polymorph transformation and hydrolysis in mildly acidic lithium bromide trihydrate (MALBTH). A mechanism of simultaneous polymorph transformation as well as controlled hydrolysis in MALBTH was proposed based on the experimental results. Under mild ammonium persulfate oxidation conditions, ox-CNC of cellulose II polymorph was released with a tunable length and relative constant lateral dimensions. The results of this study facilitate CNC production with flexible aspect ratios and improved colloidal properties allowing for expanding potential applications at the interfaces.

Chapter 7 summarizes this work and presents the outlook for future work.

Reference

(1) Liska, A. J.; Heier, C. D. The limits to complexity: A thermodynamic history of bioenergy. *Biofuels, Bioproducts and Biorefining* **2013**, *7*, 573-581.

(2) Lynd, L.; Laser, M. *Cellulosic biofuels: Importance, recalcitrance, and pretreatment*; John Wiley & Sons, 2013.

(3) Huber, G. W.; Iborra, S.; Corma, A. Synthesis of transportation fuels from biomass: chemistry, catalysts, and engineering. *Chemical Reviews* **2006**, *106*, 4044-4098.

(4) Luterbacher, J. S.; Rand, J. M.; Alonso, D. M.; Han, J.; Youngquist, J. T.; Maravelias, C. T.; Pfleger, B. F.; Dumesic, J. A. Nonenzymatic sugar production from biomass using biomass-derived γ-valerolactone. *Science* **2014**, *343*, 277-280.

(5) Ragauskas, A. J.; Beckham, G. T.; Biddy, M. J.; Chandra, R.; Chen, F.; Davis, M. F.; Davison, B. H.; Dixon, R. A.; Gilna, P.; Keller, M. Lignin valorization: improving lignin processing in the biorefinery. *Science* **2014**, *344*, 1246843.

(6) Bozell, J. J.; Petersen, G. R. Technology development for the production of biobased products from biorefinery carbohydrates—the US Department of Energy's "top 10" revisited. *Green Chemistry* **2010**, *12*, 539-554.

(7) Chheda, J. N.; Huber, G. W.; Dumesic, J. A. Liquid-phase catalytic processing of biomass-derived oxygenated hydrocarbons to fuels and chemicals. *Angewandte Chemie* **2007**, *46*, 7164-7183.

(8) McKendry, P. Energy production from biomass (part 1): overview of biomass. *Bioresource Technology* **2002**, *83*, 37-46.

(9) Limayem, A.; Ricke, S. C. Lignocellulosic biomass for bioethanol production: current perspectives, potential issues and future prospects. *Progress in Energy and Combustion Science* **2012**, *38*, 449-467.

(10) Perlack, R. D.; Eaton, L. M.; Turhollow Jr, A. F.; Langholtz, M. H.; Brandt, C. C.; Downing, M. E.; Graham, R. L.; Wright, L. L.; Kavkewitz, J. M.; Shamey, A. M. US billion-ton update: biomass supply for a bioenergy and bioproducts industry. **2011**.

(11) Mottiar, Y.; Vanholme, R.; Boerjan, W.; Ralph, J.; Mansfield, S. D. Designer lignins: harnessing the plasticity of lignification. *Current Opinion in Biotechnology* **2016**, *37*, 190-200.

(12) Rowell, R. M. *Handbook of wood chemistry and wood composites*; CRC press, 2012.

(13) Kubicek, C. P. *Fungi and lignocellulosic biomass*; John Wiley & Sons, 2012.

(14) Leonowicz, A.; Matuszewska, A.; Luterek, J.; Ziegenhagen, D.; Wojtaś-Wasilewska, M.; Cho, N.-S.; Hofrichter, M.; Rogalski, J. Biodegradation of lignin by white rot fungi. *Fungal genetics and biology* **1999**, *27*, 175-185.

(15) Ralph, J.; Brunow, G.; Boerjan, W. Lignins. *eLS* **2007**.

(16) Isikgor, F. H.; Becer, C. R. Lignocellulosic biomass: a sustainable platform for the production of bio-based chemicals and polymers. *Polym. Chem.* **2015**, *6*, 4497-4559.

(17) Marriott, P. E.; Gómez, L. D.; McQueen-Mason, S. J. Unlocking the potential of lignocellulosic biomass through plant science. *New Phytologist* **2016**, *209*, 1366-1381.

(18) Klemm, D.; Heublein, B.; Fink, H. P.; Bohn, A. Cellulose: fascinating biopolymer and sustainable raw material. *Angewandte Chemie* **2005**, *44*, 3358-3393.

(19) Nishiyama, Y.; Langan, P.; Chanzy, H. Crystal structure and hydrogen-bonding system in cellulose Iβ from synchrotron X-ray and neutron fiber diffraction. *Journal of the American Chemical Society* **2002**, *124*, 9074-9082.

(20) Moon, R. J.; Martini, A.; Nairn, J.; Simonsen, J.; Youngblood, J. Cellulose nanomaterials review: structure, properties and nanocomposites. *Chemical Society Reviews* **2011**, *40*, 3941-3994.

(21) Davison, B. H.; Parks, J.; Davis, M. F.; Donohoe, B. S. *Plant cell walls: basics of structure, chemistry, accessibility and the influence on conversion*; John Wiley & Sons, 2013.

(22) Scheller, H. V.; Ulvskov, P. Hemicelluloses. *Annual review of plant biology* **2010**, *61*, 263-289.

(23) Vogel, J. Unique aspects of the grass cell wall. *Current opinion in plant biology* **2008**, *11*, 301-307.

(24) Lan, W.; Lu, F.; Regner, M.; Zhu, Y.; Rencoret, J.; Ralph, S. A.; Zakai, U. I.; Morreel, K.; Boerjan, W.; Ralph, J. Tricin, a flavonoid monomer in monocot lignification. *Plant physiology* **2015**, *167*, 1284-1295.

(25) Heitner, C.; Dimmel, D.; Schmidt, J. *Lignin and lignans: Advances in chemistry*; CRC press, 2016.

(26) Clark, J. H.; Deswarte, F. *Introduction to chemicals from biomass*; John Wiley & Sons, 2015.

(27) Isikgor, F. H.; Becer, C. R. Lignocellulosic biomass: a sustainable platform for the production of bio-based chemicals and polymers. *Polymer Chemistry* **2015**, *6*, 4497-4559.

(28) Akpinar, O.; Erdogan, K.; Bostanci, S. Production of xylooligosaccharides by controlled acid hydrolysis of lignocellulosic materials. *Carbohydrate Research* **2009**, *344*, 660-666.

(29) Grishkewich, N.; Mohammed, N.; Tang, J.; Tam, K. C. Recent advances in the application of cellulose nanocrystals. *Current Opinion in Colloid & Interface Science* **2017**, *29*, 32-45.

(30) Wang, X.; Yao, C.; Wang, F.; Li, Z. Cellulose-based nanomaterials for energy applications. *Small* **2017**, *13*, 1702240.

(31) Siqueira, G.; Bras, J.; Dufresne, A. Cellulosic bionanocomposites: A review of preparation, properties and applications. *Polymers* **2010**, *2*, 728-765.

(32) Sun, Z.; Fridrich, B. l.; de Santi, A.; Elangovan, S.; Barta, K. Bright side of lignin depolymerization: Toward new platform chemicals. *Chemical Reviews* **2018**, *118*, 614-678.

(33) Wang, M.; Li, Z.; Fang, X.; Wang, L.; Qu, Y. Cellulolytic enzyme production and enzymatic hydrolysis for second-generation bioethanol production. In *Biotechnology in China III: Biofuels and Bioenergy*; Springer: 2012, p 1-24.

(34) Akishima, Y.; Isogai, A.; Kuga, S.; Onabe, F.; Usada, M. Kinetic studies on enzymatic hydrolysis of celluloses for evaluation of amorphous structures. *Carbohydrate Polymers* **1992**, *19*, 11-15.

(35) Mansfield, S. D.; Mooney, C.; Saddler, J. N. Substrate and enzyme characteristics that limit cellulose hydrolysis. *Biotechnology Progress* **1999**, *15*, 804-816.

(36) Chandra, R. P.; Bura, R.; Mabee, W.; Berlin, d. A.; Pan, X.; Saddler, J. Substrate pretreatment: The key to effective enzymatic hydrolysis of lignocellulosics? In *Biofuels*; Springer: 2007, p 67-93.

(37) Li, C.; Cheng, G.; Balan, V.; Kent, M. S.; Ong, M.; Chundawat, S. P.; daCosta Sousa, L.; Melnichenko, Y. B.; Dale, B. E.; Simmons, B. A. Influence of physico-chemical changes on enzymatic digestibility of ionic liquid and AFEX pretreated corn stover. *Bioresource Technology* **2011**, *102*, 6928-6936.

(38) Kleman-Leyer, K. M.; SiiKa-Aho, M.; Teeri, T. T.; Kirk, T. K. The cellulases endoglucanase I and cellobiohydrolase II of trichoderma reesei act synergistically to solubilize native cotton cellulose but not to decrease its molecular size. *Applied and environmental microbiology* **1996**, *62*, 2883-2887.

(39) Zhang, Y.-H. P.; Cui, J.; Lynd, L. R.; Kuang, L. R. A transition from cellulose swelling to cellulose dissolution by o-phosphoric acid: evidence from enzymatic hydrolysis and supramolecular structure. *Biomacromolecules* **2006**, *7*, 644-648.

(40) Alvira, P.; Tomas-Pejo, E.; Ballesteros, M.; Negro, M. J. Pretreatment technologies for an efficient bioethanol production process based on enzymatic hydrolysis: A review. *Bioresource Technology* **2010**, *101*, 4851-61.

(41) Yang, Q.; Pan, X. Correlation between lignin physicochemical properties and inhibition to enzymatic hydrolysis of cellulose. *Biotechnology and Bioengineering* **2016**, *113*, 1213-1224.

(42) Bubner, P.; Dohr, J.; Plank, H.; Mayrhofer, C.; Nidetzky, B. Cellulases dig deep in situ observation of the mesoscopic structural dynamics of enzymatic cellulose degradation. *Journal of Biological Chemistry* **2012**, *287*, 2759-2765.

(43) Huang, Y.-B.; Fu, Y. Hydrolysis of cellulose to glucose by solid acid catalysts. *Green Chemistry* **2013**, *15*, 1095.

(44) Wang, J.; Xi, J.; Wang, Y. Recent advances in the catalytic production of glucose from lignocellulosic biomass. *Greem Chemistry* **2015**, *17*, 737-751.

(45) Rinaldi, R.; Schuth, F. Acid hydrolysis of cellulose as the entry point into biorefinery schemes. *ChemSusChem* **2009**, *2*, 1096-107.

(46) Loerbroks, C.; Heimermann, A.; Thiel, W. Solvents effects on the mechanism of cellulose hydrolysis: a QM/MM study. *Journal of Computational Chemistry* **2015**, *36*, 1114-1123.

(47) Loerbroks, C.; Rinaldi, R.; Thiel, W. The Electronic Nature of the 1, 4-β-Glycosidic Bond and Its Chemical Environment: DFT Insights into Cellulose Chemistry. *Chemistry-A European Journal* **2013**, *19*, 16282-16294.

(48) Dee, S. J.; Bell, A. T. A study of the acid-catalyzed hydrolysis of cellulose dissolved in ionic liquids and the factors influencing the dehydration of glucose and the formation of humins. *ChemSusChem* **2011**, *4*, 1166-73.

(49) Jones, J.; Semrau, K. Wood hydrolysis for ethanol production—previous experience and the economics of selected processes. *Biomass* **1984**, *5*, 109-135.

(50) Rahman, S.; Choudhury, J.; Ahmad, A. Production of xylose from oil palm empty fruit bunch fiber using sulfuric acid. *Biochemical Engineering Journal* **2006**, *30*, 97-103.

(51) Harmer, M. A.; Fan, A.; Liauw, A.; Kumar, R. K. A new route to high yield sugars from biomass: phosphoric–sulfuric acid. *Chemical Communications* **2009**, 6610-6612.

(52) Amarasekara, A. S.; Wiredu, B. Aryl sulfonic acid catalyzed hydrolysis of cellulose in water. *Applied Catalysis A: General* **2012**, *417*, 259-262.

(53) Kupiainen, L.; Ahola, J.; Tanskanen, J. Hydrolysis of organosolv wheat pulp in formic acid at high temperature for glucose production. *Bioresource Technology* **2012**, *116*, 29-35.

(54) vom Stein, T.; Grande, P.; Sibilla, F.; Commandeur, U.; Fischer, R.; Leitner, W.; Domínguez de María, P. Salt-assisted organic-acid-catalyzed depolymerization of cellulose. *Green Chemistry* **2010**, *12*, 1844.

(55) Takagaki, A.; Tagusagawa, C.; Domen, K. Glucose production from saccharides using layered transition metal oxide and exfoliated nanosheets as a water-tolerant solid acid catalyst. *Chemical Communications* **2008**, 5363-5365.

(56) Tagusagawa, C.; Takagaki, A.; Iguchi, A.; Takanabe, K.; Kondo, J. N.; Ebitani, K.; Hayashi, S.; Tatsumi, T.; Domen, K. Highly active mesoporous Nb–W oxide solid-acid catalyst. *Angewandte Chemie* **2010**, *122*, 1146-1150.

(57) Zhang, F.; Deng, X.; Fang, Z.; Zeng, H.; Tian, X.; Kozinski, J. Hydrolysis of microcrystalline cellulose over Zn-Ca-Fe oxide catalyst. *Petrochemical Technology* **2011**, *40*, 43-48.

(58) Rinaldi, R.; Palkovits, R.; Schuth, F. Depolymerization of cellulose using solid catalysts in ionic liquids. *Angewandte Chemie* **2008**, *47*, 8047-50.

(59) Shuai, L.; Pan, X. Hydrolysis of cellulose by cellulase-mimetic solid catalyst. *Energy & Environmental Science* **2012**, *5*, 6889-6894.

(60) Suganuma, S.; Nakajima, K.; Kitano, M.; Yamaguchi, D.; Kato, H.; Hayashi, S. Hydrolysis of cellulose by amorphous carbon bearing SO3H, COOH, and OH groups. *Journal of the American Chemical Society* **2008**, *130*, 12787-12793.

(61) Wu, Y.; Fu, Z.; Yin, D.; Xu, Q.; Liu, F.; Lu, C.; Mao, L. Microwave-assisted hydrolysis of crystalline cellulose catalyzed by biomass char sulfonic acids. *Green Chemistry* **2010**, *12*, 696-700.

(62) Luterbacher, J.; Alonso, D. M.; Dumesic, J. Targeted chemical upgrading of lignocellulosic biomass to platform molecules. *Green Chemistry* **2014**, *16*, 4816-4838.

(63) Shuai, L.; Luterbacher, J. Organic solvent effects in biomass conversion reactions. *ChemSusChem* **2016**, *9*, 133-155.

(64) Lidström, P.; Tierney, J.; Wathey, B.; Westman, J. Microwave assisted organic synthesis—a review. *Tetrahedron* **2001**, *57*, 9225-9283.

(65) Fan, J.; De Bruyn, M.; Budarin, V. L.; Gronnow, M. J.; Shuttleworth, P. S.; Breeden, S.; Macquarrie, D. J.; Clark, J. H. Direct microwave-assisted hydrothermal depolymerization of cellulose. *Journal of the American Chemical Society* **2013**, *135*, 11728-11731.

(66) Bandura, A. V.; Lvov, S. N. The ionization constant of water over wide ranges of temperature and density. *Journal of Physical and Chemical Reference Data* **2006**, *35*, 15-30.

(67) Buffiere, J.; Ahvenainen, P.; Borrega, M.; Svedström, K.; Sixta, H. Supercritical water hydrolysis: a green pathway for producing low-molecular-weight cellulose. *Green Chemistry* **2016**, *18*, 6516-6525.

(68) Sasaki, M.; Adschiri, T.; Arai, K. Production of cellulose II from native cellulose by near- and supercritical water solubilization. *Journal of Agricultural and Food Chemistry* **2003**, *51*, 5376-5381.

(69) Olanrewaju, K. B. *Reaction kinetics of cellulose hydrolysis in subcritical and supercritical water*; The University of Iowa, 2012.

(70) Zhao, Y.; Lu, W.-J.; Wang, H.-T. Supercritical hydrolysis of cellulose for oligosaccharide production in combined technology. *Chemical Engineering Journal* **2009**, *150*, 411-417.

(71) Tolonen, L. K.; Juvonen, M.; Niemelä, K.; Mikkelson, A.; Tenkanen, M.; Sixta, H. Supercritical water treatment for cello-oligosaccharide production from microcrystalline cellulose. *Carbohydrate Research* **2015**, *401*, 16-23.

(72) Mellmer, M. A.; Sener, C.; Gallo, J. M. R.; Luterbacher, J. S.; Alonso, D. M.; Dumesic, J. A. Solvent effects in acid-catalyzed biomass conversion reactions. *Angewandte Chemie* **2014**, *53*, 11872-11875.

(73) Mellmer, M. A.; Alonso, D. M.; Luterbacher, J. S.; Gallo, J. M. R.; Dumesic, J. A. Effects of γ-valerolactone in hydrolysis of lignocellulosic biomass to monosaccharides. *Green Chemistry* **2014**, *16*, 4659-4662.

(74) Meine, N.; Rinaldi, R.; Schuth, F. Solvent-free catalytic depolymerization of cellulose to water-soluble oligosaccharides. *ChemSusChem* **2012**, *5*, 1449-54.

(75) Hick, S. M.; Griebel, C.; Restrepo, D. T.; Truitt, J. H.; Buker, E. J.; Bylda, C.; Blair, R. G. Mechanocatalysis for biomass-derived chemicals and fuels. *Green Chemistry* **2010**, *12*, 468.

(76) Käldström, M.; Meine, N.; Farès, C.; Rinaldi, R.; Schüth, F. Fractionation of 'water-soluble lignocellulose' into C5/C6 sugars and sulfur-free lignins. *Greem Chemistry* **2014**, *16*, 2454-2462.

(77) Dong, Y.; Schneider, L.; Hu, T.; Jaakkola, M.; Holm, J.; Leveque, J. M.; Lassi, U. Direct acid-catalysed mechanical depolymerisation of fibre sludge to reducing sugars using planetary milling. *Biomass and Bioenergy* **2016**, *86*, 36-42.

(78) Upton, B. M.; Kasko, A. M. Strategies for the conversion of lignin to high-value polymeric materials: Review and perspective. *Chemical Reviews* **2015**, *116*, 2275-2306.

(79) Mahmood, N.; Yuan, Z.; Schmidt, J.; Xu, C. C. Depolymerization of lignins and their applications for the preparation of polyols and rigid polyurethane foams: A review. *Renewable and Sustainable Energy Reviews* **2016**, *60*, 317-329.

(80) Rinaldi, R.; Jastrzebski, R.; Clough, M. T.; Ralph, J.; Kennema, M.; Bruijnincx, P. C.; Weckhuysen, B. M. Paving the way for lignin valorisation: recent advances in bioengineering, biorefining and catalysis

Angewandte Chemie **2016**, *55*, 8164-8215.

(81) Schutyser, W.; Renders, T.; Van den Bosch, S.; Koelewijn, S.-F.; Beckham, G. T.; Sels, B. F. Chemicals from lignin: an interplay of lignocellulose fractionation, depolymerisation, and upgrading. *Chemical Society Reviews* **2018**, *47*, 852-908.

(82) Rahimi, A.; Ulbrich, A.; Coon, J. J.; Stahl, S. S. Formic-acid-induced depolymerization of oxidized lignin to aromatics. *Nature* **2014**, *515*, 249-52.

(83) Deuss, P. J.; Scott, M.; Tran, F.; Westwood, N. J.; de Vries, J. G.; Barta, K. Aromatic monomers by in situ conversion of reactive intermediates in the acid-catalyzed depolymerization of lignin. *Journal of the American Chemical Society* **2015**, *137*, 7456-7467.

(84) Shuai, L.; Questell-Santiago, Y. M.; Luterbacher, J. S. A mild biomass pretreatment using γ-valerolactone for concentrated sugar production. *Green Chemistry* **2016**, *18*, 937-943.

(85) Li, C.; Zhao, X.; Wang, A.; Huber, G. W.; Zhang, T. Catalytic transformation of lignin for the production of chemicals and fuels. *Chemical Reviews* **2015**, *115*, 11559-11624.

(86) Mortensen, P. M.; Grunwaldt, J.-D.; Jensen, P. A.; Knudsen, K.; Jensen, A. D. A review of catalytic upgrading of bio-oil to engine fuels. *Applied Catalysis A: General* **2011**, *407*, 1-19.

(87) Luterbacher, J. S.; Azarpira, A.; Motagamwala, A. H.; Lu, F.; Ralph, J.; Dumesic, J. A. Lignin monomer production integrated into the γ-valerolactone sugar platform. *Energy & Environmental Science* **2015**, *8*, 2657-2663.

(88) Grande, P. M.; Viell, J.; Theyssen, N.; Marquardt, W.; de María, P. D.; Leitner, W. Fractionation of lignocellulosic biomass using the OrganoCat process. *Green Chemistry* **2015**, *17*, 3533-3539.

(89) Nguyen, T. Y.; Cai, C. M.; Kumar, R.; Wyman, C. E. Co-solvent pretreatment reduces costly enzyme requirements for high sugar and ethanol yields from lignocellulosic biomass. *ChemSusChem* **2015**, *8*, 1716-1725.

(90) Cai, C. M.; Nagane, N.; Kumar, R.; Wyman, C. E. Coupling metal halides with a co-solvent to produce furfural and 5-HMF at high yields directly from lignocellulosic biomass as an integrated biofuels strategy. *Green Chemistry* **2014**, *16*, 3819-3829.

(91) Renders, T.; Van den Bosch, S.; Koelewijn, S.-F.; Schutyser, W.; Sels, B. Lignin-first biomass fractionation: the advent of active stabilisation strategies. *Energy & Environmental Science* **2017**, *10*, 1551-1557.

(92) Shuai, L.; Amiri, M. T.; Questell-Santiago, Y. M.; Heroguel, F.; Li, Y.; Kim, H.; Meilan, R.;

Chapple, C.; Ralph, J.; Luterbacher, J. S. Formaldehyde stabilization facilitates lignin monomer production during biomass depolymerization. *Science* **2016**, *354*, 329-333.

(93) Lan, W.; Talebi Amiri, M.; Hunston, C. M.; Luterbacher, J. Protection group effects during α, γ-diol lignin stabilization promote high-selectivity monomer production. *Angewandte Chemie* **2017**, *130*, 1-6.

(94) Deuss, P. J.; Scott, M.; Tran, F.; Westwood, N. J.; de Vries, J. G.; Barta, K. Aromatic monomers by in situ conversion of reactive intermediates in the acid-catalyzed depolymerization of lignin. *Journal of the American Chemical Society* **2015**, *137*, 7456-67.

(95) Sen, S.; Martin, J. D.; Argyropoulos, D. S. Review of cellulose non-derivatizing solvent interactions with emphasis on activity in inorganic molten salt hydrates. *ACS Sustainable Chemistry & Engineering* **2013**, *1*, 858-870.

(96) Richard, P. S.; Scott, K. S.; John, D.; Robin, D. Dissolution of cellulose with ionic liquids. *Journal of the American Chemical Society* **2002**, *124*, 4974.

(97) Li, C.; Zhao, Z. K. Efficient acid-catalyzed hydrolysis of cellulose in ionic liquid. *Advanced Synthesis & Catalysis* **2007**, *349*, 1847-1850.

(98) Li, C.; Wang, Q.; Zhao, Z. K. Acid in ionic liquid: An efficient system for hydrolysis of lignocellulose. *Green Chemistry* **2008**, *10*, 177-182.

(99) Binder, J. B.; Raines, R. T. Fermentable sugars by chemical hydrolysis of biomass. *Proceedings of the National Academy of Sciences* **2010**, *107*, 4516-4521.

(100) Caes, B. R.; Van Oosbree, T. R.; Lu, F.; Ralph, J.; Maravelias, C. T.; Raines, R. T. Simulated moving bed chromatography: Separation and recovery of sugars and ionic liquid from biomass hydrolysates. *ChemSusChem* **2013**, *6*, 2083-2089.

(101) Vanoye, L.; Fanselow, M.; Holbrey, J. D.; Atkins, M. P.; Seddon, K. R. Kinetic model for the hydrolysis of lignocellulosic biomass in the ionic liquid, 1-ethyl-3-methyl-imidazolium chloride. *Green chemistry* **2009**, *11*, 390-396.

(102) Sievers, C.; Valenzuela-Olarte, M. B.; Marzialetti, T.; Musin, I.; Agrawal, P. K.; Jones, C. W. Ionic-liquid-phase hydrolysis of pine wood. *Industrial & Engineering Chemistry Research* **2009**, *48*, 1277-1286.

(103) Sun, N.; Liu, H.; Sathitsuksanoh, N.; Stavila, V.; Sawant, M.; Bonito, A.; Tran, K.; George, A.; Sale, K. L.; Singh, S. Production and extraction of sugars from switchgrass hydrolyzed in ionic liquids. *Biotechnology for biofuels* **2013**, *6*, 1.

(104) Dee, S. J.; Bell, A. T. A study of the acid-catalyzed hydrolysis of cellulose dissolved in ionic liquids and the factors influencing the dehydration of glucose and the formation of humins. *ChemSusChem* **2011**, *4*, 1166-1173.

(105) da Costa Lopes, A. M.; Bogel-Łukasik, R. Acidic ionic liquids as sustainable approach of cellulose and lignocellulosic biomass conversion without additional catalysts. *ChemSusChem* **2015**, *8*, 947-965.

(106) Hu, X.; Xiao, Y.; Niu, K.; Zhao, Y.; Zhang, B.; Hu, B. Functional ionic liquids for hydrolysis

of lignocellulose. *Carbohydrate Polymers* **2013**, *97*, 172-176.

(107) Brennan, T. C.; Datta, S.; Blanch, H. W.; Simmons, B. A.; Holmes, B. M. Recovery of sugars from ionic liquid biomass liquor by solvent extraction. *BioEnergy Research* **2010**, *3*, 123-133.

(108) Leipner, H.; Fischer, S.; Brendler, E.; Voigt, W. Structural changes of cellulose dissolved in molten salt hydrates. *Macromolecular Chemistry and Physics* **2000**, *201*, 2041-2049.

(109) Fischer, S.; Leipner, H.; Thümmler, K.; Brendler, E.; Peters, J. Inorganic molten salts as solvents for cellulose. *Cellulose* **2003**, *10*, 227-236.

(110) Sen, S.; Losey, B. P.; Gordon, E. E.; Argyropoulos, D. S.; Martin, J. D. Ionic liquid character of zinc chloride hydrates define solvent characteristics that afford the solubility of cellulose. *The Journal of Physical Chemistry B* **2016**, *120*, 1134-1141.

(111) Liu, Z.; Zhang, C.; Liu, R.; Zhang, W.; Kang, H.; Li, P.; Huang, Y. Dissolution of cellobiose in the aqueous solutions of chloride salts: Hofmeister series consideration. *Cellulose* **2016**, *23*, 295-305.

(112) Fischer, S.; Voigt, W.; Fischer, K. The behaviour of cellulose in hydrated melts of the composition LiX nH2O (X= I^-, NO_3^-, CH_3COO^-, $ClO4^-$). *Cellulose* **1999**, *6*, 213-219.

(113) de Almeida, R. M.; Li, J.; Nederlof, C.; O'Connor, P.; Makkee, M.; Moulijn, J. A. Cellulose conversion to isosorbide in molten salt hydrate media. *ChemSusChem* **2010**, *3*, 325-328.

(114) Pan, X.; Shuai, L. Saccharification of lignocellulosic biomass. Wisconsin Research Foundation: 2015.

(115) Yang, Y.-J.; Shin, J.-M.; Kang, T. H.; Kimura, S.; Wada, M.; Kim, U.-J. Cellulose dissolution in aqueous lithium bromide solutions. *Cellulose* **2014**, *21*, 1175-1181.

(116) Wang, H.; Zhang, L.; Deng, T.; Ruan, H.; Hou, X.; Cort, J. R.; Yang, B. $ZnCl_2$ induced catalytic conversion of softwood lignin to aromatics and hydrocarbons. *Green Chemistry* **2016**, *18*, 2802-2810.

(117) Cao, N.; Xu, Q.; Chen, L. Acid hydrolysis of cellulose in zinc chloride solution. *Applied Biochemistry and Biotechnology* **1995**, *51*, 21-28.

(118) Wei, W.; Wu, S. Depolymerization of cellulose into high-value chemicals by using synergy of zinc chloride hydrate and sulfate ion promoted titania catalyst. *Bioresource Technology* **2017**, *241*, 760-766.

(119) van den Bergh, J.; Babich, I. V.; O'Connor, P.; Moulijn, J. A. Production of monosugars from lignocellulosic biomass in molten salt hydrates: process design and techno-economic analysis. *Industrial & engineering chemistry research* **2017**, *56*, 13423-13433.

(120) Bi, Z.; Lai, B.; Zhao, Y.; Yan, L. Fast disassembly of lignocellulosic biomass to lignin and sugars by molten salt hydrate at low temperature for overall biorefinery. *ACS Omega* **2018**, *3*, 2984-2993.

Chapter 2 A facile and fast method for quantitating lignin in lignocellulosic biomass using acidic lithium bromide trihydrate (ALBTH)

This chapter has been published, in part, under the same title.

Li, N.; Pan, X.; Alexander, J. *Green Chemistry* **2016**, *18*, 5367-5376.

Abstract:

Lignin quantitation of lignocellulosic biomass is an essential and routine assay in the areas of plant chemistry, forage, biomass conversion, and pulp & paper. The two-step sulfuric acid method (or Klason method) is the most widely used protocol for lignin quantitation, but the method is a time-consuming and labor-intensive procedure. In this study, a facile and quick method was developed to quantitate lignin in lignocellulosic biomass. The new method used acidic lithium bromide trihydrate (ALBTH, $LiBr{\cdot}3H_2O$) as reaction medium, which was able to quickly and completely dissolve and hydrolyze cellulose and hemicelluloses in the biomass under mild conditions and leave lignin as insoluble residue for gravimetric quantitation. The soluble lignin generated in the ALBTH assay was determined by UV spectrophotometry. The recommended conditions for the ALBTH method were 60 wt% LiBr solution containing 40 mM HCl, 110 °C, and 30 min. The ALBTH method was applied to different species of biomass including softwood (Douglas fir), hardwood (aspen, poplar, and eucalyptus), and herbage (corn stover and switchgrass). The results indicated that the ALBTH method gave comparable lignin (both insoluble and soluble lignin) quantity with the Klason method for the biomass investigated. The ALBTH method is a one-step procedure and much faster for lignin quantitation (~30 min) than the Klason method (>3 h). In

addition, the ALBTH assay was conducted in glass vial at atmospheric pressure, and no autoclave was required. The ALBTH method also avoided the potential hazard of concentrated sulfuric acid.

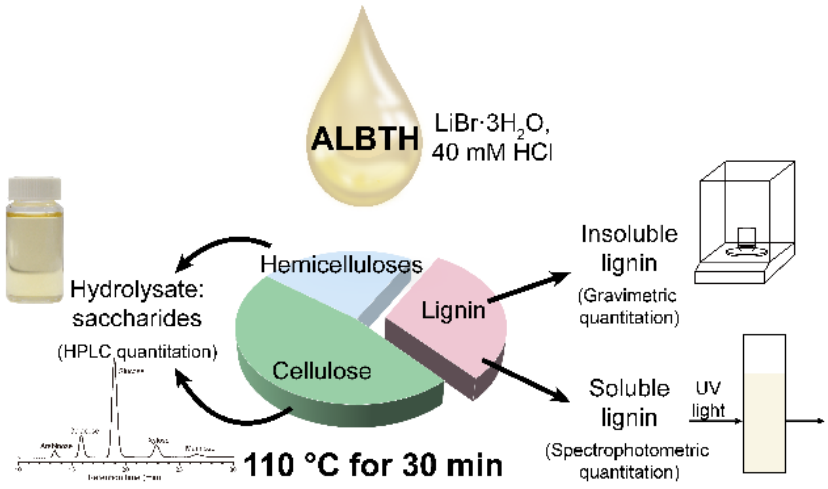

2.1 Introduction

Lignin is the most abundant natural aromatic polymer on the earth and one of the three major components of lignocellulosic biomass. In plant cell wall, lignin besieges and coheres with cellulose and hemicelluloses, endowing mechanical strength to plant stem and providing robust protection and barrier against biological and chemical attacks. On the other hand, the presence of lignin dramatically affects the efficiency of biomass utilizations, for example, the forage digestibility by ruminants, the fiberization of wood chips during pulping for paper production, and bioconversion of lignocellulosics to fuels and chemicals.[1-5] Tremendous efforts have been made to develop technologies for removing and separating lignin from lignocellulosics in order to enhance the utilization of the cell wall carbohydrates (cellulose and hemicelluloses) for fibers, chemicals, and biofuels in paper industry and biorefinery.[6,7] In addition, a great deal of research has been conducted to explore the valorization of the separated lignin from pulping and biorefining processes, such as organosolv, kraft, lignosulfonate, and steam-explosion lignin, into value-added

products including aromatic hydrocarbons, phenolic derivatives, carbon fibers, lignin-based polymers, and resins.[8-11] In all these research activities, lignin quantitation is a routine procedure for biomass composition analysis and process development and evaluation. Many methods have been developed and evaluated for lignin quantitation, including wet chemistry and instrumental protocols, which fall into two categories, indirect and direct quantitation methods, as discussed below.[12-14]

The most popular indirect method for the quantitation of lignin is known as acetyl bromide (AcBr) method.[15] Milligram-size biomass sample is digested in the solution of 25% AcBr in acetic acid at 70 °C. Lignin undergoes the bromination of α-hydroxyl groups and the acetylation of the unsubstituted hydroxyl groups, and is consequently dissolved in acetic acid. The dissolved lignin is subsequently quantitated using an ultraviolet (UV) spectrophotometer at 280 nm. Acetyl bromide method has been proven to be a prompt method with acceptable precision. Several modifications have been made to improve this method, for example, introducing glass fiber filter to simplify the procedure and reduce sample size[5a] and adding perchloric acid to improve solubilization of biomass samples.[16,17b] However, the acetyl bromide method still has some inherent shortcomings. For example, it is complicated to determine the specific absorptivity of lignin from different biomass species; the furan products derived from sugar dehydration interfere with the spectrophotometric quantitation of lignin at 280 nm, which have absorptions in the range of 270 – 290 nm.

The direct methods quantitate lignin by dissolving and hydrolyzing cellulose and hemicelluloses from lignocellulosic biomass and leaving lignin as insoluble residue to be quantitated gravimetrically. Two-stage hydrolysis with sulfuric acid (or so-called Klason method) is the most prevalent lignin quantitation procedure, in which biomass sample is first treated in

concentrated sulfuric acid (72 wt%) at ambient temperature (20-30 °C) for 1 h to swell and dissolve cellulose and hemicelluloses, and the mixture is then diluted with water to 3-4 wt% sulfuric acid and subsequently heated at elevated temperature (100 – 121°C) to hydrolyze the carbohydrates to monomeric sugars. The insoluble solid residue is gravimetrically quantitated, known as acid-insoluble lignin (AIL) or Klason lignin. The fraction of dissolved lignin, called acid-soluble lignin (ASL), is spectrophotometrically quantitated. The sugars in the hydrolysate are analyzed using gas chromatography (GC) or high performance liquid chromatography (HPLC), if necessary. Based on the Klason procedure, two standard protocols, the Technical Association of the Pulp and Paper Industry (TAPPI) method TAPPI T 222-om02: Acid insoluble lignin in wood and pulp and the National Renewable Energy Laboratory (NREL) protocol NREL/TP-510-42618: Determination of structure carbohydrates and lignin in biomass, have been widely used in paper industry and biomass conversion areas, respectively. However, the Klason method requires hazardous concentrated sulfuric acid as reaction medium and suffers from labor-intensive procedures and tedious experimental operation. In particular, insufficient swelling and dissolution of cellulose often occurs during the first step of treatment with concentrated (72 wt%) H_2SO_4, which results in overestimation of lignin. This is one of the reasons why lignin result fluctuates between operators and laboratories. The acid-induced formation of humins from sugars through furan intermediates is another source of lignin overestimation.[18-20]

Besides concentrated acids (e.g., sulfuric and phosphoric acids), ionic solvents (e.g., organic and inorganic ionic liquids) also show excellent performance in swelling and dissolving cellulose and hemicelluloses. The inorganic ionic liquids (molten salt hydrates) usually have excellent abilities to dissolve and hydrolyze carbohydrates (cellulose and hemicelluloses) but poor (limited) ability to dissolve lignin, which therefore makes it possible to quantitate insoluble lignin

gravimetrically and the soluble sugars derived from cellulose and hemicellulose chromatographically, respectively. The ability of the molten salt hydrates to dissolve cellulose is dependent on the combination of their cations and anions. It was reported that several inorganic molten salt hydrate systems (e.g., $ZnCl_2 \cdot 3\text{-}4H_2O$, $LiClO_4 \cdot 3H_2O$, $LiI \cdot 2H_2O$ and $LiBr \cdot 3H_2O$) were able to dissolve cellulose by disrupting the inter- and intra- molecular hydrogen bonds of cellulose and coordinating with hydroxyl groups of cellulose in the first coordination sphere of the cations.[21-26] Recently, we found that cellulose and hemicelluloses of lignocellulosic biomass could be quickly and completely saccharified in the acidic lithium bromide hydrate system without any pretreatment, while lignin was isolated as solid residue with high purity,[26] which triggered the present study to develop a facile and fast lignin quantitation method based on this biomass saccharification technology.

In this work, a facile protocol was established for fast quantitation of lignin in lignocellulosic biomass using acidic lithium bromide trihydrate (ALBTH, $LiBr \cdot 3H_2O$), in which cellulose and hemicelluloses were dissolved and hydrolyzed into monosaccharides, and lignin was left over as insoluble residue for gravimetric quantitation. Experimental procedure and conditions of the ALBTH method were optimized to establish a reliable, accurate, and precise quantitative method for lignin. The changes of the cell wall components during the reaction and the potential effects on the lignin quantitation were also investigated. The residual carbohydrates in the insoluble lignin from the ALBTH method were analyzed using the two-step acid hydrolysis method, and the chemical structures of the lignin were characterized with 2D-HSQC NMR to verify the representation of the ALBTH lignin as the lignin fraction in the biomass. The lignin contents of various biomass species, including softwood (Douglas fir), hardwood (poplar, aspen, and eucalyptus), and herbage (corn stover and switchgrass), were determined using the ALBTH

method and compared with the values from the NREL method.

2.2 Experimental

2.2.1 Biomass sample preparation

Lignocellulosic biomass (poplar NE222, aspen, eucalyptus, and Douglas fir, corn stover, and switchgrass) was ground using a Wiley mill and sieved to collect the fraction between 20 and 100 mesh for analysis. The ground biomass was Soxhlet-extracted with water for 8 h (only for herbaceous biomass) and 95% ethanol for 16 h to remove extractives.

2.2.2 Lignin quantification by the ALBTH method

The extractive-free biomass powder (0.3 g, weighed to the nearest 0.1 mg) was added into a 40-mL glass vial with screw top, together with 4.50 mL of acidic 60 wt% LiBr solution containing HCl. It is critical that the acid catalyst should be mixed with lithium bromide solution to form a homogeneous solution (with light yellowish color) before adding biomass. The mixture was agitated using a magnetic stirring bar (400 rpm) at room temperature for 2 min, and then the vial was immersed into an oil bath preheated to the target temperature with magnetic stirring (400 rpm). The reaction was quenched at the preset reaction time by placing the vial into ice water. The contents of the vial were quantitatively transferred into a 50-mL volumetric flask and diluted to the mark with DI water. The mixture was filtered under vacuum through a pre-weighted filtering crucible (30 mL, low form with medium porosity). The transparent filtrate was collected and stored in a refrigerator for subsequent analysis of soluble lignin, sugars, and sugar decomposition products. All the solids remaining in the volumetric flask were carefully washed out into the filtering crucible and thoroughly rinsed with 150 mL deionized water. The solid residues together with the crucible were dried at 105 °C overnight and then gravimetrically quantitated. The crucible

with the insoluble solid residue was ignited in a muffle furnace at 575 °C for 12 h to determine the ash content in the residue for correcting insoluble lignin content. Insoluble lignin (IL) on the extractive-containing basis was calculated using Eq. 2.1. Soluble lignin (SL) was quantitated on a UV-Visible spectrophotometer using a standard quartz cuvette with 1-cm pathlength and was calculated on the extractive-containing basis using Eq. 2.2 according to the Beer-Lambert law. The recommended step-by-step procedure of ALBTH method is provided in ESI. All experiments were conducted at least in duplicate, and the average and standard deviation were reported.

$$IL\,(\%) = \frac{m_{c+r} - m_c - m_a}{m_s} \times (100 - \sigma) \tag{2.1}$$

$$SL\ (\%) = \frac{Abs' \ V_f \ d}{\varepsilon \ m_s \ 1.0} \ (100 - \sigma) \tag{2.2}$$

where m_s is the oven dry weight of extractives-free biomass sample (g); m_{c+r} is the oven dry weight of the crucible with insoluble solid residue (g); m_c is the oven dry weight of the crucible (g); m_a is the oven dry weight of the ash (g); Abs' is the UV absorbance of the filtrate at 240 nm (for woody biomass) or 320 nm (for herbaceous biomass) after δ times dilution (Note: for woody biomass, a correction is needed, as explicated in Results and Discussion, to subtract the UV absorbance of hydroxymethylfurfural (HMF) and furfural at 240 nm; for herbaceous biomass, no correction is needed because of the negligible interference of HMF and furfural absorptions at 320 nm); V_f is the total volume of the filtrate (50 mL); δ is the dilution factor; ε is the absorptivity of biomass lignin at specific wavelength (25 $g^{-1}L\ cm^{-1}$ for woody biomass at 240 nm and 30 $g^{-1}L\ cm^{-1}$ for herbaceous biomass at 320 nm, respectively, adopted from the NREL method); σ is the weight percentage of the extractives in the oven dry biomass sample.

2.2.3 Klason lignin quantitation by NREL method

Quantitation of lignin by the two-stage sulfuric acid hydrolysis was conducted following the NREL

standard protocol.[27] In brief, 0.3 g biomass (weighed to the nearest 0.1 mg) was treated in 72 % H_2SO_4 at 30 °C for 60 min. The slurry was diluted to 4% H_2SO_4 and autoclaved at 121 °C for 60 min. After filtration, the acid-insoluble lignin (AIL) and the acid-soluble lignin (ASL) were quantitated gravimetrically and spectrophotometrically, respectively.

2.2.4 Chromatographic analysis

Monosaccharides in the filtrates (hydrolysates) above were quantitated using high performance ion chromatography (HPIC) on a Dionex ICS-3000 system equipped with an integrated amperometric detector and a CarboPac PA1 column (4 mm×250 mm) at 30 °C. Deionized water (18 MΩ·cm) was used as eluent at a flow rate of 0.7 mL/min according to the following gradient: 0-25 min, 100% water; 25.1-35 min, 30% water and 70% 0.1 M NaOH; and 35.1-42 min, 100% water. Post-column eluent of 0.5 M NaOH at a flow rate of 0.3 mL/min was used to ensure baseline stability and detector sensitivity.[3] The dehydration products (HMF and furfural) of the monosaccharides were determined using high performance liquid chromatography (HPLC) on a Dionex ICS-3000 system equipped with a Supelcogel C-610H column (7.8×300 mm) at 30 °C and an UV detector at 210 nm. An isocratic flow of 0.1% phosphoric acid was used as the mobile phase at 0.6 mL/min.[3]

2.2.5 NMR analysis

Poplar sample was ground using a Wiley mill and a ball mill sequentially and swelled/dissolved in 0.7 mL of premixed DMSO-d_6/pyridine-d_5 (4:1) for whole cell wall NMR according the protocol previously described.[28] The insoluble lignin collected from the ALBTH method was air-dried and directly dissolved in 0.7 mL of DMSO-d_6 solution for NMR analysis. ^{1}H-^{13}C heteronuclear single quantum correlation (HSQC) spectra were recorded on a Brucker AVANCE 500MHz instrument equipped with a DCH cryoprobe. Bruker pulse program “hsqcetgpsisp2.2 (adiabatic-pulse

fashion)" was used with spectral widths of 12 ppm (from 11 to -1 ppm) and 220 ppm (from 200 to -20 ppm) for the ^{1}H and ^{13}C dimensions, respectively. The acquisition time was 200 ms (^{1}H) and 8 ms (^{13}C), with the inter-scan relaxation delay of 1 s. The processing of spectra was conducted using Topspin 3.2 software with the final 2D data matrix size of 2k × 1k data points.

2.2.6 SEM/EDS analysis

Field emission scanning electron microscopy (FESEM, Leo Co., Oberkochen, Germany) coupled with energy dispersive spectroscopy (EDS) was used to observe the morphology and to determine the elemental distribution of the ALBTH lignin residue. Prior to microscopic observation, the ALBTH lignin residue was firmly attached on the surface of the conductive tape fixed on the aluminum mount and sputter coated with a thin layer of gold. The accelerating voltage was 10.0 kV for morphology observation and 15.0 kV for EDS analysis, respectively.

2.3 Results and Discussion

2.3.1 Description of the ALBTH method

Lithium bromide trihydrate ($LiBr{\cdot}3H_2O$) belongs to a family of molten salt hydrates, which are the unique concentrated aqueous solutions of inorganic salts. The concentration of a molten salt hydrate varies from salt to salt, dependent on the coordination number of the salt cation.[29] In a perfect molten salt hydrate, all water molecules are tightly bound to the inner coordination sphere of the cation, leaving the anion naked in the system.[21] For example, as shown in Figure 2.1, in the molten salt hydrate of lithium bromide used in this study, lithium cation (Li^{+}) has octahedral coordination geometry and needs 6 oxygen atoms from water to coordinate with. Since the oxygen of each water molecule is shared by two lithium ions, the stoichiometric ratio of LiBr to H_2O is 1:3. As water molecules was mostly trapped by Li^{+}, Br^{-} is naked and free in the solution. The free

bromide anion (Br^-) is able to associate with the H of cellulose hydroxyl groups and form hydrogen bonds with cellulose. In addition, Li^+ is very oxophilic so that it can interact with the O of cellulose hydroxyl group when the cleavage of hydrate-Li^+ coordination at elevated temperature releases the free coordination sites of Li^+,[30,31] in particular, when part of the water in the system is consumed for the hydrolysis of cellulose and hemicelluloses. In summary, the cellulose–Br^- and cellulose–Li^+ associations or interactions disrupt the inter- and intra-molecular hydrogen bonds of cellulose, breaking the tight crystalline matrix of cellulose, and thereby leading to the swelling and dissolution of cellulose. The dissolution generates a homogeneous reaction medium and facilitates the hydrolysis of cellulose and hemicelluloses under mild reaction conditions. In addition, the Hammett acidity of Brønsted acid increases exaggeratedly in molten salt hydrate,[32] compared with that in water at the same acid concentration. As a result, the rate of acid-catalyzed breakage of glycosidic bonds in cellulose and hemicelluloses is kinetically prompted.

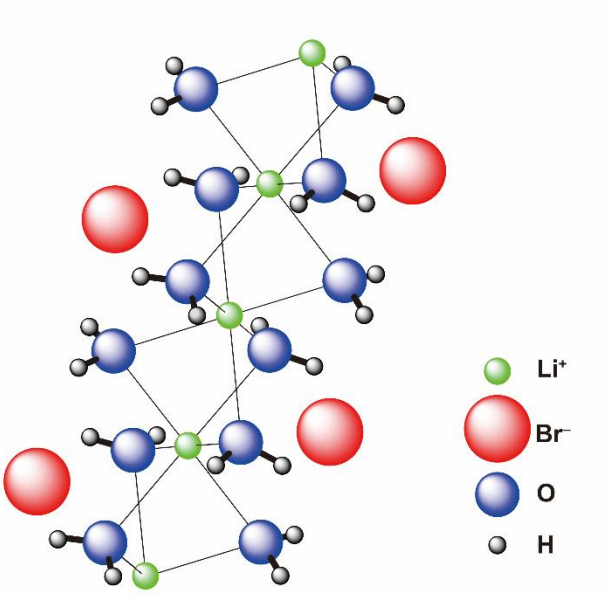

Figure 2.1 Illustration of lithium bromide trihydrate ($LiBr \cdot 3H_2O$) structure.

The overall procedure of the ALBTH method and the changes of cell wall components are illustrated in Scheme 2.1. Experimental detail is described in the section of Experimental and in

the recommended protocol in ESI. In brief, biomass sample was treated in acidic lithium bromide solution; cellulose and hemicelluloses of the biomass were dissolved and hydrolyzed into monosaccharides (such as glucose, xylose, mannose, galactose, and arabinose), and lignin was left over as insoluble residue and collected for gravimetric quantitation. Similar to Klason lignin quantitation, under the conditions of the temperature and acidity used, a small portion of the monosaccharides released from cellulose and hemicelluloses might be dehydrated to hydroxymethylfurfural (HMF, from hexoses) and furfural (from pentoses), respectively. Further, HMF and furfural could condense via a 2,5-dioxo-6-hydroxyhexnanal (DHH) route to humins.[18,19] The humins are the major source of pseudo lignin, which leads to positive bias in insoluble lignin (IL) quantitation.[20] A small portion of lignin was dissolved in ALBTH method, called soluble-lignin (SL), which can be quantitated using UV spectrophotometry, as discussed below in detail.

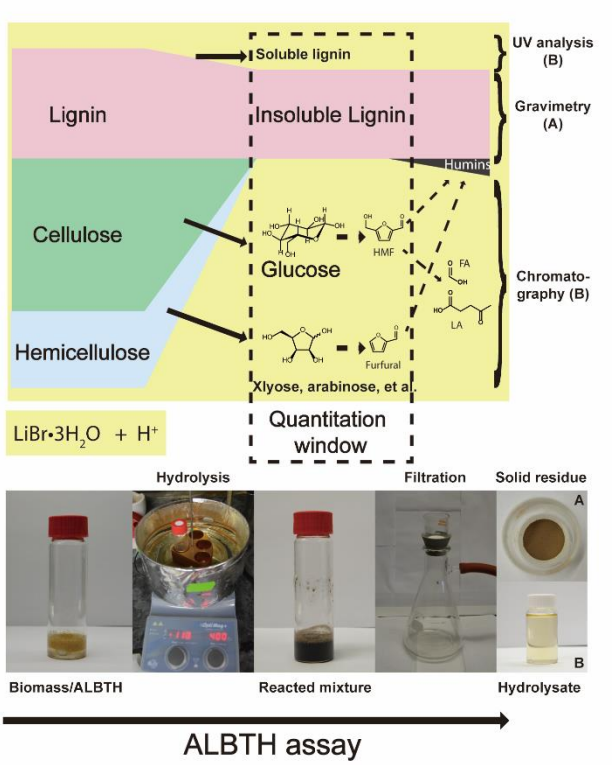

Scheme 2.1 Schematic presentation of ALBTH method for lignin quantitation.

2.3.2 Factors affecting lignin quantitation using the ALBTH method

Extractives

Depending on species, varying amount of extractives exist in lignocellulosic biomass, including water-extractives (such as protein, inorganic salts, and non-structural carbohydrates) and organic-extractives (such as waxes, chlorophyll, resin, and other minor components). Some of the extractives, in particular the organic-extractives, could be hardly digested (dissolved) in the ALBTH medium and would attach to lignin as insoluble residue, leading to overestimation (positive bias) of lignin and thus affecting the accuracy of lignin quantitation.

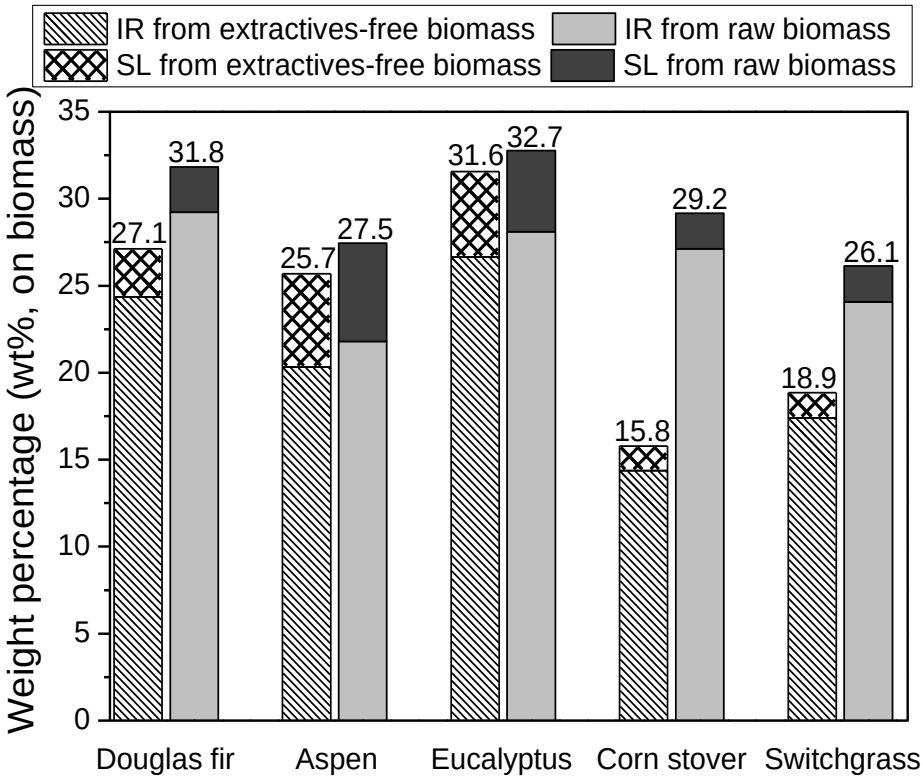

Figure 2.2 The effect of extractives on lignin quantitation with the ALBTH method.

To examine the effect of the extractives on lignin quantitation, the lignin content of different biomass with and without extractives, including softwood (Douglas fir), hardwood (aspen and eucalyptus), and herbage (corn stover and switchgrass), was quantitated using the ALBTH method,

respectively. As shown in Figure 2.2, the lignin contents determined from raw (extractives-containing) Douglas fir, aspen, eucalyptus, corn stover, and switchgrass were 4.7, 1.8, 1.1, 13.4, and 7.2% higher than those determined from extractives-free biomass, respectively. The results suggested that the extractives in raw biomass probably precipitated along with lignin directly or after condensation in the acidic lithium bromide, resulting in pseudo lignin. To verify this hypothesis, the extractives in corn stover and switchgrass, which had the largest lignin overestimation above, were isolated with hot water extraction and subjected to the ALBTH assay. The hot-water extractives represented 91 and 85% of total extractives in corn stover and switchgrass, respectively. As shown in Table S2.1, the extractives resulted in 12~15% (on dry extractives) insoluble pseudo lignin after the ALBTH treatment. Similar observation that the extractives affected lignin quantitation was reported in NREL method.[33] Therefore, the removal of the extractives is essential and a prerequisite for accurate lignin quantitation by the ALBTH method, which is also mandated in the TAPPI and NREL methods. Unless otherwise indicated, extractives-free biomass was used in the following experiments.

Reaction conditions (acid concentration, temperature, and time)

For accurate and precise quantitation of lignin, it is crucial to completely remove (dissolve and hydrolyze) cellulose and hemicelluloses with limited formation of furans and humins that could lead to the quantitation bias. In this section, the effects of the key reaction parameters (acid concentration, reaction temperature, and reaction duration) on the quantitation of lignin were investigated.

Cellulose can be dissolved in the molten salt hydrate ($LiBr{\cdot}3H_2O$) efficiently, as discussed above.[34] However, effective hydrolysis of the dissolved cellulose does need a Brønsted acid as catalyst.[24] Therefore, the effect of acid concentration on the hydrolysis of cellulose and

hemicelluloses in ALBTH assay and consequently on lignin quantitation was investigated using extractives-free aspen in 60 wt% LiBr at 110 °C with varied HCl concentrations. It is worth noting that 60 wt% LiBr solution, rather than 61.6 wt% for $LiBr \cdot 3H_2O$ was used in this study, because our previous biomass saccharification studies indicated that the performance of biomass hydrolysis in 60 wt% and 61.6 wt% was similar, and actually the former was slightly better than the latter,[35] because the slightly more water in 60 wt% LiBr solution promoted the hydrolysis of cellulose and hemicelluloses. As illustrated in Figure 2.3A and 2.3B, the lowest insoluble residue yield (20.3 wt%) was observed at 40 mM HCl, along with 5.6 wt% soluble-lignin. Lower acid concentration (10 mM HCl) resulted in higher total insoluble residue (22.6 %) because cellulose and hemicelluloses in the biomass were not completely hydrolyzed, which was verified by the presence of oligosaccharides in the insoluble residue and the low yield of glucose (11.1%) in the hydrolysate using 10 mM HCl. However, if excessive acid was added (e.g., 60 mM), a positive bias toward the insoluble residue (21.3 %) was observed, which was probably caused by the formation of humins because high acid concentration accelerates the dehydration of saccharides to HMF and furfural and the subsequent condensation to humins. These observations suggested that 40 mM HCl was an appropriate acid concentration for the ALBTH method.

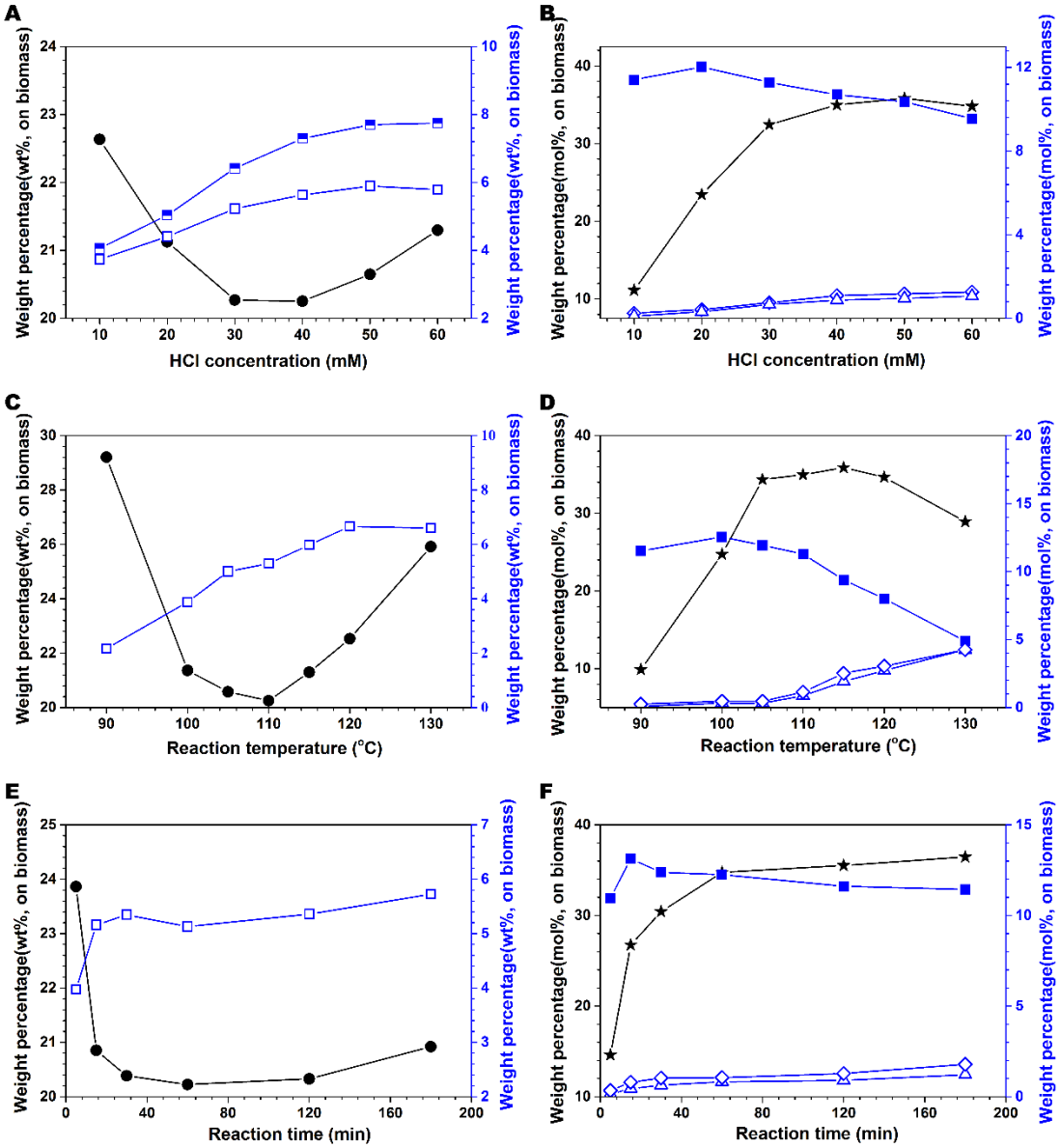

Figure 2.3 Effects of reaction conditions: HCl concentration (A and B), reaction temperature (C and D), and reaction time (E and F) on insoluble lignin (black solid circle) and soluble lignin (blue half-up square without furans correction and blue open square after correction) contents, as well as glucose (black solid star), xylose (blue solid square), HMF (blue open triangle), furfural yields (blue open diamond). Note: The results are based on the initial oven dry weight of aspen and the molar conversion factors of glucose, xylose, HMF, and furfural are 0.9, 0.88, 0.778, and 0.727, respectively.

Reaction temperature also plays an important role in the efficient and complete hydrolysis of cellulose and hemicelluloses and the isolation of lignin from biomass. Notably, microcrystalline

cellulose (Avicel) could hardly reach a complete hydrolysis at the temperature lower than 100 °C in 60% LiBr even with extended reaction time. The observation suggested that the efficient and complete hydrolysis of cellulose required high-enough temperature to activate the cleavage of glycosidic bond.[34] However, high reaction temperature tended to increase sugar decomposition. Therefore, it is important to tailor the reaction temperature so that it provides enough energy to surpass the energy barrier against cellulose hydrolysis but avoids over-heating to cause sugar dehydration to furans. As shown in Figure 2.3C and 2.3D, elevating reaction temperature from 90 to 110 °C significantly reduced the insoluble residue content from 29.2 to 20.3 wt%, indicating that more carbohydrates were removed at higher temperature. However, further elevating reaction temperature to 130 °C reversely increased the insoluble residue to 25.9 wt%, which presumably resulted from the formation of humins and apparently resulted in an overestimation of lignin in the biomass.

The temporal curves of aspen hydrolysis in acidic LiBr solution at 40 mM HCl at 110 °C are presented in Figure 2.3E and 2.3F. The yield of the insoluble residue dropped sharply to 20.8% in the first 15 min, and then decreased slowly to 20.4% at 30 min and 20.2% at 60 min, respectively. The observations indicated that the majority of carbohydrates were promptly removed from the biomass matrix within the first 15 min, and then the dissolution of the carbohydrates slowed down, probably because the residual carbohydrates are relatively more resistant against the dissolution and hydrolysis due to the linkages to lignin in lignin carbohydrate complex (LCC). Meanwhile, further extending the reaction led to a slight increase in the insoluble residue, especially after 120 min. For example, the insoluble residue increased to 21.3% at 180 min. This was probably ascribed to the gradually accumulated humins. Unlike other non-aqueous ionic liquids, the presence of water (40 wt%) in the ALBTH method probably inhibited the dehydration of monomeric

saccharides, thus significantly reducing the formation of furans and humins in the hydrolysis process.[36]

The results and discussion above suggest that the following condition: 40 mM HCl concentration in 60 wt% LiBr, 110 °C, and 30 min reaction time, is suitable for the ALBTH method to quantitate lignin in lignocellulosic biomass.

Effect of HMF and furfural from sugar dehydration on quantitation of soluble lignin

Similar to the Klason method, the ALBTH method yields a small portion of lignin as soluble lignin (SL), which can be quantitated using UV spectrophotometry. To avoid the overwhelming interference of LiBr absorption between 200-230 nm, the ALBTH method chose 240 nm (shoulder absorption) as the quantitation wavelength for the SL from woody biomass, which is identical to the NREL method. A small amount of furfural and HMF were generated in the ALBTH method, and they have absorption at 240 nm as well in addition to their maximum absorptions at 277 and 285 nm, respectively. This interference from furfural and HMF at 240 nm with lignin quantitation cannot be disparaged, because they have relatively large extinction coefficients. Therefore, SL absorbance at 240 nm needs to be corrected by deducting the contributions of HMF and furfural according to Eq 2.3.

$$Abs' = Abs_T - Abs_f \quad (2.3)$$

Where, Abs' is the corrected absorbance of SL at 240 nm; Abs_T is the total absorbance of the hydrolysate at 240 nm; and Abs_f is the absorbance of furans (furfural and HMF) at 240 nm.

The detailed methods to determine Abs_f by direct HPLC quantitative analysis or pseudo double-wavelength spectrophotometric method are described and discussed in detail in ESI.

Effect of humins on quantitation of insoluble lignin

The formation of humins from the dehydration products of carbohydrates is inevitable under acidic

condition. When quantitating insoluble lignin, the humins would attach to lignin, generating positive bias to the lignin content, as discussed above. Although the dehydration of carbohydrates to humins was suppressed in the ALBTH method because of the presence of water in the system, small amount of humins could still form, in particular under severe conditions. To evaluate the potential effect of humins on the lignin assay, microcrystalline cellulose (Avicel) was used as a model compound and experienced the ALBTH assay. As summarized in Table S2.2, under the conditions of 40 mM HCl and 110 °C, 0.35% and 1.35% humins were formed at 30 and 120 min, respectively. When HCl concentration was elevated to 150 mM, 4.14 and 6.78% humins were generated at 30 and 120 min, respectively, which were still much less than those formed during cellulose hydrolysis in non-aqueous ionic liquids.[36] These observations suggest that the formation of humins be negligible during the ALBTH assay under the recommended ALBTH conditions (40 mM HCl, 110 °C, 30 min) and barely have significant effect on lignin quantitation.

2.3.3 Characterization of the ALBTH lignin

To verify whether the insoluble residue of the ALBTH method could represent the lignin fraction of biomass, the insoluble residue was characterized via composition analysis, elemental analysis (SEM-EDS), and 2D NMR (HSQC). Firstly, the insoluble residue collected from the ALBTH procedure was subjected to the two-step sulfuric acid hydrolysis (NREL protocol) to test whether residual carbohydrates remained in the insoluble residues. As shown in Table S2.3, only trace amounts of carbohydrates were detected in the insoluble residues collected from the ALBTH assay of different species of biomass for 30-120 min. The results suggested that the ALBTH method was able to remove carbohydrates from biomass completely within 30 min. Secondly, the insoluble lignin residue from aspen was examined with SEM-EDS. The SEM image (Figure S2.3) of the ALBTH residue indicated that the particle size of the residue was less than 10 μm, and the fiber

structure of the original biomass disappeared, suggesting the complete destruction of cell wall because of the removal and hydrolysis of the carbohydrates. In addition, no bromine related peak was not observed in the energy dispersive spectroscopy (EDS) analysis, indicating that no bromination of lignin occurred during the ALBTH assay. Furthermore, the O/C molar ratio of the residue was 0.58, which was similar to that of milled wood lignin (MWL) and cellulolytic enzyme lignin (CEL) from hardwoods.[37] The evidences above suggest that the insoluble residue from the ALBTH assay represent lignin moiety.

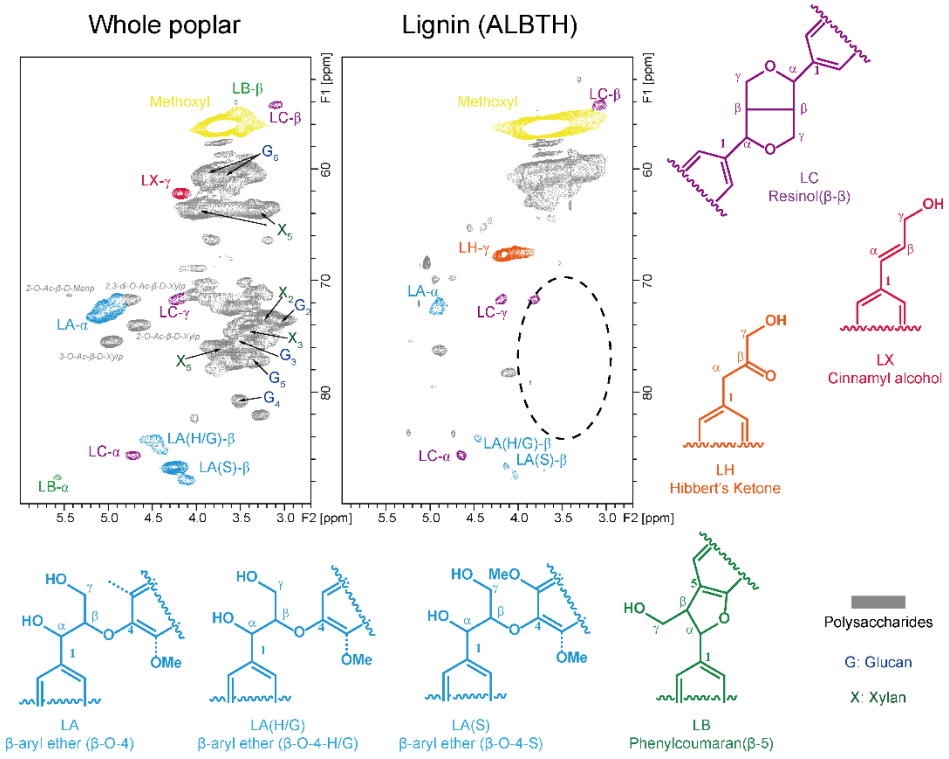

Figure 2.4 The aliphatic regions of 2D ^{1}H-^{13}C correlation (HSQC) spectra from ball-milled poplar cell wall dispersed in DMSO-d_6/pyridine-d_5 (left) and poplar lignin isolated by ALBTH method dissolved in DMSO-d_6 (right). Correlation signals are categorized and color-coded by the type of aromatic units (S: syringyl, G: guaiacyl, H: *p*-hydroxyphenyl, LA: β-aryl ether, LB: phenylcoumaran, LC: resinol, LX: cinnamyl alcohol, LH: Hibbert's ketone)

The purity and structure of the insoluble residue from ALBTH assay were further examined

using NMR. It is well known that the Klason lignin is highly condensed and insoluble in any organic solvent. Whereas, the ALBTH lignin from hardwood was found to be extremely soluble in many organic solvents such as tetrahydrofuran (THF), acetic acid/water (95:5, v/v), dioxane/water (9:1, v/v), and dimethyl sulfoxide (DMSO). Therefore, the ALBTH lignin was directly dissolved in DMSO-d_6 for NMR characterization without any derivation. ^{1}H-^{13}C HSQC NMR spectrum of the ALBTH lignin from poplar is presented in Figure 2.4 and compared with that of poplar whole cell wall sample. The peak assignments were made according to the spectra of lignin, carbohydrates, and whole-cell-wall plants reported in previous publications.[28,38,39] As illustrated in Figure 2.4, the ALBTH residue was a strikingly clean fraction of lignin with negligible carbohydrates contours. Polysaccharide peaks were barely detected except for the C_3/H_3 correlation of 3-*O*-Ac-β-D-Xylp at δ_C/δ_H 76.2/4.88 ppm, which was in agreement with the result of residue carbohydrates analysis above in Table S2.3. The inter-aryl ether linkages, such as β–*O*–4 aryl ether (A) and α–*O*–5 aryl ether (B), was ruptured, as identified by the significant reduction of the aliphatic contours at δ_C/δ_H72.0/4.88 (LA-α), 84.1/4.44 (LA(H/G)-β), 86.6/4.12 and 87.4/4.04 (LA(S)-β) ppm and the disappearance of the contours at 97.9/5.35 (LB-α) and 54.0/3.55 (LB-β). The formation of new correlation contour at 67.7/4.17 was assigned to Hibbert's ketone structure, which was produced from the acid catalyzed breakage of β–*O*–4 aryl ether.[40] The aliphatic ethers in β–β structure were relative stable since the corresponding contours at 85.7/4.64 (LC-α), 71.6/3.81, and 71.6/4.17 (LC-γ) ppm were rarely modified. The above observations suggested that the ALBTH residue was almost pure lignin with negligible carbohydrates, and ether linkages in the lignin were selectively cleaved. Lignin was depolymerized in the ALBTH protocol but still retained its polymeric structure in the form of insoluble solid residue, which allowed the ALBTH lignin to be quantitated gravimetrically.

2.3.4 Comparison between the ALBTH and the NREL methods

To verify the reliability of the ALBTH assay for lignin quantitation, the method was applied to different types of lignocellulosic species, including softwood (Douglas fir), hardwood (poplar, aspen, and eucalyptus), and herbage (corn stover and switchgrass), and compared with the NREL method. As summarized in Table 2.1, the lignin contents determined by the above two methods are well comparable. It seems that the ALBTH method gave slightly lower insoluble lignin content for most biomass, in particular for woody biomass, than the NREL method. This was probably attributed to more complete removal of carbohydrates, partial depolymerization of lignin (leading to soluble lignin), and negligible formation of humins in the ALBTH method. Corn stover, showed disparity as the ALBTH method gave slightly higher insoluble lignin content than the NREL method. We repeated the lignin quantitation of corn stover for multiple times, and similar results were obtained. The first rationalization was that this might result from the high ash content of corn stover, as the presence of ash might consume (neutralize) the acid catalyst and thereby lead to incomplete removal of carbohydrates. However, it was not supported by the experimental results. When the IL fraction of the ALBTH method from corn stover was analyzed, the residual carbohydrates in the IL were negligible. Moreover, when more acid (HCl) was added, the IL content of the corn stover was not reduced but slightly increased due to the formation of humins. Another explanation could be the presence of phenolic acids (*p*-coumaric and ferulic acids) in corn stover, which are linked with cell wall carbohydrates via ester bonds. Ralph reported the presence of *p*-coumaric and ferulic acids in Klason lignin residues from grasses.[41] Because the acid concentration in ALBTH method was much lower than that in Klason method, it was reasonable to expect that more phenolic acids retained in ALBTH lignin than in Klason lignin. This was verified by the HSQC spectrum of the ALBTH IL from corn stover, in which the *p*CA contours predominated in the aromatic region (Figure S2.4).

Table 2.1 Comparison of the NREL-LAP and the ALBTH methods for lignin quantitation of various species of biomass

Biomass	Method	IL ± SD (%)	SL ± SD (%)	TL ± SD (%)
Douglas fir	NREL-LAP	25.9 ± 0.0	2.0 ± 0.2	28.0 ± 0.2
	ALBTH-30 min	24.0 ± 0.2	2.9 ± 0.2	26.9 ± 0.1
	ALBTH-120 min	24.4 ± 0.3	2.7 ± 0.2	27.1 ± 0.3
Poplar	NREL-LAP	22.2 ± 0.4	5.6 ± 0.0	27.8 ± 0.3
	ALBTH-30 min	20.7 ± 0.2	6.0 ± 0.1	26.7 ± 0.1
	ALBTH-120 min	21.0 ± 0.2	5.9 ± 0.1	26.9 ± 0.2
Aspen	NREL-LAP	22.0 ± 0.0	5.3 ± 0.1	27.3 ± 0.0
	ALBTH-30 min	20.5 ± 0.2	5.5 ± 0.3	26.1 ± 0.3
	ALBTH-120 min	20.4 ± 0.1	5.4 ± 0.0	25.8 ± 0.1
Eucalyptus	NREL-LAP	28.4 ± 0.4	5.2 ± 0.4	33.7 ± 0.0
	ALBTH-30 min	26.1 ± 0.0	5.6 ± 0.1	31.7 ± 0.1
	ALBTH-120 min	26.8 ± 0.0	5.1 ± 0.1	32.0 ± 0.1
Corn stover	NREL-LAP	12.8 ± 0.1	1.1 ± 0.0	13.9 ± 0.1
	ALBTH-30 min	13.8 ± 0.1	1.4 ± 0.0	15.2 ± 0.2
	ALBTH-120 min	14.2 ± 0.3	1.5 ± 0.1	15.7 ± 0.3
Switchgrass	NREL-LAP	17.5 ± 0.2	0.9 ± 0.0	18.4 ± 0.2
	ALBTH-30 min	17.1 ± 0.1	1.5 ± 0.0	18.6 ± 0.1
	ALBTH-120 min	17.6 ± 0.3	1.5 ± 0.0	19.1 ± 0.3

Note: IL – insoluble lignin; SL – soluble lignin; TL – total lignin (= IL + SL); SD – standard deviation.

The dissolution and hydrolysis of the carbohydrates from biomass are always accompanied by yielding a small amount of dissolved lignin, called soluble lignin. It was reported that the quantity of the soluble lignin in Klason method reached the maximum in the first-step treatment with 72% H_2SO_4 and decreased slightly during the second-step hydrolysis in dilute H_2SO_4 (3 or 4%) because part of the soluble lignin became insoluble through intermolecular condensation at elevated temperature in an acidic meidum.[42] The results in Table 2.1 indicated that for most of the biomass investigated, the soluble lignin contents determined with the ALBTH methods were slightly higher than those determined by NREL method, suggesting that the self-condensation of soluble lignin

was insignificant in the ALBTH assay.

It is desirable if the ALBTH method is able to quantitate not only lignin but also the carbohydrates, analogous to the Klason method. However, the preliminary investigation found that the quantities of the monomeric saccharides detected by high performance ion chromatography in the ALBTH hydrolysate were lower than those in the NREL hydrolysate, which was presumably caused by the incomplete hydrolysis of carbohydrates to monomeric sugars. It was evidenced by the detection of oligosaccharides in the ALBTH hydrolysate. When the hydrolysate was diluted and underwent post hydrolysis in an autoclave, extra monomeric saccharides were released. Further study is under way to modify the ALBTH method for fast, simultaneous, and precise quantitation of both lignin and the carbohydrates in lignocellulosic biomass.

2.3.5 Prospective of the ALBTH method

In summary, the ALBTH method for the quantitation of lignin in lignocellulosic biomass has the following advantages. The reaction medium (acidic lithium bromide trihydrate) is easy to access and ready to prepare, and hazardous concentrated sulfuric acid is eliminated. The reaction medium has high boiling point (approximately 154 °C) and low vapor pressure, which allows that the reaction at 110 °C can be conducted in a glass vial at atmospheric pressure, and no autoclave is required for the hydrolysis. In addition, 60% LiBr solution has much lower viscosity than 72% H_2SO_4, facilitating the sample mixing for homogeneous reaction. The ALBTH assay is a one-step procedure and eliminates numerous liquid transfer operations required in the Klason method. The hydrolysis can be finished within as short as 30 min in the ALBTH method, which is much shorter than that in the TAPPI and NREL methods (3-6 h), as compared in Figure S2.5. This is particularly attractive when a large number of samples are analyzed in screening experiments. A recommended step-by-step ALBTH protocol is provided in the Appendix.

2.4 Conclusions

In this study, a facile and quick method was developed to quantitate lignin in lignocellulosic biomass. This method used acidic lithium bromide trihydrate (ALBTH, $LiBr \cdot 3H_2O$) as a reaction medium, which was able to quickly and completely dissolve and hydrolyze cellulose and hemicelluloses in the biomass and leave lignin as in insoluble residue for gravimetric quantitation. As the same as in Klason method, a small portion of the lignin was dissolved during the ALBTH assay. The soluble lignin was determined by UW spectrophotometry. The recommended conditions for the ALBTH method are 60 w% LiBr solution with 40 mM HCl, 110 °C, and 30 min. The conditions ensured the complete hydrolysis of carbohydrates from the biomass and minimized the formation of humins to reduce the interference with lignin quantitation. The ALBTH method was applied to different species of biomass including softwood (Douglas fir), hardwood (aspen, poplar, and eucalyptus), and herbage (corn stover and switchgrass). The results indicated that the ALBTH method gave a comparable lignin quantitation with the Klason (NREL) method for the biomass investigated. In addition, the ALBTH method is a one-step procedure and much faster for lignin quantitation (30 min), compared to the NREL and TAPPI methods (3-6 h). Furthermore, the ALBTH assay can be conducted in a glass vial at atmospheric pressure because of the high boiling point and low vapor pressure of the LiBr solution, and no autoclave is required. Finally, the ALBTH method avoids the potential hazard of concentrated sulfuric acid. The present study mainly focused on the quantitation of lignin, but the ALBTH method was potentially viable in carbohydrate quantitation after further methodology development.

Appendix

Table S2.1 Formation of pseudo lignin fraction from extractives of herbaceous biomass by ALBTH method

Extractives[a]	IL[b] (%)	SL[c] (%)	Arabinose (%)	Galactose (%)	Glucose (%)	Xylose (%)	Mannose (%)
Corn stover	11.7	6.2	0.6	n.d.	0.9	0.3	n.d.
Switchgrass	14.9	4.5	0.6	0.5	5.9	0.4	n.d.

Note: a. Extractives were isolated from hot-water extraction from corn stover and switchgrass;

b and c denoted the pseudo insoluble lignin and soluble lignin from the extractives, respectively;

n.d. denoted not detected.

Calculation was based on the dry weight of the isolated extractives.

Table S2.2 Formation of humins from cellulose in ALBTH assay at 110 °C

	40 mM HCl		150 mM HCl	
	30 min	120 min	30 min	60 min
Humins yield (wt%)	0.35	1.35	4.14	6.78

Table S2.3 Residual carbohydrates in insoluble lignin of various biomass by ALBTH method

Method	ALBTH-lignin residue				
	Arabinan (%)	Galactan (%)	Glucan (%)	Xylan (%)	Mannan (%)
Poplar-30 min	n.d.	n.d.	0.05	0.11	n.d.
Poplar-60 min	n.d.	n.d.	0.04	0.08	n.d.
Poplar-120 min	n.d.	n.d.	0.04	0.06	n.d.
Switchgrass-30 min	0.34	n.d.	0.04	0.06	n.d.
Switchgrass-60 min	0.29	n.d.	0.04	0.04	n.d.
Switchgrass-120 min	0.27	n.d.	0.04	0.03	n.d.
Corn stover-30 min	0.18	n.d.	0.26	0.06	n.d.
Corn stover-60 min	0.14	n.d.	0.08	0.04	n.d.
Corn stover-120 min	0.13	n.d.	0.04	0.02	n.d.
Aspen-30min	n.d.	0.01	0.04	0.07	n.d.
Douglas fir-30 min	0.01	0.02	0.04	0.02	0.02
Eucalyptus-30 min	n.d.	0.02	0.05	0.08	n.d.

Note: * percentage of residual carbohydrates, based on initial biomass feedstocks

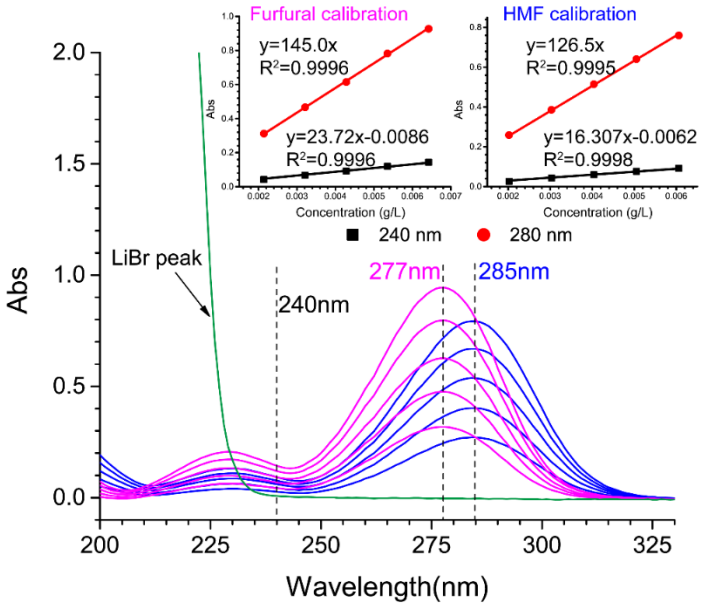

Figure S2.1 UV spectra of HMF (blue, 2.02 to 6.06 mg/L) and furfural (magenta, 2.14 to 6.42 mg/L) and acidic lithium bromide solution (green, 220 mg/L LiBr).

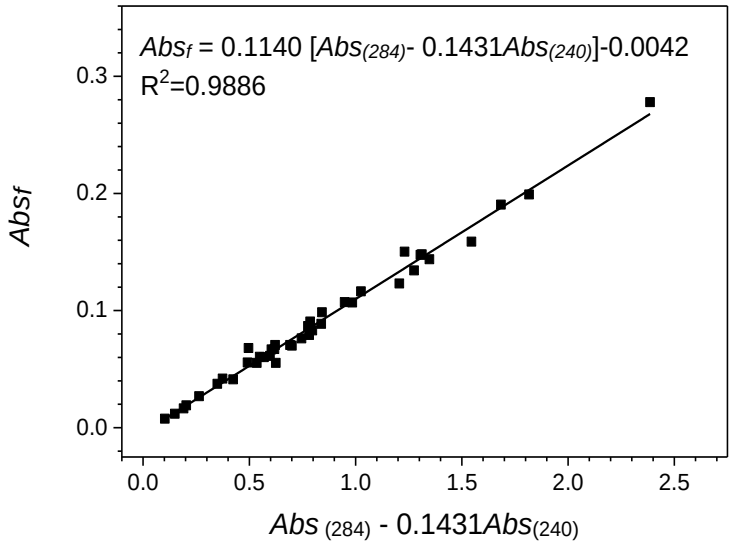

Figure S2.2 Linear correlation of absorption deduction ($Abs_{(284)} - 0.1431Abs_{(240)}$) with furan absorption correction (Abs_f) based on the multiple linear regression results.

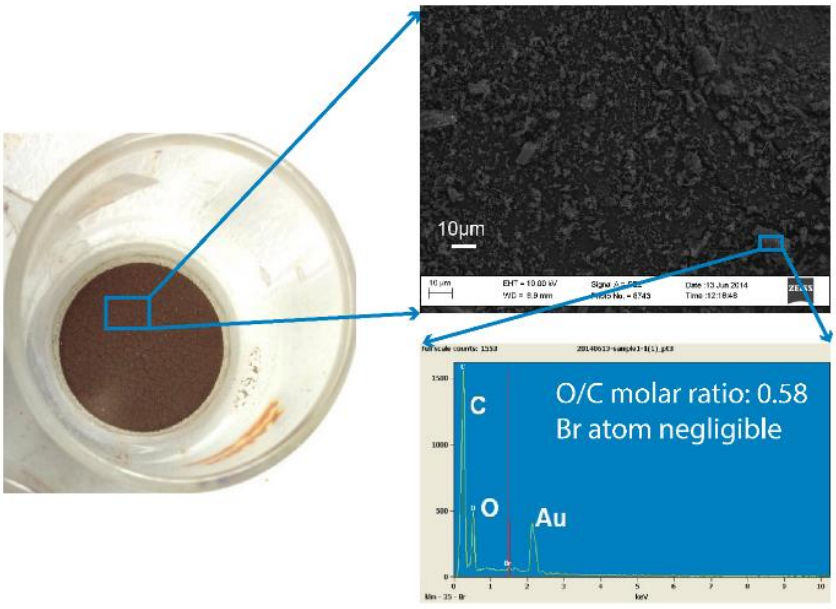

Figure S2.3 SEM-EDS analysis of ALBTH lignin residue from extractives-free aspen.

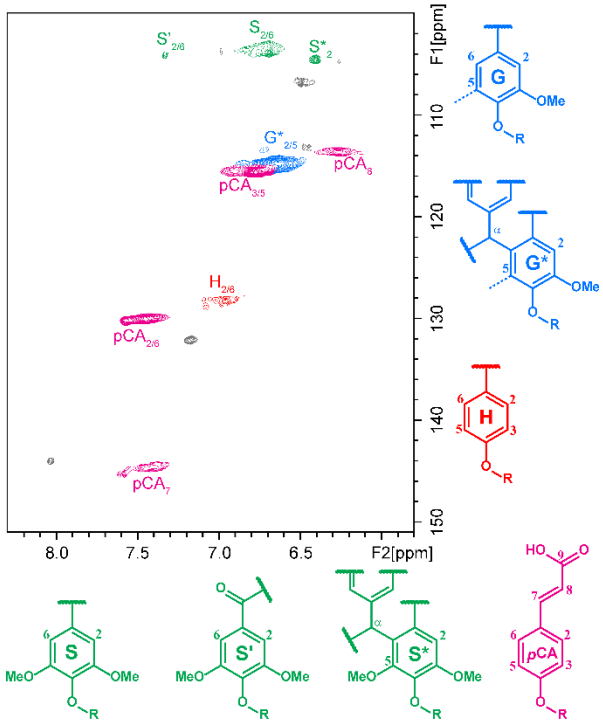

Figure S2.4 The aromatic region of 2D ^{1}H-^{13}C correlation (HSQC) spectrum from corn stover lignin residue by ALBTH method dissolved in DMSO-d_6. Correlation signals were categorized and color coded by the type of aromatic units (S: syringyl, G: guaiacyl, H: *p*-hydroxyphenyl, *p*CA: *p*-coumarate).

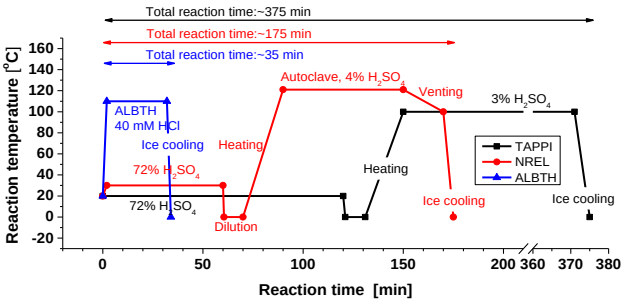

Figure S2.5 Comparison of ALBTH, NREL and TAPPI reaction duration for lignin quantitation.

The determination of Abs_f in equation (3) by direct HPLC quantitative analysis and pseudo double-wavelength spectrophotometric method

To diminish the interference of HMF and furfural from sugar dehydration on soluble lignin quantitation, we started with directly subtracting the absorbance of furfural and HMF. Specifically, first, standard calibration curves of absorbance vs. concentration were created for furfural and HMF using a UV spectrophotometer. As shown in Figure S2.1, the absorbance of both furfural and HMF followed the Beer-Lambert law at 240 nm (Eq. S2.1) for furfural and (Eq. S2.2) for HMF, respectively), where Abs_{240} is the absorbance of the furans at 240 nm, and c (g/L) is the concentration of the furan standards. Second, the concentrations of furfural and HMF in the hydrolysate from the ALBTH method after n times dilution (n, dilution factor for SL quantitation of the hydrolysate) were determined by HPLC analysis as $c_{furfural}$ and c_{HMF} (g/L), respectively. Then, the contributions of furfural and HMF to the absorbance of the hydrolysate at 240 nm (Abs_f) could be calculated from Eq. S2.3.

$$Abs_{240} = 23.72c - 0.0086 \quad \text{(S2.1)}$$

$$Abs_{240} = 16.31c - 0.0062 \quad \text{(S2.2)}$$

$$Abs_f = 23.72c_{furfural} + 16.31c_{HMF} - 0.0148 \quad \text{(S2.3)}$$

Another alternative is to use the pseudo double-wavelength spectrophotometric method, in which the portion of absorption from furfural and HMF at 240 nm (Abs_f) was estimated from the absorbance of the hydrolysate at two wavelengths, 284 nm (the isosbestic wavelength of furfural and HMF in water) and 240 nm (the characteristic wavelength of SL), according to an empirical equation regressed from the experimental data, and therefore no HPLC analysis was required to quantitate furfural and HMF. In detail, the Abs_f calculated from HPLC analysis and corresponding absorbance at 240 and 284 nm ($Abs_{(240)}$ and $Abs_{(284)}$) of the hydrolysates from 40 sets of experimental data from different biomass under different conditions were regressed using a multiple linear regression model in Origin Lab 9.1. As shown in Figure S2.2, a linear correlation between Abs_f and $[Abs_{(284)} - 0.1431Abs_{(240)}]$ was found with $R^2 = 0.9886$. Therefore, instead of using HPLC to quantitate furan compounds and then determining the absorbance correction (Abs_f) at 240 nm from furfural and HMF with Eq. S2.3 above, Abs_f can be directly estimated using empirical Eq. S2.4 after reading the absorbance ($Abs_{(240)}$ and $Abs_{(284)}$) of the hydrolysate at 240 nm

and 284 nm, respectively. In summary, Because of the elimination of the HPLC analysis of furfural and HMF, the pseudo double-wavelength method is recommended for the ALBTH method to quantitate SL of woody biomass. As mentioned above, no correction is needed for herbaceous biomass because of the negligible interference of HMF and furfural absorptions at 320 nm.

$$Abs_f = 0.1140\left[Abs_{(284)} - 0.1431Abs_{(240)}\right] - 0.0042 \quad \text{(S2.4)}$$

Recommended ALBTH Protocol for Lignin Quantitation in Lignocellulosic Biomass

1. Scope

This procedure is for the fast quantitation of lignin content of lignocellulosic biomass.

2. Apparatus

2.1 Wiley mill
2.2 Soxhlet extraction setup
2.3 Analytical balance with 0.1 mg readability
2.4 Drying oven for moisture determination at temperature of 105 ± 2 °C
2.5 Muffle furnace for ash determination at temperature of 575 ± 25 °C
2.6 Oil bath heated by hot plate with magnetic stirrer and temperature controller
2.7 Desiccator with fresh desiccant
2.8 Magnetic stirrer
2.9 Vacuum filtration set with a vacuum pump/water aspirator and filtration flask
2.10 Glass filtrating crucibles (30 mL, low form with medium pore size)
2.11 UV-Visible spectrophotometer with quartz cuvettes (1cm path-length)

3. Procedure

3.1 Sample preparation
3.1.1 Biomass grounding: Grind chipped or chopped air-dry biomass using a Wiley mill to pass a 2-mm screen. Sieve the ground biomass and collect the fraction between 20 and 100 mesh

for analysis.

3.1.2 Removal and determination of extractives: Extract woody biomass with 95% ethanol for 16 h or herbaceous biomass with hot-water for 8 h followed by 95% ethanol for 16 h using Soxhlet extractor according to NREL/TP-510-42619 “Determination of Extractives in Biomass”.

3.1.3 Determine moisture content of the extractives-free biomass

3.2 ALBTH hydrolysis of the biomass sample

3.2.1 Dry filtering crucibles in a drying oven at 105 ± 2 °C for at least 6 hours (or until constant weight). Transfer the crucibles from the oven to a desiccator and cool down for 30 ± 5 min. Weigh the crucibles and record the values to the nearest 0.1 mg.

3.2.2 Weigh 300.0 ± 5.0 mg of sample into a 40 mL glass vial with screw top.

3.2.3 Add 4.50 ± 0.10 mL of 60 % LiBr solution with 40 mM HCl to the vial. Mix the solution and the biomass with magnetic stirring at room temperature for two minutes. Ensure the solid sample evenly soaked in the solution. Seal the vial with an open top cap with Teflon lined septa.

Note: To prepare 100 mL 60% LiBr solution (1.71 g/mL, 20 °C) with 40 mM HCl, weigh 102.6 g of anhydrous LiBr, dissolve in 68.1 g of water. Cool down the solution to room temperature and add 0.394 g of 37% HCl. Vortex the solution and store it in a bottle with a cap.

3.2.4 Put the vial in an oil bath at 110 ± 2 °C, turn on the magnetic stirring at 400 ± 50 rpm, and hydrolyze the sample for 30 ± 3 min.

3.2.5 Upon the end of the hydrolysis, take the vial from the oil bath to an ice water bath. Transfer the hydrolyzed sample to a 50-mL volumetric flask, rinse the vial with water and transfer all solids completely into the flask, and fill the flask with deionized water to the mark.

3.3 Gravimetrical quantitation of insoluble lignin

3.3.1 Filter the hydrolysate in the volumetric flask under vacuum through a pre-weighed filtering crucible. Collect 20 mL the filtrate (before washing and dilution) and store in a sample storage bottle for the determination of soluble lignin and furan compounds.

3.3.2 Transfer all the remaining solids out of the volumetric flask into the filtering crucible by deionized water. Wash thoroughly the insoluble residue on the crucible with deionized water to remove residual LiBr and HCl.

3.3.3 Place the crucible together with the insoluble residue in a drying oven at 105 ± 2 °C for a minimum of 12 h or until a constant weight is achieved.

3.3.4 Move the crucible into a desiccator to cool down for 30 ± 5 min and record the weight of the crucible with the insoluble residue to the nearest 0.1 mg.

3.3.5 Place the crucible together with insoluble residue in Muffle furnace at 575 ± 25 °C for a minimum of 12 h or until a constant weight is achieved.

3.3.6 Cool down the crucible with remaining ash in a desiccator for 30 ± 5 min and record the weight of the crucible with ash to the nearest 0.1 mg.

3.4 Spectrophotometric evaluation of soluble lignin

3.4.1 Acquire a background spectrum of deionized water on a UV-Visible spectrophotometer.

3.4.2 Scan the hydrolysate aliquot collected in step 3.3.1 from 200 nm to 350 nm wavelength on the UV-Visible spectrophotometer. Dilute the samples with deionized water, if necessary, so that the absorbance at the interested wavelength (240 nm for woody biomass and 320 nm for herbage) falls into the range of 0.2-0.8. Read and record the absorbance at 240 nm and 284 nm for woody biomass and the absorbance at 320 nm for herbaceous biomass.

4. Calculation for lignin quantitation

4.1 Calculate the insoluble lignin (*IL*, wt%) of the biomass sample

$$IL\ (\%) = \frac{(m_{c+r} - m_c) - (m_{c+a} - m_c)}{m_{ods}} \times \frac{(100 - \sigma)}{100} \times 100$$

$$m_{ods} = m_s \times \frac{x}{100}$$

Where:

m_{ods}, (g), oven dry weight of extractives-free biomass sample;

x, (wt%), weight percentage dryness of the extractives-free biomass sample, x = 100 – moisture (%);

m_s, (g), air dry weight of extractives-free biomass sample;

m_c, (g), oven dry weight of the net filtering crucible after reaching constant weight;

m_{c+r}, (g), oven dry weight of the filtering crucible plus ALBTH insoluble residue;

m_{c+a}, (g), dry weight of the filtering crucible plus ALBTH ash after furnace ignition;

σ, (wt%), weight percentage of the extractives in the oven dry biomass sample.

4.2 Calculate the soluble lignin (*SL*, wt%) of the biomass sample

$$SL(\%) = \frac{Abs' \times V_f \times \delta}{\varepsilon \times m_{ods} \times 1} \times \frac{(100 - \sigma)}{100} \times 100$$

$$Abs' = Abs_T - Abs_f$$

$$Abs_f = 0.1140\left[Abs_{(284)} - 0.1431 Abs_{(240)}\right] - 0.0042$$

Where:

V_f (L), total volume of the filtrate (50 mL);

δ, dilution factor;

ε, absorptivity of biomass lignin at the appropriate wavelength, 25 $g^{-1} \cdot L \cdot cm^{-1}$ for woody biomass at 240 nm and 30 $g^{-1} \cdot L \cdot cm^{-1}$ for herbaceous biomass at 320 nm, respectively, adopted from the NREL method;

Abs', corrected UV absorbance of the diluted filtrate after subtracting UV absorbance of hydroxymethylfurfural (HMF) and furfural at 240 nm for woody biomass (No correction is necessary for herbaceous biomass hydrolysate because of the negligible absorbance of HMF and furfural absorptions at 320 nm. For herbaceous biomass, $Abs' = Abs_T$= absorbance at 320 nm);

Abs_T, total UV absorbance of the diluted hydrolysate at appropriate wavelength (240 nm for woody biomass and 320 nm for herbaceous biomass);

Abs_f, UV absorbance of the furan fractions (HMF and furfural) in the diluted hydrolysate at 240 nm wavelength for woody biomass, Abs_f approximately equals zero for herbaceous biomass at 320 nm;

$Abs_{(284)}$, total UV absorbance of the diluted hydrolysate at 284 nm wavelength;

$Abs_{(240)}$, total UV absorbance of the diluted hydrolysate at 240 nm wavelength;

σ, (wt%), weight percentage of the extractives in the oven dry biomass sample.

Reference

(1) Dimmel, D.; Gellerstedt, G. *Chemistry of Alkaline Pulping*; CRC Press: Boca Raton, 2009.

(2) Ragauskas, A. J.; Williams, C. K.; Davison, B. H.; Britovsek, G.; Cairney, J.; Eckert, C. A.; Frederick, W. J.; Hallett, J. P.; Leak, D. J.; Liotta, C. L. The path forward for biofuels and biomaterials. *science* **2006**, *311*, 484-489.

(3) Shuai, L.; Yang, Q.; Zhu, J.; Lu, F.; Weimer, P.; Ralph, J.; Pan, X. Comparative study of SPORL and dilute-acid pretreatments of spruce for cellulosic ethanol production. *Bioresource Technology* **2010**, *101*, 3106-3114.

(4) Grabber, J. H. How do lignin composition, structure, and cross-linking affect degradability? A review of cell wall model studies. *Crop Science* **2005**, *45*, 820-831.

(5) Chandra, R. P.; Bura, R.; Mabee, W.; Berlin, d. A.; Pan, X.; Saddler, J. Substrate pretreatment: The key to effective enzymatic hydrolysis of lignocellulosics? In *Biofuels*; Springer: 2007, p 67-93.

(6) Alvira, P.; Tomás-Pejó, E.; Ballesteros, M.; Negro, M. Pretreatment technologies for an efficient bioethanol production process based on enzymatic hydrolysis: a review. *Bioresource Technology* **2010**, *101*, 4851-4861.

(7) Sixta, H. *Handbook of pulp*; Wiley-vch: Weinheim, 2006.

(8) Upton, B. M.; Kasko, A. M. Strategies for the conversion of lignin to high-value polymeric materials: Review and perspective. *Chemical Reviews* **2015**, *116*, 2275-2306.

(9) Ragauskas, A. J.; Beckham, G. T.; Biddy, M. J.; Chandra, R.; Chen, F.; Davis, M. F.; Davison, B. H.; Dixon, R. A.; Gilna, P.; Keller, M. Lignin valorization: improving lignin processing in the biorefinery. *Science* **2014**, *344*, 1246843.

(10) Stewart, D. Lignin as a base material for materials applications: Chemistry, application and economics. *Industrial Crops and Products* **2008**, *27*, 202-207.

(11) Behling, R.; Valange, S.; Chatel, G. Heterogeneous catalytic oxidation for lignin valorization into valuable chemicals: What results? What limitations? What trends? *Green Chemistry* **2016**, *18*, 1839-1854.

(12) Hatfield, R.; Fukushima, R. S. Can lignin be accurately measured? *Crop science* **2005**, *45*, 832-839.

(13) Sluiter, J. B.; Ruiz, R. O.; Scarlata, C. J.; Sluiter, A. D.; Templeton, D. W. Compositional analysis of lignocellulosic feedstocks. 1. Review and description of methods. *Journal of Agricultural and Food Chemistry* **2010**, *58*, 9043-9053.

(14) Templeton, D. W.; Scarlata, C. J.; Sluiter, J. B.; Wolfrum, E. J. Compositional analysis of lignocellulosic feedstocks. 2. Method uncertainties. *Journal of Agricultural and Food Chemistry* **2010**, *58*, 9054-9062.

(15) Johnson, D. B.; Moore, W.; Zank, L. The spectrophotometric determination of lignin in small wood samples. *Tappi* **1961**, *44*, 793-798.

(16) Iiyama, K.; Wallis, A. An improved acetyl bromide procedure for determining lignin in woods and wood pulps. *Wood science and technology* **1988**, *22*, 271-280.

(17) Morrison, I. Improvements in the acetyl bromide technique to determine lignin and digestibility and its application to legumes. *Journal of the Science of Food and Agriculture* **1972**, *23*, 1463-1469.

(18) Zhang, X.; Hewetson, B. B.; Mosier, N. S. Kinetics of maleic acid and aluminum chloride catalyzed dehydration and degradation of glucose. *Energy & Fuels* **2015**, *29*, 2387-2393.

(19) van Zandvoort, I.; Wang, Y.; Rasrendra, C. B.; van Eck, E. R.; Bruijnincx, P. C.; Heeres, H. J.; Weckhuysen, B. M. Formation, molecular structure, and morphology of humins in biomass conversion: influence of feedstock and processing conditions. *ChemSusChem* **2013**, *6*, 1745-1758.

(20) Sannigrahi, P.; Kim, D. H.; Jung, S.; Ragauskas, A. Pseudo-lignin and pretreatment chemistry. *Energy & Environmental Science* **2011**, *4*, 1306-1310.

(21) Sen, S.; Martin, J. D.; Argyropoulos, D. S. Review of cellulose non-derivatizing solvent interactions with emphasis on activity in inorganic molten salt hydrates. *ACS Sustainable Chemistry & Engineering* **2013**, *1*, 858-870.

(22) Wilcox, R. J.; Losey, B. P.; Folmer, J. C.; Martin, J. D.; Zeller, M.; Sommer, R. Crystalline and Liquid Structure of Zinc Chloride Trihydrate: A Unique Ionic Liquid. *Inorganic Chemistry* **2015**, *54*, 1109-1119.

(23) Yang, Y.-J.; Shin, J.-M.; Kang, T. H.; Kimura, S.; Wada, M.; Kim, U.-J. Cellulose dissolution in aqueous lithium bromide solutions. *Cellulose* **2014**, *21*, 1175-1181.

(24) Cao, N.; Xu, Q.; Chen, L. Acid hydrolysis of cellulose in zinc chloride solution. *Applied Biochemistry and Biotechnology* **1995**, *51*, 21-28.

(25) Fischer, S.; Voigt, W.; Fischer, K. The behaviour of cellulose in hydrated melts of the composition LiX nH2O (X= I^-, NO_3^-, CH_3COO^-, $ClO4^-$). *Cellulose* **1999**, *6*, 213-219.

(26) Pan, X.; Shuai, L. Saccharification of lignocellulosic biomass. Wisconsin Research Foundation: 2015.

(27) Sluiter, A.; Hames, B.; Ruiz, R.; Scarlata, C.; Sluiter, J.; Templeton, D.; Crocker, D. Determination of structural carbohydrates and lignin in biomass. National Renewable Energy Laboratory (NREL) Laboratory Analytical Procedures (LAP) for standard biomass analysis. 2007.

(28) Mansfield, S. D.; Kim, H.; Lu, F.; Ralph, J. Whole plant cell wall characterization using solution-state 2D NMR. *Nature protocols* **2012**, *7*, 1579-1589.

(29) Leipner, H.; Fischer, S.; Brendler, E.; Voigt, W. Structural changes of cellulose dissolved in molten salt hydrates. *Macromolecular Chemistry and Physics* **2000**, *201*, 2041-2049.

(30) Fischer, S.; Leipner, H.; Thümmler, K.; Brendler, E.; Peters, J. Inorganic molten salts as solvents for cellulose. *Cellulose* **2003**, *10*, 227-236.

(31) Fischer, S.; Thümmler, K.; Pfeiffer, K.; Liebert, T.; Heinze, T. Evaluation of molten

inorganic salt hydrates as reaction medium for the derivatization of cellulose. *Cellulose* **2002**, *9*, 293-300.

(32) Duffy, J. A.; Ingram, M. D. Acidic nature of metal aquo complexes: Proton-transfer equilibriums in concentrated aqueous media. *Inorg. Chem.* **1978**, *17*, 2798-2802.

(33) Thammasouk, K.; Tandjo, D.; Penner, M. H. Influence of extractives on the analysis of herbaceous biomass. *Journal of Agricultural and Food Chemistry* **1997**, *45*, 437-443.

(34) Mei, C.; Pan, X. Dissolution of cellulose in aqueous lithium bromide solution. In *The 245th ACS National Meeting*; AMER CHEMICAL SOC 1155 16TH ST, NW, WASHINGTON, DC 20036 USA: New Orleans, 2013; Vol. 245.

(35) Mei, C. One-step saccharification of lignocellulosic biomass in inorganic molten salt hydrates. UW-Madison, 2013.

(36) Dee, S. J.; Bell, A. T. A study of the acid-catalyzed hydrolysis of cellulose dissolved in ionic liquids and the factors influencing the dehydration of glucose and the formation of humins. *ChemSusChem* **2011**, *4*, 1166-1173.

(37) Stewart, J. J. Isolation and characterization of lignin from populus. University of British Columbia, 2005.

(38) Kim, H.; Ralph, J. Solution-state 2D NMR of ball-milled plant cell wall gels in DMSO-d_6/pyridine-d_5. *Organic & biomolecular chemistry* **2010**, *8*, 576-591.

(39) Wen, J.-L.; Sun, S.-L.; Xue, B.-L.; Sun, R.-C. Recent advances in characterization of lignin polymer by solution-state nuclear magnetic resonance (NMR) methodology. *Materials* **2013**, *6*, 359-391.

(40) Yokoyama, T. Revisiting the Mechanism of β-O-4 Bond Cleavage During Acidolysis of Lignin. Part 6: A Review. *Journal of Wood Chemistry and Technology* **2014**, *35*, 27-42.

(41) Hatfield, R. D.; Jung, H. J. G.; Ralph, J.; Buxton, D. R.; Weimer, P. J. A comparison of the insoluble residues produced by the Klason lignin and acid detergent lignin procedures. *Journal of the Science of Food and Agriculture* **1994**, *65*, 51-58.

(42) Yasuda, S.; Fukushima, K.; Kakehi, A. Formation and chemical structures of acid-soluble lignin I: sulfuric acid treatment time and acid-soluble lignin content of hardwood. *Journal of wood science* **2001**, *47*, 69-72.

Chapter 3 An uncondensed lignin depolymerized and isolated from lignocellulosic biomass: A mechanistic study

This chapter has been submitted for publication, in part, under the same title.

Abstract

This study demonstrated that lignin could be efficiently depolymerized in the solid state, with minimal condensation, and separated from dissolved and hydrolyzed cellulose and hemicelluloses, using an acidic lithium bromide trihydrate (ALBTH) system under mild conditions (with 40 mM HCl at 110 °C). The resultant ALBTH lignins contained abundant uncondensed moieties (i.e., Hibbert's ketones and benzodioxanes), from partial depolymerization, and could readily be isolated from biomass sources representing the three classes (hardwood, softwood, and grasses). Reactions using lignin model compounds (LMCs, guaiacylglycerol-β-guaiacyl ether and various aromatic monomers) confirmed the formation of the uncondensed moieties and revealed the synergy between LiBr and acid in inducing the crucial intermediate α-benzyl carbocations, which then led to cleavage of the β–*O*–4 aryl ether bonds to produce Hibbert's ketones, demethylation to produce benzodioxanes, and condensation reactions. Unlike in the LMC reactions, the condensation of the real lignin in biomass under ALBTH conditions was greatly diminished, possibly due to lignin's remaining in the solid state, limiting its mobility and accessibility of the α-benzyl carbocation to the electron-rich aromatic sites for condensation. This study provided a new approach to effectively isolate depolymerized lignin from lignocellulose in a less condensed form for boosting its downstream valorization.

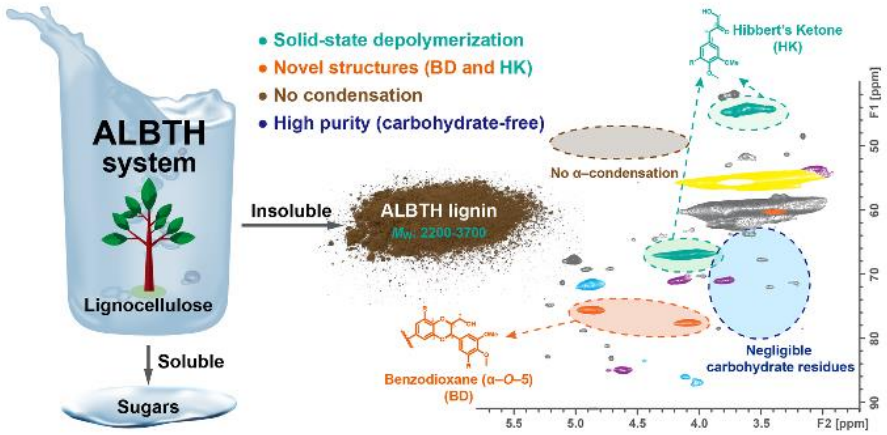

3.1 Introduction

Lignin, as a major cell wall component of lignocellulosic biomass, is the most abundant aromatic biopolymer on earth. Lignin valorization has emerged as a consensus requirement for profitability, based on efficiently utilizing the entire lignocellulosic biomass. In view of the structural and functional nature of lignin, a broad array of potential applications is anticipated, including as dispersants, aromatic platform chemicals, fuel precursors, pharmaceutical products and ingredients for adhesives, resins, biocomposites, and carbon fibers.[1-5] In efforts to separate lignin from lignocellulose and achieve value-added utilization, chemocatalytic depolymerization of lignin by cleaving the inter-unit ether linkages (mostly β–*O*–4 aryl ether bonds) but avoiding condensation (repolymerization) reactions is recognized to be a prerequisite.

Acid is prevalently used for lignin depolymerization, cleaving β–*O*–4 aryl ether bonds initiated by an α-benzyl carbocation intermediate. Acid-catalyzed lignin depolymerization has been extensively studied in many solvent systems, including ionic liquids[6-8] and various organic solvents such as γ-valerolactone,[9] dioxane,[10-14] methanol,[15] ethanol,[16,17] formic acid,[18] and acetic acid.[19,20] However, acid catalyzed lignin depolymerization is always accompanied by condensation reactions that take place either before or after the cleavage of the β-ether units. Before cleaving

the β–*O*–4 aryl ether bond, the α-benzyl carbocation can attack an electron-rich aromatic ring in an electrophilic aromatic substitution reaction, leading to formation of a new C–C linkage that defines condensation.[21-23] After the cleavage of the β–*O*–4 aryl ether bond, the resultant C2 aldehyde and Hibbert's ketone (**HK**) end-groups are vulnerable to aldol condensation under acidic conditions, forming other inert C–C linkages.[10,24] Previous studies have explored different means of avoiding or reducing the condensation reactions by introducing trapping/capturing reagents or pretreatment by, for example, trapping the α-benzyl carbocation using aromatic compounds such as phenol,[22,23] protecting the α-benzyl carbon from condensation by forming a 1,3-dioxane structure with the α- and γ-hydroxyls of lignin using formaldehyde[12] or other aldehydes,[25] or *in situ* capturing the unstable post-cleavage carbonyls, e.g., the C2 aldehyde and **HK**, by producing acetals using diols such as ethylene glycol.[10,11,15]

Intrinsically, the success of lignin depolymerization to produce uncondensed lignin relies on the competition between ether cleavage and condensation. As the occurrence of condensation requires two adjacent lignin moieties or species (i.e., is between the α-benzyl carbocation and the electron-rich aromatic ring, or between the C2 aldehydes and/or **HK**s), preventing the lignin moieties from direct contact can block or reduce condensation. Therefore, it is hypothesized that lignin condensation could be avoided or minimized by limiting the accessibility or mobility of the reactive lignin moieties (intermediates) by, e.g., keeping lignin in the solid state during the acid-catalyzed depolymerization (the cleavage of the β–*O*–4 aryl ether bond), and using mild conditions (low acid concentration and moderate temperature) such as in the LiBr system described below.

According to our previous studies, the acidic lithium bromide trihydrate (ALBTH, $LiBr{\cdot}3H_2O$) system exhibited an extraordinary ability to swell, dissolve, and hydrolyze polysaccharides (cellulose and hemicelluloses) in lignocellulose.[26,27] The lignin fraction (ALBTH lignin) could be

quantitatively obtained as the insoluble residue remaining after hydrolyzing the carbohydrates.[28] It was highly soluble in many common organic solvents, such as THF, acetone, acetic acid/water (95/5, v/v), dioxane/water (9:1, v/v), and DMSO (unpublished data). This feature distinguishes it from other isolated lignins such as Klason lignin and kraft lignin and indicates the uniqueness of the lignin depolymerization in the ALBTH system. In addition, when the technical lignins from different pulping and biorefining processes were treated in the ALBTH system under mild conditions, the cleavage of the aryl ether bonds was also observed, leading to further reductions in molecular weight.[29] It is therefore of significant interest to investigate lignins' chemical changes in the ALBTH system, to provide new insights into the lignin depolymerization mechanisms and to determine the characteristics and potential utilization of the ALBTH lignin. In this study, the native lignin in different lignocellulosic feedstocks and lignin model compounds (LMCs) were utilized to elucidate the mechanisms and pathways of lignin depolymerization and condensation in the ALBTH system.

3.2 Experimental

3.2.1 Chemicals

Chips of hardwood (aspen, poplar and eucalyptus) and softwood (Douglas fir), and coarsely chopped grasses (switchgrass and corn stover) were ground with a Wiley-mill, and the fraction between 20 and 100 mesh was collected as lignocellulosic materials for this study. Chemicals including 3,4,5-trimethoxylbenzyl alcohol (TMBA), guaiacol (**GA**), creosol (**CS**), anhydrous lithium bromide (LiBr), hydrochloric acid (HCl), dimethylsulfoxide (DMSO-d_6), pyridine-d_5, pyridine, tetrahydrofuran (THF), acetonitrile, *N*-methyl-*N*-trimethylsilyl-trifluoroacetamide (MSTFA) were purchased from Fisher Scientific (Pittsburgh, PA), VWR (Radnor, PA), and Sigma

Aldrich (St. Louis, MO). Guaiacylglycerol-β-guaiacyl ether (**GG**) was synthesized and provided by Dr. Gaojin Lyu with ~99% purity, as determined by NMR.[30]

3.2.2 Isolation of the ALBTH lignin fraction from biomass

The ground biomass was mixed with ALBTH solution (60% (w/w) LiBr with 40 mM HCl) at room temperature in a 40-mL glass vial fitted with a Teflon-lined screw cap; a magnetic stir-bar was added. The mixture in the vial was heated in an oil bath at 110 °C with magnetic stirring (400 rpm) to hydrolyze cellulose and hemicelluloses to soluble fractions. After the preset reaction time, the reaction was quenched by placing the vial into an ice-water bath. The insoluble ALBTH lignin fraction was collected by vacuum filtration on a filtering crucible and thoroughly washed with deionized (DI) water. The solid sample was dried at 50 °C under vacuum for subsequent analyses.

3.2.3 Reactions of lignin model compounds (LMCs) in ALBTH

Various aromatic monomers and dimers (including **GA**, **CS**, TMBA, and **GG**) were used as LMCs to investigate the reaction mechanism in lithium bromide trihydrate (60%, w/w) medium with or without an acid catalyst. A dilute acid solution (10 mM HCl) in the absence of LiBr was used as the control. Due to the limited solubility of LMCs in 60% LiBr at room temperature, LMCs (individually or in pairs) were first dissolved in dioxane prior to mixing with ALBTH (the final ratio of dioxane to ALBTH was ~5/95, v/v). The mixture was then sonicated for 5 min to obtain a homogeneous suspension of LMCs in ALBTH. During subsequent heating, the suspension became a transparent solution. The reaction was conducted following the same procedure as for the biomass above but with reduced reaction severity (temperature: 100 °C and acid concentration: 10 mM HCl). During the reaction, aliquots were taken for analysis at preset intervals. After the reaction, the mixture was extracted triply with CH_2Cl_2 to recover products. The CH_2Cl_2 phase was washed with water to remove the salts. The aqueous phase was filtered to collect the insoluble

products (especially from the **GG** reactions). The insoluble products were washed with DI-water and dissolved in acetone. The products in CH_2Cl_2 and acetone were combined, dried over anhydrous Na_2SO_4, and the solvents were removed by rotary evaporation at reduced pressure. Samples were stored at -4 °C for subsequent analyses.

3.2.4 Acetylation of ALBTH lignin

Lignin (0.1 g) was dispersed/dissolved in 1 mL pyridine in a 20-mL glass vial, and then acetic anhydride (1 mL) was added. The mixture was sealed and allowed to react at room temperature for 72 h. The lignin acetate was precipitated in acidic water (pH < 2) with constant stirring, collected by filtration, washed with DI-water, and vacuum-dried.

3.2.5 NMR spectroscopic analysis

The nuclear magnetic resonance (NMR) spectra were recorded on a Bruker AVANCE III 500 MHz spectrometer equipped with a DCH (^{13}C-optimized) cryoprobe (Billerica, MA). The lignin sample (50 mg, unacetylated) was dissolved in 0.5 mL of dimethylsulfoxide-d_6 (DMSO-d_6) or DMSO-d_6/pyridine-d_5 (4:1, v/v). Heteronuclear single-quantum coherence (HSQC) spectra were recorded at 25 °C using Bruker's standard hsqcetgpsisp2.2 pulse program (acquisition time 200 ms and 8 ms in ^{1}H and ^{13}C dimensions, respectively; inter-scan relaxation delay 1 s). Data processing was performed using Bruker's Topspin 3.5 software to a final matrix size of 2k × 1k data points.

The relative abundance of each interunit linkage R_i, appearing in the aliphatic region of HSQC spectra, from lignin samples was calculated by the following equation:

$$R_i\ \% = I_i / [I_A + I_B + I_C + I_{HK} + I_{BD}] \times 100\% \quad (3.1)$$

Where I_i, I_A, I_B, I_C, I_{HK}, and I_{BD} denote the α-H/C correlation peak integrals of the target inter-unit linkage i, β–*O*–4 aryl ether **A**, phenylcoumaran (β–5) **B**, resinol (β–β) **C**, **HK**, and

benzodioxane **BD** structures; **HK** has two α-protons per unit, so its integral is halved in the relative abundance calculation.

3.2.6 Gel-permeation chromatographic (GPC) analysis

The number-average and weight-average molecular weights (M_n and M_w, respectively) of the ALBTH lignins (after acetylation) and the products of LMCs were estimated on a Dionex ICS-3000 system equipped with three tandem 300 mm × 7.8 mm (l × i.d.) Phenogel 5U columns (10000, 500, and 50 Å, respectively) and a 50 mm × 7.8 mm (l × i.d.) Phenogel 5U guard column (Phenomenex, Torrance, CA). The eluent was an isocratic 100% THF (HPLC grade without stabilizer) at a flow rate of 1.0 mL/min and the column temperature was kept at 30 °C. Each sample (~0.5%) in THF was injected after passing through a 0.45 μm filter and the fractionated lignin in the column eluent was detected by a variable wavelength detector (VWD) at 280 nm. The apparent molecular weight was calibrated using polystyrene standards and **GG** at 254 nm.

3.2.7 Gas chromatography-mass spectrometric (GC-MS) analysis

Qualitative analysis of the LMC reaction products was conducted on a GC-MS system (GCMS-QP 2010S, Shimadzu Co., Addison, IL) with a SHRXI-5MS column (30 m × 0.25 mm, L. × I.D., with 0.25 μm film thickness). The injection port was at 280 °C, and the carrier gas was helium at a flow rate of 8 mL/min in a split mode (split ratio, 5:1). The programmed GC oven temperature profile started with a 30 °C isotherm for 5 min, followed by a 5 °C/min ramping to 220 °C and a subsequent 10 °C/min ramping to 300 °C, then held at the temperature for 5 min. The products from the **GG** reaction were silylated to improve the sample volatility. Specifically, an approximately 50 μL sample was mixed and reacted with 500 μL *N*-methyl-*N*-trimethylsilyl-trifluoroacetamide (MSTFA)/pyridine mixture (1:1, v/v) at room temperature for 2 h.

3.2.8 High-performance liquid chromatographic (HPLC) analysis

The LMC reaction products were quantitated on a Dionex ICS-3000 system equipped with a YMC-Triart C18 column (250 × 4.6 mm, I.D. × L.) at 30 °C and a VWD set at 210 nm. Both samples and standards were diluted with 20% acetonitrile in water to ensure full dissolution and filtered through a 0.45-μm syringe filter prior to injection. The mobile phase was an isocratic acetonitrile/water solution (20/80, v/v) with addition of 0.1% phosphoric acid at 0.8 mL/min. The column was reconditioned using an isocratic acetonitrile/water solution (60/40, v/v) for 10 min after each run.

3.3 Results and Discussion

3.3.1 Formation of HK and BD moieties from lignin depolymerization in the ALBTH system

Feedstocks (aspen, poplar, eucalyptus, Douglas fir, switchgrass, and corn stover) representing the three major biomass classes (hardwoods, softwoods, and grasses), were treated in the ALBTH system under mild reaction conditions (110 °C, LiBr 60% (w/w) and 40 mM HCl) to investigate lignin depolymerization in the process of ALBTH treatment. Because of the complete dissolution and hydrolysis of cellulose and hemicelluloses to aqueous soluble fractions,[28] the ALBTH lignin could be quantitatively collected for GPC and HSQC NMR analyses. The GPC-estimated molecular weights of the lignins are listed in Table 3.1 and compared with those of the corresponding isolated lignins [such as milled wood lignin (MWL) and cellulolytic enzyme lignin (CEL)] reported in the literature.[31-34] MWL and CEL fractions are generally considered to incur only minor modifications to the native lignin and therefore acceptable to represent the native lignin in the biomass. However, the molecular weights of MWL and CEL are slightly lower than that assumed for native lignin, because they only represent the solvent-extractable (low molecular

weight) portions of the native lignin.

The weight-average molecular weight (M_w) dropped to below 3000 Da for the hardwood (aspen, poplar, and eucalyptus) ALBTH lignins and 3700 Da for the softwood (Douglas fir), after treatment in ALBTH for 30 min. These M_w values are markedly lower than those of isolated lignins (CEL and MWL, 7K-20K Da). The results suggest that the native lignin in woody biomass was extensively depolymerized in the ALBTH system. Extending the ALBTH treatment to 120 min, the M_w of the lignins did not further decrease, suggesting that the cleavage of the β–*O*–4 aryl ether bonds was less prevalent and/or that lignin condensation was occurring, as discussed below. Similarly, the native lignin in grassy biomass such as corn stover and switchgrass was depolymerized to low molecular weight polymers (M_w 3100~4100 Da) in the ALBTH system.

Table 3.1 Average molecular weights and polydispersity indices of the representative isolated lignins and ALBTH lignins from various biomass

Biomass	Treatment	M_n	M_w	PDI
Poplar	MWL[31]	4100	10000	2.4
	ALBTH-30 min	1200	2900	2.5
	ALBTH-120 min	1100	3200	2.9
Aspen	MWL[32]	4500	23300	5.2
	ALBTH-30 min	1000	2200	2.2
Eucalyptus	CEL[33]	5500	17200	3.1
	ALBTH-120 min	1100	2500	2.2
Douglas fir	CEL[33]	5500	21800	4.0
	ALBTH-30 min	1100	3700	3.3
	ALBTH-120 min	1100	3600	3.3
Corn stover	MWL[34]	3500	8400	2.4
	ALBTH-30 min	1250	4110	3.3
Switchgrass	MWL[33]	2100	5100	2.5
	ALBTH-120 min	1000	3100	3.1

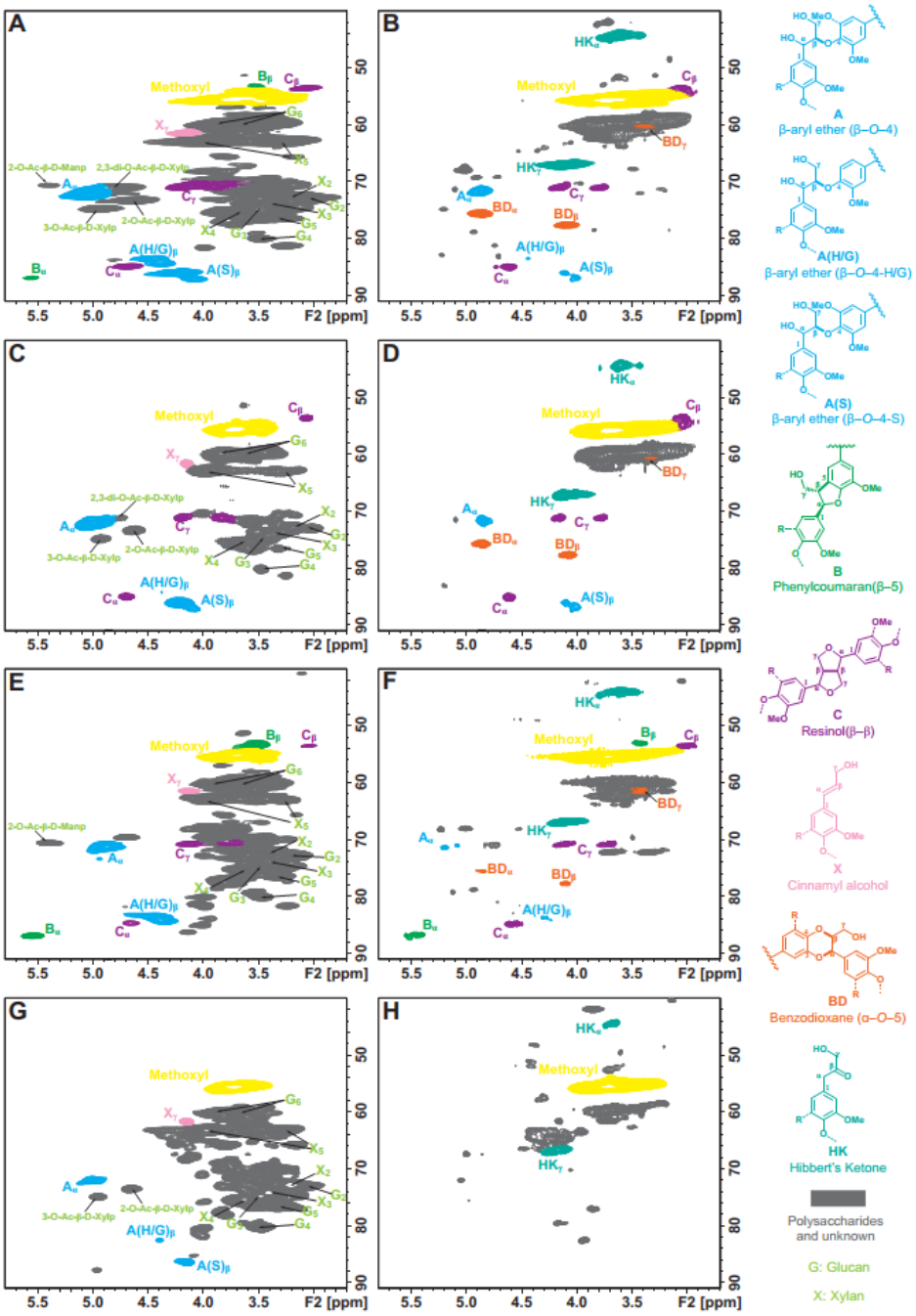

Figure 3.1 The aliphatic regions of 2D ^{1}H–^{13}C correlation (HSQC) spectra of the ball-milled plant cell walls dispersed in DMSO-d_6/pyridine-d_5 (A: aspen, C: eucalyptus, E: Douglas fir, and G: corn stover) and the lignins isolated by acidic lithium bromide trihydrate treatment in DMSO-d_6 (D: eucalyptus and F: Douglas fir) and in DMSO-d_6/pyridine-d_5 (B: aspen and H: corn stover). Correlation signals are categorized and color-coded by the type of aromatic units. (**A**, β–*O*–4 aryl ether; **B**, phenylcoumaran (β–5); **C**, resinol (β–β); **X**, cinnamyl alcohol end-group; **HK**, Hibbert's ketone; and **BD**, benzodioxane)

To reveal the structural changes in lignin during the depolymerization, the ALBTH lignins from aspen, eucalyptus, Douglas fir, and corn stover were characterized using HSQC NMR. Their spectra were compared with those from the whole cell wall (WCW) of the corresponding raw biomass, as shown in Figure 3.1 (the aliphatic region) and Figure S3.1 (the aromatic region). Many of the major contours in the δ_C/δ_H 65-85/2.5-4.5 ppm region of the WCW spectra (left column) assigned to the non-anomeric carbohydrates, are mostly absent in the ALBTH lignin spectra (right column), verifying the excellent ability of ALBTH to dissolve and hydrolyze the carbohydrates from the biomass to leave a relatively pure lignin fraction. As shown in Figure 3.1A, 3.1C, 3.1E, and 3.1G (left column), the native biomass lignins had abundant β-ether units **A** (with their characteristic β–*O*–4 aryl ether linkages) along with a small amounts of phenylcoumarans **B** (β–5) and resinols **C** (β–β), which are in agreement with other studies.[35,36] After a mild ALBTH treatment, the signals from the β-ether units were attenuated and some new chemical structures including the **HK** and **BD** moieties were revealed. The assignment of the Hibbert's ketone moiety **HK** was made by the cross peaks at δ_C/δ_H 44.5/3.67 ppm (α-position) and 67.1/4.19 ppm (γ-position) according to the study on LMCs,[13] and the assignment of the *trans*-benzodioxane moiety **BD** was made by the cross peaks at δ_C/δ_H 75.6/4.86 ppm (α-position) and 77.5/4.07 ppm (β-position) according to the study on C-lignin and C-DHP polymers derived from caffeyl alcohol polymerization.[37] Notably the resonance peaks from both moieties were distinctive from other lignin signals and were consistently observed in the ALBTH lignins from all woody biomass species used in this study. The ALBTH lignin from grasses (corn stover, Figure 3.1H), only had **HK**, but not **BD** moieties resolved, possibly due to its low β–*O*–4 aryl ether content and the presence of *p*-coumarates and ferulates. The identification of **HK** and **BD** moieties suggests that the condensation to form the inert C–C linkages was less significant (or reduced) during the

cleavage of the β–*O*–4 aryl ether bonds in ALBTH. More evidence and discussion will be provided below from the LMC study. A striking feature of the reaction was the generation of **BD** units, obviously also from β-ether units and involving a demethylation. As far as we are aware, this is the first time that **BD** units have been detected from an acid-catalyzed lignin depolymerization. **BD** units were originally discovered in vanilla seed coats that make their lignins entirely from caffeyl alcohol,[37] with its "C-lignin" being recently touted as an ideal lignin structure that can survive acidic treatments but can be readily depolymerized to valuable 4-propanolcatechol and its derivatives.[38,39] These observations suggest that the ALBTH system has the uniqueness to yield uncondensed and valuable lignin moieties/structures, compared with other acidic solvent systems for lignin depolymerization. The presence of **G**, **S**, and **H** units in lignin before/after the ALBTH treatment are most readily discerned from the aromatic regions of the HSQC spectra and can be verified with reference to Figure S3.1. Notably, the formation of **HK** and **BD** moieties significantly changed the chemical shifts of **G** and **S** units in the aromatic regions.

Using semi-quantitative analysis, the relative abundance of various units in the lignins was estimated, as shown in Table 3.2. The phenylpropanoid units in hardwood species such as aspen were mainly the β–*O*–4 aryl ether **A** and resinol **C** moieties with a trace amount of the phenylcoumaran **B** moiety. After the ALBTH treatment, the relative abundance of the resinol **C** moiety remained unchanged, while the β-ether **A** decreased from 86% to 24% and phenylcoumaran **B** was no longer detectable. Notably, **HK** and **BD** (as novel uncondensed lignin depolymerization products) formed in 44% and 22% levels, respectively. For softwood species (e.g., Douglas fir), the relative level of resinol **C** rose from 8% to 15%, whereas the β-ether **A** and phenylcoumaran **B** moieties decreased from 73% and 19% to 12% and 17%, respectively. These results suggested that the ease of cleaving the lignin linkages during the ALBTH treatment followed the order of β-

ether > phenylcoumaran > resinol (i.e., **A** > **B** > **C**). In other words, the ALBTH system was able to cleave the β-ethers **A** in lignin fairly selectively, leading to uncondensed **HK** and **BD** moieties. Notably, it was observed that the hardwood lignin had much higher level of the **BD** moiety (over 22%) than the softwood lignin (5%) after the ALBTH treatment. Apparently, the **S** type lignin (abundant in hardwood) has more chances to demethylate one of the two methoxyl groups, or one is easier to demethylate, to form a **BD** moiety than the **G** type lignin in softwood that has only one methoxyl group per unit.

Table 3.2 Relative abundance of the major inter-unit linkages in the native and ALBTH lignins by the semi-quantitative HSQC NMR analysis

Lignin Unit		**C**	**B**	**A**	**HK**	**BD**
Aspen	WCW	11.8	2.4	85.8		
	ALBTH	10.0		24.1	44.0	22.0
Eucalyptus	WCW	16.1		83.9		
	ALBTH	17.9		28.2	30.6	23.3
D. fir	WCW	8.1	19.4	72.5		
	ALBTH	14.5	16.6	12.3	52.0	4.6

As mentioned above, the acid-catalyzed lignin depolymerization has been extensively studied in the systems such as acidic ionic liquid,[6] aqueous dilute acid,[40] steam explosion,[34] and in acidic organic solvents such as methanol, GVL, and dioxane.[9,11,13] However, the HK from cleavage of the β-ether units was not observed or barely visible in the HSQC NMR spectra of the lignins from these processes. There are presumably two reasons. First, the competing C6–C2 type cleavage might be more favorable than the C6–C3 type cleavage in the traditional acid systems (especially in H_2SO_4-catalyzed systems), resulting in abundant C2 aldehyde end-groups that promptly succumb to aldol condensations.[10,41-43] This was supported by the finding that the cleavage pathways were dependent on the types of acid and solvent systems used.[44] Second, the **HK** (C3

type ketone) end-groups might be preferentially stabilized or prevented from condensation in the ALBTH system because, in the solid state, the lignin moiety was less accessible and less mobile, limiting the opportunity for condensation reactions, as further discussed below. In summary, the observations above suggest that the ALBTH system is able to selectively cleave the β–*O*–4 aryl ether bonds under mild reaction conditions and generate depolymerized and less condensed lignins containing novel **HK** and **BD** moieties. Compared with other acidic systems, the ALBTH system showed considerable potential to isolate "good" lignin from lignocellulosic biomass for valorization.

3.3.2 Reactions of LMCs in ALBTH

Guaiacylglycerol-β-guaiacyl ether (**GG**), a popular β–*O*–4 aryl ether model compound, was used to investigate the lignin depolymerization in ALBTH. The decomposition of **GG** and the yield of guaiacol (**GA**) are presented as a function of reaction time in Fig 3.2. **GG** and **GA** were quantitated by HPLC (Figure S3.2). In order to investigate the possible synergy of LiBr and acid in ALBTH, the **GG** reaction was conducted at 100 °C in three disparate solvent systems: acidic lithium bromide trihydrate (ALBTH) with 10 mM HCl, neutral lithium bromide trihydrate (NLBTH) without acid, and dilute acid (DA) solution with 10 mM HCl but without LiBr.

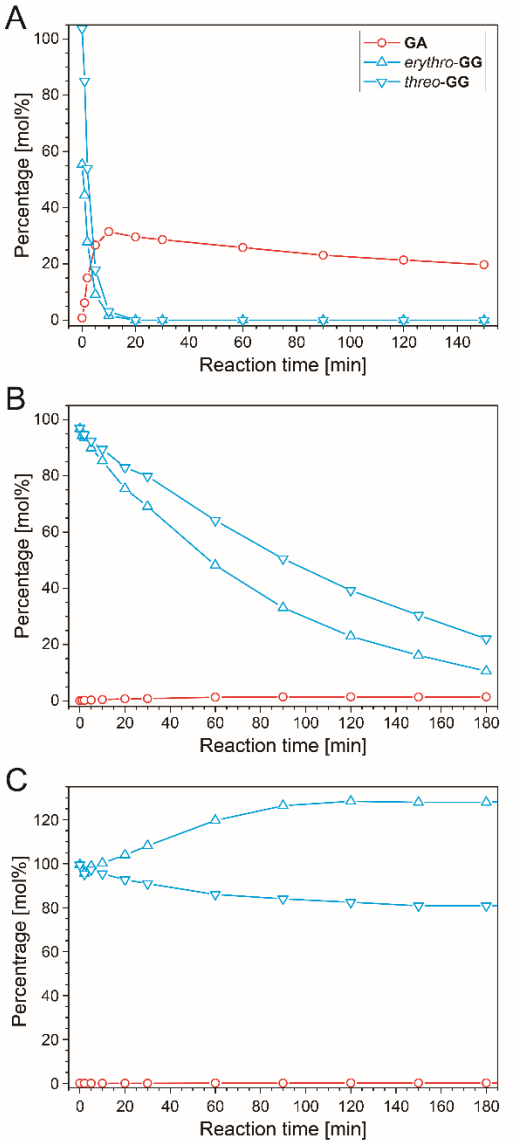

Figure 3.2 Reactions of guaiacylglycerol-β-guaiacyl ether (**GG**) in acidic lithium bromide trihydrate (A), neutral lithium bromide trihydrate without acid (B), and acidic water solution (C). Reaction conditions: 100 °C, 1 g/L GG dimer concentration, and 10 mM HCl for A and C.

In ALBTH (Figure 3.2A), **GG** was completely consumed within 10 min, yielding 34% **GA**; extending the reaction, no additional **GA** was released. Without acid catalyst, the conversion of **GG** was slow in NLBTH (Figure 3.2B). The **GG** content (both the *erythro* and *threo* diastereomers) gradually decreased with time, and over 80% conversion was reached at 180 min. In this case, the *erythro*-isomer was depleted more rapidly, as has been previously observed under

alkaline degradation conditions.[45] However, the yield of **GA** was negligible (less than 2%). This observation indicated that most of **GG** was slowly transformed in NLBTH, but no **GA** was released, possibly because either the β–*O*–4 aryl ether bonds were not cleaved, or the released **GA** promptly condensed with **GG** decomposition products. The analysis results of **GG** condensation products in NLBTH below apparently support the former was the primary reason.

The results in Figure 3.2B also verified that the presence of acid was essential to effective cleavage of the β-ether. However, acid alone (10 mM HCl in water) without LiBr did not break down **GG** at 100 °C (Figure 3.2C). The total **GG** content in the system remained without apparent change over 3 h and without formation of **GA**, although *threo*-**GG** partially isomerized to *erythro*-**GG**, resulting in the apparent equilibrium favoring *erythro*-isomer. Notably, higher reaction temperatures and higher acid concentrations (e.g., 150 °C with 200 mM H_2SO_4) were usually necessary to catalyze the cleavage of the **GG** in the aqueous dilute acid.[40] The observation of the effective cleavage of **GG** under milder conditions (very low acid concentration and moderate temperature, 10 mM HCl and 100 °C) in lithium bromide trihydrate was presumably ascribed to (1) the synergy between the acid and LiBr in cleaving the β–*O*–4 aryl ether bond, and (2) enhanced acidity of the Brønsted acid in LiBr trihydrate.[46] The aforementioned results demonstrated that both acid and LiBr trihydrate synergistically depolymerized lignin in the ALBTH system under mild conditions. Similar synergistic effect of acid and LiBr trihydrate in ALBTH was reported in the hydrolysis and dehydration of polysaccharides to furfurals.[46,47]

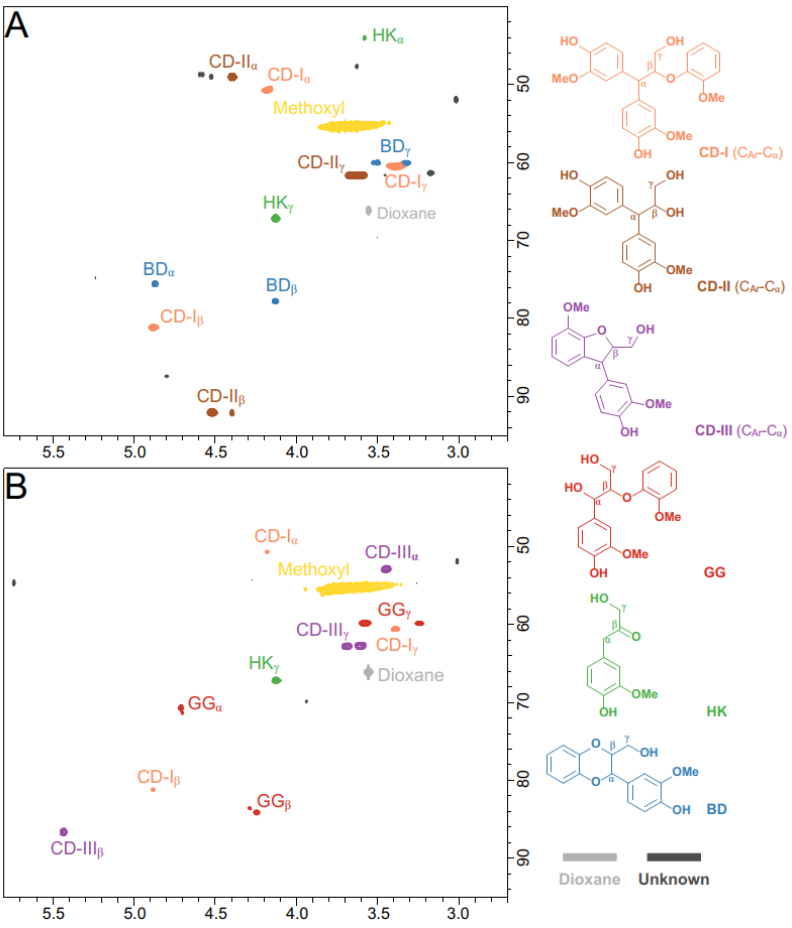

Figure 3.3 HSQC NMR spectra of **GG** reaction products in LiBr trihydrate reaction at 100 °C with 10 mM HCl for 10 min (A) and without acid (B) for 240 min.

The structures of **GG** products in ALBTH and NLBTH were further characterized by HSQC-NMR analysis. **HK** and **BD** moieties were detected from the ALBTH-treated **GG** (Figure 3.3A), whereas only a negligible amount of **HK** but no **BD** was identified from the NLBTH-treated **GG** (Figure 3.3B). **HK** was also detected in HPLC analysis of **GG** treated in both ALBTH and NLBTH (Figure S3.2). The formation of **HK** and **BD** was further confirmed by the GC-MS analysis (Figure S3.3B) of the ALBTH-treated **GG**, in which a **HK** monomer and 4-(3-(hydroxymethyl)-2,3-dihydrobenzo-[*b*][1,4]dioxin-2-yl)-2-methoxyphenol (a **BD** dimer) were detected. These verified our previous observation that both **HK** and **BD** moieties are formed during lignin depolymerization

in ALBTH. No **BD** was identified in NLBTH-treated **GG**, suggesting that acid was crucial to generate the uncondensed **BD** structures in the LiBr trihydrate system. The relatively low abundance of the **BD** moieties from **GG** was consistent with our biomass HSQC-NMR results above, in which **G** units (softwood lignin) were less prone to form the **BD** structures than **S** units (hardwood lignin).

Condensation products from **GG** were also detected in the HPLC analysis (Figure S3.2) and further confirmed by GPC analysis (Figure S3.4). Both ALBTH and NLBTH systems yielded higher molecular weight fractions from **GG**. As shown in Figure S3.4, the sample from the ALBTH system had a broad peak A (M_w: 750 Da, M_n: 630 Da) and a sharp peak B (M_w: 290 Da, M_n: 290 Da) with the A to B intensity ratio (A/B) = 2.1. For the sample from the NLBTH system, the peaks A and B represented the M_w/M_n of 780/660 and 290/280, respectively, with A/B = 4.3. These results indicate that the products from the NLBTH-treated **GG** had more condensed structures and slightly higher molecular weight than that from the ALBTH-treated **GG**. This is in agreement with the results shown in Figure 3.2B where **GG** was consumed but did not release **GA**, implying that condensation was predominant over cleavage of the β–*O*–4 aryl ether bond in NLBTH.

The structures of the condensation products from **GG** were investigated by GC-MS and NMR (HSQC, HSQC-TOCSY, COSY) analyses. In the ALBTH-treated **GG** sample, the dipehenylmethane-type condensation products were unveiled, including the 4-(3-hydroxy-1-(3-hydroxy-4-methoxyphenyl)-2-(2-methoxyphenoxy) propyl)-2-methoxyphenol trimer (**CD-I** type condensation) and 3-(4-hydroxy-3-methoxyphenyl)-3-(3-hydroxy-4-methoxyphenyl) propane-1,2-diol dimer (**CD-II** type condensation) (Figures 3.3A and S3.3B). In the NLBTH-treated **GG** sample, the phenyl-dihydrobenzofuran type condensation products (e.g., 4-(2-(hydroxymethyl) -

7-methoxy-2,3-dihydrobenzofuran-3-yl)-2-methoxyphenol, a dimer from intramolecular condensation, **CD-III** type condensation) were the most abundant together with a small amount of **CD-I** type condensation products (Figures 3.3B and S3.3A). This observation further established that the cleavage of the β–*O*–4 aryl ether bond was not the dominant reaction of **GG** in NLBTH. It was apparent that condensation mostly occurred via the α-benzyl carbocation by its electrophilic aromatic substitution on the electron-rich aromatic rings, forming a new C–C linkage. The identification of condensation products above brings new insight into the competition between the lignin depolymerization and condensation via the α-benzyl carbocation intermediate as catalyzed by both LiBr trihydrate and acid.

3.3.3 Proposed mechanisms of lignin reactions in LiBr trihydrate system

Based on the results and discussions above, pathways of lignin depolymerization to form **BD** and **HK** moieties and condensation reactions in the LiBr trihydrate system are proposed, as illustrated in Figures 3.4 and S3.5. In this system, the α-benzyl carbocation is logically the essential intermediate toward various products. There are two feasible routes to form the α-benzyl carbocation. Route I, which has been extensively elucidated in acidic systems, is initiated by acid-induced protonation of the benzyl alcohol and followed by dehydration to form the α-carbocation. Alternatively, in Route II, LiBr is postulated to catalyze the slow formation of the α-benzyl carbocation via reversible substitution of the α-hydroxyl by the bromide in the system. Route II is proposed based on the observation that condensation reactions occurred when **GG** was treated in NLBTH (LiBr alone without acid). In addition, Route II was supported by the experiment in which 3,4,5-trimethoxylbenzyl alcohol (TMBA) was treated in NLBTH system. As shown in Figure S3.6A, both the α-brominated intermediate of TMBA and its subsequent condensation product were detected, suggesting that LiBr alone did lead to the formation of the α-carbocation which

then attacked the electron-rich 2/6-position on the aromatic ring of TMBA, resulting in the condensation products. The α-benzyl carbocation then can be subsequently transferred from the α- to the β-position either by the small equilibrium in Route III via an enol ether intermediate or in Route IV via direct hydride shift.[41] Following trapping of the β-carbocation by H_2O, cleavage of the β–*O*–4 aryl ether bond occurs, releasing the **HK** and **GA** moieties. As **GA** was barely detected in the absence of acids, both Routes III and IV were presumed to be exclusively acid-catalyzed processes.

The reactive α-benzyl carbocation intermediate can also lead to the formation of **BD** moieties via Route V, which is supported by the results above that the **BD** structures were identified in the products from both native lignins and **GG** in ALBTH. The nucleophilic methoxyl oxygen on the **GA** ring of **GG** can intramolecularly trap the α-benzyl carbocation, resulting in a **BD** moiety from β–*O*–4 aryl ethers after demethylation. It seems that trapping the α-benzyl carbocation by C3/5-methoxyl is the first step in the **BD** formation followed by the demethylation. Otherwise, other demethylation structures besides **BD** should have been identified from the GC-MS and NMR analyses. In addition, no **BD** moiety is detected in NLBTH system, suggesting the essentiality of an acid to the **BD** formation. It is worth mentioning that the detection of the **BD** moiety has never been reported in the products from acidolysis of lignin or LMCs. The conversion of β–*O*–4 aryl ethers to **BD** (an acid-tolerant structure) suggests the possibility of a new strategy for lignocellulosic biomass valorization in the ALBTH system, i.e., hydrolyzing polysaccharides efficiently to their component sugars[26,28] and converting all lignin β-ethers to benzodioxanes in an isolated lignin that is then converted to catechol-type monomers by hydrogenolysis.[38]

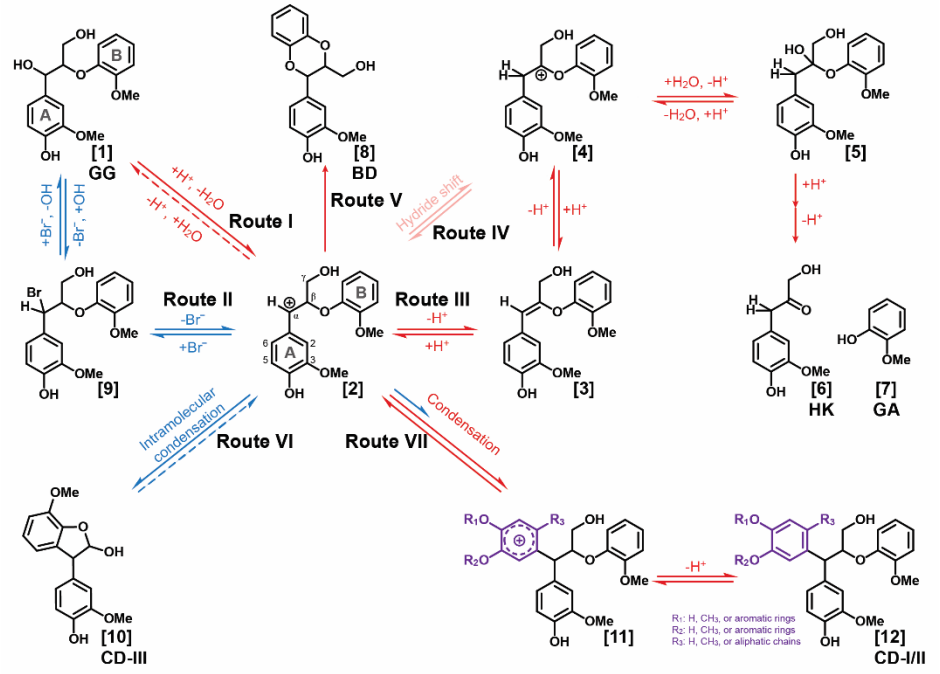

Figure 3.4 Proposed lignin depolymerization and condensation mechanisms.

Based on the identified condensation products from the **GG** studies above, two condensation routes are proposed. In Route VI (Figure 3.4), intramolecular condensation occurs via electrophilic aromatic substitution by the α-carbocation on the electron-rich C5-carbon on the B-ring. The resultant phenyl-dihydrobenzofuran structure (**CD-III**) was detected only in the NLBTH system, the analog of which was also reported in the previous model compound study using 1-phenyl-2-phenoxy-1,3-propanediol (**PD**) and 1-(4-hydroxyphenyl)-2-phenoxy-1,3-propanediol (**HH**) in dilute H_2SO_4.[40,43,48] However, the **CD-III** structures were not detected from **GG** dimers under the acidic condition in several LMC studies including our own. The observation in this study suggested that the presence of acid might greatly inhibit the intramolecular condensation of **GG** from occurring in the LiBr trihydrate system, possibly due to the overwhelming prevalence of the intermolecular condensation. As proposed in Route VII, the α-benzyl carbocation readily attacks the electron rich carbon on the aromatic rings. The reactive sites on the ring may vary depending

on the ring substituents. For example, the favorable sites are the C1 position (*para* to the hydroxyl substituent) for **GA** (R_1: H, R_2: CH_3, and R_3: H) and the C6 position (*para* to the methoxyl substituent) for lignin units (R_1: H, R_2: CH_3, and R_3: aliphatic sidechain) in Figure 3.4. Three factors may affect the regioselectivity of the electrophilic substitution (condensation) of the aromatic rings: 1) the electron denoting substituents activate the aromatic rings mostly at their *para* and *ortho* positions and their activation power follows the order OH > OMe > methyl ≈ sidechain of lignin; 2) the substituents that form extra resonance structures with the aromatic rings favor the *ortho*/*para* substitution; and 3) larger substituents (e.g., aliphatic sidechains) sterically inhibit the substitution at their *ortho* positions.

In analogy with traditional acid-catalyzed lignin depolymerization,[49] the trapping of an α-benzyl carbocation by the aromatic rings is considered to be the major condensation reaction in the ALBTH system. Each of the aromatic rings of **GG**, even after condensation, has active electron-rich sites, which are able to condense with a new α-benzyl carbocation to form C–C linkages. As a result, the intermolecular condensation reactions could generate high molecular weight products, such as those detected in the GPC analysis (Figure S3.4).

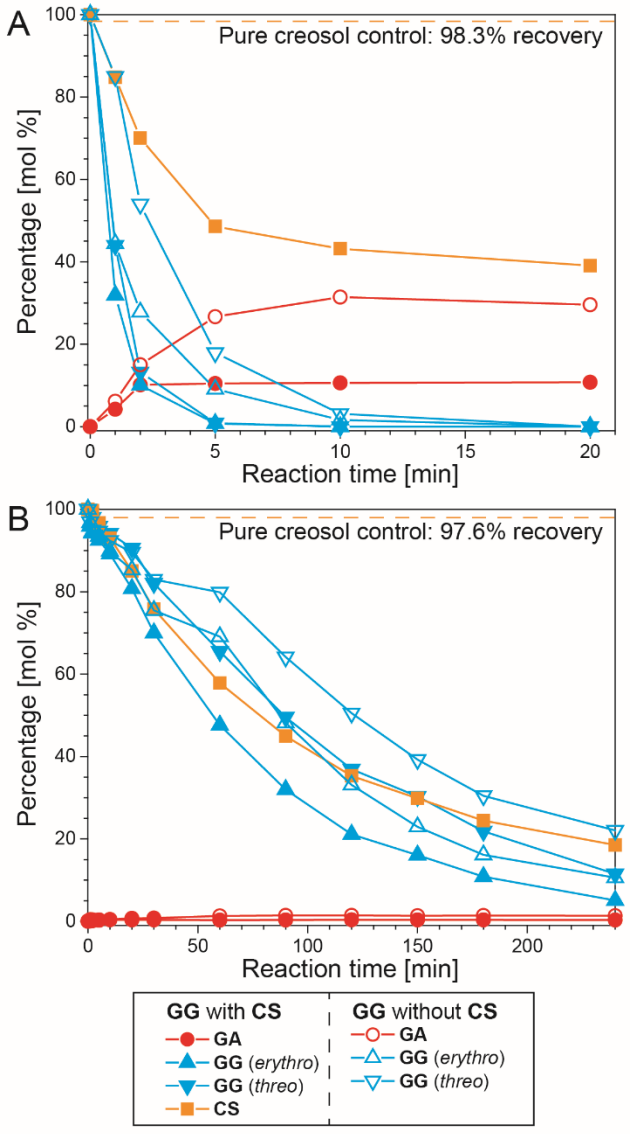

Figure 3.5 Reaction of **GG** with **CS** in ALBTH with 10 mM HCl (A) and NLBTH (B). Reaction conditions: 100 °C, **GG** to **CS** ratio: 1/1 (w/w); no addition of **CS** as control.

In order to further probe the condensation reactions occurring in ALBTH, TMBA (an α-carbocation generator) was reacted with **GA** and creosol (**CS**), and the products were analyzed with GC-MS, as shown in Figure S3.6B and S3.6C. The results confirmed the proposed Route VII (Figure 3.4) in which the C–C condensation mostly occurred between the α-benzyl carbocation and electron-rich aromatic rings. Creosol (**CS**) is a monomeric lignin-mimic without carbocation-

forming ability that, alone, was stable in ALBTH and NLBTH (~98% recoverable at 100 °C). When **CS** was introduced into the **GG** system in LiBr trihydrate, CS was significantly consumed, indicating that **CS** reacted with **GG** (Figure 3.5). In the ALBTH system (Figure 3.5A), the maximum yield of **GA** decreased significantly from 31.4 to 10.7% when **CS** was added, indicating that the addition of **CS** inhibited the cleavage of the β–*O*–4 aryl ether bond in **GG** that would generate **GA**. This is because, under the acidic condition, the protonation of the benzyl alcohol of **GG** readily happens and yields the α-benzyl carbocation, and its trapping by the excess creosol in the system forms the C_{α}–C_{aryl} linkage, which apparently blocks the pathway to cleavage of the β–*O*–4 aryl ether linkage via the analog of Route III or IV. In NLBTH (Figure 3.5B), the **GG** consumption was much slower than in ALBTH, as only LiBr contributed to formation of the α-benzyl carbocation. In this case, the presence of **CS** produced no significant changes to **GG** consumption, indicating that the rate-limiting step of the condensation reactions in NLBTH is the formation of α-benzyl carbocation.

To summarize the findings of the mechanistic studies using LMCs, both LiBr and acid can induce the formation of the α-benzyl carbocation intermediate, which is crucial to lignin depolymerization and **BD** formation. Although LiBr exerts synergistic effects on the formation of the α-benzyl carbocation, the acid dominates the catalysis of both the formation of the α-benzyl carbocation and the subsequent cleavage of the β–*O*–4 aryl ether bonds to yield **HK** and demethylation to yield **BD** moieties. The undesirable competing pathway is the formation of C–C bonds between the α-benzyl carbocation and the electron-rich aromatic rings, which is catalyzed by both LiBr and acid.

3.3.4 Suppressed lignin condensation in ALBTH system

In any process of lignin isolation and depolymerization for downstream valorization,

condensation is intrinsically undesirable. Although the LMC studies above demonstrated the possible condensation reactions occurring in ALBTH and NLBTH systems, the condensation products (containing C_{α}–C_{aryl} bonds), interestingly, remained at a minimal level in the real ALBTH lignins. In the HSQC NMR spectra (Figure 3.1B, 3.1D, 3.1F, and 3.1H), the $^{1}H/^{13}C$ correlation signals at δ_C/δ_H (45-52)/(4.0-5.0) ppm from the assignment of the condensation structures at the C_{α} position were negligible. This observation indicated that the C–C condensation between the α-carbocation and an aromatic carbon was greatly suppressed during the ALBTH treatment of lignocellulosic biomass. The condensation disparity between the real lignin and LMCs might result from their solubility, status, and mobility in ALBTH (i.e., the accessibility of electron-rich aromatics to the α-benzyl carbocation). In the case of the LMC reactions, the small aromatic molecules are either well dispersed or are dissolved in the system. Once the α-benzyl carbocation is formed, the nearby electron-rich (nucleophilic) aromatic carbons can readily succumb to attack by the carbocation, resulting in the C–C condensation products. On the other hand, lignin and lignin moieties are insoluble and tend to coil and aggregate as large particles in the ALBTH medium. The α-benzyl carbocation and the electron-rich aromatic rings from larger lignin polymers are therefore less mobile and have fewer chances to react with each other because of the steric and physical hindrance. Instead, the intramolecular cleavage of β–*O*–4 aryl ether bonds and the formation of **BD** from the α-benzyl carbocation are promoted. As a result, the ALBTH lignin has abundant uncondensed moieties (**HK** and **BD**) with limited condensation structures, which is consistent with our findings that the ALBTH lignin has low molecular weight and good solubility in many organic solvents.

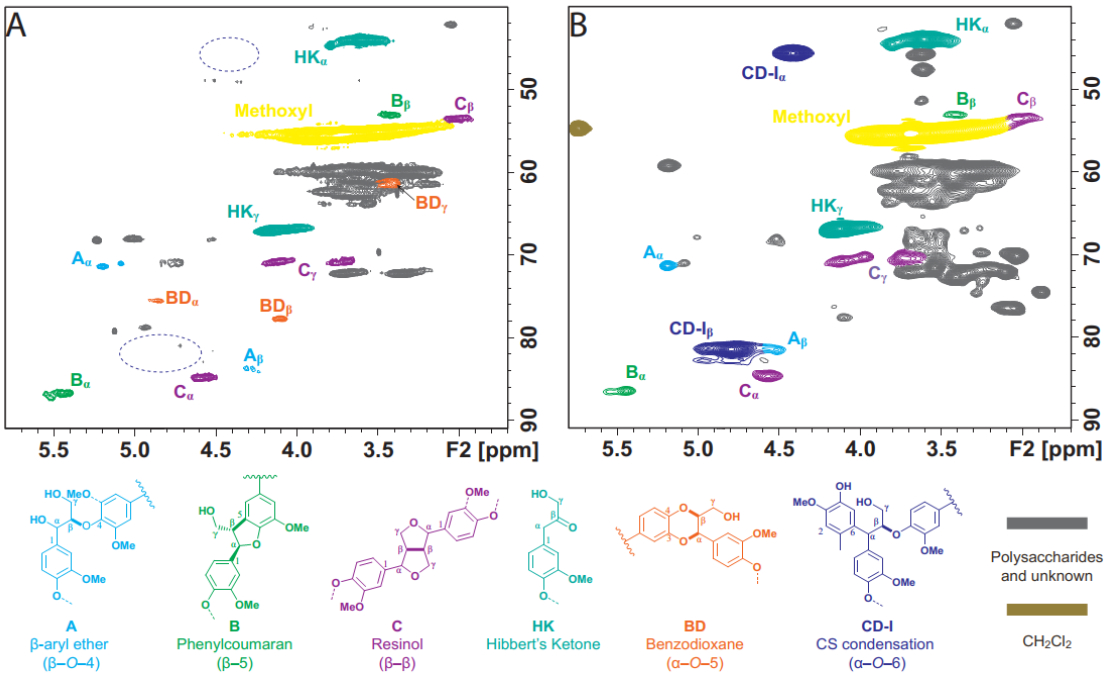

Figure 3.6 Evaluation of the condensation in ALBTH lignin from Douglas fir without creosol (A) and with addition of creosol (B, 5.5/1, w/w) at 110 °C.

In order to verify the hypothesis that the condensation is unfavorable in real lignin due to limited mobility and accessibility, the lignocellulosic biomass (e.g., Douglas fir) was treated in ALBTH in the presence of a monomeric lignin model nucleophile (**CS**). As expected, the resultant lignin featured significant correlation signals at δ_C/δ_H 45.4/4.41 ppm (α-position) and 81.4/4.80 ppm (β-position) due to the condensation with **CS** (Figure 3.6B), whereas the lignin without **CS** had negligible signals corresponding to condensation structures (Figure 3.6A, the same as Figure 3.1E). The results indicated that **CS**, as a small and mobile nucleophile, condensed readily with the lignin α-benzyl carbocation and formed the C_α–C_{aryl} bonds; in contrast the condensation between two real lignin polymers was limited. These observations confirmed that the aromatic carbons and the α-benzyl carbocation in the solid-state lignin are less accessible to each other, avoiding the condensation reactions in ALBTH.

3.4 Conclusions

In this study, we illustrated how the treatment of lignocellulose in the ALBTH system achieved depolymerization and separation of lignin in its solid state after nearly quantitative hydrolysis of polysaccharides to sugars. A pure lignin could be isolated from various woody and grassy biomass sources, also essentially quantitatively. The lignin was extensively depolymerized with a minimal level of condensation. The most vulnerable β–*O*–4 aryl ether bonds were selectively cleaved/transformed to uncondensed **HK** and **BD** moieties. Notably, **BD** was identified and confirmed for the first time in an acid-depolymerized lignin; its appearance suggests the possibility of using simpler routes toward catechol-type monomers that may be attractive for lignin valorization.

Model compound studies using **GG** revealed that the formation of the α-benzyl carbocation is the prerequisite for both the depolymerization and condensation. LiBr and HCl in the ALBTH system synergistically catalyze the formation of the α-benzyl carbocation, which subsequently leads to either an **HK** moiety via the cleavage of the β–*O*–4 aryl ether bond or a **BD** moiety via the demethylation of methoxyls on the aromatic rings. The α-benzyl carbocation may also attack lignin's electron-rich aromatic rings, resulting in the undesirable condensation products. However, we found that the level of condensation (formation of C_{α}–C_{aryl} bonds) in real ALBTH lignin was surprisingly low. It was postulated that the solid-state lignin reactions in ALBTH suppressed the condensation due to the reduced mobility and accessibility of the rigid lignin moieties (α-benzyl carbocations and electron-rich aromatic carbons) to each other. These findings reveal a new strategy for fractionation and depolymerization of lignin in the solid state to yield less condensed lignin products for downstream valorization.

Appendix

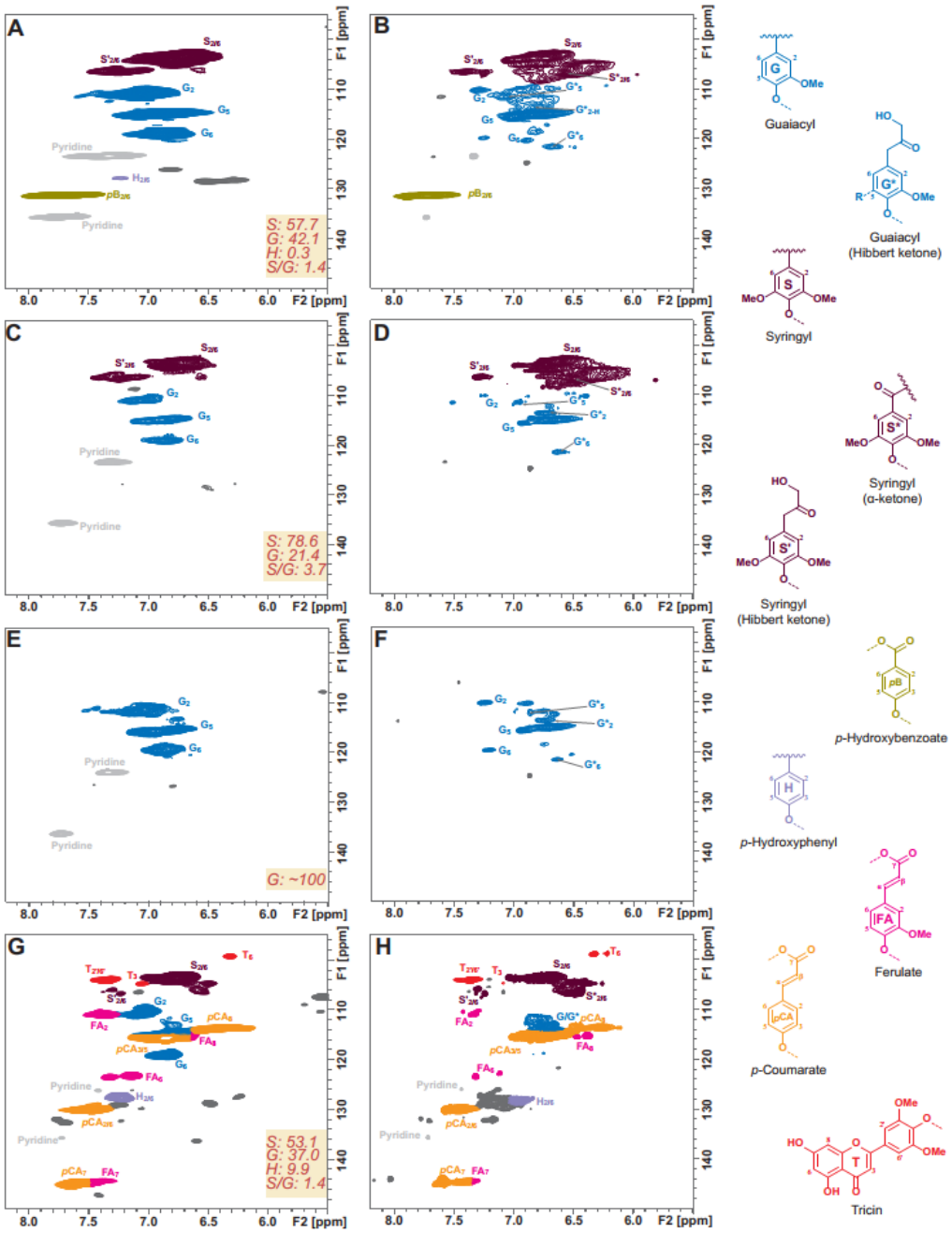

Figure S3.1 The aromatic regions of 2D ^{1}H–^{13}C correlation (HSQC) spectra of the ball-milled plant cell walls dispersed in DMSO-d_6/pyridine-d_5 (A: aspen, C: eucalyptus, E: Douglas fir, and G: corn stover) and the lignins isolated by acidic lithium bromide trihydrate treatment in DMSO-d_6 (D: eucalyptus and F: Douglas fir) and in DMSO-d_6/pyridine-d_5 (B: aspen and H: corn stover). Correlation signals are categorized and color-coded by the type of aromatic units. (**S**, syringyl; **G**, guaiacyl; **H**, *p*-hydroxyphenyl; ***p*CA**, *p*-coumarate; **FA**, ferulate; ***p*BA**, *p*-hydroxybenzoate; **T**,

tricin)

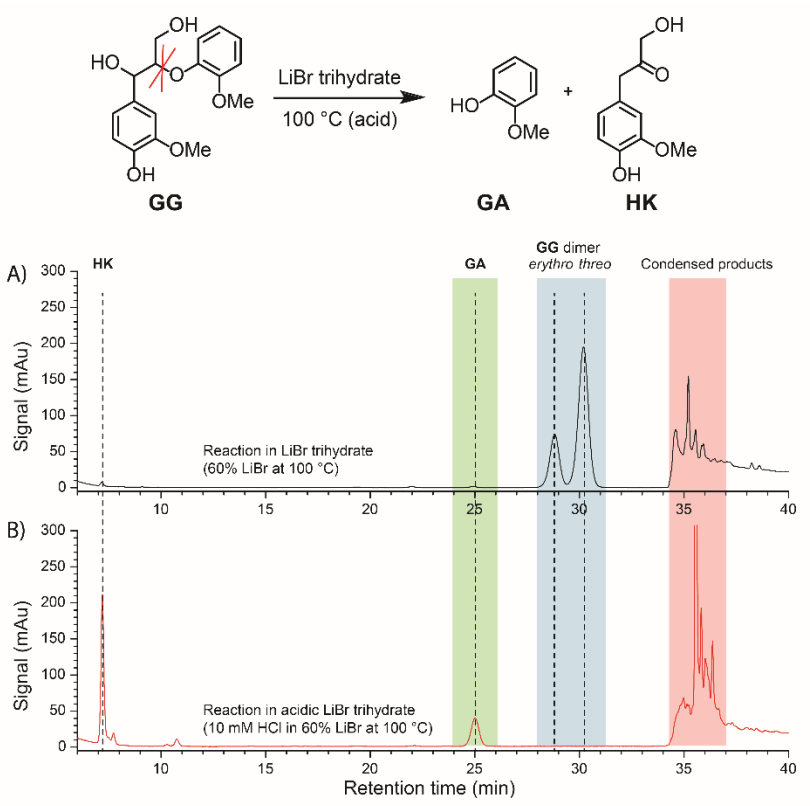

Figure S3.2 Reverse-phase HPLC analysis of the catalytic cleavage of the β–*O*–4 aryl ether bond of model **GG** in LiBr trihydrate without acid (A) and with 10 mM HCl (B) for 60 min. Note: **HK** monomer was not quantitatively analyzed due to its poor stability.

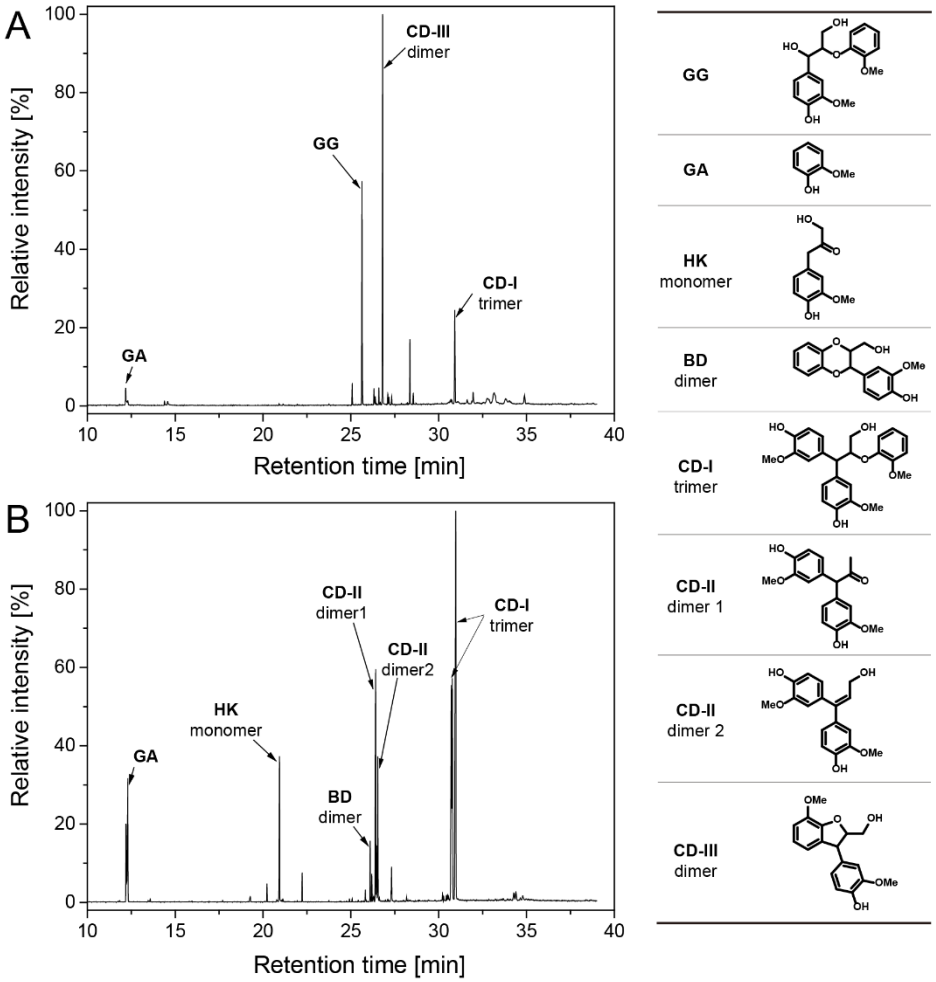

Figure S3.3 GC-MS identification of the low molecular weight products of **GG** reaction in NLBTH (A) and ALBTH (B). Reaction conditions: A, 100 °C for 240 min without acid; B, 100 °C for 20 min with 10 mM HCl.

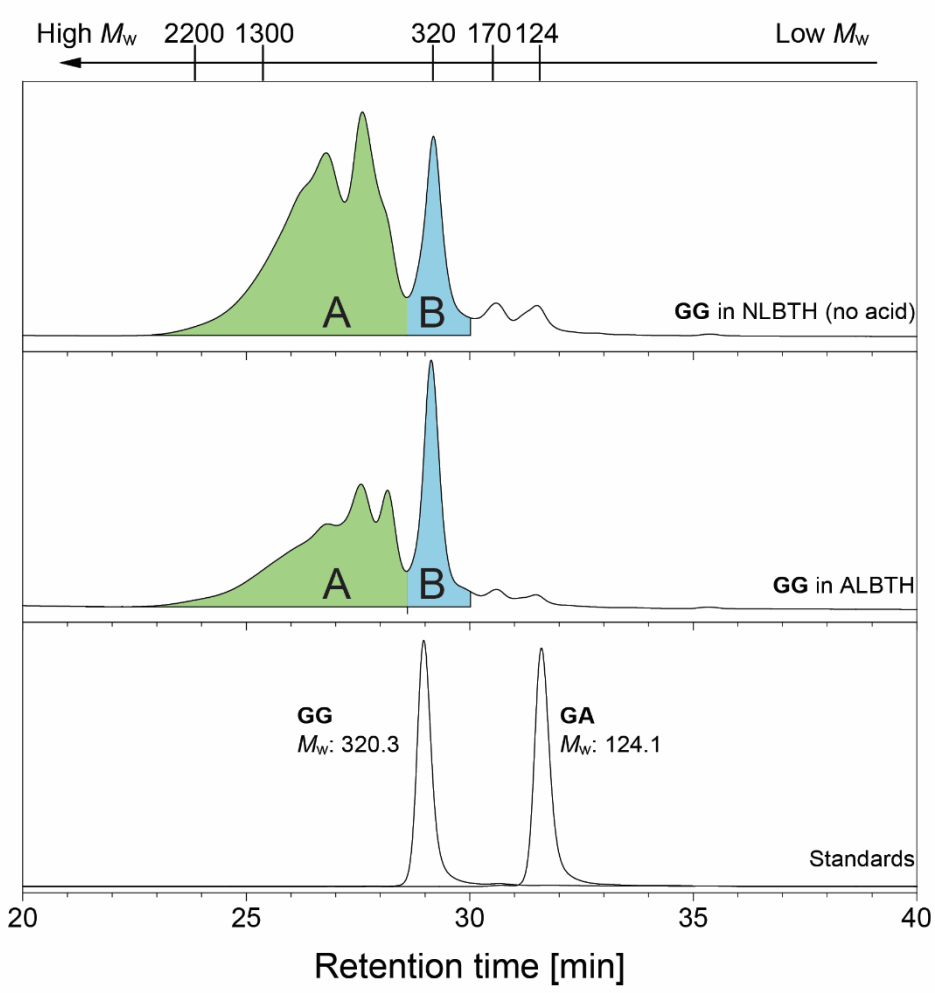

Figure S3.4 GPC chromatograms of the **GG** condensation products in the NLBTH (top) and ALBTH (middle). Note: The samples after NMR analysis were precipitated into acidic water for GPC analysis.

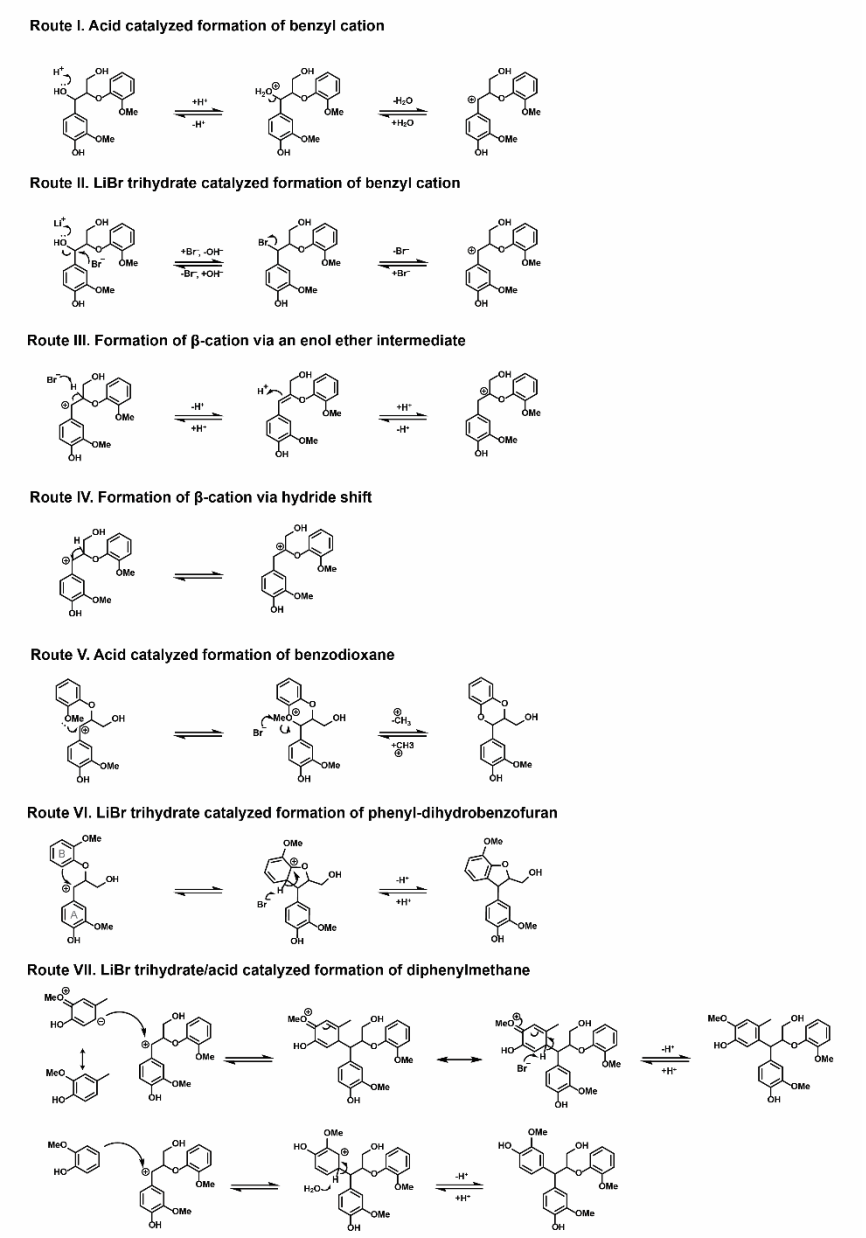

Figure S3.5 The detailed reaction pathways of the proposed reaction mechanisms.

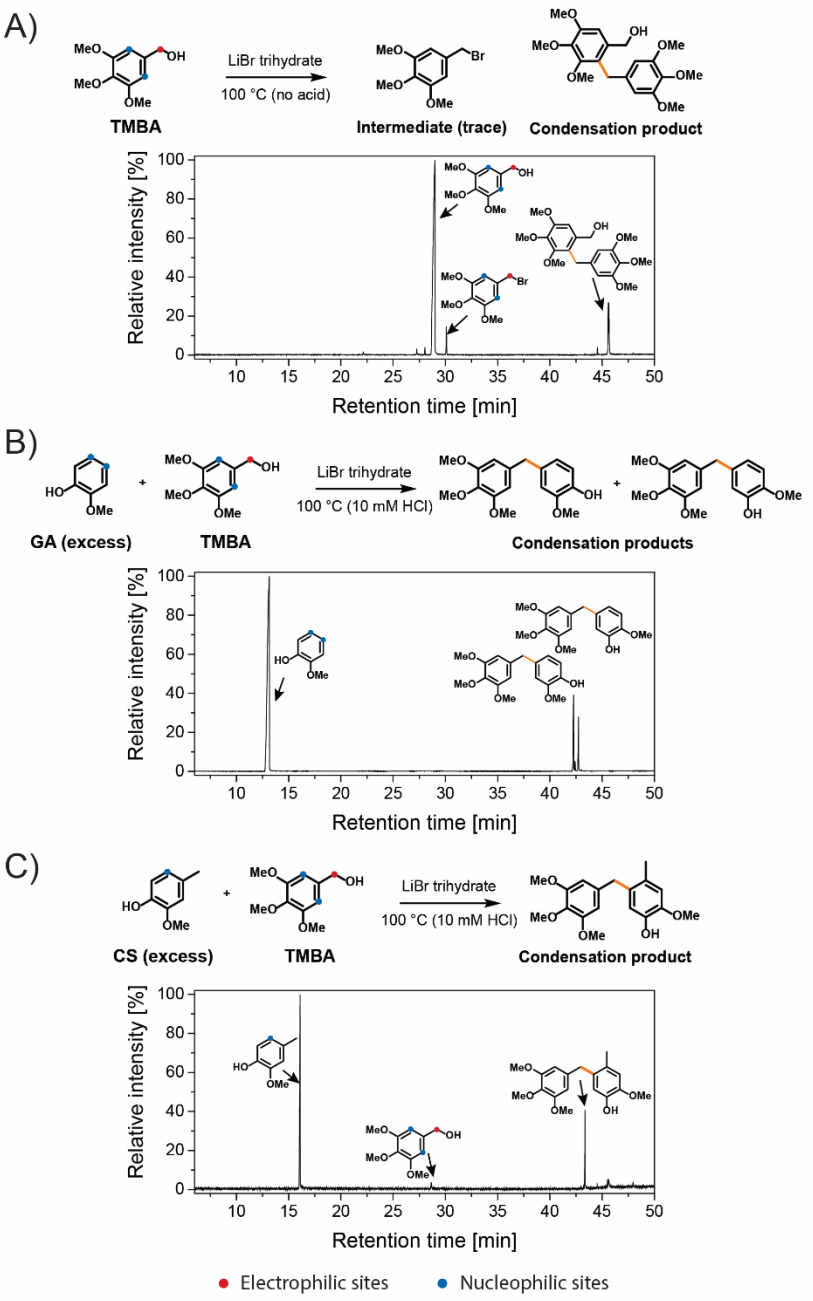

Figure S3.6 The condensation between monomeric models. A. Reaction of TMBA in NLBTH at 100 °C for 30 min; B. Reaction of TMBA with excess **GA** in ALBTH at 100 °C for 30 min; and C. Reaction of TMBA with excess **CS** in ALBTH at 100 °C for 30 min.

Raw data. NMR spectra

GG in ALBTH (COSY)

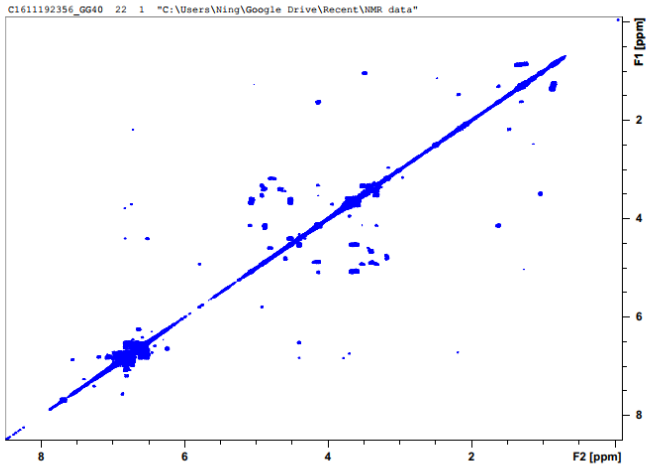

GG in NLBTH (COSY)

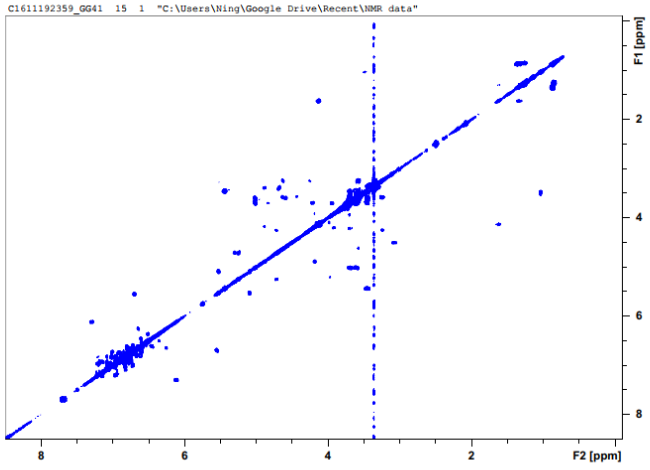

GG in ALBTH (HSQC-TOCSY)

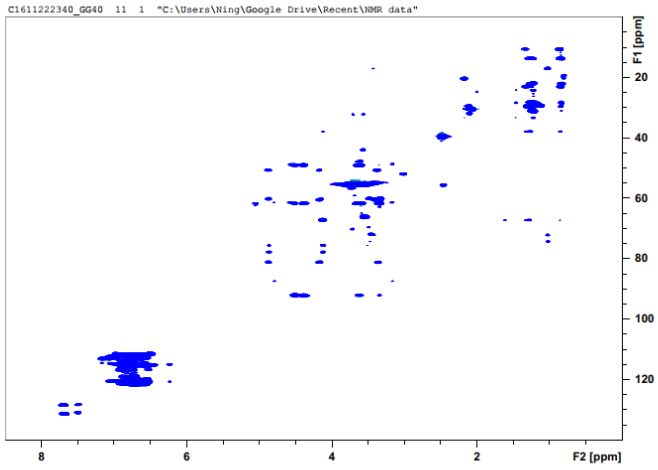

GG in NLBTH (HSQC-TOCSY)

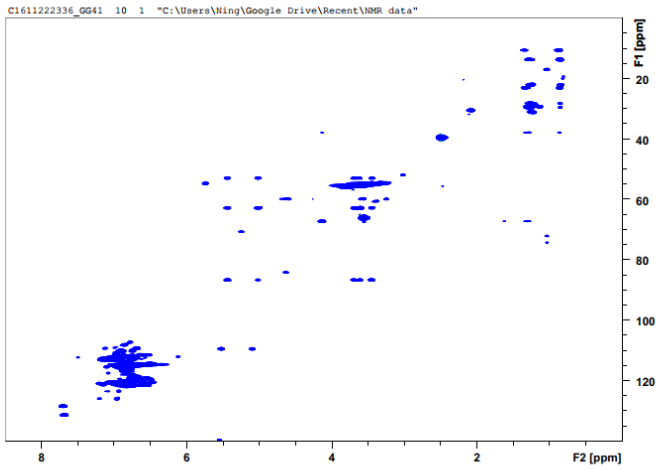

Reference

(1) Upton, B. M.; Kasko, A. M. Strategies for the conversion of lignin to high-value polymeric materials: Review and perspective. *Chemical Reviews* **2015**, *116*, 2275-2306.

(2) Mahmood, N.; Yuan, Z.; Schmidt, J.; Xu, C. C. Depolymerization of lignins and their applications for the preparation of polyols and rigid polyurethane foams: A review. *Renewable and Sustainable Energy Reviews* **2016**, *60*, 317-329.

(3) Rinaldi, R.; Jastrzebski, R.; Clough, M. T.; Ralph, J.; Kennema, M.; Bruijnincx, P. C.; Weckhuysen, B. M. Paving the way for lignin valorisation: recent advances in bioengineering, biorefining and catalysis. *Angewandte Chemie* **2016**, *55*, 8164-8215.

(4) Xu, C.; Arancon, R. A. D.; Labidi, J.; Luque, R. Lignin depolymerisation strategies: Towards valuable chemicals and fuels. *Chemical Society Reviews* **2014**, *43*, 7485-7500.

(5) Sun, Z.; Fridrich, B. l.; de Santi, A.; Elangovan, S.; Barta, K. Bright side of lignin depolymerization: Toward new platform chemicals. *Chemical Reviews* **2018**, *118*, 614-678.

(6) De Gregorio, G. F.; Weber, C. C.; Gräsvik, J.; Welton, T.; Brandt, A.; Hallett, J. P. Mechanistic insights into lignin depolymerisation in acidic ionic liquids. *Green Chemistry* **2016**, *18*, 5456-5465.

(7) Cox, B. J.; Ekerdt, J. G. Depolymerization of oak wood lignin under mild conditions using the acidic ionic liquid 1-H-3-methylimidazolium chloride as both solvent and catalyst. *Bioresource Technology* **2012**, *118*, 584-588.

(8) Cox, B. J.; Jia, S.; Zhang, Z. C.; Ekerdt, J. G. Catalytic degradation of lignin model compounds in acidic imidazolium based ionic liquids: Hammett acidity and anion effects. *Polymer Degradation and Stability* **2011**, *96*, 426-431.

(9) Luterbacher, J. S.; Azarpira, A.; Motagamwala, A. H.; Lu, F.; Ralph, J.; Dumesic, J. A. Lignin monomer production integrated into the γ-valerolactone sugar platform. *Energy & Environmental Science* **2015**, *8*, 2657-2663.

(10) Deuss, P. J.; Scott, M.; Tran, F.; Westwood, N. J.; de Vries, J. G.; Barta, K. Aromatic monomers by in situ conversion of reactive intermediates in the acid-catalyzed depolymerization of lignin. *Journal of the American Chemical Society* **2015**, *137*, 7456-67.

(11) Lahive, C. W.; Deuss, P. J.; Lancefield, C. S.; Sun, Z.; Cordes, D. B.; Young, C. M.; Tran, F.; Slawin, A. M.; de Vries, J. G.; Kamer, P. C.; Westwood, N. J.; Barta, K. Advanced model compounds for understanding acid-catalyzed lignin depolymerization: Identification of renewable aromatics and a lignin-derived solvent. *Journal of the American Chemical Society* **2016**, *138*, 8900-11.

(12) Shuai, L.; Amiri, M. T.; Questell-Santiago, Y. M.; Heroguel, F.; Li, Y.; Kim, H.; Meilan, R.; Chapple, C.; Ralph, J.; Luterbacher, J. S. Formaldehyde stabilization facilitates lignin monomer production during biomass depolymerization. *Science* **2016**, *354*, 329-333.

(13) Miles-Barrett, D. M.; Neal, A. R.; Hand, C.; Montgomery, J. R.; Panovic, I.; Ojo, O. S.; Lancefield, C. S.; Cordes, D. B.; Slawin, A. M.; Lebl, T.; Westwood, N. J. The synthesis and analysis of lignin-bound Hibbert ketone structures in technical lignins. *Organic & Biomolecular Chemistry* **2016**, *14*, 10023-10030.

(14) Yokoyama, T. Revisiting the mechanism of β-*O*-4 bond cleavage during acidolysis of lignin. Part 6: A review. *Journal of Wood Chemistry and Technology* **2014**, *35*, 27-42.

(15) Deuss, P. J.; Lancefield, C. S.; Narani, A.; de Vries, J. G.; Westwood, N. J.; Barta, K. Phenolic acetals from lignins of varying compositions via iron (III) triflate catalysed depolymerisation. *Green Chemistry* **2017**, *19*, 2774-2782.

(16) Aziz, S.; Sarkanen, K. Organosolv pulping (a review). *Tappi Journal* **1989**, *72*, 169-175.

(17) Pan, X.; Arato, C.; Gilkes, N.; Gregg, D.; Mabee, W.; Pye, K.; Xiao, Z.; Zhang, X.; Saddler, J. Biorefining of softwoods using ethanol organosolv pulping: Preliminary evaluation of process streams for manufacture of fuel-grade ethanol and co-products. *Biotechnology and Bioengineering* **2005**, *90*, 473-481.

(18) Rahimi, A.; Ulbrich, A.; Coon, J. J.; Stahl, S. S. Formic-acid-induced depolymerization of oxidized lignin to aromatics. *Nature* **2014**, *515*, 249-52.

(19) Nimz, H.; Casten, R. Chemical processing of lignocellulosics. *European Journal of Wood and Wood Products* **1986**, *44*, 207-212.

(20) Pan, X.-J.; Sano, Y. Atmospheric acetic acid pulping of rice straw IV: Physico-chemical characterization of acetic acid lignins from rice straw and woods. part 2. Chemical structures. *Holzforschung* **1999**, *53*, 590-596.

(21) Li, J.; Henriksson, G.; Gellerstedt, G. Lignin depolymerization/repolymerization and its critical role for delignification of aspen wood by steam explosion. *Bioresource Technology* **2007**, *98*, 3061-8.

(22) Funaoka, M.; Kako, T.; Abe, I. Condensation of lignin during heating of wood. *Wood Science and Technology* **1990**, *24*, 277-288.

(23) Shimada, K.; Hosoya, S.; Ikeda, T. Condensation reactions of softwood and hardwood lignin model compounds under organic acid cooking conditions. *Journal of Wood Chemistry and Technology* **1997**, *17*, 57-72.

(24) Imai, T.; Yokoyama, T.; Matsumoto, Y. Revisiting the mechanism of β-*O*-4 bond cleavage during acidolysis of lignin IV: dependence of acidolysis reaction on the type of acid. *Journal of Wood Science* **2011**, *57*, 219-225.

(25) Lan, W.; Talebi Amiri, M.; Hunston, C. M.; Luterbacher, J. Protection group effects during α, γ-diol lignin stabilization promote high-selectivity monomer production. *Angewandte Chemie* **2017**, *130*, 1-6.

(26) Pan, X.; Shuai, L. Saccharification of lignocellulosic biomass. Wisconsin Research Foundation: 2015.

(27) Shuai, L. Transforming lignocelluloses to sugars and liquid fuels. University of Wisconsin-Madison, 2012.

(28) Li, N.; Pan, X.; Alexander, J. A facile and fast method for quantitating lignin in lignocellulosic biomass using acidic lithium bromide trihydrate (ALBTH). *Green Chemistry* **2016**, *18*, 5367-5376.

(29) Yang, X.; Li, N.; Lin, X.; Pan, X.; Zhou, Y. Selective cleavage of the aryl ether bonds in lignin for depolymerization by acidic lithium bromide molten salt hydrate under mild

conditions. *Journal of Agricultural and Food Chemistry* **2016**, *64*, 8379-8387.

(30) Liu, Y.; Lyu, G.; Ji, X.; Yang, G.; Chen, J.; Lucia, L. A. Analytical pyrolysis pathways of guaiacyl glycerol-β-guaiacyl ether by Py-GC/MS. *BioResources* **2016**, *11*, 5816-5828.

(31) Kim, J.-Y.; Shin, E.-J.; Eom, I.-Y.; Won, K.; Kim, Y. H.; Choi, D.; Choi, I.-G.; Choi, J. W. Structural features of lignin macromolecules extracted with ionic liquid from poplar wood. *Bioresource Technology* **2011**, *102*, 9020-9025.

(32) Jahan, M. S.; Mun, S. P. Isolation and characterization of lignin from tropical and temperate hardwood. *Bangladesh Journal of Scientific and Industrial Research* **2010**, *44*, 271-280.

(33) Tolbert, A.; Akinosho, H.; Khunsupat, R.; Naskar, A. K.; Ragauskas, A. J. Characterization and analysis of the molecular weight of lignin for biorefining studies. *Biofuels, Bioproducts and Biorefining* **2014**, *8*, 836-856.

(34) Wang, G.; Chen, H. Enhanced lignin extraction process from steam exploded corn stalk. *Separation and Purification Technology* **2016**, *157*, 93-101.

(35) Heitner, C.; Dimmel, D.; Schmidt, J. *Lignin and lignans: Advances in chemistry*; CRC press, 2016.

(36) Mansfield, S. D.; Kim, H.; Lu, F.; Ralph, J. Whole plant cell wall characterization using solution-state 2D NMR. *Nature protocols* **2012**, *7*, 1579-89.

(37) Chen, F.; Tobimatsu, Y.; Havkin-Frenkel, D.; Dixon, R. A.; Ralph, J. A polymer of caffeyl alcohol in plant seeds. *Proceedings of the National Academy of Sciences* **2012**, *109*, 1772-1777.

(38) Li, Y.; Shuai, L.; Kim, H.; Motagamwala, A. H.; Mobley, J. K.; Yue, F.; Havkin-Frenkel, D.; Luterbacher, J. S.; Dumesic, J. A.; Ralph, J. "Ideal lignin" facilitates full biomass utilization. *Nature Communication* **2018**. (submitted)

(39) Barta, K.; Warner, G. R.; Beach, E. S.; Anastas, P. T. Depolymerization of organosolv lignin to aromatic compounds over Cu-doped porous metal oxides. *Green Chemistry* **2014**, *16*, 191-196.

(40) Sturgeon, M. R.; Kim, S.; Lawrence, K.; Paton, R. S.; Chmely, S. C.; Nimlos, M.; Foust, T. D.; Beckham, G. T. A mechanistic investigation of acid-catalyzed cleavage of aryl-ether linkages: implications for lignin depolymerization in acidic environments. *ACS Sustainable Chemistry & Engineering* **2013**, *2*, 472-485.

(41) Ito, H.; Imai, T.; Lundquist, K.; Yokoyama, T.; Matsumoto, Y. Revisiting the mechanism of β-*O*-4 bond cleavage during acidolysis of lignin. Part 3: Search for the rate-determining step of a non-phenolic C6-C3 type model compound. *Journal of Wood Chemistry and Technology* **2011**, *31*, 172-182.

(42) Hoo, L. H.; Sarkanen, K. V.; Anderson, C. D. Formation of C6 C2-enol ethers in the acid-catalyzed hydrolysis of erythro-veratrylglycerol-β-(2-methoxyphenyl) ether. *Journal of Wood Chemistry and Technology* **1983**, *3*, 223-243.

(43) Yasuda, S.; Ota, K. Chemical structures of sulfuric acid lignin-Pt. X. Reaction of

syringylglycerol-β-syringyl ether and condensation of syringyl nucleus with guaiacyl lignin model compounds in sulfuric acid. *Holzforschung* **1987**, *41*, 59-65.

(44) Imai, T.; Yokoyama, T.; Matsumoto, Y. Revisiting the mechanism of β-*O*-4 bond cleavage during acidolysis of lignin: Part 5: On the characteristics of acidolysis using hydrobromic acid. *Journal of Wood Chemistry and Technology* **2012**, *32*, 165-174.

(45) Obst, J. R. Kinetics of alkaline cleavage of β-aryl ether bonds in lignin models: significance to delignification. *Holzforschung* **1983**, *37*, 23-28.

(46) Sadula, S.; Oesterling, O.; Nardone, A.; Dinkelacker, B.; Saha, B. One-pot integrated processing of biopolymers to furfurals in molten salt hydrate: understanding synergy in acidity. *Green Chemistry* **2017**, *19*, 3888-3898.

(47) Yoo, C. G.; Zhang, S.; Pan, X. Effective conversion of biomass into bromomethylfurfural, furfural, and depolymerized lignin in lithium bromide molten salt hydrate of a biphasic system. *RSC Advances* **2017**, *7*, 300-308.

(48) Zhang, C.; Li, H.; Lu, J.; Zhang, X.; MacArthur, K. E.; Heggen, M.; Wang, F. Promoting lignin depolymerization and restraining the condensation via an oxidation−hydrogenation strategy. *ACS Catalysis* **2017**, *7*, 3419-3429.

(49) Li, C.; Zhao, X.; Wang, A.; Huber, G. W.; Zhang, T. Catalytic transformation of lignin for the production of chemicals and fuels. *Chemical Reviews* **2015**, *115*, 11559-624.

Chapter 4 Fractionation and controlled hydrolysis of lignocellulose for production of mono-, oligosaccharides and uncondensed lignin

This chapter has been filled, in part, for US Patent application No. 62610472, WARF, Dec. 26, 2017.

Abstract

A simultaneous fractionation and hydrolysis process was demonstrated to produce mono- and oligosaccharides from lignocellulose under mild conditions (110 °C and 0.02-0.24 M HCl) with high feedstock loading (30-80%, w/v) in acidic lithium bromide trihydrate (ALBTH). The lignin fraction, which had undergone negligible condensation, was isolated. The chemical structure of oligosaccharides was investigated and used to elucidate the formation of oligosaccharides produced through controlled hydrolysis and simultaneous glycosylation. In a single-batch operation, poplar at 30% (w/v) solid loading could yield up to 29.7% of glucooligosaccharides (accounting to 63.3% of glucan in poplar) in 60 min. In a fed-batch operation, biomass loading could be ramped to 60% (w/v), yielding maximum soluble mono- and oligosaccharides from glucan (91.0%, oligomer to monomer ratio=1.10) and xylan (90.7%, oligomer to monomer ratio=0.63). The MALDI-TOF MS analysis revealed the degree of polymerization (*DP*) of the oligosaccharides to be in the range of 2-10. The 2D-HSQC NMR identified new glycosidic bonds other than β–1,4 glycosidic bond in the resultant oligosaccharides, including α/β–1,1, α–1,2, α/β–1,3, α–1,4, and α/β–1,6 glycosidic bonds. Using cellulose as a model compound, saccharification at 30% (w/v) substrate loading confirmed the oligosaccharides were generated not only from

controlled hydrolysis of cellulose, but also by glycosylation with glucose, with contributions by controlled hydrolysis and glucose glycosylation of 45% and 55%, respectively.

4.1 Introduction

Sugars are an indispensable resource in the natural world. Sugars, existing primarily in plants in monosaccharide, oligosaccharide and polysaccharide forms, are synthesized through photosynthesis and utilized for energy storage and structural support. Utilizing the predominate form found in nature (lignocellulose, consisting of cellulose and hemicelluloses) ensures sustainable supplies of a renewable resource.[1,2] These abundant plant polysaccharides have been widely recognized as the most promising sources of sugars for future biorefining to fuels, chemicals, and materials via the so-called sugar platform.

Extracting sugars from lignocellulosic biomass is a prerequisite for biorefining based on the sugar platform. Naturally co-existing in plant cell walls with hemicelluloses and lignin, cellulose is the most recalcitrant fraction of the biomass. In order to extract sugars from lignocellulose, various saccharification methods (including pretreatment followed by enzymatic hydrolysis and acid catalyzed hydrolysis) have been extensively studied.[2-5] In the saccharification process, the concentration of resultant sugars is proportional to the initial lignocellulose loading. High final sugar concentrations (above 100 g/L) obtained by increasing lignocellulose loading, are beneficial to downstream operations (i.e., reducing operational costs and energy consumption, and simplifying product purification and chemical recovery).[6,7] Higher lignocellulose loading, however, also increased the viscosity of the saccharification mixture which inevitably impaired the saccharification efficiency, due to deteriorated mass as well as heat transfer.[8] Thus in order to

obtain high resultant sugar concentrations using high lignocellulose loading conditions, it will be necessary to reduce the viscosity of saccharification mixture.

Hydrolysis of polysaccharides (such as cellulose and hemicelluloses) involves the cleavage of the inter-unit glycosidic bonds, and the oligosaccharides intermediates in this process are subsequently converted to monosaccharides (i.e., the hydrolysates generally consist of both mono- and oligosaccharides). Selective production of oligosaccharides, derived from controlled and incomplete hydrolysis of polysaccharides, have drawn increasing attention because they have shown great potential as prebiotics and biofunctional dietary fibers.[9] For example, fructan and xylan were hydrolyzed in dilute HCl (0.54 M) and H_2SO_4 (0.25 M) under mild reaction conditions resulting in oligosaccharides subsequently used in prebiotic production.[10,11] Hydrolysis of cellulosic feedstocks also generated significant amounts of oligosaccharides. Oligosaccharide yields from cellulose could reach up to 50% in certain hydrolysis processes, such as the supercritical water hydrolysis and acidic hydrolysis in γ-valerolactone (GVL).[12,13] The lack of followup investigation of the oligosaccaride chemical structures however, has prevented full realization of their potential to be value-added products.

In our previous studies, saccharification of lignocellulosic biomass was developed in acidic lithium bromide trihydrate (ALBTH) under a normal biomass loading range (1-10%, w/v) to achieve high monosaccharide yields.[14,15] In this study, we explored a facile approach to extract both oligosaccharides and monosaccharides from poplar utilizing the ALBTH system at high biomass loading concentrations (30%-80%, w/v). The process was optimized with the aim of high-yields of aqueous soluble saccharides under mild conditions, while keeping lignin as insoluble and less condensed fractions. The oligosaccharides were isolated and analyzed by matrix assisted laser desorption/ionization time-of-flight mass spectrometry (MALDI-TOF MS) and heteronuclear

single quantum correlation nuclear magnetic resonance spectroscopy (2D-HSQC NMR) in order to identify their chemical structures. Cellulose was employed as a model substrate to elucidate the mechanisms involved in the oligosaccharide formation.

4.2 Experimental

4.2.1 Raw material

Poplar NE222 (harvested in Rhinlander, WI) chips were ground using a Wiley mill, and particles between 20 and 100 mesh were collected as raw material for the present study. The chemical composition of the poplar was determined to be: insoluble lignin 21.4±0.2%, soluble lignin 6.0±0.1%, glucan 46.9±0.0%, arabinan 0.3±0.0%, galactan 0.6±0.0%, xylan 14.5±0.0%, mannan 0.5±0.0% and 95% ethanol extractives 1.8±0.1%. Microcrystalline cellulose (Avicel PH-101, average particle size: ~50 μm,) was purchased from Sigma-Aldrich and used as received.

4.2.2 Biomass saccharification in ALBTH

Saccharification was conducted in 40 mL glass vials with pressure-relief screw tops. In a batch process, poplar powder or microcrystalline cellulose was directly mixed with ALBTH with HCl as the acid catalyst. The mixture was stirred or sonicated in the case of high solid loading at ambient temperature for 5 min before inserting the vial into an aluminum heating block in an oil bath. In the fed-batch experiment, fresh poplar power or microcrystalline cellulose was successively added after liquefaction of the biomass in the previous loading was achieved. After incubating for 10-120 min, the saccharification reaction was quenched by immersing the reaction vial in ice water and diluting the mixture with DI water. Insoluble residues (IR) were collected by filtration using a pre-weighted filtering crucible (30 mL, low form with medium porosity), washed thoroughly with water, and then gravimetrically quantitated. The residual carbohydrates in the IR

were analyzed using the two-step H_2SO_4 hydrolysis (NREL method).[16] The quantification of monosaccharides, oligosaccharides, and sugar degradation products from the resultant supernatant was performed as follows.

Following a post-hydrolysis procedure to convert all oligosaccharides to monosaccharides, the oligosaccharides from glucan (OS-G) and the oligosaccharides from xylan (OS-X)) were quantitated. Briefly, hydrolysate samples (the supernatant above) were diluted with 4% sulfuric acid to a sugar concentration ≤ 5 g/L and hydrolyzed at 121 °C for 1h in an autoclave unit. The total monosaccharides in the hydrolysate were quantitated using a high performance anion exchange chromatography (HPAEC) method described below. The yield of oligosaccharides was calculated from the difference in monosaccharide concentrations before and after post-hydrolysis.

4.2.3 Chromatographic analysis

Chromatographic quantitation of saccharides

Monosaccharides (arabinose, galactose, glucose, xylose, and mannose), cellobiose, isomaltose, gentiobiose, and levoglucosan (LGA) were quantitated using the HPAEC on an ICS-3000 system (Dionex, Sunnyvale, CA) equipped with a pulsed amperometric detector and a 250 mm × 4 mm CarboPac PA1 column (Thermo Scientific, Sunnyvale, CA) at 30 °C. A gradient eluent containing A: deionized water (18 MΩ·cm) and B: 100 mM NaOH was programed: 0-40 min, 80% A and 20% B; 40.1-49 min, 30% A and 70% B; and 49.1-58 min, 80% A and 20% B. An isocratic post-column eluent of 0.5 M NaOH was used at a flow rate of 0.3 mL/min to ensure the baseline stability and to enhance the detector sensitivity.[17]

Chromatographic quantitation of sugar degradation products

Sugar degradation products [5-hydroxymethyl furfural (HMF) and furfural] were quantitated using high performance liquid chromatography (HPLC) on an ICS-3000 system (Dionex, Sunnyvale,

CA) equipped with a 300 mm × 7.8 mm C-610H column (Supelco, Bellefonte, PA) at 30 °C and a UV detector at 280 nm. An isocratic flow of 0.1% phosphoric acid was applied as the mobile phase at 0.6 mL/min.[17]

Calculation equations

IR (wt%) = Mass of insoluble residues / Mass of starting biomass × 100% (4.1)

Product yield (%) = Product mass × Conversion factor / Mass of starting biomass × 100% (4.2)

Conversion factors for glucose, xylose, cellobiose, isomaltose, gentiobiose, LGA, HMF, and furfural are: 0.90, 0.88, 0.95, 0.95, 0.95, 1.0, 1.29, and 1.38, respectively.

OS-G/OS-X (%) = Total monosaccharide yield (after post-hydrolysis) – Monosaccharide yield – Levoglucosan yield (4.3)

4.2.4 MALDI_TOF MS analysis

The MS oligosaccharide spectra were collected on an AB Sciex 4800 MALDI TOF/TOF mass spectrometer (Foster City, CA) equipped with Nd: YAG_200Hz laser at 355 nm. A binary matrix was used to attenuate the background signals, in particular those below m/z 500.[18] Aminopyranize (AP, 2.5 mg/mL) and 2,5 dihydroxybenzoic acid (DHB, 7.5 mg/mL) in acetonitrile were combined with an equal volume of oligosaccharides (2 mg/mL) and then placed on a stainless steel target. After air-drying, the sample spot was exposed to an accumulation of one thousand laser shots to record the MS spectrum.

4.2.5 NMR analysis

The glycosidic linkages of the oligosaccharides from the glycosylation reaction were identified using NMR spectroscopy. Oligosaccharides from poplar and cellulose were directly dissolved in D_2O with 1 wt% of 2,2-Dimethyl-2-silapentane-5-sulfonate sodium salt (DSS) as a reference. Raw

poplar and IR were ball-milled and dispersed in DMSO-d_6/pyridine-d_5. 2D-HSQC NMR spectra were recorded on a Brucker AVANCE 500 MHz instrument (Bilerica, MA) equipped with a DCH cryoprobe. The pulse program "hsqcetgpsisp 2.2 (adiabatic-pulse fashion)" was adopted with 10 ppm (from 9 to -1 ppm) and 200 ppm (from -10 to 190 ppm) sweep widths in ^{1}H and ^{13}C dimensions, respectively. The acquisition time was 200 ms (^{1}H) and 8 ms (^{13}C) and the inter-scan relaxation delay varied from 1s (general analysis) to 10 s (semi-quantitative analysis). The spectra were processed using Topspin 3.2 software to a final 2D matrix size of 2k × 1k data points.

The relative abundance of each interunit linkage R_i, appearing in the aliphatic region of HSQC spectra, from lignin samples was calculated by the following equation:

$$R_i\ \% = I_i / [I_A + I_B + I_C + I_{HK} + I_{BD}] \times 100\% \qquad (4.4)$$

Where I_i, I_A, I_B, I_C, I_{HK}, and I_{BD} denote the α–H/C correlation peak integrals of the target inter-unit linkage i, β–*O*–4 aryl ether **A**, phenylcoumaran (β–5) **B**, resinol (β–β) **C**, **HK**, and benzodioxane **BD** structures; **HK** has two α-protons per unit, so its integral is halved in the relative abundance calculation.

To estimate the relative contents of glycosidic bonds in the oligosaccharide fractions, the anomeric correlation contours of α/β–1,1, α/β–1,2, α/β–1,3, α/β–1,4, and α/β–1,6 glycosidic linkages were integrated for relative comparison due to the similar C-H environment and distinguishable chemical shifts. The anomeric integrals of α/β–1,1 glycosidic linkages were logically halved in the calculation.

4.3 Results and discussion

4.3.1 Single-batch saccharification of poplar in ALBTH

Formation of oligosaccharides was observed during the saccharification of biomass, in particular

at high solid loading, as mentioned above.[12,13] Compared to other systems for lignocellulose saccharification, ALBTH demonstrated excellent performance in dissolving and hydrolyzing cellulose at high biomass solid loading. The yields of mono- and oligosaccharides during the saccharification of poplar in ALBTH were investigated at varied substrate loadings using two acid-addition strategies, as shown in Figure 4.1.

In the first experimental design, the acid concentration in ALBTH was kept constant (40 mM) at varied poplar solid loading (Figure 4.1A). The yield of glucose decreased from 36.9% to 9.4% with increasing solid loading from 5% to 30% (w/v). The release of glucose was impaired at higher solid loading as the liquefaction of the biomass slowed down with increasing the poplar loading and took up to 30 min at 30% (w/v) loading. Interestingly, the insoluble residue (IR) after the saccharification did not proportionally increase with increasing biomass loading. IR showed only a slight increase from 21.4% to 24.9% when poplar loading was elevated from 5% to 20% (w/v). Since the poplar itself contained 21.5% ALBTH insoluble lignin (results in Chapter 2), it is safe to assume that the unhydrolyzed or undissolved carbohydrates in the IR fractions was less than 3%, indicating ALBTH insoluble lignin was fractionated as IR at high purity.

Varying the biomass loading also influenced the oligosaccharide yield. The yields of OS-G increased from 5.4 to 30.3% when the poplar loading was elevated from 5% to 20% (w/v). Since the intial poplar feedstock contained 46.9% glucan, the maximum OS-G yield (30.3%) based on the the poplar mass is equivalent to 64.6% conversion of total glucan to OS-G. Further increasing the poplar loading to 30% resulted in an IR yield of 32%, indicating a certain amount of carbohydrates remained insoluble and also resulted in reduced yields of glucose (9.4%) and OS-G (29.7%). Along with glucan, poplar contains 14.5% xylan. When compared with glucose yields, xylose yields were nearly constant (8.4-10.5%) within a biomass loading range of 5-30% w/v. This

is due to xylan being more vulnerable to acid catalyzed hydrolysis even at low acid concentrations. Approximately 1.3% HMF and 1.9% furfural were detected at 5% (w/v) poplar loading. The yields gradually decreased to 0.1% (HMF) and 0.3% (furfural) when the poplar loading was increased to 30% (w/v). At constant acid catalyst concentrations, the ratio of acid to substrate decreased with poplar loading, which limited the efficiency of hydrolysis and dehydration reactions thus leading to low yields of monosaccharides and furans at high substrate loadings.

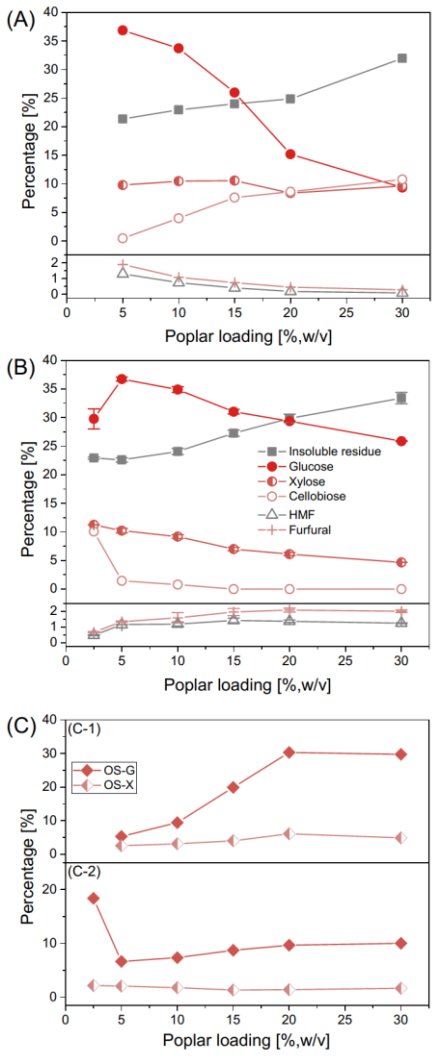

Figure 4.1 Effects of poplar loading (2.5%-30%, w/v) on yields of insoluble residue (IR), aqueous soluble mono- and oligosaccharides, and sugar degradation products at varied acid concentrations

in ALBTH conditions of 110 °C and 60 min. Note: Constant HCl concentration design (40 mM, A and C-1); constant HCl to poplar ratio design (0.8 mmol $_{HCl}$/g $_{poplar}$, B and C-2).

In the second experimental design, poplar saccharification was conducted at a constant acid to poplar ratio (0.8 mmol $_{HCl}$/g $_{poplar}$). This allowed the acid concentration (20-240 mM) to increase proportionally with the poplar loading. The highest glucose yield (36.7%) was still achieved at 5% (w/v) poplar loading and further increases in poplar loading led to a reduced glucose yield of 25.9% at 30% (w/v) loading (Figure 4.1B). Although relation of glucose yield to poplar loading was similar to that in the first strategy, cellulose (glucan) was more extensively hydrolyzed i.e., higher glucose yields than those in the previous experimental design. Liquefaction took less than 3.5 min at even 30% (w/v) poplar loading. It suggests that the sufficient acid catalyst facilitates rapid liquefaction of poplar and extensive hydrolysis of cellulose in ALBTH. The OS-G yields increased from 6.7% to 10.0% when the poplar loading was elevated from 5% (w/v) to 30% (w/v), but the overall yields were nearly 2-3 fold lower than those in the previous saccharification design. The inhibition of oligosaccharide formation is thought to be due to extensive hydrolysis of carbohydrates which also leads to increased amounts of undesired side-products. At a high HCl concentration (120 mM), yields of HMF and furfural were over 1.3 % and 2.0%, respectively. The IR fraction turned black due to humin formation and increased to 33% based on the total poplar mass. Humin formation is assumed to result from the acid catalyzed condensation of furan compounds and monosaccharides.[19] The above results indicate that increasing acid concentration with poplar loading could improve hydrolysis efficiency but decrease oligosaccharide yields and increase sugar degradation products.

In the batch reaction, it was found that 30% (w/v) poplar was the maximum loading (Figure S4.1 in the Appendix) in order to ensure homogeneous mixing. With additional poplar loading,

the ALBTH medium failed to wet the entire biomass even after 1h of sonification. As the acid concentration in ALBTH plays a crucial role in hydrolysis (saccharification) of poplar and the formation of side-products, saccharification at 30% (w/v) poplar loading was further investigated by varying the acid concentration from 40 to 240 mM (Figure 4.2).

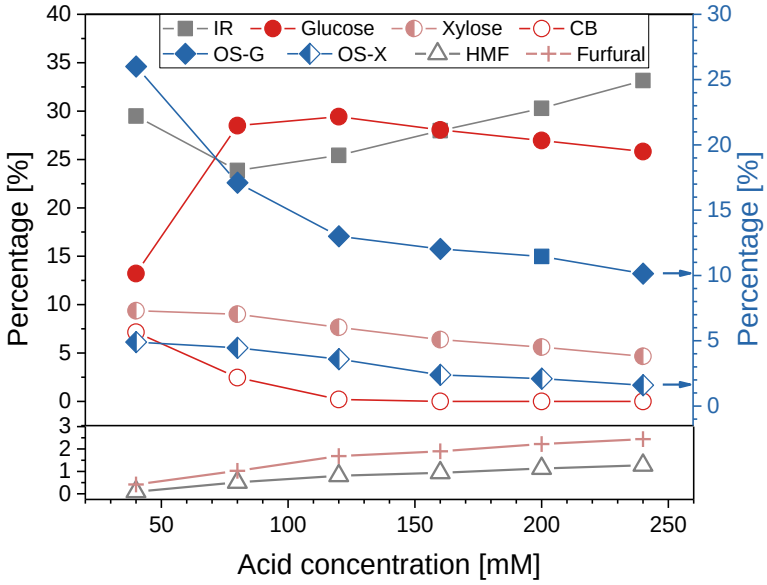

Figure 4.2 Saccharification of poplar at 30% (w/v) loading in ALBTH at varied acid concentration for production of aqueous soluble monosaccharides and oligosaccharides at 110 °C and 60 min.

Increasing acid concentration was proven to shorten liquefaction time. For example, liquefaction of poplar at 30 % (w/v) loading took approximately 30, 8, and 4 min at 40, 80, and 120 mM HCl, respectively. At over 120 mM HCl, liquefaction of poplar was achieved within 3.5 min as shown in Figure S4.1. After saccharification, IR yields first decreased to 23.9% at 80 mM HCl concentration and then gradually increased to 33.2% at 240 mM HCl (Figure 4.2). The initial decrease of IR yields was due to the enhanced hydrolysis of cellulose, which was consistent with the increase in glucose yields. The accumulation of IR at high HCl concentrations was attributed

to acid catalyzed degradation of sugars, as discussed above. At 120 mM HCl, the glucose yields reached 29.4%, equivalent to 63% of total poplar glucan. When the acid concentration was higher than 120 mM, the yields of glucose and xylose started leveling off. It was observed that OS-G yields dropped sharply from 26.0% at 40 mM HCl to 13.0% at 120 mM HCl. It was suggested that the high yield formation of oligosaccharides was dependent on controlled hydrolysis of polysaccharides at low acid concentrations.

4.3.2 A fed-batch technique to enhance the yield of oligosaccharides

The maximum loading of biomass in a single batch was limited due to mixing issues. As biomass underwent prompt liquefaction in the ALBTH system, a fed-batch technique was adopted to further elevate the total biomass loading, which can be easily achieved in industrial operations.[20] In the fed-batch process, 30% (w/v) of poplar was initially loaded. After 5 min when the initial batch of poplar was liquefied, an extra 10% (w/v) of poplar was added. Then, 5% (w/v) of poplar was added every 5 min until 60% (w/v) poplar loading was achieved at 25 min. It was also feasible to increase the solid loading to 80% (30% +10% +10% +10% +10% +10%, w/v) within 60 min. As the lignin fraction was insoluble during the saccharification process, accumulated lignin at the ultra-high biomass loading (i.e., 80%, w/v) eventually deteriorated the rheological properties of the saccharification mixture. As a result, 80% (w/v) poplar loading was the upper limit in this study.

Poplar saccharification proceeded effectively at 60% (w/v) poplar loading. The carbohydrate distribution during poplar saccharification at 60% (w/v) loading in ALBTH under various reaction times (30 and 90 min) and acid (HCl) concentrations (120-240 mM) are summarized in Figure 4.3. After 30 min saccharification at 120 mM HCl, 78.7% of glucan was hydrolyzed to 28.1% glucose and 50.6% OS-G, while 90.5% of xylan was hydrolyzed to 44.3% xylose and 46.2% OS-X. The

oligosaccharide to monosaccharide ratio was higher for glucan (oligomer to monomer ratio (O/M) =1.80) compared to that for xylan (O/M=1.04). There were still 17.4% of glucan and 8.7% of xylan remained insoluble, contributing to the IR fraction. These results demonstrate that xylan is more vulnerable to hydrolysis than glucan. Formation of sugar degradation productions was minor (less than 4% of the total carbohydrates) at 30 min. Extending the reaction time to 90 min, hydrolysis of glucan to glucose increased to 43.4%, while the insoluble residual glucan decreased to 3.0%. OS-G yields were basically unaffected by extending reaction time. Up to 91.0% of glucan and 90.7% of xylan were converted to aqueous soluble mono- and oligosaccharides in ALBTH, which included 43.4% glucose and 47.6% OS-G from glucan and 55.6% xylose and 35.1% OS-X from xylan, respectively. This is the first report of high yields of aqueous soluble sugars obtained from lignocellulose saccharification at such high substrate loading.

Increasing the initial HCl concentration in the fed-batch process increased yields of monosaccharides but decreased oligosaccharide yields. In addition, high acid concentrations enhanced the formation of sugar degradation products. Degradation products were 2.6 fold higherat 240 mM HCl than at 120 mM HCl. These results suggest that extending the reaction time at relative low acid concentrations was preferable for maximizing overall yield of the aqueous soluble mono- and oligosaccharides while limiting undesirable side-products.

The above experiments, even with high poplar loading, demonstrated that oligosaccharides could be produced from poplar via controlled hydrolysis in ALBTH. At 30% (w/v) poplar loading, the O/M of hydrolysis products were in the range of 0.39-0.60 for those from glucan and 0.34-0.52 from xylan. At 60% (w/v) loading, the range of O/M increased to 0.78-1.10 for glucan and 0.63-1.10 for xylan. It suggests that oligosaccharides are preferentially formed at higher substrate loading.

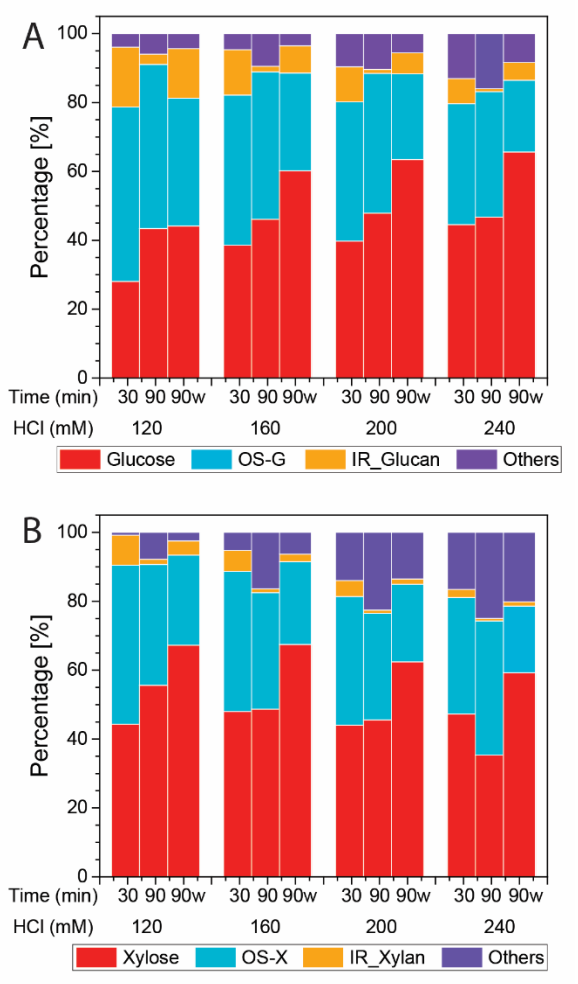

Figure 4.3 Distribution of carbohydrate fractions from ALBTH saccharification of poplar (A. glucan and B. xylan) using a fed-batch technique for a total of 60% (w/v) loading at 110 °C. (Glucose, Xylose, OS-G, OS-X denote the fractions of glucose, xylose, OS-G, OS-X, respectively, in the hydrolysates; IR_Glucan and IR_Xylan denote the insoluble glucan and xylan fractions in the insoluble residues; Others represents additional components including sugar degradation by-products, such as HMF, furfural, humins, etc.; 90w denotes the water addition step in which the hydrate number of ALBTH was transformed from ~3 to 6 by adding extra DI water at 30 min and the total saccharification time was 90 min.)

Another advantage of the fed-batch process in ALBTH involves the co-production of concentrated monomeric sugars with oligosaccharides. As shown in Table S4.1, the monomeric sugar concentrations in the hydrolysates reached 106 g/L (glucose) and 28.5 g/L (xylose) at 60% (w/v) poplar loading and 130 g/L (glucose) and 37 g/L (xylose) at 80% (w/v) poplar loading. These

concentrated fermentable sugar syrups could greatly ease downstream purification and bio-conversion to produce biofuels and biochemicals. Hydrolysis to monosaccharides could be further optimized utilizing a water addition step during hydrolysis. After 30 min of saccharification at 60% (w/v) poplar loading, extra DI water was added to change the hydrate number of ALBTH from 3 to 6 as the hydrolysis intrinsically is a water-addition reaction. Introducing the extra water in the system is postulated to drive the reaction toward monosaccharide production. As shown in Figure 4.3, the conversion of glucan to glucose increased from 46.8% to 65.6% after water addition at 240 mM HCl. Using a preparative ion exclusion column (packed with Dowex 50WX2 resins, Li^+ form), base-line separation between the sugars (glucose and xylose) and LiBr was achieved with over 98% recovery of sugars and 100% recovery of LiBr (Figure S4.2). This chromatography separation method could be incorporated to the simulated moving bed technique for industrial level separation of the hydrolysates.[21]

4.3.3 Structures of the oligosaccharides

In order to probe the structural information of the resulting oligosaccharides and the underlying mechanism of the ALBTH saccharification process, the oligosaccharide fractions were separated from the hydrolysate and purified by precipitation in anti-solvents (ethanol and acetone) followed by freeze-drying. The purified oligosaccharides were in the form of a white powder. The molecular weight distribution of the oligosaccharides was determined using MALDI-TOF MS, as illustrated in Figure 4.4. The oligosaccharides derived from saccharification of poplar were composed of an average of 2-10 sugar units, in agreement with observations from other studies that the oligosaccharides with *DP*>10 were marginally soluble in an aqueous solution.[22] Mass peaks of the oligosaccharides were determined using the formula [GnXm-M, m/z = 18 + 162n + 132m + 23(Na^+)/39(K^+)]. The letters n and m represent the number of anhydrous glucose (G) and xylose

(X) units, respectively, in the oligosaccharides. M stands for the metal adducts which facilitate ionization of the oligosaccharides, including Na^+ and K^+. Under relatively mild conditions (120 mM HCl and 60% (w/v) poplar loading for 30 min), the most intense peaks corresponded to oligosaccharides with a *DP* of 3-5. The oligosaccharides contained either exclusively anhydrous glucose units (Gn-M) or anhydrous glucose units together with one or two anhydrous xylose units (GnXm-M). These results suggest that xylose units can bind to OS-G during ALBTH saccharification.

A

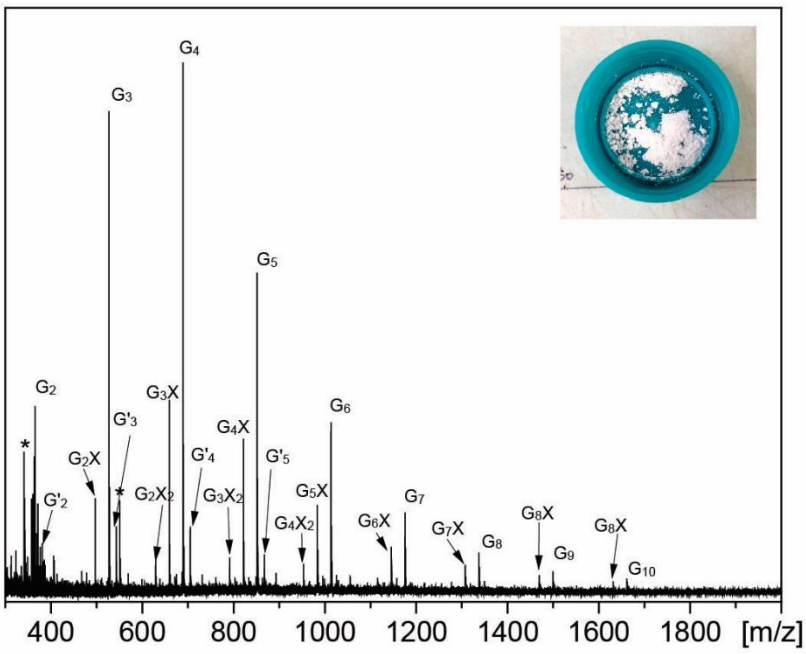

B Table of mass peaks

Peak	Formula	Mass	Rel. Intensity (%)
G_2	G_2-Na	365.1	35.4
G'_2	G_2-K	381.1	9.6
G_2X	G_2X-Na	497.2	18.1
G_3	G_3-Na	527.2	90.8
G'_3	G_3-K	543.1	12.8
G_2X_2	G_2X_2-Na	629.2	6.5
G_3X	G_3X-Na	659.3	36.6
G_4	G_4-Na	689.3	100.0
G'_4	G_4-K	705.2	12.8
G_3X_2	G_3X_2-Na	791.3	7.0
G_4X	G_4X-Na	821.3	29.3
G_5	G_5-Na	851.3	60.4
G'_5	G_5-K	867.2	7.5
G_4X_2	G_4X_2-Na	953.4	5.8
G_5X	G_5X-Na	983.4	16.8
G_6	G_6-Na	1013.4	32.4
G_6X	G_6X-Na	1145.4	9.0
G_7	G_7-Na	1175.4	15.4
G_7X	G_7X-Na	1307.5	5.6
G_8	G_8-Na	1337.5	7.9
G_8X	G_8X-Na	1469.5	3.6
G_9	G_9-Na	1499.5	4.4
G_9X	G_9X-Na	1631.5	2.5
G_{10}	G_{10}-Na	1661.6	3.0

Figure 4.4 The MALDI-TOF MS spectrum (A) and the assignment table (B) of the oligosaccharide fractions from ALBTH saccharification at 60% (w/v) poplar loading under mild conditions. (T: 110 °C, 120 mM HCl, 30 min)

Oligosaccharides are generally viewed as intermediates in the process of polysaccharide hydrolysis to monosaccharides under acidic conditions. Since glucose and xylose units are exclusively linked via β–1,4 glycosidic bonds in native cellulose and xylan chains, the

oligosaccharides derived from partial hydrolysis of these polysaccharides should present a high degree of β–1,4 glycosidic bonds. The glycosidic linkages in the oligosaccharide fraction were identified using 2D HSQC NMR as shown in Figure 4.5. Although most of ^{1}H-^{13}C correlation signals at the C2, C3, C4, and C6 positions of glucose and xylose units overlapped in the region of δ_C/δ_H (62.0-82.4 ppm)/ (3.10-4.00 ppm), assignments of the glycosidic linkages could be made using the distinguishable anomeric (C1) correlation based on the assignments of disaccharide standards and the reported oligosaccharides.[23] The presence of β–1,4 linkages in the oligosaccharides was confirmed from ^{1}H-^{13}C correlation of the anomeric non-reducing C1 at δ_C/δ_H 105.3/4.51 ppm and the C-H in the C4 position at δ_C/δ_H 81.1/3.65 ppm. This indicates that controlled hydrolysis of cellulose contributes to the formation of oligosaccharides. Other glycosidic linkages which did not exist previously in the native biomass were also identified, including α/β–1,1 , α–1,2, α/β–1,3, α–1,4, and α/β–1,6 glycosidic bonds. These results suggest that not only hydrolysis but also glycosylation occurs during the saccharification of poplar using the ALBTH system. Monosaccharides (glucose and xylose) derived from cellulose and hemicellulose hydrolysis might react with the oligosaccharide intermediates, leading to formation of new glycosidic bonds. Since there was overlap between the anomeric C1 signals of the β–1,6 glycosylic linkage and the β–1,4 glycosylic linkage, the appearance of the characteristic correlation contours of CH_2 in the C6 position at δ_C/δ_H 71.5/3.86 ppm and 71.5/4.18 ppm f justified the presence of β–1,6 glycosidic linkage. The correlation signal at δ_C/δ_H 4.45/104.4 ppm from anomeric xylose units linked by β–1,4 glycosidic bonds was not identified, but the anomeric correlation between xylose and glucose glycosylic linkages was resolved, confirming that xylose units were added to OS-G. This observation was in agreement with the MALDI-TOF MS results above. Since these new glycosylic linkages synthesized were distinct to these in the native lignocellulose, their formation

must occur during the acid catalyzed saccharification process in the ALBTH system via intermolecular glycosylation reactions. Based on the MALDI-TOF MS and 2D-HSQC NMR characterization of the oligosaccharide fractions as well as the chromatographic analysis of the hydrolysates, both the controlled hydrolysis of polysaccharides and the simultaneous glycosylation reactions may occur during the process of lignocellulose saccharification in the ALBTH system. This top-down process provides a new insight into synthesis of oligosaccharides with varied glycosidic linkages using inexpensive lignocellulose feedstocks.

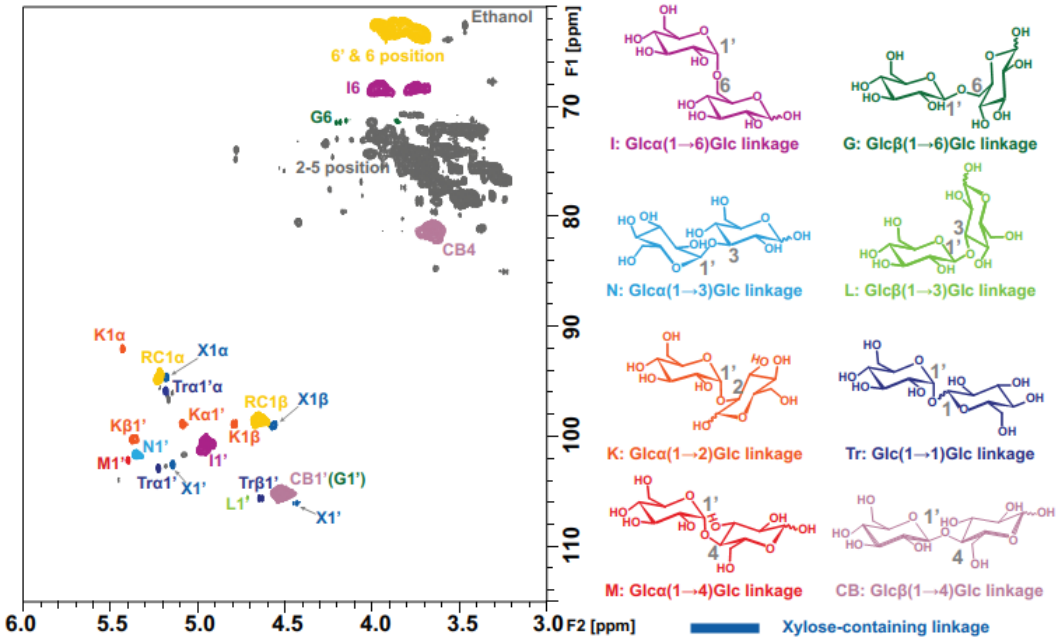

Figure 4.5 ^{1}H-^{13}C HSQC NMR spectrum of oligosaccharides in D_2O from ALBTH saccharification of poplar at 60% (w/v) loading and 110 °C for 90 min. [Oligosaccharide fractions were isolated by anti-solvent (ethanol/acetone) precipitation]

4.3.4 Lignin fraction from the ALBTH saccharification at high poplar loading

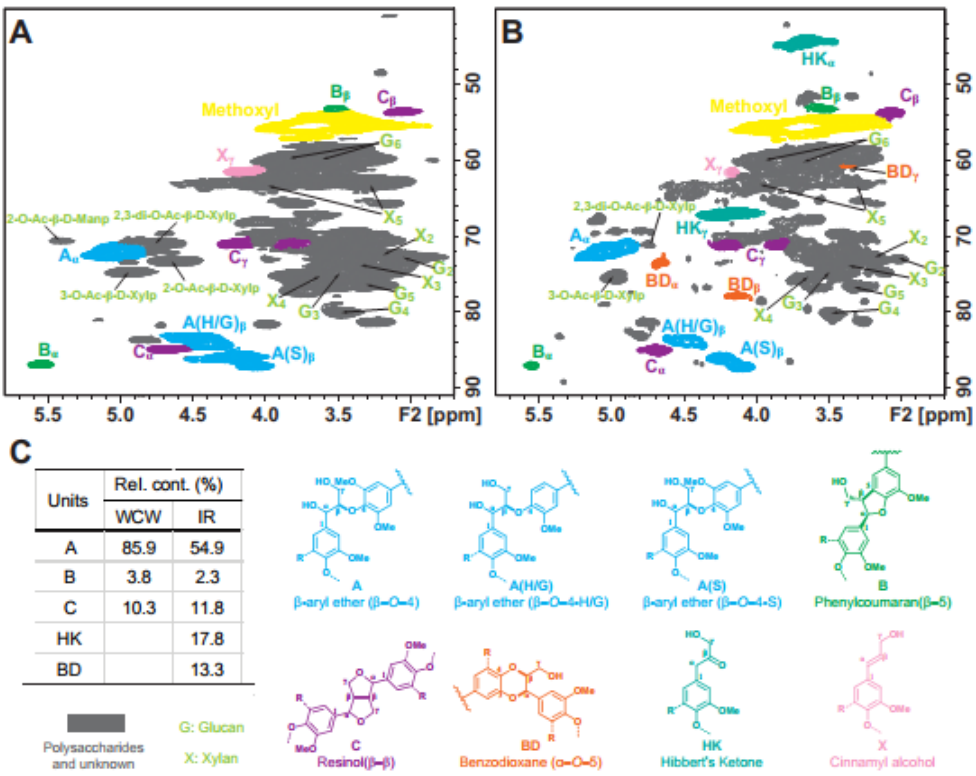

Figure 4.6 The aliphatic regions of 2D ^{1}H-^{13}C correlation (HSQC) spectra from ball-milled poplar cell walls (A) and insoluble saccharification residuals (B) dispersed in DMSO-d_6/pyridine-d_5 and the relative contents of the bonding units (C).

In Chapter 3, the uncondensed lignin with Hibbert's ketone (**HK**) and benzodioxane (**BD**) structures was isolated from lignocellulose in ALBTH by thorough dissolution and hydrolysis of the carbohydrates at low biomass loading. In this chapter, hydrolysis of carbohydrate was conducted under mild conditions to maximize the mono- and oligosaccharide yields at high poplar loading. The ALBTH saccharification at 60% (w/v) poplar loading yielded 25.9%-29.3% IR in which the lignin fraction was predominated (Table S4.1). As illustrated from the 2D-HSQC NMR spectra (Figures 4.6 and S4.3), the IR fractions from poplar saccharification had analogous chemical structures to the ALBTH lignin previously reported in Chapter 3. Carbohydrate related contours also appeared due to a small amount of residual carbohydrates in IR. Due to the mild

saccharification conditions, the lignin present in the IR fraction preserved 64% of the β–*O*–4 aryl ethers, together with uncondensed structures **HK** (21%) and **BD** (15%). Since the majority of the carbohydrates were converted to mono- and oligosaccharides, high-purity lignin could be further upgraded for production of value-added aromatic monomers and oligomers.

4.3.5 Elucidation and confirmation of oligosaccharide formation from cellulose (a top-down process)

To understand the formation of oligosaccharides during the saccharification of lignocellulose in the ALBTH system, cellulose was used as a model substrate to elucidate the mechanism of the oligosaccharide formation, thus eliminating interference from the lignin and hemicellulose fractions. Our previous studies demonstrated that the ALBTH system is capable of disrupting the inter- and intra-molecular hydrogen bonds in cellulose and thereby dissolving cellulose.[14,15] The dissolved cellulose is vulnerable to acidic hydrolysis due to the cleavage of β–1,4 glycosylic bonds, resulting in mono- and oligosaccharides.

OS-G formation during cellulose hydrolysis in ALBTH

The cellulose substrate (Avicel) is insoluble in water and ALBTH at ambient temperature and has a high water retention value. It was found that at 30% (w/v) cellulose loading, a critical point was reached where ALBTH could fully wet cellulose but leave no free solvent. It was then set as the maximum cellulose loading. If the saccharification temperatureis increased to 110 °C, cellulose was liquefied using ALBTH within 2 min and turned to a fully transparent solution in 5-8 min (Figure S4.4). Given these observations, the hydrolysis of cellulose in ALBTH is postulated to be a homogeneous process. Compared to heterogeneous hydrolysis processes in which favor production of monosaccharides, homogenous processes under mild conditions favor

oligosaccharide production.[24,25]

As shown in Figure 4.7, less than 0.3% IR was left over after 5 min, suggesting that cellulose was quantitatively dissolved. Up to 59.7 % OS-X and 32.0% glucose were detected in the hydrolysate (O/M=1.87) whereas hydrolysis of cellulose in organic solvents (such as GVL/water, 9:1, v/v) yielded less than 25% of OS-X with O/M ratio less than 0.6.[12] In another saccharification process (supercritical water hydrolysis), maximum OS-G yields could rapidly reach 50% at extremely high temperatures (360 °C, 0.5 s), while the yield of total aqueous soluble mono- and oligosaccharides was less than 70% with significant amounts of side-products.[13] As far as we are aware, the mechanocatalytic depolymerization of cellulose is the only approach that could obtain OS-G yields higher than 60%. This is possibly due to the nature of the solid state reaction,[22] though scaling-up the mechanocatalytic process still remain challenging because of the necessity for extensive ball milling treatment as well as the presence of concentrated H_2SO_4.[26]

Further extending the hydrolysis time, OS-G yields gradually decreased from 48.1% at 10 min to 36.0% at 60 min, while the yield of glucose increased to 49.0% at 20 min and then proceeded to level off. The increase in glucose yields at the initial stage is attributed to the hydrolysis of cellulose to glucose. Using cellobiose (the β–1,4 glycosidically linked disaccharide) as an indicator of cellulose hydrolysis, cellobiose yields dwindled with hydrolysis time from 14.0% at 5 min to 2.9% and 2.0% at 20 min and 60 min, respectively. This demonstrates that the depletion of cellobiose accompanies the leveling-off of glucose yields.

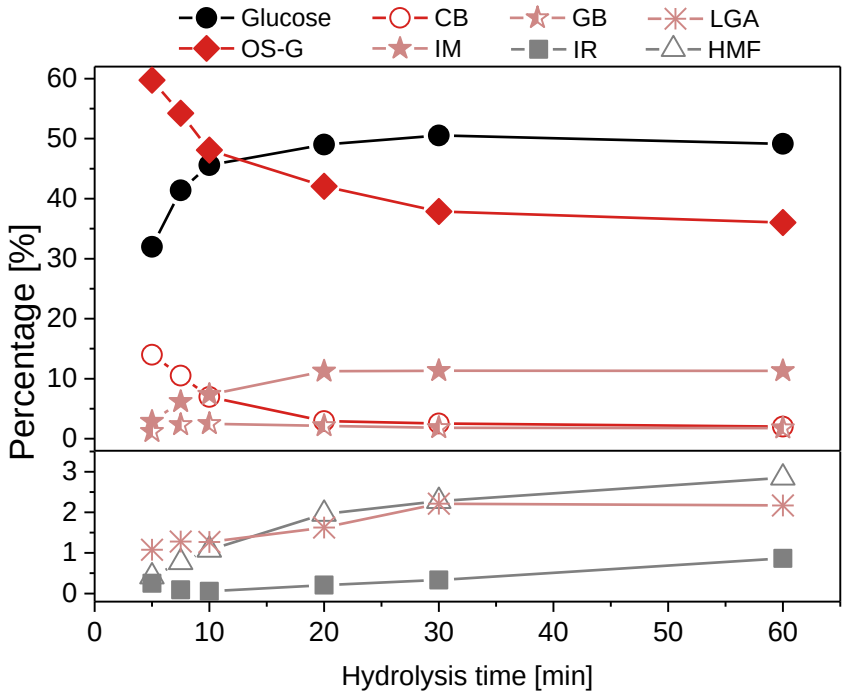

Figure 4.7 Homogenous hydrolysis of cellulose at high substrate loading (30%) in ALBTH (40 mM HCl) to yield OS-G, glucose and glucose degradation products as a function of ALBTH hydrolysis time at 110 °C. (Note: Yields were based on mol% anhydrous glucose unit (AGU) in cellulose expect IR yield which was based on wt% of cellulose)

Table 4.1 Homogeneous hydrolysis of cellulose in ALBTH to yield OS-X and glucose as a function of temperature, acid concentration and reaction time

T (°C)	HCl (mM)	t (min)	Glucose yield (%)	OS-G yield (%)				IR (wt%)	LGA yield (%)	HMF yield (%)
				Total	IM	GB	CB			
90	20	90	29.3	52.9	2.8	0.8	9.8	12.1	0.8	0.4
90	40	150	41.3	51.1	6.6	2.3	8.5	3.7	1.1	0.6
100	20	20	22.3	62.9	1.2	0.3	11.4	10.9	1.6	0.2
100	20	60	33.9	58.0	3.2	1.1	10.8	3.6	2.3	0.5
100	40	10	28.2	66.8	1.8	1.0	12.8	4.8	1.9	0.3
100	40	20	39.2	55.3	5.1	2.1	9.3	0.5	2.5	0.6
110	20	10	29.1	64.0	1.7	0.6	13.4	2.5	2.2	0.4
110	20	20	39.9	54.2	5.2	0.9	9.3	N.D.	3.1	0.8

The leveling off of glucose yields after extended hydrolysis is due to the glycosylation of glucose to OS-G (detailed discussion in Chapter 5). Isomaltose and gentiobiose (α/β–1,6 linked disaccharides) were the primary glycosylation dimers produced in ALBTH. Neither was present in the native cellulose chains, suggesting that glycosylation occurred during cellulose hydrolysis in the ALBTH system. The yields of isomaltose and gentiobiose increased with reaction time to maximum yield of 11.3% and 1.8%, respectively. Gentiobiose yields began declining slightly after reaching a maximum yield at 10 min, while isomaltose yields continued increasing with time. The detection of isomaltose and gentiobiose further confirms that new glycosylic bonds were formed during the process of cellulose saccharification in ALBTH.

Sugar degradation is basically inevitable under acidic conditions. Compared to other acidic hydrolysis processes, the formation of side-products caused by sugar degradation was insignificant during the ALBTH reaction. LGA (via reversible intra-molecular dehydration) and HMF (irreversible dehydration reaction) were detected in a yield range of 1.1-2.2% and 0.4-2.9%, respectively. Negligible amounts of humins (black floccules, less than 0.9% in yield), a result of degradation and condensation of HMF and monosaccharides, were detected within 60 min.

These results indicate that cellulose was homogenously hydrolyzed to glucose and OS-G in the ALBTH system at 30% (w/v) cellulose loading, and glycosylation reactions could also contribute to OS-G formation. In order to maximize OS-G yields, reaction conditions were optimized (Table 4.1). At low reaction temperature (90 °C), the dissolution and hydrolysis of cellulose in ALBTH was limited with cellulose liquefaction taking up to 60 min. After 90 min of reaction, up to 12.1% remained as insoluble cellulose which was neither dissolved nor hydrolyzed. Yields of glucose and OS-G were 29.3% and 52.9%, respectively. Under these conditions, OS-G were generated primarily from the incomplete hydrolysis of cellulose. Cellobiose yield was 9.8%.

Only small amounts of isomaltose (2.8%) and gentiobiose (0.8%) were synthesized, suggesting that the acid catalyzed glycosylation was minor. Increasing the reaction temperature to 100 °C, the liquefaction time shrank to ~12 min at 20 mM HCl and to ~7 min at 40 mM HCl. After 10 min of hydrolysis, 66.8% OS-G and 28.2% glucose were released along with 4.8% of insoluble cellulose residues. Increasing the temperature to 110 °C at 20 mM HCl achieved a similar OS-G yield, but increased isomaltose and gentiobiose yields. Increasing acid concentrations and extending reaction times favored both hydrolysis of cellulose and the release of glucose. Under varied conditions of time, temperature and acid concentration, the maximum glucose yield did not exceed 41%, and OS-G yields were consistently over 50%. As the concentration of glucose increased with hydrolysis, the glycosylation reactions became increasingly significant and retarded the subsequent cleavage of glycosidic bonds. This suggests that both controlled hydrolysis of cellulose and simultaneousglycosylation of glucose contributes to OS-G formation.

In order to further elucidate the mechanism of OS-G formation in ALBTH, the following experiments were designed. The first one involved replacing one third of the cellulose with glucose and cellobiose (equivalent mole glucose units) which resulted in similar glucose and OS-G yields at 110 and 130 °C to the cellulose only control, indicating cellobiose is promptly hydrolyzed to glucose and contributes to OS-G yields via glycosylation. The second experiment involved the effect of adding extra glucose during cellulose hydrolysis on the yield of aqueous soluble sugars. As shown in Table S4.2, under equivalent cellulose loading conditions, the addition of glucose contributed to minor increase in the yield of OS-G from 54.2 to 55.4%, but significantly increased the yields of isomaltose and cellobiose, 25% and 27% higher than the control, respectively. As glycosylation products are not expected to contain β–1,4 glycosylic bonds, the addition of glucose might inhibit the hydrolysis of cellobiose, leading to the accumulation of cellobiose in the system.

Characterization of the oligosaccharides from cellulose hydrolysis

The OS-G from cellulose (30% loading, w/v) saccharification in ALBTH were isolated and purified by the anti-solvent precipitation and characterized using MALDI-TOF MS and 2D-HSQC NMR. For the MALDI-TOF MS spectrum (Figure S4.5), the adduct peaks followed the formula [Gn-M, m/z=18+162n+7(Li^+)/23(Na^+)/39(K^+)], indicating that the OS-G were composed exclusively of anhydrous glucose units. When compared to the spectrum of oligosaccharides from poplar saccharification, there were no anhydrous xylose units linked to OS-G. This observation confirms that xylose units in the poplar oligosaccharides were derived from hydrolysis of xylan in poplar. The *DP* of OS-G from cellulose was primarily from 2 to 10, although trace amounts of OS-G with *DP* up to 16 were detected at the baseline level (Figure S4.5).

The 2D-HSQC NMR spectrum of OS-G from cellulose (Figure 4.8) showed analogous correlation signals for the glycosidic linkages. When compared to that from poplar, the OS-X related signals disappeared. This is consistent with the results from the MALDI-TOF MS analysis. The identical glycosidic linkages of OS-G derived from either cellulose or poplar suggests the formation of OS-G during the saccharification of both cellulose and poplar follow the same mechanism.

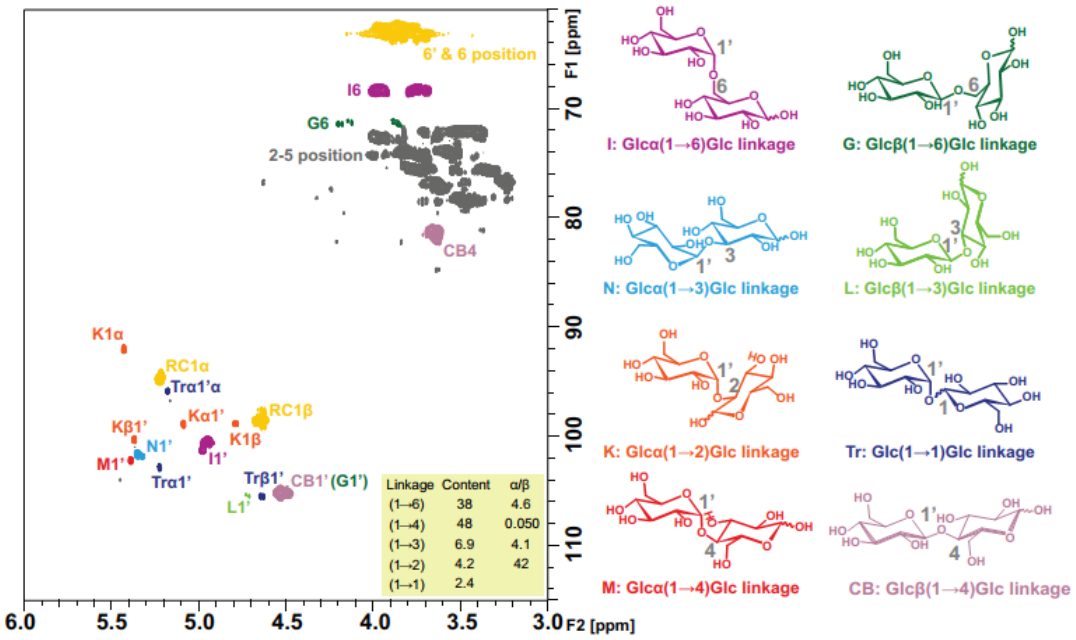

Figure 4.8 ^{1}H-^{13}C HSQC NMR spectrum of OS-G in D_2O from cellulose hydrolysis (30% loading, w/v) in ALBTH (40 mM) at 110 °C for 10 min. [OS-G were isolated by anti-solvent (acetone) precipitation of the hydrolysate; the content of each glycosylic linkage was estimated based on the total glycosylic linkage detected]

In order to evaluate the regio- and stereo-selectivity of the glycosidic bonds in OS-G, a semi-quantitative 2D-HSQC NMR experiment was conducted with a relaxation delay of 10 s. There are several potential factors which could influence the quantitative reliability of the HSQC experiment, including the deviation of coupling constant $^{1}J_{C\text{-}H}$, resonance offset, and relaxation effects (both longitudinal relaxation T1 and transverse relaxation T2).[27,28] Based on the MALDI-TOF MS analysis, the molecular weight of the OS-G was primarily below 1500 Da, so any T2 effects are assumed to be insignificant. The one bond coupling constants ($^{1}J_{C\text{-}H}$) of the anomeric C1-H1 correlations demonstrated little variation (ranging from 158-172 Hz for the $^{1}J_{C\text{-}H}$ of β–anomers, which was 10-15 Hz higher than that of α–anomers). Taking these factors into consideration, the relative abundance of glycosylic linkages in OS-G could be semi-quantitatively estimated using

the general hsqcetgpsisp 2.2 program with a sufficient D1 (10 s). As illustrated in Figure 4.8, 48% and 38% of the glycosylic bonds were determined to be (1→4) and (1→6) glycosidic linkages, respectively. The β–anomer was dominant (95%) in the (1→4) linkages, while the α–anomer was more prevelant in the (1→6) linkages. The β–1,4 glycosidic linkage was inherited exclusively from cellulose and the rest of the glycosidic linkages were created via acid-catalyzed glycosylation reactions. The estimated relative contribution of hydrolysis and glycosylation to OS-G formation from cellulose was approximately 45% and 55%, respectively. The occurrence of the detected glycosidic linkages followed the order of α–1,6 (32%) > β–1,6 (7%) > α–1,3 (6%) > α–1,2 (4%) > α–1,4 (2%) ≈ α/β–1,1 (2%) > β–1,3 (1%). It was reported that the oligosaccharides linked via α/β–1,6, α/β–1,2, and α/β–1,3 glycosylic bonds had potential prebiotic functions.[29-31] Using oligosaccharides produced from the saccharification of lignocellulose and cellulose as potential prebiotics (functional food additives) would be attractive to further explore.

4.4 Conclusions

In this study, saccharification of poplar and cellulose in the ALBTH system at high biomass loading was demonstrated to produce mono- and oligosaccharides under mild conditions (110 °C, 0.02-0.24 M HCl). In a single-batch saccharification, poplar at 30% (w/v) solid loading resulted in maximum yields of OS-G and glucose of 29.7% and 9.4%, respectively, in 60 min. Saccharification of poplar in a fed-batch process increased the poplar loading to 60%-80% (w/v), yielding maximum soluble mono- and oligosaccharides from glucan (91.0%, oligomer to monomer ratio=1.10) and xylan (90.7%, oligomer to monomer ratio=0.63). The oligosaccharide fraction had *DP* 2-10 with an inherited β–1,4 glycosidic bond and newly synthesized α/β–1,1, α–1,2, α/β–1,3, α–1,4, and α/β–1,6 glycosidic bonds. The yield of oligosaccharides was due to both controlled

hydrolysis of polysaccharides and simultaneous glycosylation of monomeric sugars in ALBTH. During the ALBTH saccharification of lignocellulose, carbohydrates were nearly qunatitively transformed to both a concentrated monosaccharide solution (up to 167 g/L) and an oligosaccharide powder with potential prebiotic functions, while the isolated lignin fraction containing abundant β–*O*–4 aryl ethers and uncondensed structures could be further upgraded to value-added aromatics.

Appendix

Table S4.1 Yields of insoluble residues (IR), soluble lignin (Sol. lignin), glucose, xylose, cellobiose (CB), HMF and furfural from 60% (w/v) poplar loading in a fed-batch experiment

HCl (mM)	Time (min)	IR (%)	Sol. lignin (%)	Glucose		Xylose		CB.	HMF yield (%)	Furfural yield (%)
				Yield (%)	Conc.[a] (g/L)	Yield (%)	Conc.[a] (g/L)	Yield (%)		
120	90	25.9	4.1	20.4	92.1	8.1	37.3	3.1	0.3	0.6
160	90	26.1	4.0	21.6	97.8	7.1	32.7	1.1	0.4	0.8
200	90	26.8	3.9	22.4	101.9	6.6	30.7	0.7	0.5	1.0
240	90	28.1	3.7	23.0	105.8	6.0	28.5	0.5	0.4	0.8
200[b]	120	29.3	3.6	17.5	97.3	6.5	37.0	1.6	0.3	0.6
320c	120	29.0	3.4	20.9	130.1	5.8	37.4	0.3	0.5	1.0

Note: a. The concentration of glucose and xylose in hydrolysates was directly determined by HPAEX after filtering the IR fractions;

b. 80% loading was achieved by fed-batch addition of poplar 30% (0 min) with 200 mM HCl+10% (5 min)+10% (10 min)+10% (15 min)+ 10% (20 min)+ 10% (35 min);

c. 80% loading was achieved by fed-batch addition of poplar 30% (0 min) with 200 mM HCl+10% (5 min)+10% (10 min)+10% with 40 mM HCl (15 min)+ 10% with 40 mM HCl (20 min)+ 10% with 40 mM HCl (35 min).

Table S4.2 Effects of glucose and cellobiose addition on homogenous hydrolysis of cellulose in ALBTH

T (°C)	Loading (%, w/v) Cell/CB/G	HCl/t (mM/min)	Glucose Yield (%)	OS-G yield (%)				IR (wt%)	LGA yield (%)	HMF yield (%)
				Total	IM	GB	CB			
110	30/0/0	20/20	39.9	54.2	5.2	0.9	9.3	N.D.	3.1	0.8
	30/0/10	20/20	39.6	55.4	6.5	0.8	11.8	0.4	2.8	0.8
	30/0/0	40/10	45.6	48.1	7.4	1.2	6.6	N.D.	1.3	1.1
	20/10/0	40/10	49.8	44.4	8.6	1.0	5.3	N.D.	1.3	1.4
	20/0/10	40/10	51.4	44.2	9.3	1.0	7.1	N.D.	1.4	1.5
130	30/0/0	40/10	53.2	36.1	8.4	0.9	0.8	N.D.	2.0	3.1
	20/10/0	40/10	53.7	35.1	8.6	0.7	1.0	N.D.	2.1	3.6
	20/0/10	40/10	54.3	35.5	8.6	0.8	0.9	N.D.	1.6	3.7

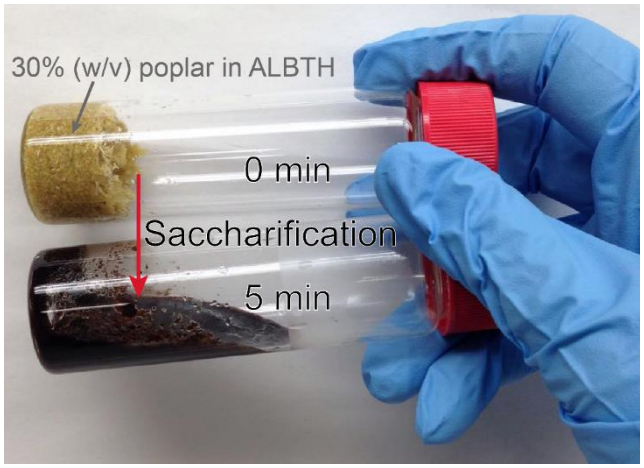

Figure S4.1 Liquefaction of poplar at 30% (w/v) loading in ALBTH at 110 °C for 5 min.

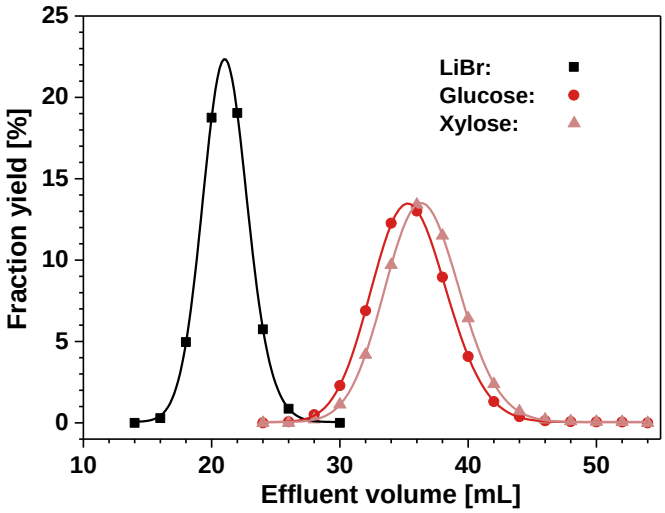

Figure S4.2 Chromatographic separation of LiBr, glucose and xylose on a preparative ion exclusion column. (18cm ×1.5 cm, Dowex 50WX2 resin, Li^+ form)

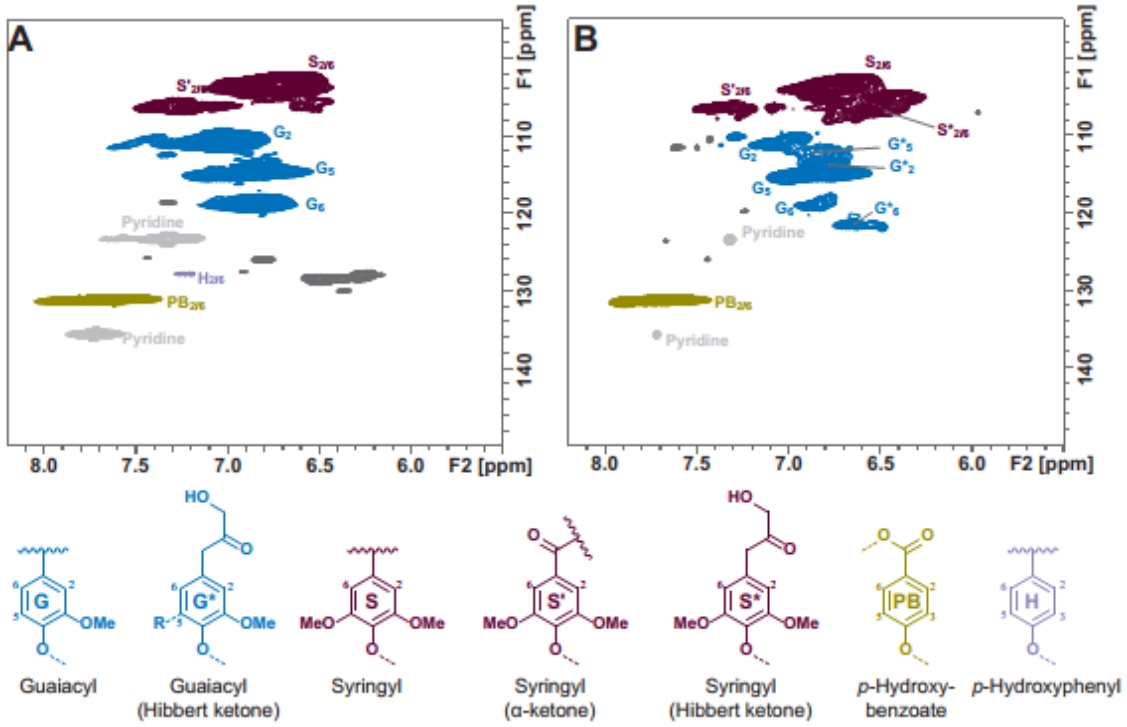

Figure S4.3 The aromatic regions of 2D ^{1}H-^{13}C correlation (HSQC) spectra of ball-milled poplar cell walls (A) and insoluble saccharification residuals (B) dispersed in DMSO-d_6/pyridine-d_5.

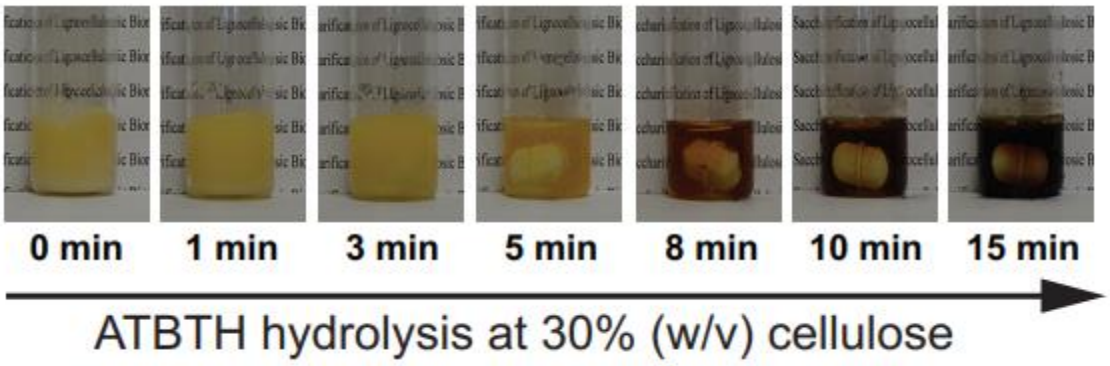

Figure S4.4 Dissolution and hydrolysis of cellulose at 30% (w/v) loading in ALBTH (40 mM HCl) at 110 °C.

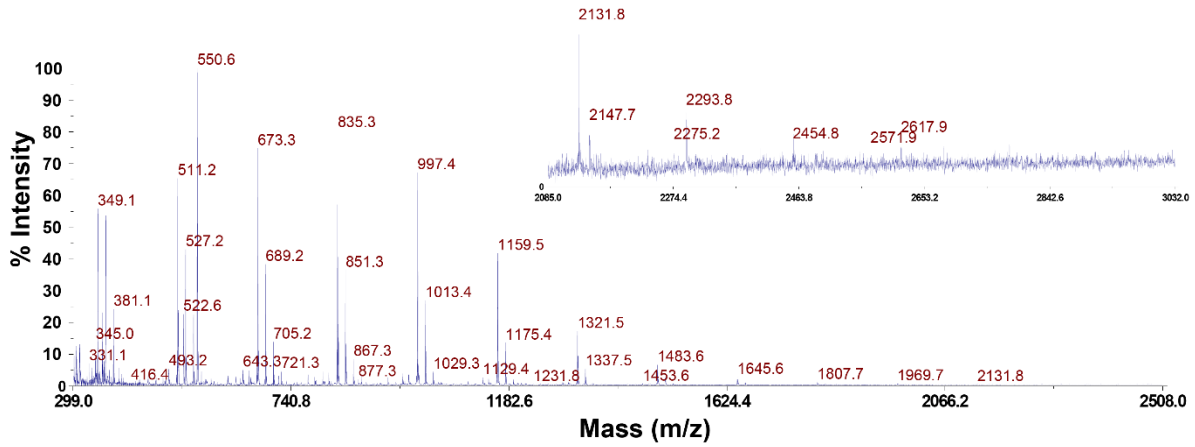

Figure S4.5 MALDI-TOF MS spectrum of oligosaccharides from ALBTH saccharification of cellulose at 30% (w/v) loading for 10 min under mild reaction conditions. (T: 110 °C and 40 mM)

Reference

(1) Alvira, P.; Tomás-Pejó, E.; Ballesteros, M.; Negro, M. Pretreatment technologies for an efficient bioethanol production process based on enzymatic hydrolysis: a review. *Bioresource Technology* **2010**, *101*, 4851-4861.

(2) Wang, J.; Xi, J.; Wang, Y. Recent advances in the catalytic production of glucose from lignocellulosic biomass. *Green Chemistry* **2015**, *17*, 737-751.

(3) Rinaldi, R. Plant biomass fractionation meets catalysis. *Angewandte Chemie* **2014**, *53*, 8559-8560.

(4) Chandra, R. P.; Bura, R.; Mabee, W.; Berlin, d. A.; Pan, X.; Saddler, J. Substrate pretreatment: The key to effective enzymatic hydrolysis of lignocellulosics? In *Biofuels*; Springer: 2007, p 67-93.

(5) Luterbacher, J.; Alonso, D. M.; Dumesic, J. Targeted chemical upgrading of lignocellulosic biomass to platform molecules. *Green Chemistry* **2014**, *16*, 4816-4838.

(6) Modenbach, A. A.; Nokes, S. E. Enzymatic hydrolysis of biomass at high-solids loadings–a review. *Biomass and Bioenergy* **2013**, *56*, 526-544.

(7) Kristensen, J. B.; Felby, C.; Jørgensen, H. Yield-determining factors in high-solids enzymatic hydrolysis of lignocellulose. *Biotechnology for Biofuels* **2009**, *2*, 11.

(8) Du, J.; Cao, Y.; Liu, G.; Zhao, J.; Li, X.; Qu, Y. Identifying and overcoming the effect of mass transfer limitation on decreased yield in enzymatic hydrolysis of lignocellulose at high solid concentrations. *Bioresource Technology* **2017**, *229*, 88-95.

(9) Gullón, P.; Moura, P.; Esteves, M. a. P.; Girio, F. M.; Domínguez, H.; Parajó, J. C.

Assessment on the fermentability of xylooligosaccharides from rice husks by probiotic bacteria. *Journal of Agricultural and Food Chemistry* **2008**, *56*, 7482-7487.

(10) Ávila-Fernández, Á.; Galicia-Lagunas, N.; Rodríguez-Alegría, M. E.; Olvera, C.; López-Munguía, A. Production of functional oligosaccharides through limited acid hydrolysis of agave fructans. *Food Chemistry* **2011**, *129*, 380-386.

(11) Akpinar, O.; Erdogan, K.; Bostanci, S. Production of xylooligosaccharides by controlled acid hydrolysis of lignocellulosic materials. *Carbohydrate Research* **2009**, *344*, 660-666.

(12) Luterbacher, J. S.; Rand, J. M.; Alonso, D. M.; Han, J.; Youngquist, J. T.; Maravelias, C. T.; Pfleger, B. F.; Dumesic, J. A. Nonenzymatic sugar production from biomass using biomass-derived γ-valerolactone. *Science* **2014**, *343*, 277-280.

(13) Buffiere, J.; Ahvenainen, P.; Borrega, M.; Svedström, K.; Sixta, H. Supercritical water hydrolysis: a green pathway for producing low-molecular-weight cellulose. *Green Chemistry* **2016**, *18*, 6516-6525.

(14) Pan, X.; Shuai, L. Saccharification of lignocellulosic biomass. Wisconsin Research Foundation: 2015.

(15) Li, N.; Pan, X.; Alexander, J. A facile and fast method for quantitating lignin in lignocellulosic biomass using acidic lithium bromide trihydrate (ALBTH). *Green Chemistry* **2016**, *18*, 5367-5376.

(16) Sluiter, A.; Hames, B.; Ruiz, R.; Scarlata, C.; Sluiter, J.; Templeton, D.; Crocker, D. *Determination of structural carbohydrates and lignin in biomass*, National Renewable Energy Laboratory, 2012.

(17) Shuai, L.; Yang, Q.; Zhu, J.; Lu, F.; Weimer, P.; Ralph, J.; Pan, X. Comparative study of SPORL and dilute-acid pretreatments of spruce for cellulosic ethanol production. *Bioresource Technology* **2010**, *101*, 3106-3114.

(18) Hashir, M. A.; Stecher, G.; Bonn, G. K. Identification of low molecular weight carbohydrates employing new binary mixtures for matrix-assisted laser desorption/ionisation mass spectrometry. *Rapid Communications in Mass Spectrometry* **2008**, *22*, 2185-2194.

(19) Dee, S. J.; Bell, A. T. A study of the acid-catalyzed hydrolysis of cellulose dissolved in ionic liquids and the factors influencing the dehydration of glucose and the formation of humins. *ChemSusChem* **2011**, *4*, 1166-1173.

(20) Goldrick, S.; Ştefan, A.; Lovett, D.; Montague, G.; Lennox, B. The development of an industrial-scale fed-batch fermentation simulation. *Journal of Biotechnology* **2015**, *193*, 70-82.

(21) Caes, B. R.; Van Oosbree, T. R.; Lu, F.; Ralph, J.; Maravelias, C. T.; Raines, R. T. Simulated moving bed chromatography: Separation and recovery of sugars and ionic liquid from biomass hydrolysates. *ChemSusChem* **2013**, *6*, 2083-2089.

(22) Meine, N.; Rinaldi, R.; Schüth, F. Solvent-free catalytic depolymerization of cellulose to water-soluble oligosaccharides. *ChemSusChem* **2012**, *5*, 1449-1454.

(23) Roslund, M. U.; Tähtinen, P.; Niemitz, M.; Sjöholm, R. Complete assignments of the ^{1}H and ^{13}C chemical shifts and $J_{H,H}$ coupling constants in NMR spectra of D-glucopyranose and all D-glucopyranosyl-D-glucopyranosides. *Carbohydrate Research* **2008**, *343*, 101-112.

(24) Rinaldi, R.; Palkovits, R.; Schüth, F. Depolymerization of cellulose using solid catalysts in ionic liquids. *Angewandte Chemie International Edition* **2008**, *47*, 8047-8050.

(25) Himmel, M. E.; Ding, S.-Y.; Johnson, D. K.; Adney, W. S.; Nimlos, M. R.; Brady, J. W.; Foust, T. D. Biomass recalcitrance: engineering plants and enzymes for biofuels production. *science* **2007**, *315*, 804-807.

(26) Kaufman Rechulski, M. D.; Käldström, M.; Richter, U.; Schüth, F.; Rinaldi, R. Mechanocatalytic depolymerization of lignocellulose performed on hectogram and kilogram scales. *Industrial & Engineering Chemistry Research* **2015**, *54*, 4581-4592.

(27) Zhang, L.; Gellerstedt, G. Quantitative 2D HSQC NMR determination of polymer structures by selecting suitable internal standard references. *Magnetic Resonance in Chemistry* **2007**, *45*, 37-45.

(28) Claridge, T. D. *High-resolution NMR techniques in organic chemistry*; Elsevier, 2016; Vol. 27.

(29) Rycroft, C.; Jones, M.; Gibson, G. R.; Rastall, R. Fermentation properties of gentio-oligosaccharides. *Letters in Applied Microbiology* **2001**, *32*, 156-161.

(30) Kaulpiboon, J.; Rudeekulthamrong, P.; Watanasatitarpa, S.; Ito, K.; Pongsawasdi, P. Synthesis of long-chain isomaltooligosaccharides from tapioca starch and an in vitro investigation of their prebiotic properties. *Journal of Molecular Catalysis B: Enzymatic* **2015**, *120*, 127-135.

(31) Sanz, M. L.; Gibson, G. R.; Rastall, R. A. Influence of disaccharide structure on prebiotic selectivity in vitro. *Journal of Agricultural and Food Chemistry* **2005**, *53*, 5192-5199.

Chapter 5 High-yield synthesis of glucooligosaccharides (GlOS) from glucose via non-enzymatic glycosylation as potential prebiotics

This chapter has been filled, in part, for US Patent application No. 62610472, WARF, Dec. 26, 2017.

Abstract

This study demonstrated a process for high-single pass yield (up to 75%) and high-selectivity (~99%) synthesis of glucooligosaccharides (GlOS) from glucose via non-enzymatic glycosylation reaction in acidic lithium bromide trihydrate (ALBTH, a concentrated aqueous solution of LiBr containing a small amount of acid) system. It was revealed through MALDI-TOF MS, GPC, and HSQC NMR analysis that the synthesized GlOS were composed of 2-9 anhydrous glucose units, which were linked predominantly via α/β–1,6 glycosidic bonds (69%), followed by α/β–1,3, α/β–1,2, α/β–1,1, and α–1,4 glycosidic bonds. The enhanced glycosylation in ALBTH was attributed to the unique properties of the ALBTH including the low water concentration, the high capacity of dissolving glucose, and the enhanced acid dissociation in the system. Preliminary *in-vitro* fermentation tests with select probiotic strains verified the prebiotic potential of the GlOS.

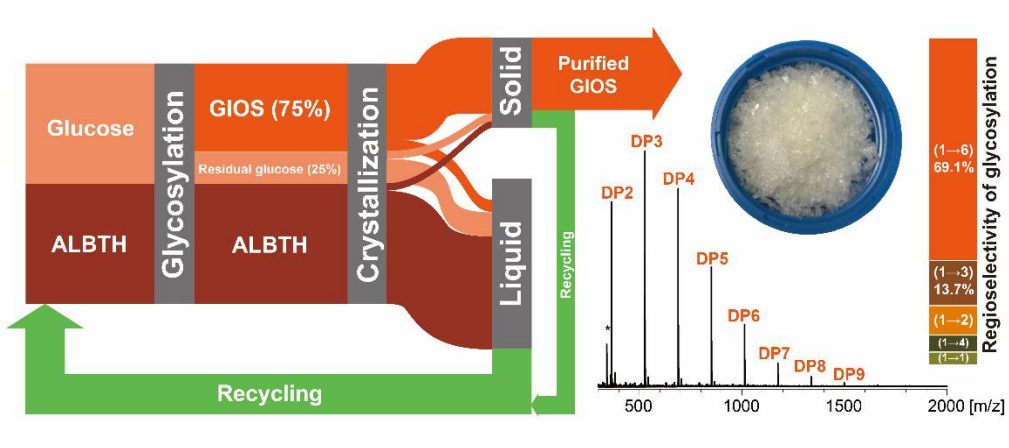

5.1 Introduction

Oligosaccharides, generally refer to the oligomers of sugar units linked by glycosidic bonds with degrees of polymerization (*DP*) between 2 and 10.[1] Certain types of oligosaccharides exhibit prebiotic properties, such as fructooligosaccharides (FOS), galactooligosaccharides (GOS), xylooligosaccharides (XOS), isomaltooligosaccharides (IMO), and pectooligosaccharides (POS), etc.[1-3]. It is believed that they can survive (not digested) from the upper gastrointestinal tract and then can be selectively metabolized by beneficial bacteria in colon, thus modulating the composition and/or activity of the gut microbiota and improving host health.[4] Intake of the prebiotics (oligosaccharides) can confer direct physiological benefits by stimulating growth of bifidobacteria and lactobacilli, which leads to increased production of short-chain fatty acids (SCFA) in the colon. SCFA have been linked to a range of systemic health implications, including inhibition of pathogenic microorganisms, constipation alleviation, obesity reduction, improvement of mineral absorption, repression of allergic symptoms, enhancement of immune system, reduction of colon cancer, and modulation of cholesterol levels.[1,4-9] Not surprisingly, there is increasing interest to exploit oligosaccharides as supplementary ingredients in food industry, which affords a boosted global market expanding from ~$3.2 billion in 2016 to ~6.0 billion as expected in 2022.[10]

The prebiotic activities of oligosaccharides greatly depend on their compositions of sugar units, the type of glycosidic linkages, and *DP*,[2,8] which are determined by the sources and production methods of the oligosaccharide. There are two different ways to get oligosaccharides, top-down approach (hydrolyzing parent polysaccharides to oligosaccharides) and bottom-up approach (synthesizing oligosaccharides from simple sugars). The top-down approach uses enzymes or acids to partially and selectively cleave the glycosidic bonds in the polysaccharides to obtain oligosaccharides.[2] For example, FOS, XOS and POX have been produced from the hydrolysis of inulin, xylan and pectin, respectively.[11-13] Since both sugar units and glycosidic linkages are inherited from their parent polysaccharides, the oligosaccharides prepared from the controlled hydrolysis have limited variation. Other challenges of this method include the high cost of the hydrolytic enzymes[14] and the limited supply of the parent polysaccharides.

In the bottom-up approach, synthesis of oligosaccharides from simple sugars is achieved by forming new glycosidic bonds between the sugars units via glycosylation and transglycosylation catalyzed by enzymes or acids. This approach is attractive because oligosaccharides with varied glycosidic bonds and sugar units can be synthesized from inexpensive and abundant simple sugars, instead of their scarce polysaccharides. Enzymatic glycosylation is to synthesize oligosaccharides using glycosyl transferases and glycosyl hydrolases. For example, IMO, GOS, and FOS were produced by α–glycosidases, galactosidase, and β–fructofuranosidase/inulosucrase, respectively, with yields ranging from 40 to 55%.[15-17]

Acids can also catalyze the glycosylation reactions. The acid-induced glycosylation of glucose was described as early as in 1954.[18] Disaccharides such as gentiobiose, isomaltose, maltose, cellobiose, nigerose, kojibiose, sophorose, and trehalose were detected when treating cellulose or glucose in acidic aqueous systems.[18-20] Recently, dimers of xylose were detected in the dilute acid

pretreatment of biomass, containing 1→1, 1→2, 1→3, and 1→4 (the most abundant) glycosidic bonds.[21] To our knowledge, the products from the acid-catalyzed glycosylation in these studies were primarily disaccharides with a yield below 20%, and no oligosaccharides were identified with *DP*>2. In addition, traditional acid-catalyzed processes unavoidably generated undesired side-products such as hydroxymethylfurfural (HMF) and organic acids due to sugar degradation at high temperature (120-140 °C) and acid concentration (over 100 mM H^+).[20]

While investigating the saccharification/hydrolysis of cellulose and lignocellulosic biomass in acidic lithium bromide trihydrate (ALBTH, $LiBr{\cdot}3H_2O$) system, oligosaccharides were detected in the hydrolysates.[22,23] They were initially believed to be the result of incomplete hydrolysis of cellulose. However, after further examining the structure of the resultant oligosaccharides, it was realized that glycosylation reaction occurred in the system since non β–1,4 glycosidic bonds were identified in the oligosaccharides, which do not naturally exist in either cellulose or its hydrolysis products. The following concept-proof tests further disclosed that oligosaccharides were synthesized from monosaccharides in the ALBTH system. This study reports a high-yield process to synthesize glucooligosaccharides (GlOS) as potential prebiotics directly from glucose in the ALBTH system. The structure, *DP*, and glycosidic bonds of the resultant GlOS were identified and estimated using matrix-assisted laser desorption/ionization-time of flight mass spectrometry (MALDI-TOF MS), gel permeation chromatography (GPC), and nuclear magnetic resonance (NMR) spectroscopy, respectively. The mechanisms underlying the enhanced glycosylation of glucose in the ALBTH system were discussed. The potential of the GlOS as prebiotics to support the growth of gut probiotics was investigated via *in-vitro* fermentation.

5.2 Experimental

5.2.1 Chemicals

D-Glucose (98%), levoglucosan (99%), levulinic acid (98%), phosphoric acid (85wt%), and aminopyrazine (98%) were purchased from Acros Organics (Pittsburgh, PA). D-Gentiobiose (98%), lithium bromide (99%), formic acid (97%), oxalic acid (98%), and 5-hydroxymethyl-2-furaldehyde (HMF, 98%) were purchased from Alfa Aesar (Tewksbury, MA). D-Maltose (94%), isomaltose (97%), acetone (99.5%), acetonitrile (HPLC grade), and acetic acid (99.8%) were purchased from Fisher Scientific (Pittsburgh, PA). Methanol (99.8%), ethyl alcohol (anhydride), sodium hydroxide (50%), hydrochloric acid (37%), sulfuric acid (98%), and citric acid (99%) were purchased from VWR (Radnor, PA). *p*-Toluenesulfonic acid monohydrate (TsOH, 98.5%), dichloroacetic acid (DCA, 99%), 2,5-hydroxybenzonic acid (DHB, 98%), and deuterium oxide (D_2O, 99.9 atom% D with 1% 3-(trimethylsilyl)-1-propanesulfonic acid, DSS) were purchased from Sigma Aldrich (St. Louis, MO). All the chemicals were used as received without further purification.

5.2.2 Glucose glycosylation reaction

Glycosylation reaction of glucose was conducted in acidic LiBr solution in a 40-mL glass reactor heated in an oil bath under atmospheric pressure. Unless specified, glucose (0.05-20.0 g) was initially mixed with 5 mL of acidic LiBr solution using a Teflon-coated magnetic stirring bar, and the mixture was heated up to the reaction temperature (50-110 °C) within 2 min and maintained at this temperature for the duration of the reaction. After the glycosylation, the reactor was quenched by immersing the glass reactor in ice water.

The GlOS from the glycosylation reaction were separated and recovered by precipitation in acetone as an anti-solvent. In brief, the syrup-like mixture after the glycosylation reaction was first diluted with methanol (equivalent to 2, 5, 15 folds of the volume of the reaction mixture) and

subsequently transferred dropwise to 300 mL acetone in a centrifuge bottle immersed in ice water with vigorous agitation to precipitate the GlOS. The acetone insoluble GlOS fraction was collected by centrifugation at 4500 rpm for 20 min, further purified by repeating the procedure of dissolution in water and precipitation in acetone, and finally freeze-dried to yield the colorless GlOS crystal for subsequence characterization.

5.2.3 Quantitation of acetone, methanol, and LiBr

Methanol and acetone were quantitated using a gas chromatography (GC-2014, Shimadzu, MD) with a flame ionization detector (FID) and a 30 m × 0.32 mm × 0.5 μm (length × inner diameter × film thickness) ZB-Wax Plus column. The oven temperature was kept at 100 °C for 5 min and gradually increased to 180 °C in 20 min. LiBr was quantitated using Mohr's titration method.[24]

5.2.4 Fermentability of the GlOS synthesized from glucose glycosylation

Lactic acid bacteria (LAB) from humin intestine including *Lactobacillus reuteri* (ATCC 6475), *Lactobacillus rhamnonsus* GG, *Lactobacillus casei* BFLM 218, and *Lactobacillus gasseri* ATCC 33323 were kindly provided from Dr. Pijkeren's lab and *Lactobacillus buchneri* (ATCC 4005), *Bifidobacterium bifidum* (ATCC 29521), and *Bifidobacterium animalis* (DSM 10140) were generously provided by USDA ARS culture collection (NRRL). The strains were reactivated at 37 °C under anaerobic conditions on MRS medium (ATCC medium 416) for LAB and on Reinforcement Clostridial Medium for *Bifidobacteria* (ATCC medium 2107).

Fermentability of the GlOS by the probiotic strains was evaluated by the anaerobic fermentation experiment in a Hungate tube at 37 °C. The modified MRS fermentation broth and Reinforcement Clostridial Medium fermentation broth were reconstituted without glucose, as described below. Modified MRS medium for LAB stains: dissolve peptone (1.0 g), beef extractive (1.0 g), yeast extractive (0.5 g), NaCl (0.4 g), dipotassium phosphate (0.4 g), ammonium citrate

(0.4 g), manganese sulfate (0.01 g), magnesium sulfate (0.02 g), Tween 80 (0.2 g), and L-cysteine-HCl (0.1 g) in 200 mL deionized (DI) water and adjust the pH to 6.80 ± 0.05 under anaerobic condition. Modified Reinforcement Clostridial broth (pre-reduced) for *Bifidobacteria*: dissolve peptone (1.0 g), beef extractive (1.0 g), yeast extractive (0.5 g), dipotassium phosphate (0.4 g), sodium chloride (0.4 g), ammonium citrate (0.4 g), manganese sulfate (0.01 g), magnesium sulfate (0.02 g), ferrous sulfate (0.002 g), Tween 80 (0.2 g), resazurin (0.0002 g), and L-cysteine-HCl (0.1 g) in 200 mL DI water and adjust the pH to 6.80 ± 0.05 under anaerobic condition. Filter-sterilized GlOS solution and glucose solution as positive control were mixed with the fermentation broth to yield a final carbohydrate concentration of 10 g/L. The pre-cultured cells were washed twice with PBS (phosphate-buffered saline) buffer, and a cell suspension of approximately O.D. = 0.1 was inoculated anaerobically for 24-48 h. The sample medium without inoculation was used as negative control. The cell growth was monitored by the changes in optical density at 600 nm (OD) from duplicated fermentation experiments.

Consumption of carbohydrate substrates and production of short-chain fatty acid (SCFA) in the fermentation broths after 24-48 h growth at 37 °C were quantitated using chromatographic methods, as described below.

5.2.5 Chromatographic quantitation of saccharides

Glucose, disaccharides (isomaltose and gentiobiose), and levoglucosan were quantitated using a high performance anion exchange chromatography (HPAEC) on an ICS-3000 system (Dionex, Sunnyvale, CA) equipped with a pulsed amperometric detector and a 250 mm × 4 mm (length × inner diameter) CarboPac PA1 column (Thermo Scientific, Sunnyvale, CA) at 30 °C. A gradient eluent containing A: deionized water (18 MΩ) and B: 100 mM NaOH was programed as 0-40 min, 80% A and 20% B; 40-49 min, 30% A and 70% B; and 49-58 min, 80% A and 20% B. An isocratic

post-column eluent of 0.5 M NaOH was used at a flow rate of 0.3 mL/min to ensure the baseline stability and to enhance the detector sensitivity.[25]

5.2.6 Quantitation of GlOS

Quantitation of the total GlOS was conducted following a post-hydrolysis procedure that converted all the GlOS ($DP \geq 2$) to glucose before HPAEC analysis. Briefly, the syrup-like mixture (including residual glucose and GlOS) after the glycosylation reaction was diluted with 4% sulfuric acid to a total sugar concentration ≤ 5 g/L and hydrolyzed at 121 °C for 1h in an autoclave unit to convert GlOS to glucose. After neutralization, glucose in the hydrolysate was quantitated using the HPAEC method described above. The free glucose in the syrup-like mixture before the hydrolysis was quantitated using the same HPAEC method. The yield and selectivity of the GlOS was then calculated following Eq. 5.1 and 5.2.

$$\text{GlOS yield (\%)} = \frac{\text{Glu(mol, post-hydrolysis)} - \text{Glu(mol, after glycosylation)} - \text{LGA (mol, after glycosylation)}}{\text{Glu(mol, before glycosylation)}} \quad (5.1)$$

$$\text{GlOS selectivity (\%)} = \frac{\text{Glu(mol, post-hydrolysis)-Glu(mol, after glycosylation)-LGA (mol, after glycosylation)}}{\text{Glu(mol, before glycosylation)-Glu(mol, after glycosylation)}} \quad (5.2)$$

5.2.7 Quantitation of sugar degradation products and SCFA

The sugar degradation products including formic acid, levulinic acid, 5-hydroxymethyl furfural (HMF), and SCFA (acetic acid, propionic acid, and butyric acid) were quantitated using a high performance liquid chromatography (HPLC) on an ICS-3000 system (Dionex, Sunnyvale, CA) equipped with a 300 mm × 7.8 mm (length × inner diameter) C-610H column (Supelco, Bellefonte, PA) at 30 °C and a VWD detector at 210 nm. Isocratic 0.1% phosphoric acid was used as the mobile phase at a flow rate 0.6 mL/min.[25]

5.2.8 Characterization of GlOS

MALDI-TOF MS analysis

The molecular weight distribution of the GlOS was estimated by mass spectrometry in a positive ionization mode using an AB Sciex 4800 MALDI TOF/TOF mass spectrometer (Foster City, CA) equipped with Nd: YAG_200Hz laser at 355 nm. To attenuate the background signals, in particular those below m/z 500, a binary matrix mixture was applied.[26] The matrix containing aminopyranize (AP, 2.5 mg/mL) with 2,5 dihydroxybenzoic acid (DHB, 7.5 mg/mL) in acetonitrile was combined with an equal volume of a GlOS sample (2 mg/mL) and then placed on a stainless steel target. After air-drying, the sample spot was exposed to an accumulation of one thousand laser shots to record a MS spectrum.

GPC analysis

The degree of polymerization of GlOS was estimated using GPC after derivatizing the hydroxyl groups of the GlOS with phenylisocyanate to form GlOS tricarbanilates. First, 30 mg GlOS was dried in a Duran bottle (100 mL) in a vacuum oven at 50 °C for 12 h. Then anhydrous pyridine (6 mL) and phenyl isocyanate (2 mL) were added. The bottle was sealed with a screw thread cap with a PTFE faced silicone liner, and the mixture was reacted in an incubating shaker at 70 °C and 80 rpm for 48 h. The derivatization reaction was quenched by adding methanol (5 mL) and then cooling in an ice bath. The mixture was transferred dropwise to a mixture of methanol/water (35 mL, 7/3, v/v) and glacial acetic acid (1 mL). The precipitates of GlOS derivatives were collected by centrifugation at 8000 rpm, washed twice with the methanol/water mixture, and then vacuum-dried at 50 °C.

GPC analysis was carried out on a Dionex ICS-3000 system (Dionex, Sunnyvale, CA) equipped with three tandem 300 mm × 7.8 mm (l × i.d.) Phenogel 5U columns (10000, 500, and 50 Å, respectively) and a 50 mm × 7.8 mm (l × i.d.) Phenogel 5U guard column (Phenomenex,

Torrance, CA). The eluent was an isocratic 100% THF (HPLC grade without stabilizer) at a flow rate of 1.0 mL/min, and the column temperature was kept at 30 °C. The derivatized GlOS (10 mg/mL in THF) was injected after passing through a 0.45 μm syringe filter and detected with a variable wavelength detector (VWD) at 270 nm. The apparent weight average molecular weight (M_w) was calibrated using polystyrene standards. The weight average degree of polymerization (*DP*) of the GlOS was calculated using Eq. 5.3.

$$DP = M_w/519 \tag{5.3}$$

where 519 g/mol is the molecular weight of the repeating unit of the derivatized GlOS.

NMR analysis

The glycosidic linkages of the GlOS from the glucose glycosylation reaction were identified using NMR spectroscopy. The GlOS were dissolved in D_2O with 1% DSS as reference. ^{1}H-^{13}C heteronuclear single quantum correlation (HSQC) spectra were recorded on a Brucker AVANCE 500 MHz instrument (Bilerica, MA) equipped with a DCH cryoprobe. Bruker pulse program "hsqcetgpsisp 2.2 (adiabatic-pulse fashion)" was used with spectral widths of 10 ppm (from 9 to -1 ppm) and 160 ppm (from 155 to -5 ppm) for the ^{1}H and ^{13}C dimensions, respectively. The acquisition time for ^{1}H and ^{13}C was 200 ms and 8 ms, respectively, with the relaxation delay of 1-10 s. The spectra were processed using Topspin 3.5 software with a final 2D matrix size of 2k × 1k data points. To estimate the regio- and stereo- selectivity, the anomeric correlation contours of α/β–1,1, α/β–1,2, α/β–1,3, α–1,4, and α/β–1,6 glycosidic linkages were integrated for relative comparison due to the similar C-H environment and distinguishable chemical shifts. The anomeric integrals of α/β–1,1 glycosidic linkages were logically halved in the calculation.

5.3 Results and discussion

5.3.1 Synthesis of GlOS from glucose glycosylation in ALBTH

The formation of new glycosidic bonds in glucose glycosylation under acidic condition is via nucleophilic substitution (Figure 5.1A). Protonation of C1 hydroxyl results in a C1 carbocation intermediate (glycosyl donor) after releasing a water molecule. The C1 carbocation is stabilized by an oxocarbenium resonance structure, and trapped by a hydroxyl group of adjacent glucose molecules (glycosyl acceptor).[27] The subsequent deprotonation by releasing a proton back to the solvent medium yields a new glycosidic bond. The glucose glycosylation reaction in the ALBTH system was investigated at varied temperatures (70-110 °C), and results are shown in Figure 5.1B and 5.1C. At the conditions shown in Figure 5.1B, over 41.6 mol% of glucose was consumed in less than 2 min. The turnover frequency (TOF) of glucose consumption exceed 20.0 $mol_{glucose} \cdot mol_{HCl}^{-1} \cdot min^{-1}$. The GlOS yield ascended to a maximum (39.5%) at 10 min with product selectivity up to 87%. The GlOS yield decreased with reaction time because undesired byproducts were formed. The GIOS selectivity also decreased with reaction time. Accompanied with the glycosylation, glucose underwent reversible intramolecular condensation to form 1,6–anhydro–β–D–glucopyranose (LGA) (Reaction 1 in Figure S5.1). Irreversible dehydration glucose formed 5-hydroxymethylfurfural (HMF) (Reaction 2 in Figure S5.1), followed by subsequent rehydration of HMF to form levulinic acid (LA) and formic acid (FA) (Reaction 3 in Figure S5.1). The glucose concentration reached an asymptote with time on stream at all temperatures suggesting that this reaction was equilibrium limited. Equilibrium was reached at around 10 min at 110 °C, after which the sugar degradation products became noticeable (Figure 5.1C). For instance, the yields of HMF and organic acids (LA and FA) increased from 1.5% and 0.9% at 10 min to 3.2% and 2.0% at 60 min, respectively.

Lowering the reaction temperature from 110 °C to 70 °C reduced the rate of glucose conversion

(expressed as TOF) from 20.0 $mol_{glucose} \cdot mol_{HCl}^{-1} \cdot min^{-1}$ to 1.8 $mol_{glucose} \cdot mol_{HCl}^{-1} \cdot min^{-1}$. However, the maximum GIOS yield increased at lower temperature. For example, the GlOS yield increased to 42.3 % at 90 °C and 60 min (Figure 5.1B) and 47.5% at 70 °C and 240 min (Figure S5.2), respectively. The yields of glucose degradation reactions were attenuated at lower temperatures. As shown in Figure 5.1C, 3.2% HMF was detected at 110 °C and 60 min, while only 0.9% and 0.1% HMF at 90 °C and 70 °C, respectively. LA and FA followed the same trend and became negligible at 70 °C. The LGA yield also decreased to less than 1.3% with decreasing temperature. At lower temperature, higher GlOS selectivity (up to 94%) could be reached (Figure 5.1B). However, further lowering temperature to 50 °C decreased the glycosylation reaction rate to very low levels. For example, glucose conversion to GlOS hardly exceeded 25% over 12 h at 50 °C. Isomaltose (an α–1,6 linked dimer of glucose) and gentiobiose (a β–1,6 linked dimer) were identified as the most abundant disaccharides from the glucose glycosylation in the ALBTH system. The highest yields of isomaltose (IM) and gentiobiose (GB) were 12.2% and 4.1 % (110 °C) and 13.8% and 2.7% (70 °C), respectively (Figure 5.1B). Gentiobiose reached the highest yield faster than isomaltose, indicating that the β–glycosidic bond might be kinetically more favorable to form than the α–glycosidic bond during the glycosylation.

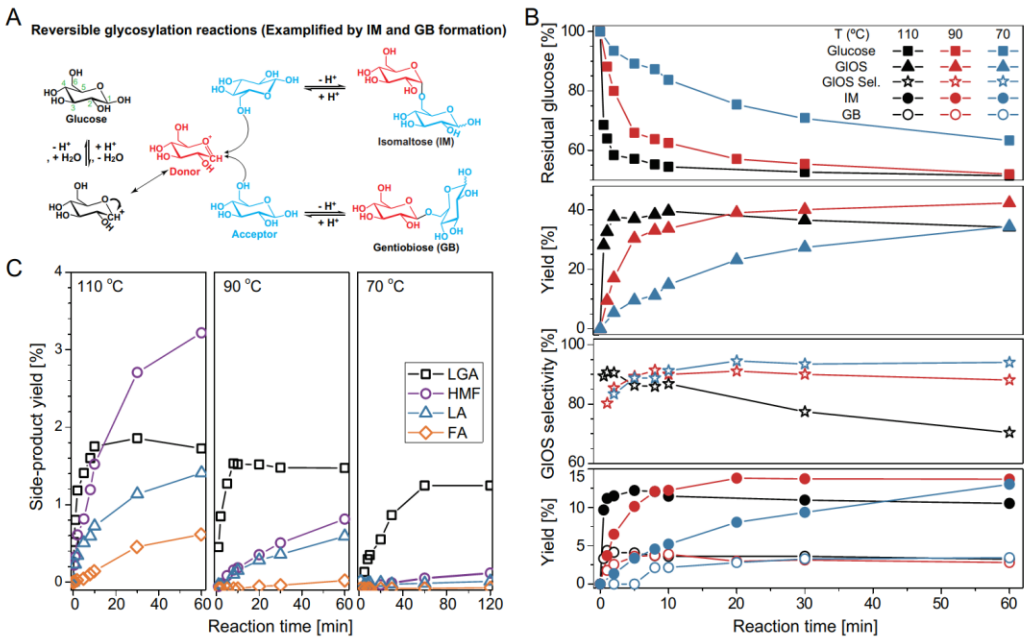

Figure 5.1 Synthesis of GlOS from glycosylation of glucose in ALBTH at three temperatures (70, 90, and 110 °C). A. Chemistry of acid-catalyzed glycosylation of glucose (e.g., formation of α/β–1,6-glycosidic linkages); B. GlOS yield and selectivity as a function of reaction time; C. Yield of side-products as a function of reaction time. The glycosylation reaction was conducted with 19% (w/w) initial glucose concentration in 60% LiBr (LiBr trihydrate) with 40 mM HCl. GlOS, IM, GB, LGA, HMF, LA, and FA denote total glucooligosaccharides, isomaltose, gentiobiose, levoglucosan, hydroxymethylfurfural, levulinic acid, and formic acid, respectively. GlOS selectivity, by definition, is the molar percentage of glucose units in the synthesized GlOS based on the total consumed glucose units.

5.3.2 Identification and characterization of GlOS

The synthesized GlOS from glucose in ALBTH were colorless crystals (Figure 5.2A). MALDI-TOF MS analysis indicated that the GlOS were a mixture of oligosaccharides of glucose with 2 to 9 recurring units (Figure 5.2A). The peaks observed in the spectrum had an interval of 162, suggesting that the oligosaccharides were exclusively composed of glucose units. The incorporation of the sugar degradation products (such as LGA, HMF, and organic acids) into GlOS was not observed because of the absence of corresponding peaks in the MS spectrum. The relative intensity of the GlOS peaks in the MALDI-TOF MS spectrum suggested that most of the

oligosaccharides were composed of 2 to 5 glucose units. *DP* of the GlOS was further estimated by GPC chromatography. As shown in Figure 5.2B, the GlOS had an average *DP* of 2.9, composed of approximately 35% disaccharides and 65% oligosaccharides (*DP*>2). The most abundant oligosaccharides were trisaccharides (45%), followed by tetrasaccharides (15%) and pentasaccharides (4%), along with only a small amount (~1%) of larger oligosaccharides (*DP*>5). These results were in agreement with the MALDI-TOF MS spectrum (Figure 5.2A), suggesting that the majority (~65%) of the oligosaccharides from glucose glycosylation in ALBTH had *DP* higher than 2. This is distinct from the traditional acid-induced glycosylation in water where the oligosaccharides with *DP*>2 were negligible.[19-21]

The glycosidic linkages formed in the GlOS were characterized using 2D-HSQC NMR in D_2O (Figs. 5.2C and S5.3). The ^{1}H-^{13}C correlation contours of the GlOS were assigned according to the references of di- and oligosaccharide standards.[28] There glycosidic linkages identified in the GlOS samples include α/β–1,1, α/β–1,2, α/β–1,3, α–1,4, and α/β–1,6 glycosidic bonds. No β–1,4 glycosidic bond was detected, which is exclusive in cellulose and has the characteristic contour of C4–H4 correlation at δ_C/δ_H 81.1/3.65 ppm. Cellobiose (β–1,4 glycosidic dimer) was not detected in the high performance anion exchange chromatogram of the GlOS (Figure S5.4), confirming that the β–1,4 glycosidic linkage was not formed during the glucose glycosylation in ALBTH.

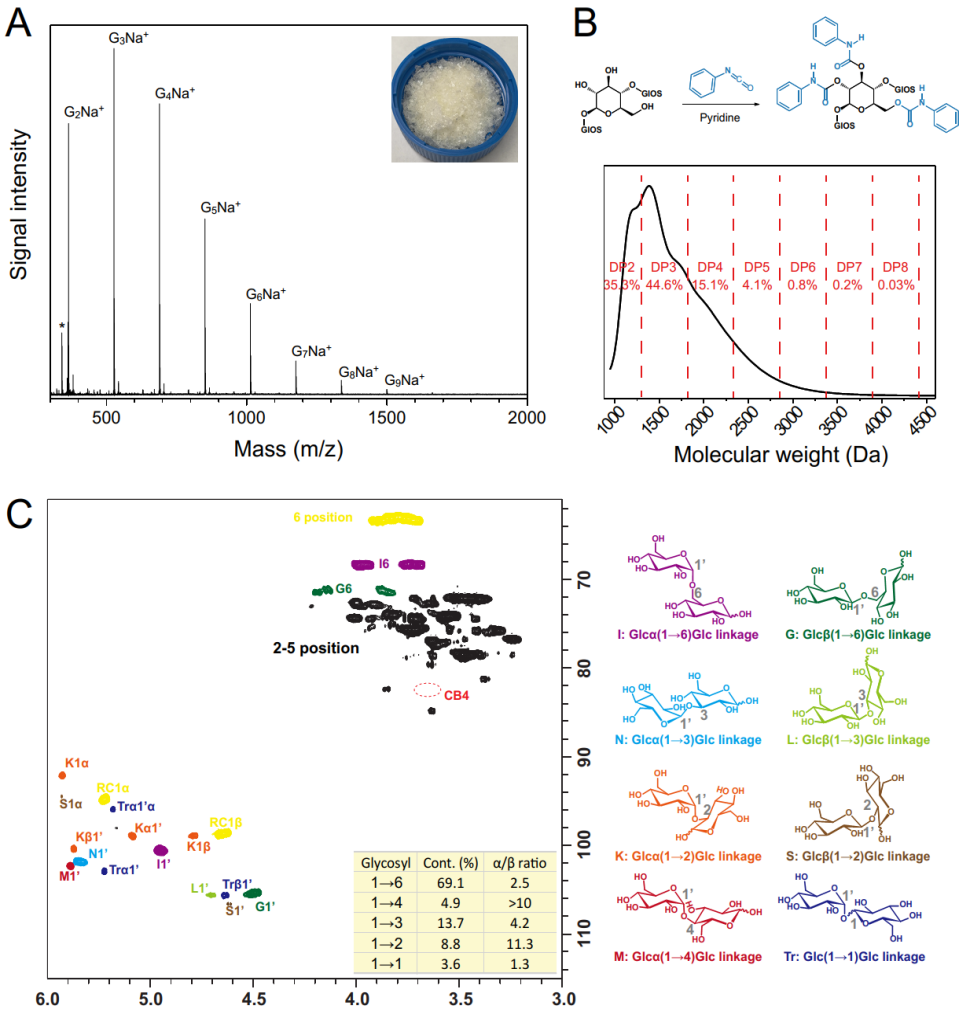

Figure 5.2 Identification and characterization of the GlOS produced from the acid catalyzed glycosylation reaction of glucose in ALBTH using the MALDI-TOF MS spectrum (A), in which the MS peaks (G_nNa^+) assigned by with their corresponding m/z values represent the GlOS containing *"n"* units of glucose *"G"*; the GPC chromatogram after derivatization of GlOS (B); and the 2D-HSQC NMR spectrum (C), in which the chemical shifts are referred by 3-(trimethylsilyl)-1-propanesulfonic acid (DSS). Note: The glycosylation was conducted at 19% (w/w) initial glucose concentration and 70 °C in ALBTH with 40 mM HCl for 2 h.

Semi-quantitative HSQC NMR analysis was conducted to investigate the regio- and stereo-selectivity of the glucose glycosylation in ALBTH (Figure 5.2C and Table S5.1). Although the standard "hsqcetgpsisp 2.2" pulse program is theoretically non-quantitative, a relative comparison of the anomeric integrals is valid because of the insignificant T2 effects on the GlOS (molecular weight less than 1500 Da) and the comparable bond coupling constants ($^1J_{C\text{-}H}$) among various

anomeric C1-H1 correlations (158-172 Hz for β–anomers and 10-15 Hz lower for α–anomers)[29-31] The semi-quantitative results indicated that the 1→6 glycosidic linkage was the most abundant one (69.1%), followed by other glycosidic linkages in the order of 1→3 (13.7%) > 1→2 (8.8%) > 1→4 (4.9%) ≈ 1→1 (3.6%). The observation suggested that the 1→6 glycosidic linkages were the most regio-selective in the glucose glycosylation reaction. In terms of the stereo-selectivity, it is apparent that the α–anomeric linkages were more selective. For example, the (1→6), (1→3), and (1→2) glycosidic linkages had α to β conformation ratios of 2.5, 4.2, and 11.3, respectively. Considering the fact that the abundance of the α–1,4 glycosidic linkage was 4.9% and no β–1,4 glycosidic linkage was observed, the α/β ratio of (1→4) glycosidic linkage was even higher than others. The prevalence of the α–glycosidic linkages (axial orientation) over the β-glycosidic bonds (equatorial orientation) was due to the anomeric effect. Although the anomeric carbocation (sp^2 hybridized) had no spatial disparity to trap a glycosyl acceptor either from the bottom (α–glycoside) or from the top (β–glycoside) side, the α-anomers were more thermodynamically favorable because of the electron repulsive interaction and hyperconjugation effect.[27] The possible reasons why 1→6 glycosidic linkages were less stereo-selective than 1→2, 1→3, and 1→4 glycosidic linkages included: 1) the primary C6 hydroxyl group is the most accessible and the least stereo-controlled glycosyl acceptor, compared to the secondary hydroxyls (C2–OH, C3–OH, and C4–OH) and the hemiacetal hydroxyl (C1–OH); 2) there is little energetic disparity in forming α– and β–1,6 glycosidic linkages. In addition, the presence of the methylene group on C6–OH reduces the steric hindrance of nucleophilic substitution between the two bulky sugar units. Similar observations were reported in the glucose glycosylation catalyzed by glycosidases and H_2SO_4.[20,32] Increasing the glycosylation temperature from 70 to 110 °C (Table S5.1) led to marginal changes in the abundance of the glycosidic bonds and the ratio of α/β conformations, indicating the regio-

and stereo-selectivity of the glycosylation was barely affected by reaction temperature in the range investigated.

5.3.3 Mechanisms underlying the enhanced glucose glycosylation in ALBTH

The results above have demonstrated the enhanced performance of glucose glycosylation in ALBTH with high GlOS yield and selectivity. This can be attributed to the unique properties of ALBTH: 1) the water-deficient nature of this system, 2) the high capacity of this system to dissolve glucose, and 3) the ability of the solvent to dissociate acids. In this section the enhanced glucose glycosylation in ALBTH is rationalized with respect to each of these properties.

Effect of water on glycosylation

As a dehydration process, glycosylation is intrinsically favorable over hydrolysis in a water deficient environment. Compared to the glycosylation in aqueous dilute sulfuric acid,[19,20] that in the ALBTH system yielded 4 times more oligosaccharides at similar conditions (Figure S5.5). The ALBETH system ($LiBr{\cdot}3H_2O$) is a concentrated LiBr solution with much less water (38.4 wt%) than the dilute aqueous acid solution (nearly 100wt% water). As shown in the proposed structure of $LiBr{\cdot}3H_2O$ in Figure 2.1, one mole of Li^+ can coordinate with 3 moles of water, and all the water molecules are confined by the interaction/coordination with lithium. In other words, it is deficient of "free" (uncoordinated) water in the ALBTH system.

To investigate the influence of water content, glucose glycosylation was conducted in LiBr hydrate solutions (from $LiBr{\cdot}2H_2O$ to $LiBr{\cdot}12H_2O$) with varied water contents (29.3-71.3 wt%) (Figure 5.3A and 5.3B). The GlOS yield increased from 9% to 39.7% as the water content was reduced from 71.3wt% ($LiBr{\cdot}12H_2O$) to 38.4wt% ($LiBr{\cdot}3H_2O$). Further decrement of the water content to 29.3wt% ($LiBr{\cdot}2H_2O$) led to an extra 5.8% increase in GlOS yield. These results clearly verified that the glycosylation of glucose was favorable when low or no "free water" was present.

The effects of water deficiency on the glycosylation reaction was further confirmed by an experiment in which extra anhydrous LiBr was added when the glucose glycosylation reaction started for 10 min with an aim at reducing free water in the system. The quantity of added anhydrous LiBr was equivalent to one third of the released water in mole, because one mole LiBr is expected to coordinate with three moles of water. Compared to the glycosylation without the addition of extra anhydrous LiBr, that with the addition led to 3.6% increase in GlOS yield at 20 min (See Section S5-I and Table S5.2 in the Appendix). This observation confirmed that LiBr is able to coordinate with the released water from glycosylation and thereby drive the reaction equilibrium toward the GlOS production.

The yields of levoglucosan, HMF and organic acids were inversely correlated to the water content in the LiBr solution (Figure 5.3B). This is in agreement with our previous study that the acid-catalyzed glucose dehydration to furans was promoted in the ALBTH system.[33] It is worth noting that the yields of these degradation side-products were less than 2% under the investigated conditions.

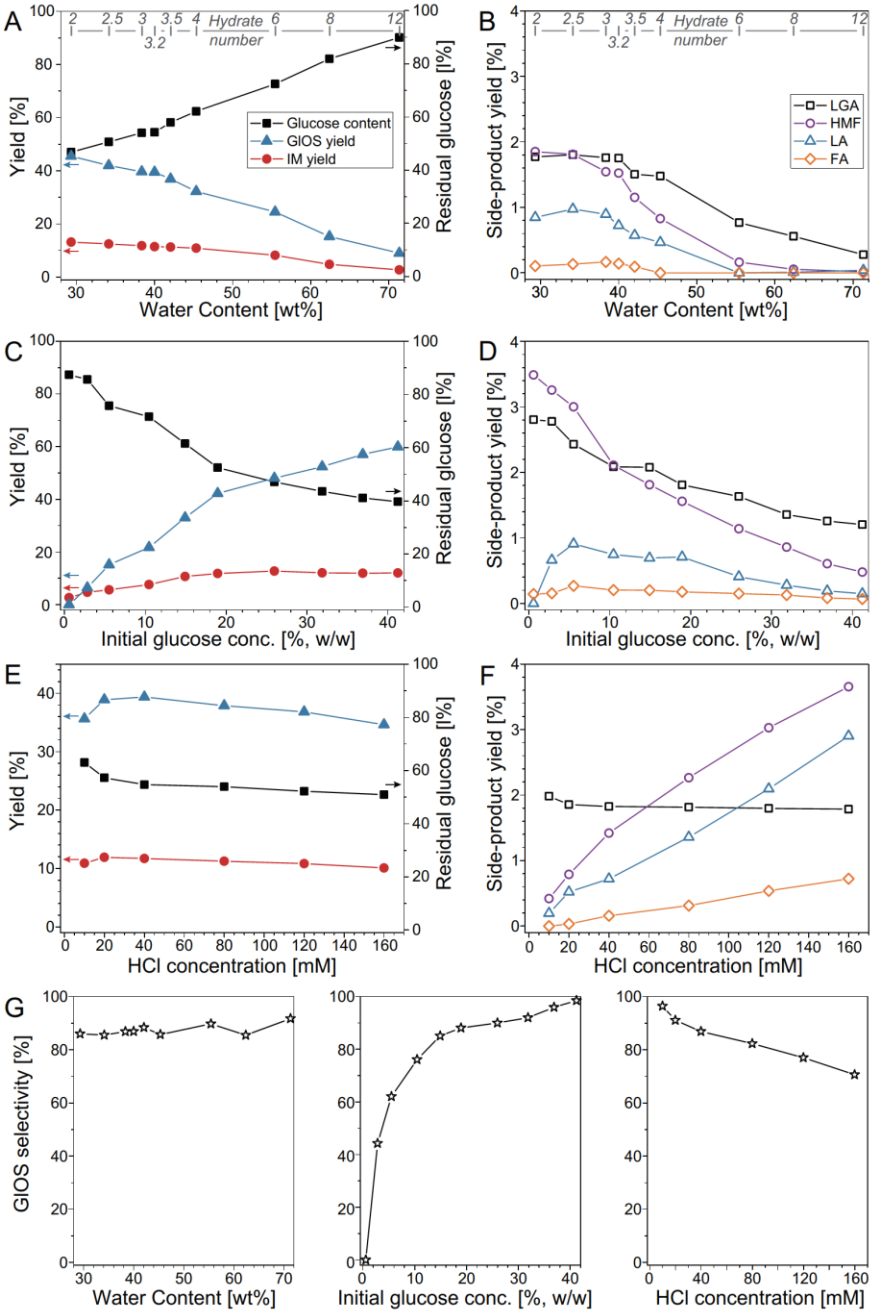

Figure 5.3 Effects of water content in LiBr solution, initial glucose concentration, HCl dosage on the yields of GlOS and side-products from the glycosylation of glucose in acidic LiBr solution. Detailed conditions: 110 °C for A, B, C, D, E, and F; 19% (w/w) initial glucose concentration for C, D, E, and F; 40wt% water content in LiBr solution for A, B, E, and F; 40 mM HCl for A, B, C, and D; all the reactions were quenched after 10 min. Note: GlOS, IM, LGA, HMF, LA, and FA denote total glucooligosaccharides, isomaltose, levoglucosan, hydroxymethylfurfural, levulinic acid, and formic acid, respectively; hydrate number of the LiBr solutions represents the molar ratio of water to LiBr.

Ultra-high capacity of dissolving glucose

During the glucose glycosylation, glucose acts as both the glycosyl donor and the glycosyl acceptor. Therefore, increasing the reactant (glucose) concentration in the system should drive the glycosylation equilibrium toward GlOS according to the Le Chatelier's principle. This assumption was verified by the experiments shown in Figure 3C where elevating the initial glucose concentration from 0.6% to 41% (w/w) greatly increased the GlOS yield. At a low glucose concentration (≤3%, w/w), over 85.6% glucose was unconverted, and the GlOS yield was less than 6.4% (Figure 5.3C). Meanwhile, more side-products were formed, including levoglucosan (2.8%), HMF (3.3%), levulinic acid (0.7%), and formic acid (0.2%) (Figure 5.3D), respectively. Increasing the glucose concentration enhanced glucose conversion, and the GlOS yield reached 48.0% and 60.0% at the 26% and 41% (w/w) glucose concentrations, respectively. The GlOS selectivity also escalated to over 95% with glucose concentrations reaching to 41% (w/w) (Figure 5.3G). The observation above proved that high initial glucose concentration is crucial to ensure high yield and selectivity of GlOS production.

It was observed that glucose had a very high solubility in ALBTH. For example, 40 g glucose promptly dissolved in 10 mL of ALBTH (equivalent to a concentration of 70%, w/w) at 110 °C, resulting in a transparent solution of glucose that could be mixed with a magnet stirring bar (Figure S5.6). At this concentration, 71% of the glucose was selectively converted to GlOS in 20 min. The glucose concentration could be further elevated to 85% (w/w, 100 g of glucose dissolved in 10 mL of ALBTH) using a fed-batch operation, which gave a GlOS yield as high as 75% within 70 min (Table S5.2). At this glucose concentration (54-85%, w/w), the yields of HMF, levoglucosan, and total organic acids were approximately 0.1%, 1.0%, and 0.2% (Table S5.2), respectively. These observations further indicate that elevating initial glucose concentration improves the GlOS

selectivity (up to 99%). As far as we know, it has not been reported that the glycosylation reaction could be carried out effectively at such a high glucose concentration (up to 85%, w/w), as previous studies conducted the glycosylation only at lower sugar concentration of 20-40% (w/w).[20,21] In summary, the ultra-high glucose concentration in ALBTH was one of the reasons leading to not only high GlOS yield (>70%) but also excellent selectivity (~99%).

The ultra-high glucose solubility in ALBTH might be ascribed to the association between glucose units and the hydrate sphere of lithium. Similar association (coordination) between glucose units and a salt hydrate ($ZnCl_2 \cdot 3H_2O$) was detected from neutron scattering results, which facilitated the dissolution of cellulose in $ZnCl_2$ solution.[34] In addition, the association between glucose units and might also contribute to the improved glycosylation at high glucose concentration, as illustrated in a postulated mechanism in Figure S5.7 how the hydrate sphere of lithium associate and bridge the glucose units to form glycosidic bonds.

Enhanced acidity in ALBTH for glycosylation

In acid catalyzed glycosylation reactions, protonation of the glucose anomeric hydroxyl group is the prerequisite to form an anomeric carbocation intermediate (Figure 5.1A).[27] Since the Hammett acidity in the ALBTH system is higher than that in aqueous solution at the same acid concentration,[22,35] the enhanced acidity might be an imperative factor for high-yield and high-selectivity synthesis of GlOS in ALBTH, because reduced acid loading (but maintaining the same acidity) suppressed the sugar degradation to side-products (Figure 5.3F). Hydrochloric acid was tested at varying concentrations in the LiBr system. As shown in Figure 5.3E, the GlOS yield first increased with HCl concentration from 35.7% at 10 mM HCl to 39.4% at 40 mM and then gradually decreased to 34.6% at 160 mM. Meanwhile, the glucose degradation products (HMF,

LA, and FA) increased continuously with the increasing acid concentration, as shown in Figure 3F. These results indicate that low HCl concentration (20-40 mM) was sufficient to catalyze the glycosylation but not enough to cause significant sugar degradation. A dilute aqueous sulfuric acid medium (40 mM H^+) without LiBr had a limited oligosaccharide yield (~8%) from glucose under a similar glycosylation condition (140 °C, 20 mM H_2SO_4, and 30 min),[20] indicating that there would be a synergetic effect of LiBr in enhancing the catalytic performance of an acid in glycosylation.

Acid catalysts with different p*Ka* values were also investigated for the glycosylation reaction in ALBTH, as shown in Table S5.3. The GlOS yield was mostly constant when the p*Ka* values of acids changed from -4.00 to 2.16. These results indicated that weak Brønsted acids, such as phosphoric acid and oxalic acid, had similar catalytic performance with strong Brønsted acids for the glycosylation. Formic acid (p*Ka* = 3.75) was still able to catalyze the glycosylation reaction, although both glucose conversion and GlOS yield were low. These results further confirmed that all these acids dissociated in the ALBTH system, which made them capable of catalyzing the glycosylation reaction. When the reaction was conducted in LiBr trihydrate without an acid catalyst (Table S5.3), approximately 12% of glucose was consumed, but no glycosylation product was generated. Only fructose and mannose were detected (data are not shown here) from glucose isomerization and epimerization, respectively, which is consistent with the observation in our previous study.[36]

5.3.4 Separation and purification of GlOS and recovery of LiBr in a conceptual process

A conceptual process to produce GlOS from glucose is presented in Figure 5.4. Fresh glucose is mixed with the ALBTH media containing a small amount of acid (e.g., 20-40 mM HCl under mild

conditions (70-110 °C and ambient pressure). The glycosylation reaction leads to a viscous syrup-like mixture including generated GlOS, unreacted glucose, HCl and the LiBr solution. The mixture is then diluted with methanol (a diluting solvent) to reduce its viscosity. Acetone (a non-solvent of GlOS) is added into the diluted mixture to homogeneously precipitate/crystallize GlOS. The establishment of this GlOS separation procedure, including the selection of the dilution solvent and the non-solvent, is described in detail in Section S5-II in the Appendix. After centrifugation, the crude GlOS crystals are collected. If necessary, further purification can be conducted to remove the small amount of glucose and LiBr co-precipitated with GlOS by consecutive operations of dissolution in methanol and precipitation in acetone (as described above). For example, repeating the purification operation twice yielded the GlOS crystals with a 98% purity. The supernatant after removal of the GlOS crystals contains acetone, methanol, unreacted glucose, and the LiBr solution, together with a small amount of un-precipitated GlOS. Acetone and methanol can be easily evaporated in a flash tank due to their distinct volatilities to LiBr trihydrate. In this operation, a portion of volatile HCl in ALBTH may be removed as well. A lab-scale test using a rotary evaporator removed over 99.9% acetone and methanol, which can be subsequently separated by distillation[37] and reused for the next batch. The quantities of residual glucose and GlOS in the recovered LiBr stream are dependent on the methanol dilution factor (Table S5.4). The presence of glucose and GlOS in the recovered LiBr stream did not deteriorate its reusability. When conducting the glycosylation reaction in the recovered LiBr solution with the addition of HCl to make up the lost portion, the yield of GlOS (55.5%) was comparable to that (56.2%) in freshly prepared LiBr solution. The GlOS synthesized in the recovered LiBr solution had the identical chemical structures as those synthesized in fresh LiBr solution, as verified with HSQC NMR analysis (Figure S5.8). It is apparent that the recovered LiBr solution is reusable for the next batch

reaction. The accumulated sugar degradation side-products in the system after multiple-time recycles could be optionally removed/separated through, for example, solvent extraction or a simulated moving bed ion exclusion chromatographic system. In summary of the proposed diagram, GlOS could be synthesized from glucose in ALBTH in a closed-cycle process.

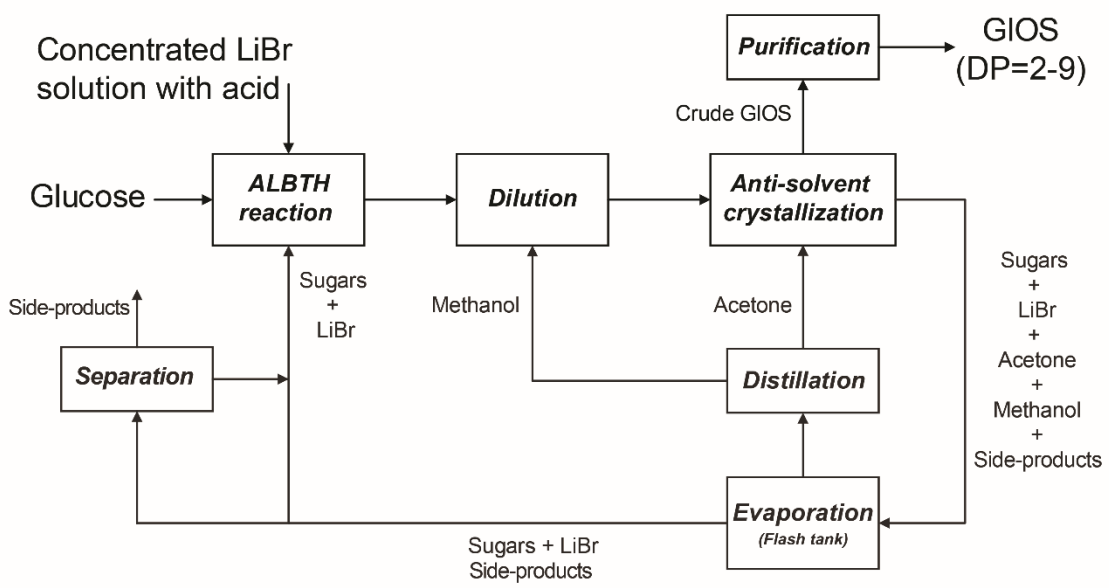

Figure 5.4 Conceptual flow diagram for synthesis and separation of the GlOS in a closed-circle process via acid-catalyzed glycosylation of glucose in ALBTH followed by the precipitation in non-solvent.

5.3.5 Preliminary evaluation of the GlOS as potential prebiotics *in vitro*

It has been reported that the isomalto-oligosaccharides and gentiobio-oligosaccharides (linked via α–1,6 and β–1,6 glycosidic bonds, respectively) had prebiotic function,[38,39] and many disaccharides with α/β–1,2, α/β–1,3, and α–1,6 glycosidic bonds exhibited high prebiotic index (PI>5) and selective promotion of the probiotic strains.[40] The GlOS synthesized from glucose in this study had abundant α–1,6 and β–1,6 glycosidic bonds, along with α/β–1,1, α–1,2, and α–1,3 glycosidic bonds. The GlOS were therefore expected to exhibit prebiotic properties.

To assess to what extent select probiotics utilize GlOS, we performed an *in vitro* growth

experiment under anaerobic conditions with five lactobacilli and two bifidobacteria strains. In the modified medium containing GlOS as the sole carbon source, probiotic bacteria proliferated after 24-h incubation but at different efficiencies, ranging from a final optical density (OD600) from 0.6 (*B. bifidum*) up to 2.0 (*L. Rhamnosus GG*) (Figure 5.5). Since our GlOS preparation contains a small amount of glucose (5 wt%), we assessed if the supported growth could be attributed to the free glucose rather than GlOS utilization. The results show that glucose was predominately metabolized in the first 3-4 h, and the GlOS contributed to the subsequent growth of the probiotic bacteria which were distinct from the limited glucose control (Figure S5.9). This provides direct evident that the select probiotics can utilize GlOS for growth. The carbohydrate analysis of the post-fermentation broth (Table S5) indicated that GlOS were partially consumed by both *Lactobacillus* and *Bifidobacterium* strains. For example, *L. rhamnosus GG* utilized gentiobiose completely, and *L. buchneri* consumed more than 90% isomaltose, but not gentiobiose. *B. animalis* consumed more than 70% disaccharides and up to 43% total oligosaccharide. The metabolic activities of the probiotic strains produced short chain fatty acids (SCFA) and lactic acids as fermentation products. The production of formic acid (0.2-0.6 g/L), acetic acid (0.6-2.3 g/L) and lactic acid (0.3-2.2 g/L) on GlOS was dependent on the strains. Direct production of propionate or butyrate was negligible by *Lactobacillus* and *Bifidobacterium* strains in this study, although both lactate and acetate could be utilized by a group of bacteria such as *Eubacterium hallii* and *Anaerostipes caccae* to produce propionate and/or butyrate.[41]

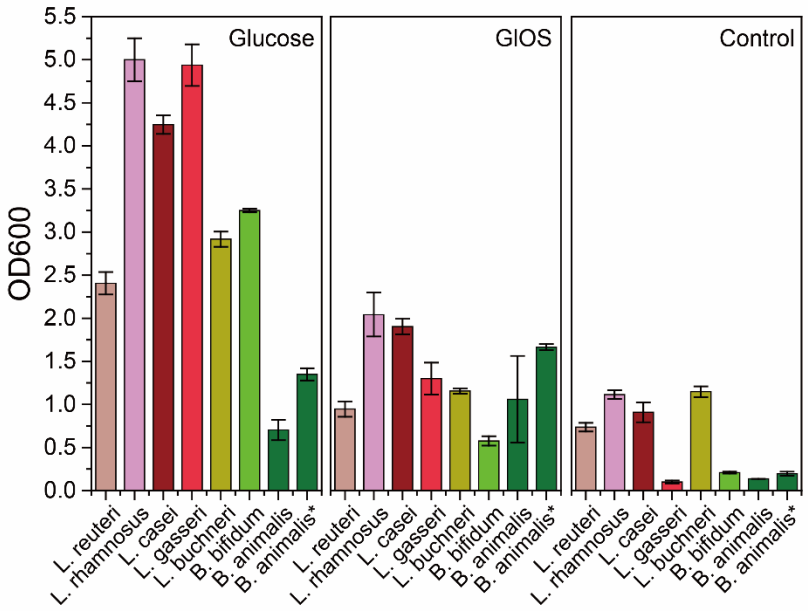

Figure 5.5 Growth of select *Lactobacillus* and *Bifidobacterium* strains on glucose, gluco-oligosaccharides (GlOS) after 24 h anaerobic incubation at 37 °C. (Note: The control media contained 0.5 g/L glucose for *Lactobacillus* strains except *L. buchneri* and 0.0 g/L glucose for *Bifidobacterium* strains and *L. buchneri*; B. animals* had 48-h incubation time.)

The preliminary results above demonstrated the prebiotic potential of the GlOS by probiotic strains. We envision that these studies will provide us with incentive to conduct more comprehensive studies of the GlOS prebiotic performance according to the criterions stated by the International Scientific Association for Probiotics and Prebiotics (ISAPP).[4] In addition, the animal and human dietary intervention experiments in the future work would be helpful to provide a comprehensive evaluation of the prebiotic influence on the overall ecosystem of the gut.

5.3.6 Preliminary test of glycosylation using other sugar monomers

In the above acidic glycosylation, glucose reacted as both the glycosyl donor (C1 oxocarbenium) and glycosyl acceptor (active hydroxyl). Besides glucose, other naturally abundant sugars (e.g. arabinose, galactose, xylose, etc.) are capable of forming C1 oxocarbeniums and providing active hydroxyls under acidic conditions. The glycosylation reactions of varied sugars were preliminarily tested in Table S5.6. All other sugars involved in ALBTH glycosylation, analog to glucose.

Specifically, hexo-oligosaccharides showed slightly higher glycosylation yield compared to the pento-oligosaccharides. This observation could direct the future glycosylation research toward manipulate functional oligosaccharide formation using varied monomeric sugars.

5.3.7 Glucose glycosylation in other molten salt hydrate systems

Various molten salt hydrate systems other than LiBr trihydrate, were tested as reaction media for oligosaccharide production from glucose. In the preliminary test, the divalent metal salts were paired with 6 hydrates and the monovalent metal salts were paired with 3 hydrates. In the case of $NaBr{\cdot}3H_2O$ and $MgCl_2{\cdot}6H_2O$, full dissolution failed at room temperature, so extra 3 hydrates were added. As shown in Table S5.7, various molten salt hydrate systems including $NaBr{\cdot}6H_2O$, $LiCl{\cdot}3H_2O$, $LiBr{\cdot}3H_2O$, $CaCl_2{\cdot}6H_2O$, and $CaBr_2{\cdot}6H_2O$, enabled GlOS production from glucose with the yields ranging from 19-42%. Having the same anion pair (either chloride or bromide), the lithium salts contributed to higher GlOS yields than the sodium and calcium salts. The disparity in GlOS yields between $LiCl{\cdot}3H_2O$ vs $LiBr{\cdot}3H_2O$ and $CaCl_2{\cdot}6H_2O$ vs $CaBr_2{\cdot}6H_2O$, revealed that bromide was more efficient than chloride to enhance the glycosylation reactions. When taken both the anion and cation factors into consideration, $LiBr{\cdot}3H_2O$ resulted in the highest GlOS yield under the conditions investigated. The yield of GlOS was negligible in $ZnCl_2{\cdot}6H_2O$, while a small amount of fructose was produced, indicating that $ZnCl_2$ hydrate system might favor the glucose isomerization reaction.

5.4 Conclusions

Acidic lithium bromide trihydrate system (ALBTH) was demonstrated to be an efficient medium for glucose glycosylation under mild conditions (moderate temperature and low acid dosage) to synthesize GlOS with high yield (~75%) and selectivity (~99%). The GlOS were composed of 2–9 glucose units linked dominantly by α/β–1,6 glycosidic bonds along with a small portion of α/β–

1,1, α/β–1,2, α/β–1,3, and α–1,4 glycosidic bonds. Several unique properties of ALBTH contributed to the enhanced glycosylation of glucose, including the water-deficient nature, the ultra-high capacity of this system to dissolve sugars, and the high dissociation of acids in this solvent system. The synthesized GlOS were separated from the reaction medium (ALBTH) by precipitation in non-solvent (acetone), and the recovered ALBTH could be directly reused for the next batch glycosylation, which established a feasible closed-cycle process for the synthesis of GlOS from glucose in ALBTH. GlOS could be utilized by select lactobacilli and bifidobacteria strains, which exemplified the potential to exploit GlOS as prebiotics. This non-enzymatic glycosylation method provided a new approach of producing high-value and functional oligosaccharide prebiotics directly from inexpensive and abundant monosaccharides.

Appendix

Section S5-I. Batch addition of anhydrous LiBr to confine the released free water from the glycosylation

In the progress of the glycosylation (dehydration) reaction, the released water can increase the water content in the system and drive the equilibrium opposite to the GlOS side, resulting in reduced GlOS yield. For example, approximately 22 g water is generated when 400 g glucose reacted in 171 g ALBTH to achieve 71.0% of GlOS yield. It thus increases the water contents from 38.4% to 45.4% and has negative effects on GlOS production. To address this issue, a strategy of adding anhydrous LiBr during the glycosylation reaction was tested with the aim to limit the free water released from the glycosylation reaction. The results in Table S5.2 clearly indicated that the addition of anhydrous LiBr (1.5 equivalent to water released, w/w) did elevate the yield of the oligosaccharides up to 74.7%, which was 3.6% higher than that in the control experiment without adding LiBr. This observation once again verified that a water deficient environment of the ALBTH system played a crucial role in GlOS production.

Section S5-II. Selection of diluting solvents and non-solvents for separation of GlOS from ALBTH

For practical consideration, efforts were made to afford the economical separation of GlOS from the reaction medium and the subsequent recycle/reuse of the LiBr solution. Unfortunately, it is challenging to separate the saccharides from the salt solution using solvent-solvent extraction approaches due to the strong inter-molecular interactions between ALBTH and saccharides.[42] We noticed that GlOS and LiBr had distinct solubility in organic solvents. For example, LiBr can dissolve in acetone where GlOS are marginally soluble. Herein, a non-solvent crystallization

approach was adopted to isolate GlOS and recover LiBr. In principle, a non-solvent should interrupt the interaction between the original solvent and solute, leading to an over-saturation and precipitation of the solute.[43] In this study, acetone was chosen as the non-solvent in virtue of the low dielectric constant (20.7) to over-saturate GlOS and the miscibility with ALBTH.[44,45]

At high glucose concentration, glycosylation of glucose yielded a highly viscous syrup. Dispersing the syrup into acetone resulted in the formation of sugar gums in which a significant amount of LiBr was entrapped. It thus deteriorated the separation of GlOS and LiBr. It was found that diluting the syrup is critical for viscosity reduction prior to the non-solvent crystallization. Deionized water was firstly tested as a dilution solvent which effectively eliminated the formation of sugar gums. However, the defect was the reduced GlOS recovery since introducing water during dilution greatly elevated the solubility of GlOS in the non-solvent, as confirmed by the previous study.[46] Alternatively, the syrup was diluted with methanol (dielectric constant 32.6). In spite of its lower polarity than water, methanol was still capable of interrupting the interactions between ALBTH and the GlOS, and formed a transparent mixture with reduced viscosity. When dropping the methanol-diluted syrup into acetone, regeneration of GlOS as white precipitates was achieved without aggregated gums.

The effect of dilution factor on the separation of GlOS from the ALBTH system was investigated. The resultant product syrup was diluted 2-15 folds with methanol and then dropped into acetone. It was found that the methanol dilution facilitated the separation and purification of the GlOS. As shown in Table S5.4, when the methanol dilution factor increased from 2 to 15, the distribution of LiBr and glucose in the precipitated GlOS fraction, decreased from 25.0% and 66.5% to 6.5% and 20.3%, respectively. Meanwhile, the yield of GlOS in the precipitate was relatively constant (less than 3% decrease with methanol dilution). It was confirmed that the

methanol dilution of the glycosylation syrup followed by the non-solvent crystallization in acetone, could effectively isolation the GlOS from the ALBTH system.

Section S5-III. Lists of Figures and Tables

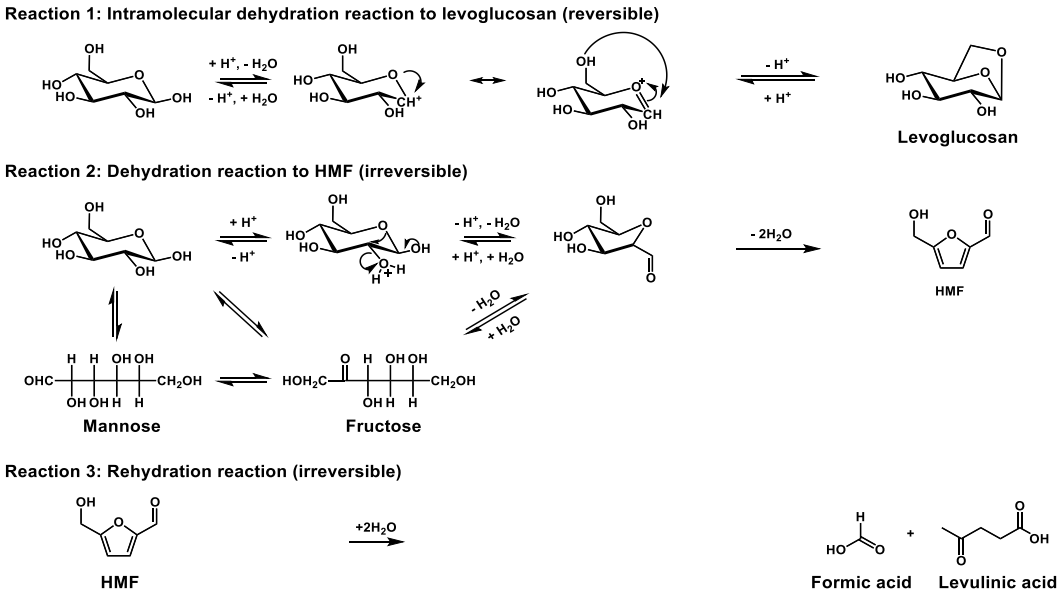

Figure S5.1 Acid catalyzed side-reactions in ALBTH during glucose glycosylation.

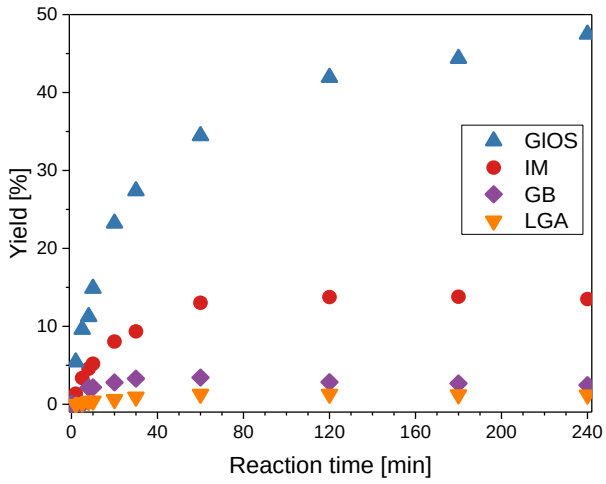

Figure S5.2 Formation of glucooligosaccharides (GlOS) and levoglucosan (LGA) in ALBTH at 70 °C as a function of reaction time. The batch reaction was conducted using 19% (w/w) initial glucose concentration in 60% LiBr with 40 mM HCl. GlOS, IM, GB, and LGA denote total

glucooligosaccharides ($DP \geq 2$), isomaltose, gentiobiose, and levoglucosan, respectively.

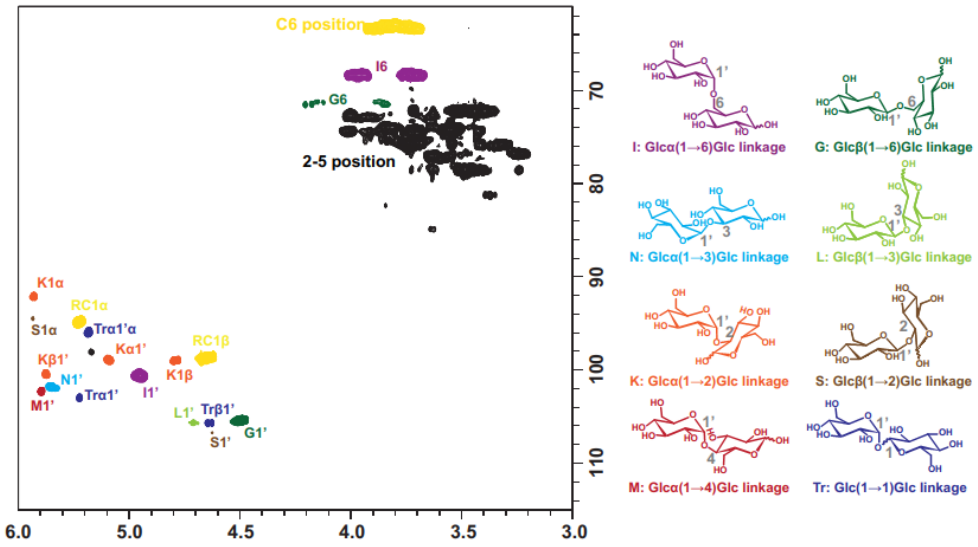

Figure S5.3 2D-HSQC NMR spectrum of the GlOS dissolved in D_2O from the acid catalyzed glycosylation in ALBTH at 110 °C for 10 min. DSS was used as a chemical shift reference.

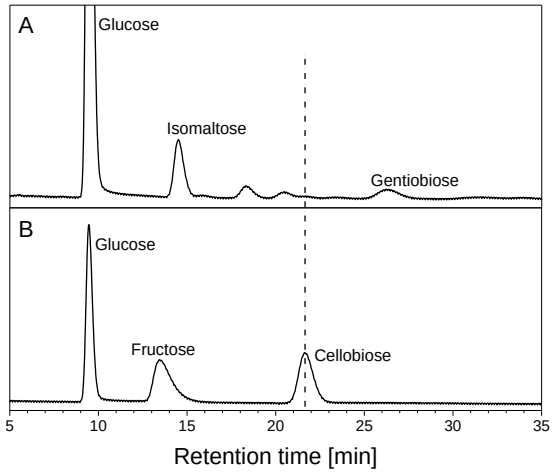

Figure S5.4 HPAEC chromatograms of GlOS samples (A) and cellobiose (B).

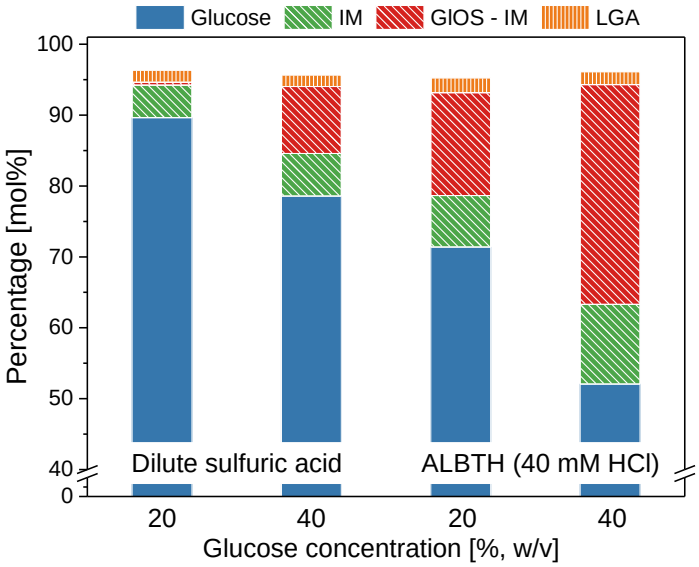

Figure S5.5 Comparison between the glycosylation reactions of glucose in dilute sulfuric acid (121 °C for 60 min) and in ALBTH (110 °C for 10 min).

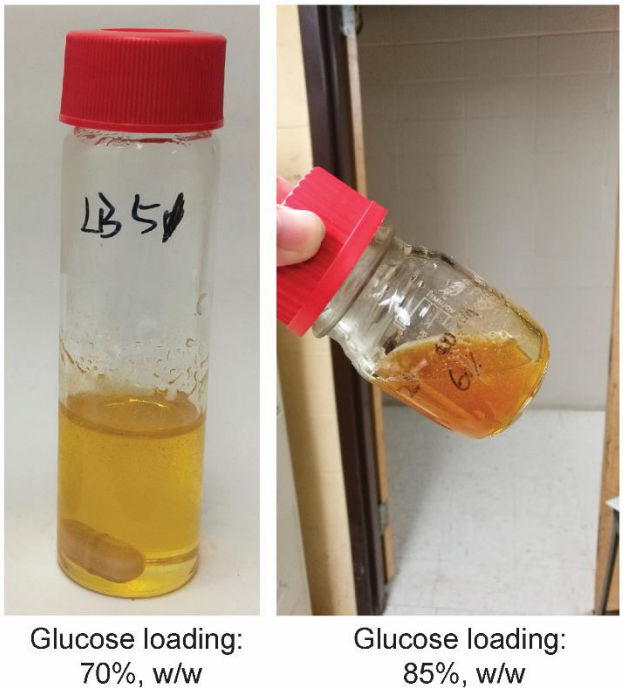

Figure S5.6 The ultra-high capacity of dissolving glucose in ALBTH with good fluidity.

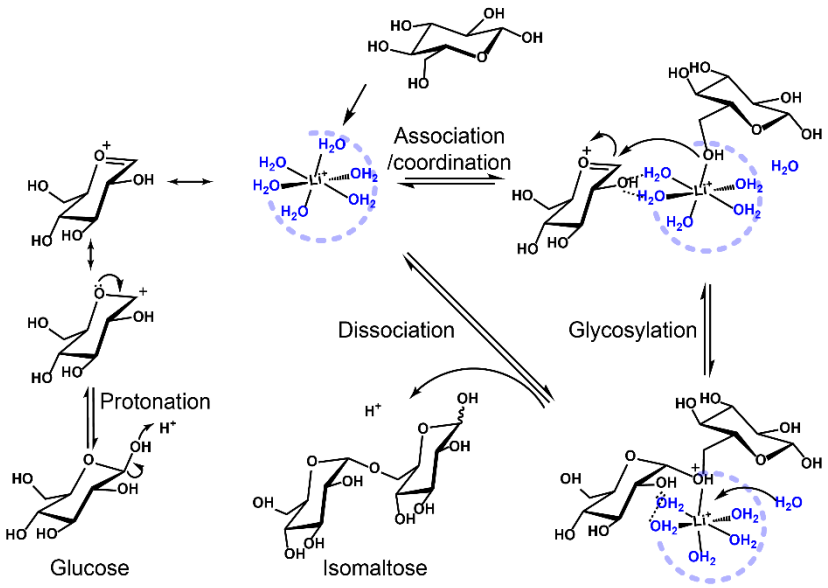

Figure S5.7 Proposed association and bridging of glucose units to facilitate the glycosylation in ALBTH using isomaltose as an example.

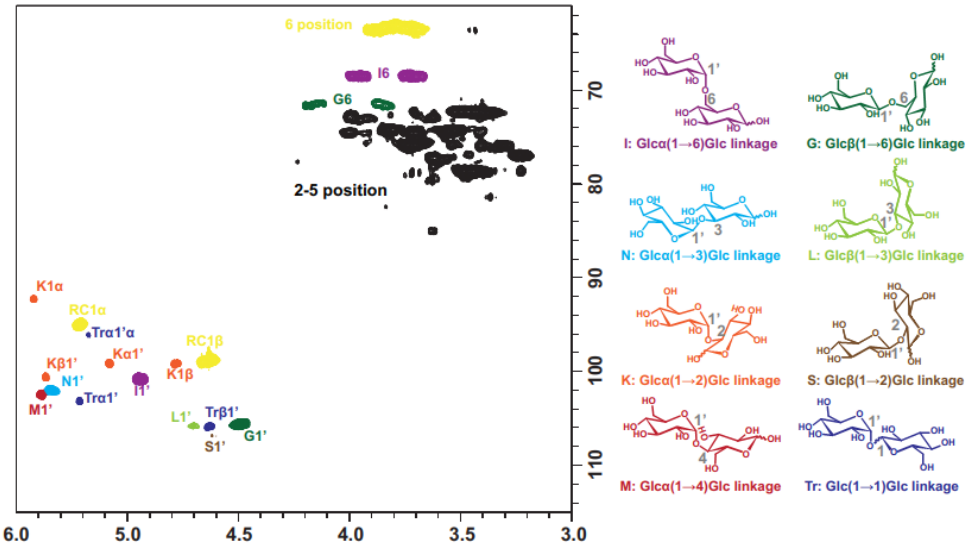

Figure S5.8 2D-HSQC NMR spectrum of the GlOS dissolved in D_2O from acid catalyzed glycosylation reaction in recycled ALBTH. DSS was used as a chemical shift reference. The GlOS were synthesized at 70 °C for 120 min.

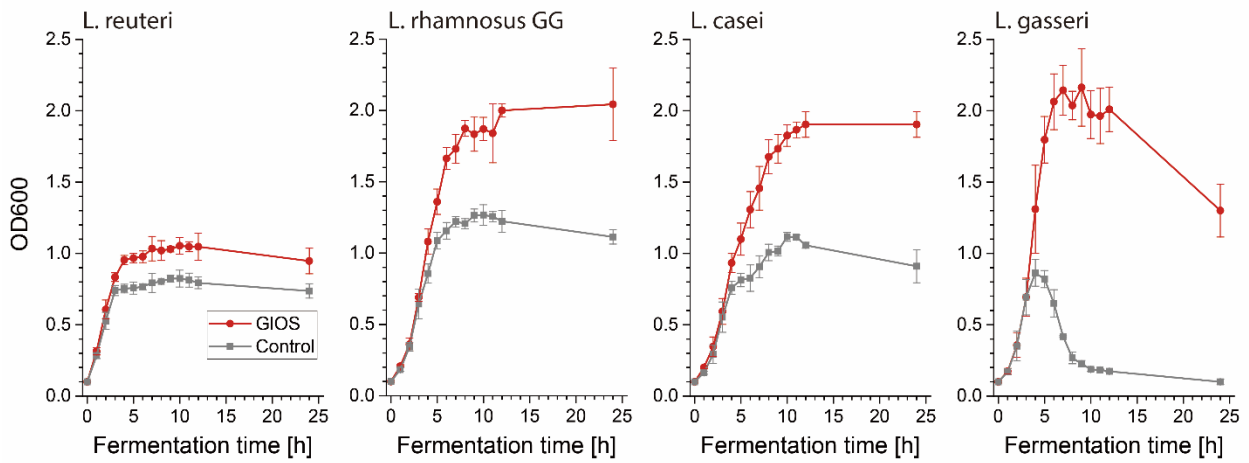

Figure S5.9 Growth curves of *L. reuteri* (ATCC 6475), *L. rhamnonsus* GG, *L. casei* BFLM 218, *L. gasseri* ATCC 33323 with GlOS (9.5 g/L) + glucose (0.5 g/L) or minimal glucose (0.5 g/L) as the carbon source.

Table S5.1 Regio- and stereo-selectivity of the glycosylation reaction of glucose in ALBTH

Glycosylic linkage	70 °C				110 °C			
	D1=10 s		D1=1 s		D1=10 s		D1=1 s	
	Cont. (%)	α/β ratio	Cont. (%)	α/β ratio	Cont. (%)	α/β ratio	Cont. (%)	α/β ratio
1→6	69.1	2.5	69.3	2.6	69.8	3.1	68.0	3.0
1→4	4.9	>10	4.5	>10	3.0	>10	3.4	>10
1→3	13.7	4.2	12.5	4.3	13.5	2.1	12.9	2.5
1→2	8.8	11.3	8.8	9.1	9.7	10.0	10.9	7.7
1→1	3.6	1.3	1.9	1.4	4.0	2.6	4.8	2.2

Table S5.2 Glucose glycosylation reaction at ultra-high initial concentration in ALBTH (40 mM HCl) at 110 °C

Loading (%, w/w)	Time (min)	Glucose content (%)	Yield (%)							GlOS selectivity (%)
			IM	GB	GlOS	LGA	HMF	LA	FA	
54[a]	10	30.6	13.5	4.3	65.9	1.2	0.2	0.1	<0.1	94.9
	20	27.9	9.2	3.4	69.1	0.9	0.3	0.1	<0.1	95.9
	20[c]	26.2	9.3	2.8	69.2	1.1	0.4	0.1	0.1	93.8
70[a]	10	39.5	12.3	4.0	58.2	0.9	0.1	0.1	<0.1	96.1
	20	27.0	8.3	4.3	71.1	0.9	0.1	0.1	<0.1	97.5
	20[c]	22.8	7.6	3.1	74.7	1.0	0.1	0.1	<0.1	96.8
75[a]	20	29.1	9.6	3.9	68.8	0.8	0.1	0.1	<0.1	97.0
80[b]	21	42.7	11.5	3.7	56.5	0.6	0.1	0.1	<0.1	98.6
85[b]	70	23.3	7.6	3.3	75.0	0.6	0.1	0.1	<0.1	97.9

Note: (a) A one-pot approach was applied to reach 54%, 70%, and 75% (w/w) initial glucose concentration by adding 20 g, 40 g and 50 g of glucose, respectively, in 10 mL of ALBTH; (b) a fed-batch strategy was applied to reach 80.4% (40 g +10 g +10 g of glucose in 10 mL of ALBTH) and 85.4% (50 g +10 g +10 g +10 g +10 g +10 g of glucose in 10 mL of ALBTH) glucose loading concentration. (c) LiBr anhydrous (one third of the released water from glycosylation in mole) was added after 10 min.

Table S5.3 Comparison of the acids (40 mM) with varied p*K*a values in catalyzing glucose glycosylation in ALBTH at 110 °C

Acids	pKa	Glucose content (%)	Yield (%)							GlOS selectivity (%)
			IM	GB	GlOS	LGA	HMF	LA	FA	
HCl	-4.00	55.6	11.7	2.6	38.0	1.6	1.8	0.7	0.2	85.8
H_2SO_4	-3.00	55.7	12.9	2.5	38.5	1.6	2.0	0.9	0.2	87.0
TsOH	-2.80	55.4	12.9	2.1	38.1	1.4	1.9	0.8	0.1	85.3
Oxalic acid	1.25	54.0	12.5	2.1	39.4	1.7	1.8	0.4	0.2	85.5
DCA	1.35	57.9	12.5	3.1	35.9	0.9	2.0	0.3	0.1	85.2
H_3PO_4	2.16	56.9	13.2	2.4	39.1	1.1	1.8	0.4	0.1	90.9
Citric acid	3.13	64.7	11.5	2.9	31.6	0.5	2.2	0.2	0.0	89.6
Formic acid	3.75	88.3	4.0	1.5	9.5	0.1	1.0	0.1	0.3	81.1
Acetic acid	4.76	100.0	0.0	0.0	0.0	0.0	0.0	0.1	0.0	--
Acetic acid[a]	4.76	95.7	2.6	0.0	3.1	0.0	0.5	0.1	0.0	70.8
Control[b]	7.00	87.8	0.0	0.0	0.0	0.0	0.0	0.0	0.0	--

Note: (a) Acid concentration: 200 mM; (b) LiBr trihydrate (60 wt%) without acid catalyst. GlOS, IM, GB, LGA, HMF, LA, and FA denote total glucooligosaccharides, isomaltose, gentiobiose, levoglucosan, hydroxymethylfurfural, levulinic acid, and formic acid, respectively.

Table S5.4 Separation of GlOS and LiBr by dilution in methanol and crystallization in acetone

		Methanol dilution		
		2×	5×	15×
After reaction	LiBr (g)	5.13	5.13	5.13
	Glucose (g)	2.18	2.22	2.17
	GlOS (g)	2.77	2.73	2.78
	IM (g)	0.68	0.65	0.69
	GB (g)	0.21	0.20	0.19
Anti-solvent precipitates	LiBr (g)	1.28	0.78	0.33
	Glucose (g)	1.45	1.07	0.44
	GlOS (g)	2.47	2.43	2.40
	IM (g)	0.58	0.52	0.43
	GB (g)	0.20	0.15	0.13
Recovered LiBr hydrate	LiBr (g)	3.70	3.98	4.62
	Glucose (g)	0.51	0.75	1.30
	GlOS (g)	0.30	0.30	0.38
	IM (g)	0.02	0.06	0.17
	GB (g)	0.01	0.02	0.13
	Methanol (g)	0.08	0.01	0.05
	Acetone (g)	0.02	0.00	0.24

Note: GlOS – total oligosaccharides; IM – isomaltose; GB – gentiobiose. Reaction condition: The glycosylation reaction was conducted at 70 °C in ALBTH with 40 mM HCl for 2 h using 37% (w/v) initial glucose concentration.

Table S5.5 Consumption of glucose and GlOS by probiotics and the resultant SCFA production after 24 h anaerobic incubation at 37 °C

	Substrate consumption (%)				SCFA conc[a] (g/L)				
	Glucose	GlOS			LcA	FA	AA	PA	BA
		TOS[b]	IM	GB					
L.buchneri	100.0	25.5	90.7	0.0	1.2	<0.1	1.1	<0.1	<0.1
L. reuteri	99.5	12.6	22.5	100.0	0.5	<0.1	0.6	<0.1	<0.1
L. rhamnosus GG	100.0	27.2	13.9	99.0	0.3	0.6	1.5	<0.1	<0.1
L.casei	98.2	20.9	21.1	95.5	1.0	0.2	1.3	<0.1	<0.1
L. gasseri	99.4	26.1	15.4	98.1	2.1	0.3	1.4	<0.1	<0.1
B. bifidum	100.0	12.7	12.1	2.4	2.2	<0.1	<0.1	<0.1	<0.1
B. animalis	10.9	40.6	42.6	47.5	0.9	0.3	1.4	<0.1	<0.1
B. animalis[c]	69.4	42.7	79.9	74.1	1.6	0.3	2.3	<0.1	<0.1

Note: (a) Production of SCFA by fermentation using GlOS, LcA, FA, AA, PA, and BA denote lactic, formic, acetic, propionic, and butyric acid, respectively, (b) TOS denotes total oligosaccharides, (c) Incubation duration: 48 h

Table S5.6 Preliminary investigation of monosaccharide conversion of arabinose, galactose, glucose, and xylose by ALBTH glycosylation at 110 °C for 10 min

Loading (%, w/w)				Conversion (%)			
Arabinose	Galactose	Glcuose	Xylose	Arabinose	Galactose	Glcuose	Xylose
	9.5	9.5			57.1	55.8	
	19.0				48.3		
		12.8	6.2			43.0	40.5
			19.0				40.7
8.0	8.0	8.0	8.0	54.1	61.1	59.4	56.2

Table S5.7 Comparison of GlOS production in various molten salt hydrate (MSH) systems

MSH	Glucose content (%)	Yield (mol %)							GlOS selectivity (%)
		IM	GB	TOS	LGA	HMF	LA	FA	
$NaBr·6H_2O$	79.8	7.5	3.6	18.8	1.1	0.1	0.0	0.0	93.3
$MgCl_2·6H_2O$	90.0	1.9	3.9	3.8	0.3	0.1	0.0	0.0	38.2
$ZnCl_2·6H_2O$	88.9	0.0	0.0	0.0	0.2	0.7	0.0	0.0	--
$LiCl·3H_2O$	65.1	10.9	4.0	30.7	1.4	0.7	0.4	0.0	88.0
$LiBr·3H_2O$	52.1	11.8	2.6	42.2	1.8	1.6	0.7	0.2	88.1
$CaCl_2·6H_2O$	79.3	6.8	2.3	14.1	1.8	0.5	0.2	0.0	68.3
$CaBr_2·6H_2O$	72.0	9.1	2.4	23.0	3.5	0.7	0.5	0.0	82.2

Other conditions: The reactions were conducted in various MSH media containing 40 mM HCl at 110 °C for 10 min. The loading of glucose was 19% (w/w).

Reference

(1) Barreteau, H.; Delattre, C.; Michaud, P. Production of oligosaccharides as promising new food additive generation. *Food Technology and Biotechnology* **2006**, *44*, 323.

(2) Moura, F. A.; Macagnan, F. T.; Silva, L. P. Oligosaccharide production by hydrolysis of polysaccharides: a review. *International Journal of Food Science & Technology* **2015**, *50*, 275-281.

(3) Bindels, L. B.; Delzenne, N. M.; Cani, P. D.; Walter, J. Towards a more comprehensive concept for prebiotics. *Nature Reviews Gastroenterology & Hepatology* **2015**, *12*, 303-310.

(4) Gibson, G. R.; Hutkins, R. W.; Sanders, M. E.; Prescott, S. L.; Reimer, R. A.; Salminen, S. J.; Scott, K.; Stanton, C.; Swanson, K. S.; Cani, P. D. The International Scientific Association for Probiotics and Prebiotics (ISAPP) consensus statement on the definition and scope of prebiotics. *Nature Reviews Gastroenterology and Hepatology* **2017**, *14*, 491-502.

(5) Swennen, K.; Courtin, C. M.; Delcour, J. A. Non-digestible oligosaccharides with prebiotic properties. *Critical reviews in food science and nutrition* **2006**, *46*, 459-471.

(6) Moure, A.; Gullón, P.; Domínguez, H.; Parajó, J. C. Advances in the manufacture, purification and applications of xylo-oligosaccharides as food additives and nutraceuticals. *Process Biochemistry* **2006**, *41*, 1913-1923.

(7) Rastall, R. A.; Gibson, G. R. Recent developments in prebiotics to selectively impact beneficial microbes and promote intestinal health. *Current Opinion in Biotechnology* **2015**, *32*, 42-46.

(8) Moreno, F. J.; Corzo, N.; Montilla, A.; Villamiel, M.; Olano, A. Current state and latest advances in the concept, production and functionality of prebiotic oligosaccharides. *Current Opinion in Food Science* **2017**, *13*, 50-55.

(9) Katsnelson, A. Prebiotics gain prominence but remain poorly defined. *Proceedings of the National Academy of Sciences* **2016**, *113*, 14168-14169.

(10) *Prebiotics: ingredients, applications and global markets*, M2 Presswire, 2017.

(11) Singh, R. S.; Singh, R. P. Production of fructooligosaccharides from inulin by endoinulinases and their prebiotic potential. *Food Technology and Biotechnology* **2010**, *48*, 435.

(12) Aachary, A. A.; Prapulla, S. G. Value addition to corncob: production and characterization of xylooligosaccharides from alkali pretreated lignin-saccharide complex using Aspergillus oryzae MTCC 5154. *Bioresource Technology* **2009**, *100*, 991-995.

(13) Gullón, B.; Gómez, B.; Martínez-Sabajanes, M.; Yáñez, R.; Parajó, J.; Alonso, J. Pectic oligosaccharides: Manufacture and functional properties. *Trends in food science & technology* **2013**, *30*, 153-161.

(14) Dao, T. H.; Zhang, J.; Bao, J. Characterization of inulin hydrolyzing enzyme (s) in commercial glucoamylases and its application in lactic acid production from Jerusalem artichoke tubers (Jat). *Bioresource Technology* **2013**, *148*, 157-162.

(15) Hancock, S. M.; Vaughan, M. D.; Withers, S. G. Engineering of glycosidases and glycosyltransferases. *Current Opinion in Chemical Biology* **2006**, *10*, 509-519.

(16) Abdul Manas, N. H.; Md. Illias, R.; Mahadi, N. M. Strategy in manipulating transglycosylation activity of glycosyl hydrolase for oligosaccharide production. *Critical Reviews in Biotechnology* **2017**, 1-22.

(17) Flores-Maltos, D. A.; Mussatto, S. I.; Contreras-Esquivel, J. C.; Rodríguez-Herrera, R.; Teixeira, J. A.; Aguilar, C. N. Biotechnological production and application of fructooligosaccharides. *Critical Reviews in Biotechnology* **2016**, *36*, 259-267.

(18) Thompson, A.; Anno, K.; Wolfrom, M.; Inatome, M. Acid reversion products from D-

glucose. *Journal of the American Chemical Society* **1954**, *76*, 1309-1311.

(19) Helm, R. F.; Young, R. A.; Conner, A. H. The reversion reactions of d-glucose during the hydrolysis of cellulose with dilute sulfuric acid. *Carbohydrate Research* **1989**, *185*, 249-260.

(20) Pilath, H. M.; Nimlos, M. R.; Mittal, A.; Himmel, M. E.; Johnson, D. K. Glucose reversion reaction kinetics. *Journal of Agricultural and Food Chemistry* **2010**, *58*, 6131-6140.

(21) Pilath, H. M.; Michener, W. E.; Katahira, R.; Mittal, A.; Clark, J. M.; Himmel, M. E.; Nimlos, M. R.; Johnson, D. K. Investigation of xylose reversion reactions that can occur during dilute acid pretreatment. *Energy & Fuels* **2013**, *27*, 7389-7397.

(22) Pan, X.; Shuai, L. Saccharification of lignocellulosic biomass. Wisconsin Research Foundation: 2015.

(23) Li, N.; Pan, X.; Alexander, J. A facile and fast method for quantitating lignin in lignocellulosic biomass using acidic lithium bromide trihydrate (ALBTH). *Green Chemistry* **2016**, *18*, 5367-5376.

(24) Sheen, H.; Kahler, H. Effect of ions on Mohr method for chloride determination. *Industrial & Engineering Chemistry Analytical Edition* **1938**, *10*, 628-629.

(25) Shuai, L.; Yang, Q.; Zhu, J.; Lu, F.; Weimer, P.; Ralph, J.; Pan, X. Comparative study of SPORL and dilute-acid pretreatments of spruce for cellulosic ethanol production. *Bioresource Technology* **2010**, *101*, 3106-3114.

(26) Hashir, M. A.; Stecher, G.; Bonn, G. K. Identification of low molecular weight carbohydrates employing new binary mixtures for matrix-assisted laser desorption/ionisation mass spectrometry. *Rapid Communications in Mass Spectrometry* **2008**, *22*, 2185-2194.

(27) Demchenko, A. V. General aspects of the glycosidic bond formation. *Handbook of Chemical Glycosylation* **2008**, *9*, 1-27.

(28) Roslund, M. U.; Tähtinen, P.; Niemitz, M.; Sjöholm, R. Complete assignments of the ^{1}H and ^{13}C chemical shifts and $J_{H,H}$ coupling constants in NMR spectra of D-glucopyranose and all D-glucopyranosyl-D-glucopyranosides. *Carbohydrate Research* **2008**, *343*, 101-112.

(29) Bock, K.; Pedersen, C. A study of ^{13}CH coupling constants in hexopyranoses. *Journal of the Chemical Society, Perkin Transactions 2* **1974**, 293-297.

(30) Claridge, T. D. *High-resolution NMR techniques in organic chemistry*; Elsevier, 2016; Vol. 27.

(31) Zhang, L.; Gellerstedt, G. Quantitative 2D HSQC NMR determination of polymer structures by selecting suitable internal standard references. *Magnetic Resonance in Chemistry* **2007**, *45*, 37-45.

(32) Kato, N.; Suyama, S.; Shirokane, M.; Kato, M.; Kobayashi, T.; Tsukagoshi, N. Novel α-glucosidase from Aspergillus nidulans with strong transglycosylation activity. *Applied and environmental microbiology* **2002**, *68*, 1250-1256.

(33) Yoo, C. G.; Zhang, S.; Pan, X. Effective conversion of biomass into bromomethylfurfural, furfural, and depolymerized lignin in lithium bromide molten salt hydrate of a biphasic

system. *RSC Advances* **2017**, *7*, 300-308.

(34) Sen, S.; Losey, B. P.; Gordon, E. E.; Argyropoulos, D. S.; Martin, J. D. Ionic liquid character of zinc chloride hydrates define solvent characteristics that afford the solubility of cellulose. *The Journal of Physical Chemistry B* **2016**, *120*, 1134-1141.

(35) Sadula, S.; Oesterling, O.; Nardone, A.; Dinkelacker, B.; Saha, B. One-pot integrated processing of biopolymers to furfurals in molten salt hydrate: understanding synergy in acidity. *Green Chemistry* **2017**, *19*, 3888-3898.

(36) Yoo, C.; Li, N.; Swannell, M.; Pan, X. Isomerization of glucose to fructose catalyzed by lithium bromide in water. *Green Chemistry* **2017**, *19*, 4402-4411.

(37) Hilal, N.; Yousef, G.; Anabtawi, M. Operating parameters effect on methanol–acetone separation by extractive distillation. *Separation Science and Technology* **2002**, *37*, 3291-3303.

(38) Rycroft, C.; Jones, M.; Gibson, G. R.; Rastall, R. Fermentation properties of gentio-oligosaccharides. *Letters in Applied Microbiology* **2001**, *32*, 156-161.

(39) Kaulpiboon, J.; Rudeekulthamrong, P.; Watanasatitarpa, S.; Ito, K.; Pongsawasdi, P. Synthesis of long-chain isomaltooligosaccharides from tapioca starch and an in vitro investigation of their prebiotic properties. *Journal of Molecular Catalysis B: Enzymatic* **2015**, *120*, 127-135.

(40) Sanz, M. L.; Gibson, G. R.; Rastall, R. A. Influence of disaccharide structure on prebiotic selectivity in vitro. *Journal of Agricultural and Food Chemistry* **2005**, *53*, 5192-5199.

(41) Belenguer, A.; Duncan, S. H.; Calder, A. G.; Holtrop, G.; Louis, P.; Lobley, G. E.; Flint, H. J. Two routes of metabolic cross-feeding between Bifidobacterium adolescentis and butyrate-producing anaerobes from the human gut. *Applied and environmental microbiology* **2006**, *72*, 3593-3599.

(42) de Almeida, R. M.; Li, J.; Nederlof, C.; O'Connor, P.; Makkee, M.; Moulijn, J. A. Cellulose conversion to isosorbide in molten salt hydrate media. *ChemSusChem* **2010**, *3*, 325-328.

(43) Liu, W.; Hou, Y.; Wu, W.; Ren, S.; Jing, Y.; Zhang, B. Solubility of glucose in ionic liquid+ antisolvent mixtures. *Industrial & Engineering Chemistry Research* **2011**, *50*, 6952-6956.

(44) Zasadowski, D.; Yang, J.; Edlund, H.; Norgren, M. Antisolvent precipitation of water-soluble hemicelluloses from TMP process water. *Carbohydrate Polymers* **2014**, *113*, 411-419.

(45) Gray, M. C.; Converse, A. O.; Wyman, C. E. Sugar monomer and oligomer solubility. In *Biotechnology for Fuels and Chemicals*; Springer: 2003, p 179-193.

(46) Alves, L. A.; Almeida e Silva, J. B.; Giulietti, M. Solubility of D-glucose in water and ethanol/water mixtures. *Journal of Chemical & Engineering Data* **2007**, *52*, 2166-2170.

Chapter 6 Tailorable cellulose II nanocrystal (CNC II) prepared in mildly acidic lithium bromide trihydrate (MALBTH)

Abstract

Preparation of cellulose II nanocrystal (CNC II) from abundant cellulose I feedstocks mandates polymorph transformation. Transforming cellulose I to cellulose II generally takes place by either mercerization treatment or dissolution/regeneration operations prior to isolating cellulose nanocrystals by selective hydrolysis and physical disintegration. In this study, we developed a facile method to prepare CNC II directly from a commercially available cellulose I feedstock (bleached kraft pulp, BKP) via simultaneous polymorph transformation and hydrolysis in mildly acidic lithium bromide trihydrate (MALBTH). BKP was simultaneously swelled and hydrolyzed in the MALBTH, yielding 64-86% of cellulose II hydrolysis residues (CHR). The integrated process of hydrolysis and polymorph transformation was monitored by scanning electron microscopy, degree of polymerization, hydrogen-deuterium exchange, wide angle X-ray diffraction, and Fourier transform infrared spectroscopy. An inter-plane transition mechanism was proposed to rationalize the polymorph transformation under swelling conditions. Subsequently the CHR was oxidized by ammonium persulfate (APS, 0.1-0.6 M), resulting in the ox-CNC with ultra-high crystallinity (above 90%), flexible surface carboxyl group (0.3-1.2 mmol/g cellulose) and excellent colloidal stability (up to -59 mV zeta potential). Depending on the conditions of MALBTH hydrolysis and APS oxidation, the ox-CNC varied in the length dimension (10-200 nm), but had a relative constant lateral size (8-10 nm), as characterized by transmission electron microscopy and atomic force microscopy. This study facilitates the production of CNC with

flexible aspect ratios and improved colloidal properties for further expanding its applications at interfaces.

6.1 Introduction

Harnessing the most abundant biopolymer (cellulose, 1.5×10^{12} ton/year) in the world has much potential[1,2] because of its inherent advantages such as renewability, sustainability, biodegradability, and non-toxicity.[3,4] Traditional cellulosic materials (e.g., cotton and wood logs), composed of hierarchical fiber units in tens of micron, are either directly utilized to produce textiles and construction materials, or further purified to manufacture paper (flexible cellulosic fiber sheets) after chemical and mechanical treatments. Alternatively, natural cellulose fibers can be downsized to isolate the elementary nanocellulose particles (at least one dimension in nanoscale), rendering extra added-value to cellulosic materials with improved optical transparency, colloidal stability, surface reactivity, mechanical strength and barrier property.[3,5-7] Enormous efforts have been made to exploit the potential of nanocellulose in the areas of biomedical engineering, environmental treatment, energy harvesting/storage, food packaging, etc.[8-10] Depending on the specific applications, cellulose nanomaterials can be either dispersed as 1-dimension individual particles for its excellent interfacial properties and surface chemical reactivity, casted to 2-dimensional films for its flexibility and strength, or molded into 3-dimensional hydrogels and aerogels for its porosity and mechanical properties.[8]

Extraction of cellulose nanocrystal (CNC) generally involves acid/enzyme hydrolysis to rupture and remove cellulose in the amorphous regions. CNC (less than 200 nm in length) is then released from the cellulosic feedstocks with assistance of mechanical disintegration. The hydrolysis conditions especially the type and concentration of acids, play a critical role in the preparation of cellulose nanocrystals. Concentrated sulfuric acid (64%) has been extensively

employed due to its excellent ability of swelling cellulose fibers and selective hydrolysis of amorphous cellulose. Negative charges were introduced on the surface of nanoparticles via the sulfonation reaction, increasing the dispersibility of nanoparticles in aqueous solution. Other concentrated strong acids such as hydrochloride acid (6M), phosphoric acids (10.7 M), as well as concentrated weak acids such as oxalic acid (50-70%) and maleic acid, were also feasible solvents for preparation of cellulose nanocrystals.[11-13]

The extracted CNC from natural fibers (cellulose I polymorph) features high aspect ratios (30-100), which facilitates a great array of applications to produce tough and flexible 2D films and reinforced 3D composite materials. CNC with low aspect ratios, as well-dispersed 1D particles, could be beneficial in applications such as Pickering emulsifiers and drug/catalyst carriers, due to the high interfacial surface coverage as well as abundant surface functional groups.[8,14,15] However, CNC with low aspect ratios was less frequently produced from cellulose I due to the recalicitrant cellulose I crystallites in the disintegration process.[16]

A feasible route to produce CNC with tunable particle sizes is to artificially modify cellulose crystallites by changing cellulose I (paralleled chain conformation) to cellulose II (anti-paralleled chain conformation). The polymorph transformation generally involves either mercerization treatment using concentrated sodium hydroxide or dissolution/regeneration processes using N-methylmorpholine N-oxide (NMMO) or ionic liquids prior to acid hydrolysis.[17-19] However, the above processes require additional operations and introduce costly and toxic solvents which have poor compatibility with subsequent cellulose hydrolysis. Herein, we developed a facile process to achieve selective hydrolysis and polymorph transformation of commercial bleached kraft pulp (BKP, cellulose I polymorph) simultaneously in the mildly acidic lithium bromide trihydrate (MALBTH) under swelling conditions. The cellulose II nanocrystal (CNC II) was then released

by either ammonia persulfate oxidation under mild conditions or by direct homogenization treatment.

6.2 Experimental

6.2.1 Cellulose feedstock

The bleached kraft pulp (BKP) board was immersed in deionized (DI) water overnight and disintegrated into individual fibers. The resulting BKP slurry was concentrated to ~10 wt% and then lyophilized for the subsequent treatment. The chemical composition of BKP showed that it contained 86.7 ± 0.4% glucan and 11.4 ± 0.2% xylan. The average degree of polymerization (*DP*) was determined to be 603.

6.2.2 Mildly acidic lithium bromide trihydrate (MALBTH) treatment

BKP was first mixed with LiBr trihydrate (solid to liquid ratio 1:10, w/v) in a 40 mL sealed reaction vial containing a magnetic stir-bar at 100 °C in order to enable full swelling of cellulose fibers. Following pretreatment, mild hydrolysis of cellulose was triggered by addition of acid (H_2SO_4, 2.5 mM) at 100 °C. The hydrolysis was subsequently quenched by dilution with DI water to yield regenerated ivory cellulose hydrolysis residue (CHR). The mixture was centrifuged at 4500 rpm for 25 min at 4 °C, followed by three washes with DI water. The suspension (1 wt% CHR) was transferred to a sealed dialysis tube (12,000 Da molecular weight cutoff) and immersed in enormous amounts of DI water for 72 h. The yield of CHR was gravimetrically determined based on the initial cellulose content in BKP. The monosaccharides released from BKP were quantified using high performance anion exchange chromatography (HPAEC) on an ICS-3000 system (Dionex, Sunnyvale, CA) equipped with a pulsed amperometric detector and a 250 mm × 4 mm (length × inner diameter) CarboPac PA1 column (Thermo Scientific, Sunnyvale, CA) at 30 °C.

6.2.3 Preparation of CNC by physical disintegration

Physical disintegration of the CHR was carried out, after dialysis using a microfluidizer (M-110EH processor, Microfluidics Corp. Westwood, MA). The slurry (1wt% CHR) was directly pumped three times through a 200 μm interaction chamber then five times through an 87 μm interaction chamber to harvest the nanocellulose particles.

6.2.4 Preparation of ox-CNC by APS oxidation

Surface modification of CNC II took place by oxidizing the CHR with ammonium persulfate (APS, 0.1-0.6 M) at 60 °C for 6-24 h. After APS oxidation, the oxidation residue was collected by centrifugation and further washed with DI water. When the supernatant turned turbid after centrifugation, the whole mixture was transferred to a sealed dialysis tube in DI water and left for 72 h. The oxidized CNC (ox-CNC) was then released by disintegration using an ultra-sonicator (Sonics Vibra Cell Newton, CT) at 80% amplitude. The yield of ox-CNC (in the supernatant after centrifugation) was calculated based on the initial cellulose content in BKP.

6.2.5 Wide-angle X-ray diffraction (WAXD) measurement

WAXD measurement was carried out using an X-ray diffractometer (Bruker D8 Discover diffractometer) with Cu-Kα micro X-ray (wavelength 1.5418 Å) and a Vantec 500 area detector. The sample was compressed to a flat cellulose pad (thickness: ~1 mm) and analyzed in a step-scan mode with 2θ angle ranging from 5° to 55°. The Segal crystallinity index (CrI) was calculated using the experimental diffraction patterns following Eq. 6.1.

$$CI(\%) = \frac{I_{c+a} - I_a}{I_{c+a}} \times 100 \qquad (6.1)$$

where I_{c+a} is the intensity corresponding to the (200) peak of cellulose Iβ at 2θ 22.7˚ and the (020) peak of cellulose II at 2θ 21.8˚, I_a is the intensity corresponding to the amorphous peaks of

cellulose Iβ at 2θ 18˚ and cellulose II at 2θ 16˚.

The average size of cellulose crystallites (*d*, nm) perpendicular to the corresponding lattice plane of the diffraction peak was estimated by the Scherrer equation (Eq. 6.2).[20]

$$d = \frac{K\lambda}{\beta \cos\theta} \quad (6.2)$$

where *K* denotes the Scherrer constant (0.9), λ denotes the radiation wavelength of the X-ray (0.15418 nm), β denotes the full width at half maximum (FWHM) of the diffraction peak in radians, θ denotes the Bragg angle of the diffraction peak.

The deconvolution of the diffraction peaks was conducted using Origin 2016 software (OriginLab Corp.) with Gaussian fitted peaks.

6.2.6 Diffraction simulation

The simulated diffraction patterns of the ideal cellulose Iβ and cellulose II crystallites were obtained using the Mercury 3.9 program (The Cambridge Crystallographic Data Centre, UK).[21] The coordinates of the asymmetric crystal units of both cellulose polymorphs were adopted from Condon et al.[22] The input FWHM was set to be 1.0 º (2θ, 0.0174 radian).

6.2.7 Polarized optical microscope (POM)

The morphology of the wetted BKP and CHR samples was characterized using a Motic microscope equipped with two crossed polarizers in reflection mode. The images were recorded via a Q-imaging G3-go camera.

6.2.8 Transmission electron microscopy (TEM)

The dimensions (both length and width) of ox-CNC particles were characterized using a Tecnai G2 TF12 TEM (FEI, Hillsboro, OR) with a four mega-pixel GatanUltra Scan 1000 camera. A diluted suspension (0.04 wt%) was gently dropped on a freshly glow-discharged carbon-coated (5-

6 nm in thickness) copper grid (VWR, 300 mesh). After 5 min, the excess liquid was blotted away and the grid was then covered with 5 µL of 1% aqueous uranyl acetate (negative staining reagent, Sigma-Aldrich) for 2 min. After removing the extra solution, the sample was dried under vacuum prior to the morphology imaging.

6.2.9 Atomic force microscopy (AFM)

The thickness of ox-CNC was determined using an AFM Workshop system (Signal Hill, CA). Diluted samples (0.005%) were dropped on freshly peeled mica slices, and air dried overnight at room temperature. AFM scanning was operated in tapping mode with resonance frequency in the range of 160-225 kHz and height topographies were analyzed using Gwyddion imaging analysis software (Department of Nanometrol, Czech Metrology Institute, Czech Republic).

6.2.10 Scanning electron microscopy (SEM)

Morphology of BKP fibers and hydrolysis residues was observed by field emission scanning electron microscopy (FE-SEM, Leo Co., Oberkochen, Germany). To prepare SEM samples, a drop of cellulose suspension after solvent exchange by t-butanol was placed on a clean aluminum foil. After vacuum drying, the foil was firmly attached on an aluminum mount by conductive tape and coated with a thin Au layer. The SEM images were recorded by an in-lens detector at 3.0 kV accelerating voltage and 4-5 mm working distance.

6.2.11 Dynamic light scattering (DLS) and zeta potential analyses

The ox-CNC suspension (0.1 wt%) was measured using a DLS analyzer (Nanobrook Omni, Holtsville, NY) at 90° scattering angle. The resultant hydrodynamic diameter was an average of 5 continuous measures. It provided a rough estimation of nanoparticle size since scattering analysis using the Stokes-Einstein equation, is based on theoretically spherical particles.

The interface zeta potential of ox-CNC was determined using a phase analysis light scattering

(PALS) potential analyzer (NanoBrook, Holtsville, NY) and fitted to the Smoluchowshi model. The zeta potential value was read after accumulation of 30 data cycles and the result was an average of 3 continuous measures.

6.2.12 Carboxyl group content

Electric conductivity titration was conducted to determine the COOH content ox-CNC. CNC suspension (50 mg in dry weight) was mixed with 10 mL of 0.01 M HCl for 5 min and then titrated against 0.01 M of standard NaOH. The consumption of NaOH (mL) by weak carboxylic acid was obtained from the resultant titration curves (Figure S6.1). Then the carboxyl content (X_c, mmol/g) was calculated following Eq. 6.3.

$$Xc=\frac{c\times(V_2-V_1)}{m} \quad (6.3)$$

where c (mol/L) is the concentration of the standard NaOH solution, V_1 and V_2 (mL), are the volumes of the standard NaOH solution at the inflection points of the titration curve; m (g), is the oven-dry weight of ox-CNC.

6.2.13 Degree of polymerization (*DP*)

DP of cellulose was estimated by a capillary viscometer method following the TAPPI T230 om-08 procedure. Cellulose samples (0.1 g) were dispersed in 10 mL of DI water and subsequently dissolved in 20 mL of 0.5 M cupriethylenediamine (CED) for 30 min. The kinematic viscosity of the solutions equilibrated to 25.0 °C was measured using a Cannon-Fenske capillary viscometer to yield the corresponding intrinsic viscosities ([η]c, ml/g). The *DP* value was calculated from Eq. 6.4.[23]

$$DP^{0.905} = 0.75[\eta] \quad (6.4)$$

where the constants of 0.905 and 0.75 are from the empirical values for the polymer-solvent system. It is also necessary to note that the *DP* value from the viscosity measurement was only

numeric estimation of the average degree of polymerization of cellulose, and might not be identical to the authentic value.

6.2.14 Attenuated total reflectance (ATR) - Fourier transform infrared (FTIR) spectroscopic analysis

The CHR and ox-CNC samples were analyzed by an ATR-FTIR spectroscopy (PerkinElmer Spectrum 100, Hopkinton, MA). Each measurement was recorded by 64 scans at 4 cm^{-1} resolution.

6.2.15 Hydrogen-deuterium exchange

Hydrogen-deuterium exchange (a facile approach to probe the accessibility of cellulose to water) was conducted in the MALBTH system. Under conditions analogous to CHR preparation, BKP fibers (10%, w/v loading) were either fully swelled in $LiBr{\cdot}3D_2O$ at 100 °C for 60 min or partially hydrolyzed in $LiBr{\cdot}3D_2O$ (containing 2.5 mM H_2SO_4, deuterated MALBTH) at 100 °C for 30 min. After incubation in an ice water bath, the mixture underwent a 10-fold dilution with D_2O, and subsequently was washed by either D_2O or H_2O. In the experimental control, BKP was treated in D_2O at 100 °C for 60 min. All samples were dried in an isothermal oven at 105 °C for 12 h, cooled down in a moisture-free desiccator and immediately analyzed using ATR-FTIR with minimal exposure to ambient moisture. The peak baseline-correction, deconvolution and integration were processed using Origin 2016 software (OriginLab Corp.)

6.2.16 Thermogravimetric analysis (TGA)

The thermal stability was determined by a Q500 thermogravimetric analyzer (TA instruments, Wilmington, DE). Cellulose samples (4.0 mg) were heated from 30 to 600 °C at a rate of 10 °C/min under a flow of nitrogen at 20 mL/min.

6.3 Results and discussion

6.3.1 Hydrolysis of BKP in MALBTH

BKP is industrially produced from wood fibers after extensive removal of lignin and hemicelluloses. It contains an abundant assembly of cellulose chains, which are composed of a well-organized crystalline region and a disordered amorphous region, depending on the arrengement of inter-/intra- chain hydrogen bonds. In the previous chapters, prompt dissolution and hydrolysis of cellulose in acidic lithium bromide trihydrate (ALBTH) were described. Upon decreasing the treatment temperature to 100 ºC, cellulose fibers were effectively swelled but still remained in a solid state (undissolved). When a tiny amount of acid (5 mM H^+) was introduced, hydrolysis of cellulose fibers took place under the swelling conditions in MALBTH, which putatively contributed to hydrolysis of amorphous cellulose together with simultaneous polymorph transformation.

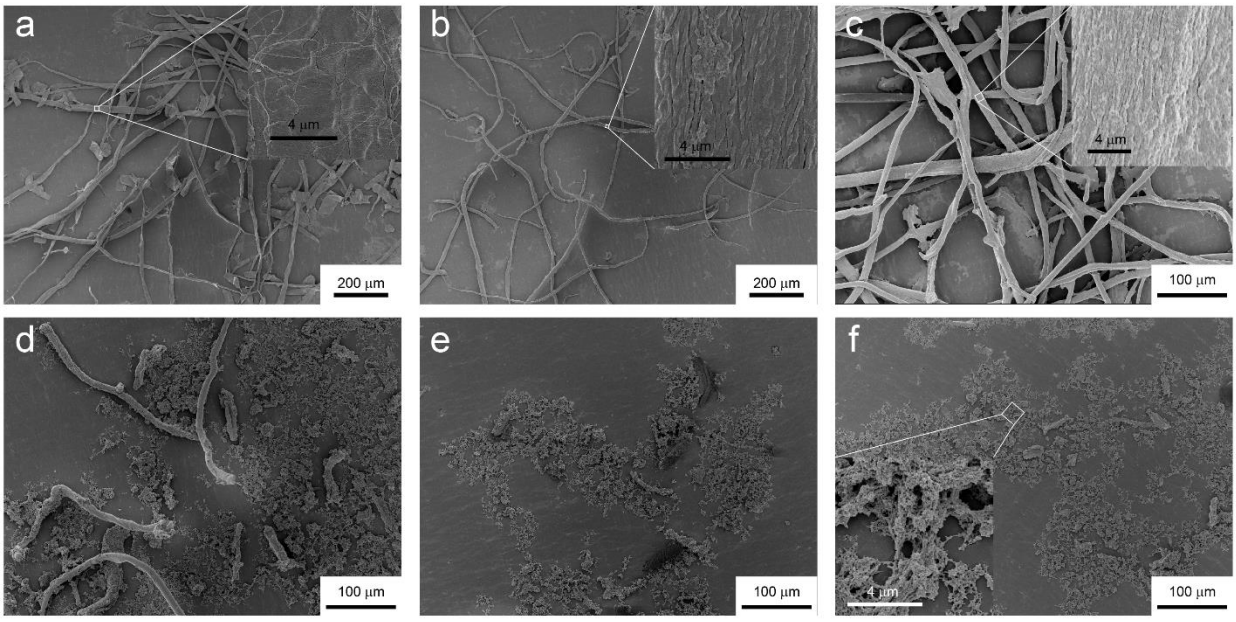

Figure 6.1 SEM images of the original BKP(a), LBTH swelled BKP(b), CHR from the MALBTH treatment (c, 10 min; d, 20 min; e, 30 min; f, 60 min).

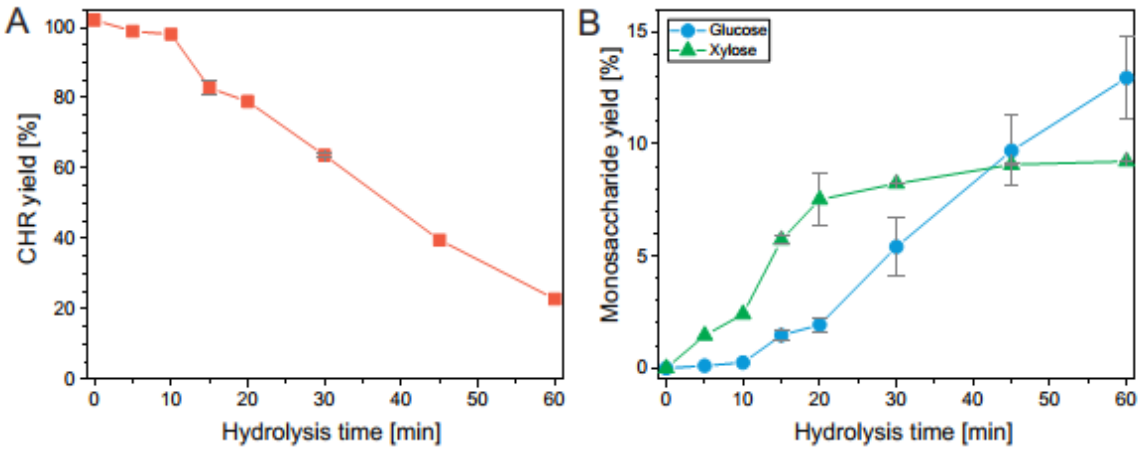

Figure 6.2 Yields of CHR, glucose and xylose as a function of hydrolysis time in the MALBTH treatment of BKP.

The apparent changes of BKP during MALBTH hydrolysis were investigated by monitoring the morphology of dry samples using SEM (Figure 6.1) and wet samples using POM (Figure S6.2). The original BKP was mainly composed of cellulose fibers with a small amount of parenchyma cells (Figure 6.1a). During the lithium bromide trihydrate (LBTH) pretreatment, the parenchyma cells were broken down under swelling conditions, and were no longer detectable. The cellulose fibers remained mostly constant in length dimension (Figure 6.1b). Compared with the smooth surface of the original BKP, a wrinkled surface was observed after the LBTH pretreatment. It was possibly induced by shrinkage of the swelled fibers upon drying. Similar surface topology was also reported during the mercerization process.[24] After the first 10 min of mild hydrolysis, the macroscopic structures of the fibers were mostly preserved. The surface morphology resembled that of LBTH pretreatment, though fractures or tiny holes appeared, possibly due to acidic corrosion. It was indicative of the hydrolysis of cellulose occurring inside the fiber cell wall under swelling conditions. Upon increasing MALBTH hydrolysis time, the BKP fibers were remarkably cut along the length dimension. The fiber fragments were less than 500 and 100 μm in length after 20 and 30 min, respectively. A certain amount of cellulose residues (especially after extensive

hydrolysis in MALBTH) contained nano-scale porous structures which were distinct from those isolated by extensive enzymatic hydrolysis or concentrated acid hydrolysis of cellulose.[25-27]

Table 6.1 Effects of hydrolysis time on crystallinity, crystalline dimension and *DP* of CHR in the MALBTH treatment of BKP

Samples	CrI (%)	Crystallite size (nm)			*DP*
		(1-10)	(110)	(200)/(020)	
Raw BKP	75.1	5.8	3.0	5.6	603
0 min	62.9	5.7	2.8	3.4	553
5 min	72.3	5.8	2.7	2.9	208
10 min	73.2	6.2	2.7	3.1	139
15 min	75.3	6.0	3.2	4.1	79
20 min	79.2	6.4	3.4	4.2	67
30 min	82.2	9.3	5.2	4.2	41
45 min	90.9	10.1	5.5	5.0	38
60 min	84.9	9.4	4.2	5.4	45

The process of hydrolyzing BKP in MALBTH was further monitored by analyzing the degree of polymerization (*DP*) of CHR, CHR yields, and released monosaccharide yields (Figure 6.2 and Table 6.1). Hydrolysis was minor under swelling condition without acidic treatment, as confirmed by insignificant *DP* reduction and no yield of monosaccharides. When acid (5 mM H^+) was added, the cellulose *DP* promptly decreased from 553 to 139 within 10 min. However, over 98% of CHR was still recovered with negligible released glucose (less than 0.3%). This indicates that the acid penetrated the cell walls, resulting in cleavage of cellulose chains, while the macro-structure of the fibers was mostly intact during the initial hydrolysis stage. Extending the hydrolysis time, the CHR yield gradually decreased from 82.8% at 15 min to 63.1% at 30 min, while 1.5-5.4% of glucose was released from BKP. The resultant CHR had a *DP* below 100. At 60 min, only 22.9% of CHR was retrieved together with a 13.0% glucose yield. It suggests that a significant amount of oligosaccharides were generated, possibly due to the homogeneous hydrolysis of cellulose inside

the cell wall. MALBTH hydrolysis produces a larger percentage of oligosaccharides when compared to other hydrolysis processes such as enzymatic hydrolysis using cellulases, in which glucose is overwhelmingly produced as opposed to oligosaccharides.[25]

To elucidate the mechanism of MALBTH mediated BKP hydrolysis, a hydrogen-deuterium exchange assay was conducted to estimate the accessibility of BKP fibers under swelling conditions. A proton in aqueous solvents can readily bind with water to form a hydronium ion. Any location on a cellulose microfibril which water can access, is equally accessible to protons which enable acidic cellulose hydrolysis. Thus the accessible region of cellulose to water also reflects the portion of cellulose which is vulnerable to acidic hydrolysis. In the hydrogen-deuterium exchange assay, hydroxyls on the accessible cellulose are specifically labeled due to the hydrogen exchange with D_2O molecules in the MALBTD medium and characterized by FTIR. As shown in Figure S6.3, the absorption peaks in the wavenumber ranges of 3200-3600 cm^{-1}, 2800-3000 cm^{-1}, and 2400-2600 cm^{-1} were assigned to the vibrational stretching of O-H, C-H, and O-D in cellulose, respectively.[28,29] Compared with CHR by MALBTH hydrolysis, the MALBTD treated CHR showed obvious vibrational signals of the O-D (Figures 3 and S3), indicating the occurrence of the hydrogen-deuterium exchange between D_2O and O-H of cellulose. After washing the MALBTD treated CHR with H_2O which could transform the surface O-D back to O-H, the O-D vibrational signals were still detectable. The regions containing the preserved O-D, represented the portion of cellulose that was exclusively accessible in MALBTD, but not in water. As water molecules are only capable of entering the amorphous region of cellulose,[28] it must be the crystalline cellulose that preserved the O-D after the MALBTD treatment. This observation provided direct evidence for our assumption that the H^+/water in MALBTH could penetrate inside the crystalline region of cellulose under swelling conditions, contributing to the enhanced

hydrolysis of cellulose.

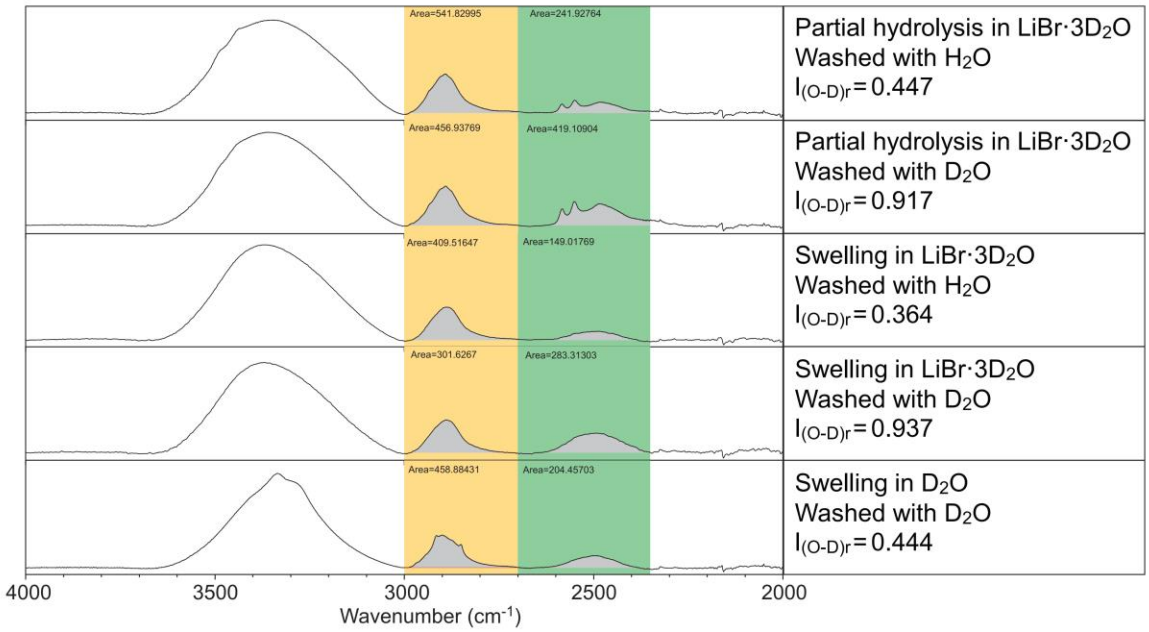

Figure 6.3 FTIR spectra of cellulose samples from the hydrogen deuterium exchange experiment. Note: The FTIR spectra were baseline corrected and integrated from 3000-2700 cm^{-1} for C-H vibrational signal and from 2700-2350 cm^{-1} for O-D vibrational signal.

Based on the preliminary deconvolution analysis, hydroxyls at C2, C3, and C6 positions of cellulose II were responsible for the three peaks at 3470, 3402, and 3269 cm^{-1}, and deuteroxyls at C2, C3, C6 position of cellulose II were responsible for the three peaks at 2583, 2551, and 2474 cm^{-1}.[29] The relative intensities of the O-D vibrational signals were illustrated in Figure 6.3 using the C-H vibrational signal as reference. Under the swelling condition in deuterated LBTH without acid, the relative intensities of O-D were 0.573 (for the amorphous and surface cellulose) and 0.364 (for the crystalline cellulose). Under the mild hydrolysis condition in deuterated MALBTH, the relative intensities of O-D were 0.470 (for the amorphous/surface cellulose) and 0.447 (for the crystalline cellulose). The decreased O-D intensity of the amorphous and surface cellulose after hydrolysis in deuterated MLABTH, indicated that amorphous cellulose was preferentially

hydrolyzed in MALBTH.

6.3.2 Polymorph transformation of cellulose in MALBTH and its proposed mechanism

The polymorph of original BKP was transformed from cellulose I to cellulose II during the MALBTH treatment as verified by both WAXD and FTIR analyses. As shown in Figure 6.4, after the MALBTH treatment, CHR showed diffraction peaks at 12.2º (1-10), 20.0º (110), and 22.1º (020), which were characteristic for cellulose II crystallites as compared to untreated BKP, which is composed of cellulose Iβ crystallites, showing diffraction peaks at 14.8º (110), 16.7º (1-10), and 22.6º (200). Based on the .cif files provided by French el al.,[22] the ideal XRD patterns were simulated using the generally accepted cellulose Iβ and cellulose II lattice units by Mercury software, as illustrated in Figure 6.4B and 6.4C. The experimental XRD patterns of original BKP and the MALBTH treated CHR were in perfect agreement with with the simulation using ideal cellulose Iβ and cellulose II crystallites, respectively. The results confirm that polymorph transformation of cellulose occurs in MALBTH. In the following sections, CHR denotes the cellulose II hydrolysis residues from the MALBTH treatment unless otherwise reported. Swelling BKP in LBTH without acid resulted in a XRD pattern distinct from cellulose I, but consistent with cellulose II (Figure 6.4). It suggests that polymorph transformation was initiated under initial swelling conditions in either LBTH or MALBTH. The LBTH or MALBTH treatment is more efficient at transforming cellulose polymorph when compared to other cellulose swelling solvents such as concentrated sulfuric acid and [BMIM]Cl.[30,31] As far as we are aware, this is the first report of polymorph transformation achieved by swelling cellulose in an aqueous solvent other than corrosive concentrated sodium hydroxide.

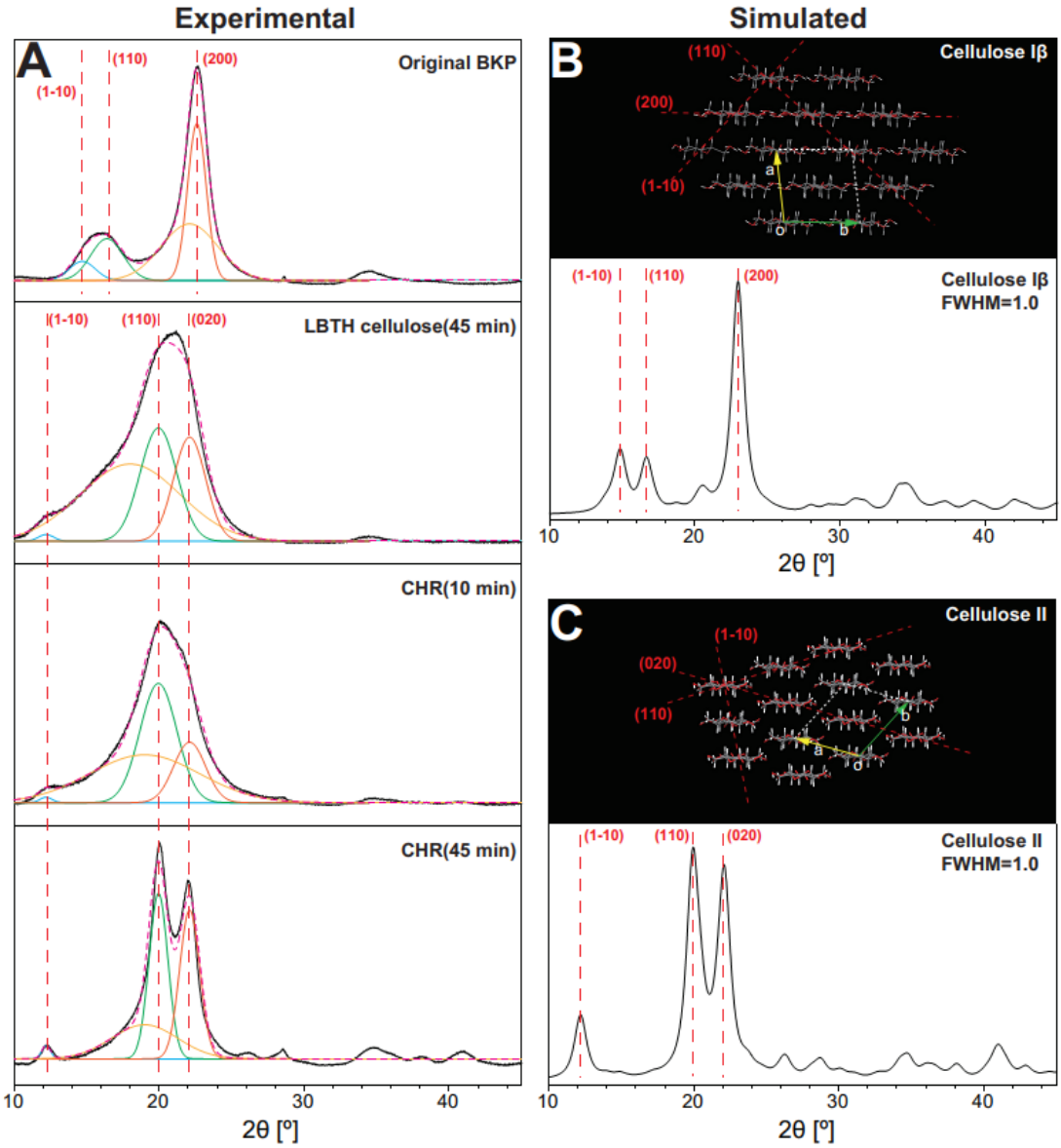

Figure 6.4 The experimental XRD patterns (A) of BKP and the MALBTH treated CHR and the simulated XRD patterns of cellulose Iβ (B) and cellulose II (C).

As illustrated in Table 6.1, the polymorph transformation under swelling conditions also led to reduced crystallinity from 75.1% for original BKP to 62.9% for swelled cellulose II fibers. The reduced crystallinity is believed to be from the generation of amorphous cellulose during the polymorph transformation. During MALBTH hydrolysis, the crystallinity of CHR gradually increased with hydrolysis time from 72.3% at 5 min to 90.9% at 45 min, confirming that crystalline

cellulose was more recalcitrant to hydrolysis than amorphous cellulose. The size corresponding to the three major crystalline planes [(1-10), (110), and (020)] of cellulose II exhibited a 50-100% increase when extending the hydrolysis time from 5 min to 45-60 min.

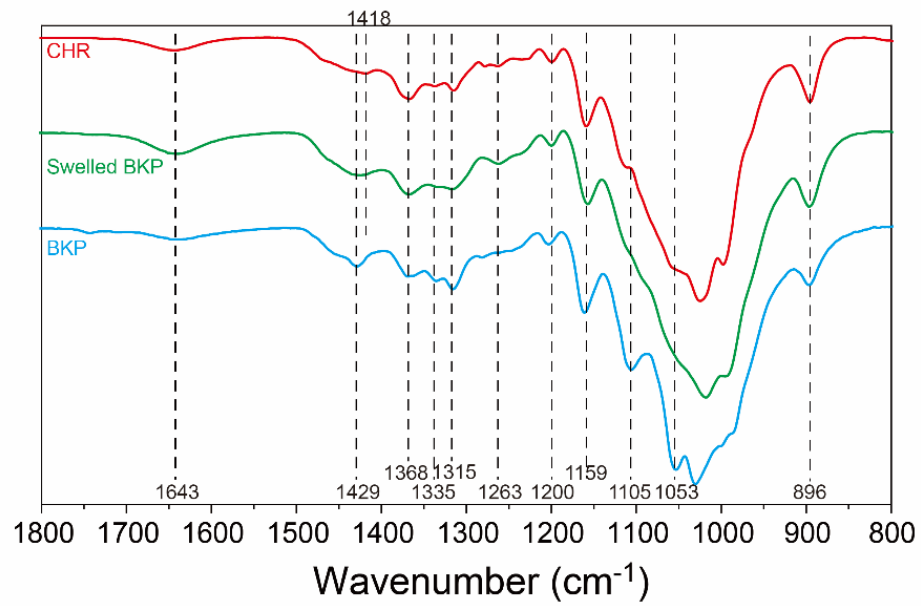

Figure 6.5 Comparison of the FTIR spectra of BKP, LBTH swelled BKP and CHR from MALBTH treated BKP in the range of 800-1800 cm^{-1}.

The transformation of cellulose I to cellulose II was also verified by the FTIR spectra (Figure 6.5). The absorption bands at 1429, 1105, and 1053 cm^{-1}, which are characteristic for cellulose I samples (e.g., BKP), disappeared after the MALBTH treatment. The vibrational frequency of CH_2 symmetric bending shifted to 1418 cm^{-1} from 1429 cm^{-1} in the CHR spectrum, consistent with that of the cellulose II crystallites in lyocell fibres.[32] It further verifies that the MALBTH treatment contributes to the polymorph transformation from cellulose I to cellulose II. In addition, the enhanced intensity of the vibrational bands at 1368 and 1263 cm^{-1} in the CHR spectrum, was consistent with the above XRD results which demonstrated that cellulose II crystallites accumulate as a consequence of polymorph transformation and subsequent hydrolysis of amorphous cellulose.

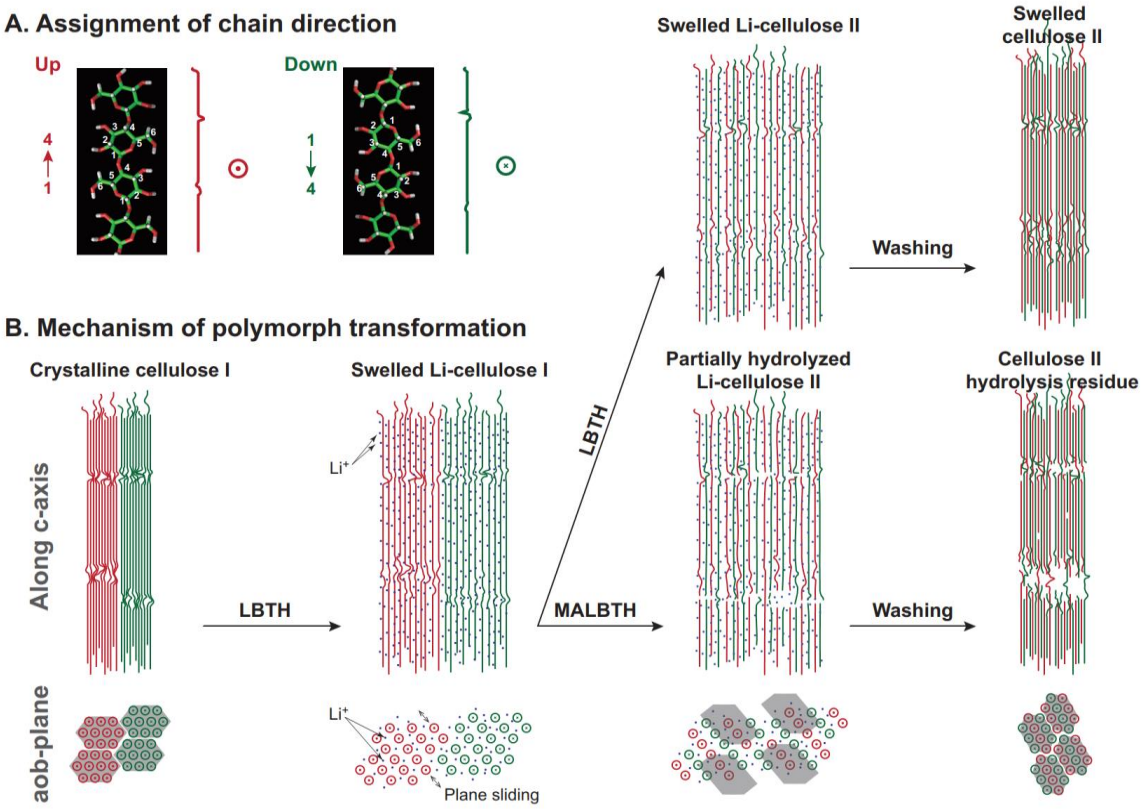

Figure 6.6 Schematic illustration to explicate the polymorph transformation of BKP under swelling conditions from cellulose I to cellulose II in MALBTH.

We propose an inter-plane transition mechanism for the transformation of cellulose I crystallites to cellulose II crystallites in MALBTH under swelling conditions (Figure 6.6). At the molecular level, the elementary fibrils in BKP are assembled by cellulose chains in a parallel direction.[33] Among the elementary fibrils, the chain directions (either up or down depending on the relative position of the C4 and C1 carbons in the glucopyranose ring as referenced by the chain axis) are randomly distributed (Figure 6.6A).[34] As evidenced by the hydrogen-deuterium exchange assay, Li^+ hydrates can penetrate into the elementary fibrils (cellulose crystallites) under swelling conditions. Partially interrupting the inter-molecular hydrogen bonds between cellulose chains, the Li^+ hydrates act as a spacer and allow the fibrils to disintegrate into layers of mobile crystalline

planes by forming the Li–cellulose I complex. Notably, the swelled cellulose fibers still retain a certain degree of structure from the original cellulose (specifically the crystalline planes). This is distinct from dissolved cellulose where all the chains are fully disintegrated and solvated. The cellulose chains in the crystalline plane are held together due to the hydrophobic interactions.[35] Under swelling conditions, the crystal planes can slide into adjacent fibrils of opposite chain direction, resulting in a Li-cellulose II complex with anti-paralleled conformation cross the planes. The inter-plane transition is believed to be a spontaneous process, as the anti-parallel arrangement of cellulose chains is considered to be thermodynamically favorable.[34] When diluted with water, the Li^+ hydrates are extracted out of the crystalline cellulose by water. Then the anti-parallel chains of cellulose form new inter-molecular hydrogen bonds, resulting in cellulose II crystals after drying.

Based on the proposed mechanism above, only crystalline cellulose I can be transformed to cellulose II via the formation of mobile crystalline planes. Polymorph transformation generates extra amorphous cellulose due to the imperfect assembly of the crystalline planes after the inter-plane transition. This is consistent with our results which demonstrated that LBTH swelled BKP had a lower crystallinity than BKP. When subjected to partial hydrolysis under the swelling conditions, the length of the crystalline planes is shortened by cleavage of the cellulose chains, primarily in the amorphous region. The shorter crystalline planes lead to higher mobility by reducing the spatial hindrance. The hypothesis that CHR forms well-organized cellulose crystallites after inter-plane transition is supported by the results [e.g., up to 90.9% crystallinity and large crystallite size: (1-10) 10.1 nm, (110) 5.5 nm, and (020) 5.0 nm after 45 min MALBTH treatment]. Similar mechanisms were also demonstrated in the mercerization induced polymorph transformation of cellulose.[34,36]

6.3.3 Disintegration of CHR to CNC II

Disintegration of CHR by chemical modification

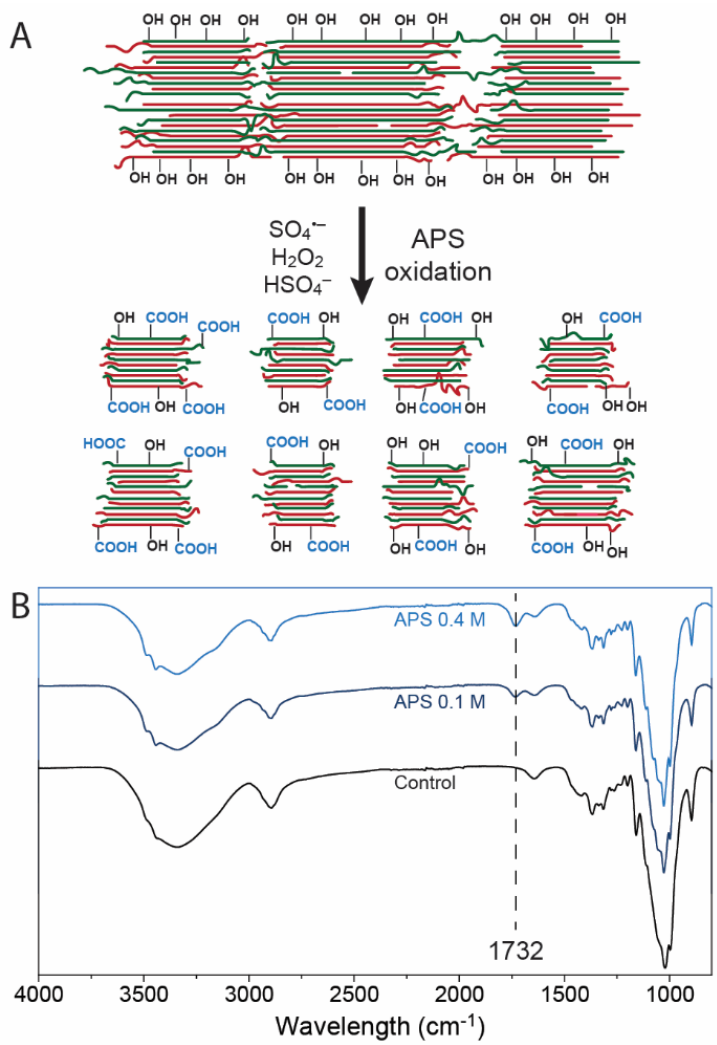

Figure 6.7 Schematic illustration of the APS oxidation process introducing surface carboxyls on ox-CNC (A) and the experimental verification by FTIR (B). Note: Control denotes the CHR after 30 min MLABTH treatment; APS oxidation conditions: temperature 60 ºC, time 12 h.

Chemical modification of CHR was introduced by ammonium persulfate (APS) oxidation to yield ox-CNC with negative surface charges. As an alternative to TEMPO reagents, APS has a strong oxidizing activity, but has low chronic toxicity and is inexpensive.[37,38] At elevated temperatures, persulfate ($S_2O_8^{2-}$) can slowly decompose to $SO_4^{\cdot-}$, HSO_4^-, and H_2O_2 (Figure 6.7A). The HSO_4^-

provides an acidic environment for further removal of amorphous cellulose and the free radicals ($SO_4^{\cdot-}$ and H_2O_2) contribute to formation of surface oxidized carboxylated cellulose. Cellulose residues produced by either LBTH swelling or MALBTH hydrolysis, were subjected to APS oxidation. Using CHR from 15 min MALBT treatment, APS oxidation results in maximum ox-CNC yields of 62.1% (Table 6.2). Both the swelled BKP and the CHR from extensive MALBTH treatment (30 min) had lower ox-CNC yields under the same APS oxidation conditions (0.1 M APS). Swelling of BKP in LBTH without acid inevitably increased the amount of amorphous cellulose during polymorph transformation. It impeded the release of ox-CNC with high crystallinity and up to 55.1% of non-dispersible precipitates with large particle sizes were detected (Figure S6.4). Extended hydrolysis in MALBTH, however, resulted in significant loss of CHR yield (over 40%) which in turn impaired the final ox-CNC yield based on the initial cellulose content in BKP. The APS oxidation didn't contribute to polymorph transformation as the ox-CNC maintained cellulose II polymorph which was identical to CHR (Figure S6.5). In the following sections, ox-CNC specifies the APS oxidized CNC of cellulose II polymorph unless otherwise mentioned.

Oxidation of CHR was demonstrated by a characteristic peak at 1732 cm^{-1} which is consistent with the C=O bond of carboxyls in FTIR spectra. The vibrational peak (1732 cm^{-1}) representing the C=O bond was detected in ox-CNC, but was absent in CHR. The intensity of this peak increased with the APS concentration (Figure 6.7B). Though a semi-quantitative analysis of the carboxyl content has been reported utilizing FTIR spectra,[37] we adopted the more quantitative electric conductivity titration method. As shown in Table 6.2, the carboxyl content increased with APS oxidation from 0.4 $mmol/g_{cellulose}$ (0.1 M APS) to 1.2 $mmol/g_{cellulose}$ (0.6 M APS), indicating concentrated APS greatly enhanced the surface oxidation of cellulose. It is worth noting that the

concentration of APS in this study was significantly lower than that applied to other cellulose feedstocks (e.g., lyocell cellulose II fibers and bleached cellulose I pulp) which generally required 1-2 M APS to achieve 1.0 mmol/$g_{cellulsoe}$ carboxyl content on CNC.[37,39] The low APS concentration requirement in this study is attributed to the enhanced surface accessibility of CHR after the MALBTH treatment. APS oxidation of CHR produced by MALBTH treatment provides a greener and economically favorable option for ox-CNC production.

The yield of ox-CNC is negatively correlated to APS concentration (Table 6.2). This primarily is due to removal of the amorphous cellulose in CHR at high APS concentrations. As no glucose was detected after APS oxidation, formation of soluble oligo- and mono-glucuronic acid may account for the the loss of ox-CNC. Crystallinity of ox-CNC could reach up to ~99%, based by the Segal method, due to extensive removal of amorphous cellulose (Table 6.2). Although the Segal method has been reported to produce a slight overestimation of cellulose II crystallinity,[40] the greatly attenuated peak of amorphous cellulose from the deconvoluted experimental XRD patterns, evidences the ultra-high crystallinity of ox-CNC.

The hydrodynamic diameter of ox-CNC was estimated by DLS analysis. While it is generally acceptable to estimate the relative changes of the ox-CNC size under varied APS oxidation conditions, it must be noted that the resultant diameter value, as fitted by isotropic particles, doesn't represent the real dimension of rod nanoparticles.[41] Using CHR from the MALBTH treatment for 15 min, increasing the APS concentration from 0.1 to 0.6 M led to decreased hydrodynamic diameters of ox-CNC from 208 to 80 nm as illustrated by Table 6.2. The effect of the APS oxidation duration was insignificant on the relative size of ox-CNC, especially after 12h whereas extended MALBTH hydrolysis could reduce the hydrodynamic diameter of ox-CNC to less than 60 nm after 0.4 M APS oxidation.

Table 6.2 Effects of APS oxidation on yield, crystallinity index (CrI), carboxyl content, hydrodynamic diameter, and zeta potential of ox-CNC

MALBTH hydrolysis (min)	APS (M)	Time (h)	Yield[a] (%)	CrI (%)	Carboxyl content (mmol/g)	Particle size (nm)[c]	Zeta potential (mV)
0 (Swelling)	0.1	12	39.7 (55.1)	82.9	- -[b]	417	-32
	0.2	12	57.3 (24.9)	85.6	- -	374	-44
	0.4	12	55.2 (2.0)	86.9	- -	132	-40
15	0.1	12	62.1	87.4	0.40	208	-49
	0.2	8	54.7	95.0	0.44	207	-48
	0.2	12	51.5	96.3	0.44	200	-53
	0.2	18	41.8	96.2	0.50	211	-54
	0.4	12	38.4	98.4	0.59	147	-53
	0.6	12	23.3	99.6	0.92	80	-59
30	0.1	6	55.2	92.9	0.42	179	-38
	0.1	12	52.6	95.2	0.41	164	-43
	0.2	6	48.4	94.3	0.36	136	-45
	0.2	12	43.2	96.4	0.43	98	-45
	0.2	18	39.9	95.5	0.49	93	-48
	0.4	12	24.6	97.7	0.57	57	-52
	0.6	12	10.1	97.4	1.20	85	-45

a. The yield is based on the initial cellulose content in BKP; the value in the parenthesis denotes the yield of un-dispersible precipitate after oxidation;
b. The carboxyl content analysis was not conducted for the LBTH swelled samples;
c. Particle size (hydrodynamic dimeter of ox-CNC) was obtained by DLS analysis.

The morphology and actual dimensions of ox-CNC were characterized by TEM and AFM. Compared to the ox-CNC I from APS oxidation of BKP without polymorph transformation, which resulted in a needle-like shape with sharp endings (Figure 6.8A), the ox-CNC from the MALBTH treated CHR had a ribbon-like shape with blunt endings (Figure 6.8B and 6.8C). It was similar to the CNC II produced by extensive hydrolysis in concentrated sulfuric acid.[42] The modified shape of the oxidized CNC particles, compared to CNC I particles, may be due to polymorph transformation under swelling conditions in MALBTH.

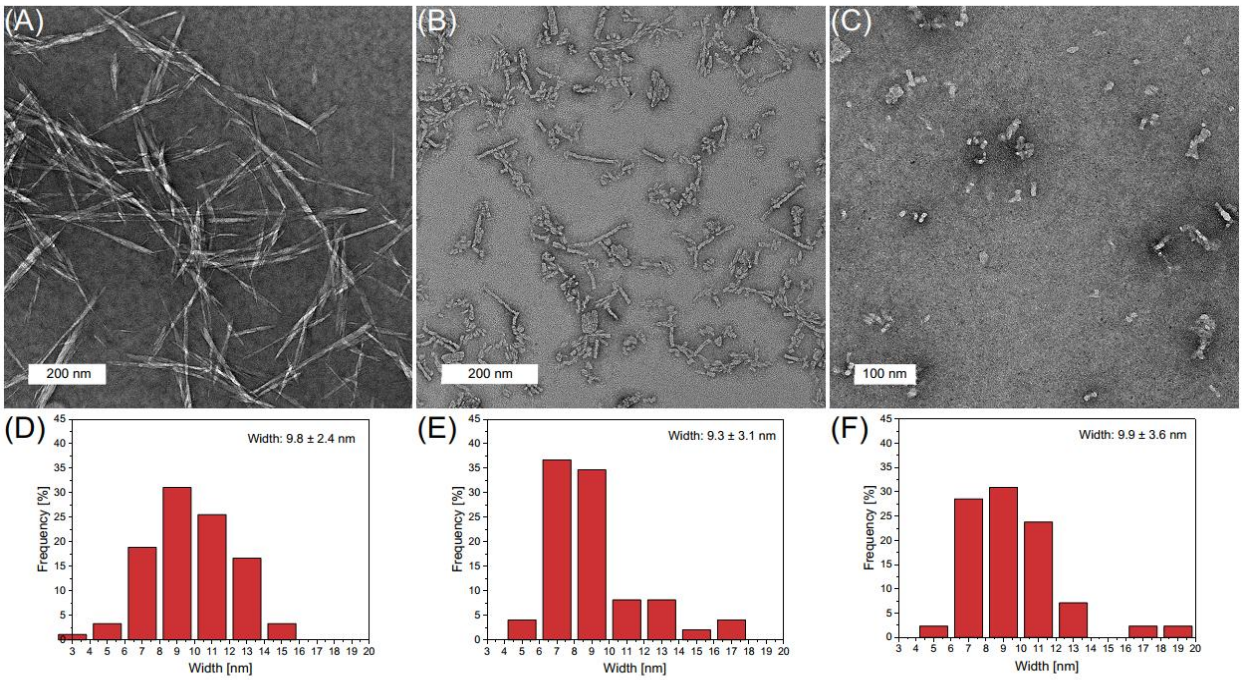

Figure 6.8 TEM images and width distribution of ox-CNC I from BKP treated with 0.8 M APS (A and D); ox-CNC from CHR (15 min MALBTH treatment) treated with 0.1 M APS (B and E); ox-CNC from CHR (15 min MALBTH treatment) treated with 0.6 M APS (C and F). APS oxidation conditions: temperature 60 °C, oxidation time 12 h.

After 0.1 M APS oxidation, the ox-CNC showed an average width of 9.3 ± 3.1 nm with the length ranging from 100 to 200 nm. Under severe oxidation conditions (0.4-0.6 M APS), the length of ox-CNC shrunk to 10-50 nm whereas the width dimension of ox-CNC (cellulose II polymorph) was relatively unaffected, having an average width of 9.9 ± 3.6 nm. There was also little effect on the thickness of ox-CNC (8.0-8.5 nm) with increasing APS concentrations (Figure S6.6). The TEM and AFM observations above demonstrate that oxidation of CHR by APS could selectively tailor the ox-CNC length with negligible impacts on the lateral dimensions. As a result, prepared ox-CNC had tunable aspect ratios ranging from ~20 to ~1 when varying APS oxidation conditions.

The ox-CNC exhibited high zeta potential ranging from -42.8 to -59.0 mV depending on the carboxyl content and the particle size. The high zeta potential (absolute value) contributed to

excellent colloidal stability of ox-CNC in water. The colloid suspension (0.5-1.0 wt%) under varied APS oxidation conditions was found to be stable for up to 6 months, as shown in Figure S6.7. In contrast, flocculation phenomena were inevitable for traditional CNC after weeks of storage.[30]

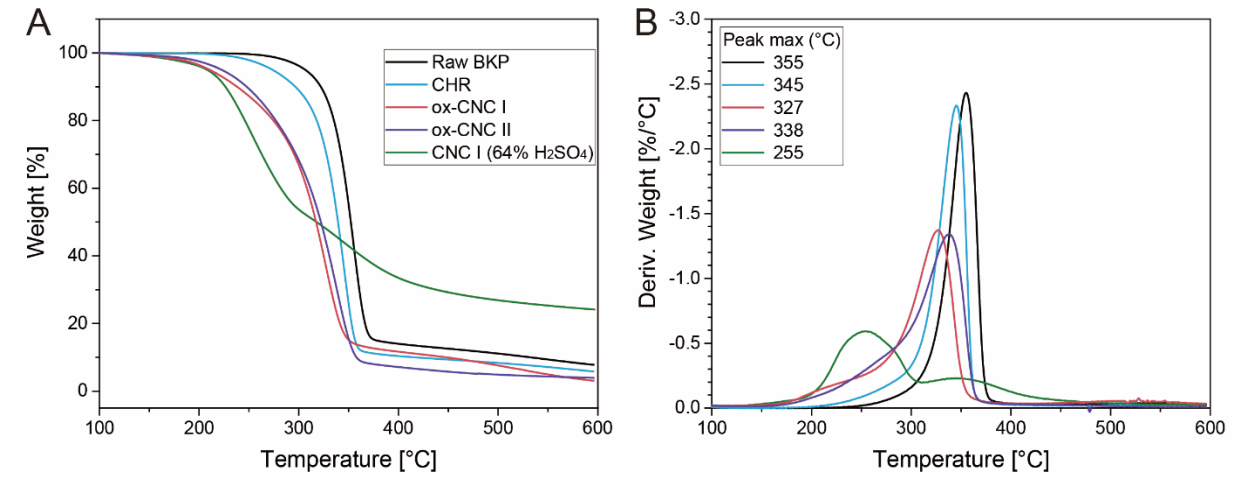

Figure 6.9 TGA and the first derivative curves of various cellulose samples.

The thermal stability of cellulose samples with different cellulose polymorphs was evaluated based on the TGA curves (Figure 6.9). The ox-CNC from the MALBTH treated CHR had a similar shape to the original BKP in the TGA curves, though the major pyrolytic degradation peaks at 338 °C was slightly lower than that of original BKP (355 °C). The slight decrease in thermal stability was ascribed to the reduced molecular weight by the MALBTH hydrolysis and the introduced carboxyl groups by the APS oxidation. Compared with ox-CNC samples of cellulose II polymorph, the ox-CNC I without the MALBTH treatment had lower stability at temperatures above 300 ºC. This is consistent with the hypothesis that thermodynamically, cellulose II is more resistant than cellulose I to thermal degradation.[43] Traditional CNC I prepared by 64% H_2SO_4 hydrolysis, displayed a downward shift in its major degradation peak (255 °C), indicating significantly

decreased thermal stability. The above result confirmed the improved thermal stability of ox-CNC derived from the MALBTH CHR, which could facilitate downstream thermal processing.

Disintegration of cellulose by homogenization

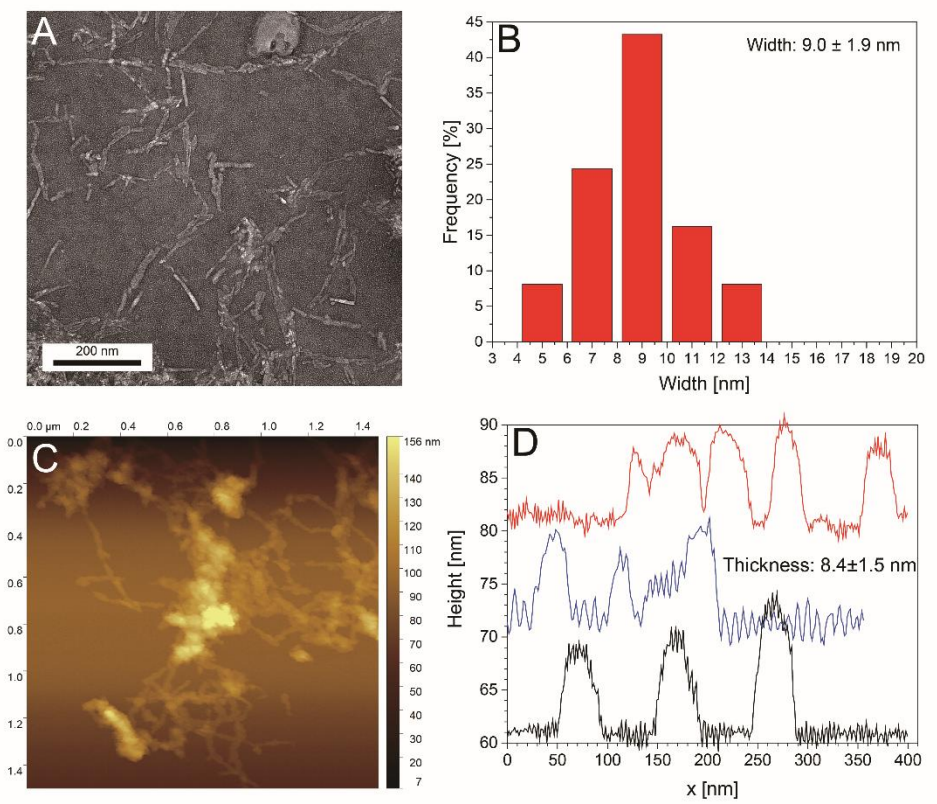

Figure 6.10 Morphology of CNC II characterized by TEM (A, B) and AFM (C, D) from the direct physical disintegration of CHR.

Instead of surface modification by APS oxidation, CHR could be directly ruptured to yield CNC employing a physical disintegration method (e.g., homogenization). After passing through an interaction chamber 5 times, CHR from 30 min MALBTH treatment, was completely disintegrated to a homogeneous CNC II suspension. Due to a lack of surface modification, CNC II showed reduced colloidal stability compared to ox-CNC. The CNC II morphology was characterized by TEM and AFM as shown in Figure 6.10. The shape of CNC II, similar to ox-CNC, had a ribbon-

like structure which was distinct from the needle-like structure of CNC I. Polymorph transformation is assumed to play an important role in the final shape of cellulose nanoparticles. The length dimension of CNC II was in the range of 100-200 nm with uniform width and thickness distribution 9.0±1.9 nm and 8.4±1.5 nm, respectively. Preliminary results don't indicate the length of CNC II to correlate with hydrolysis time, though a minimum treatment time (at least 15 min in MALBTH) is necessary to avoid clogging issues during the homogenization process.

6.4 Conclusions

In this study, the simultaneous hydrolysis and polymorph transformation of BKP (cellulose I fibers) was achieved in MALBTH to yield CHR of cellulose II polymorph. Intensified hydrolysis reduced the CHR yield but resulted in well-organized crystallites by selective hydrolysis of amorphous cellulose. The Li^+ hydrates in MALBTH were proven to penetrate inside the cellulose crystallites under swelling conditions using the hydrogen-deuterium exchange assay. The proposed inter-plane transition mechanism describes polymorph transformation and enhanced hydrolysis under swelling conditions. The APS oxidation of CHR produced ox-CNC (up to 62% yield, cellulose II polymorph) at low APS concentrations (0.1-0.6 M) by introducing the surface charges (0.3-1.2 mmol $COOH/g_{cellulose}$). The ox-CNC featured ultra-high crystallinity (above 90%), excellent dispersibility, and good thermal stability. Depending on the conditions of MALBTH hydrolysis and APS oxidation, the length of ox-CNC was tunable (10-200 nm) with relatively constant lateral dimensions (8-10 nm). The preliminary physical disintegration of CHR demonstrated the production of CNC without surface modification. This study provides a new insight into tailoring CNC by simultaneous hydrolysis and polymorph transformation of cellulose I feedstock with emphasis on its interfacial and colloidal properties.

Appendix

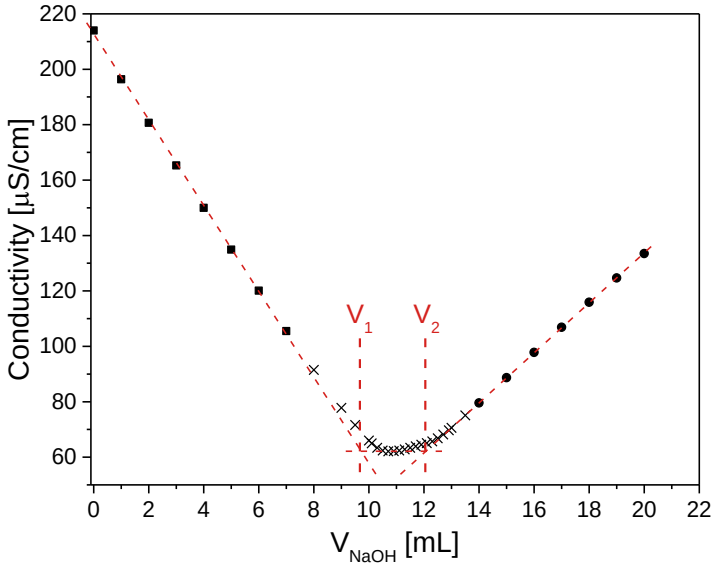

Figure S6.1 An electric conductivity titration curve for measurement of carboxyl content in ox-CNC.

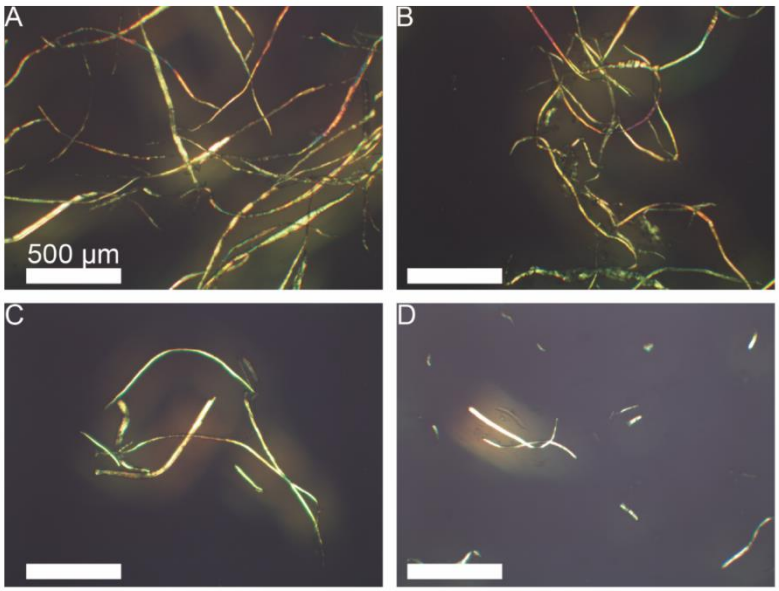

Figure S6.2 POM images of the original BKP(A), LBTH swollen BKP(B), CHR from the MALBTH treatment (C, 10 min and D, 20 min). Scale bar: 500 µm

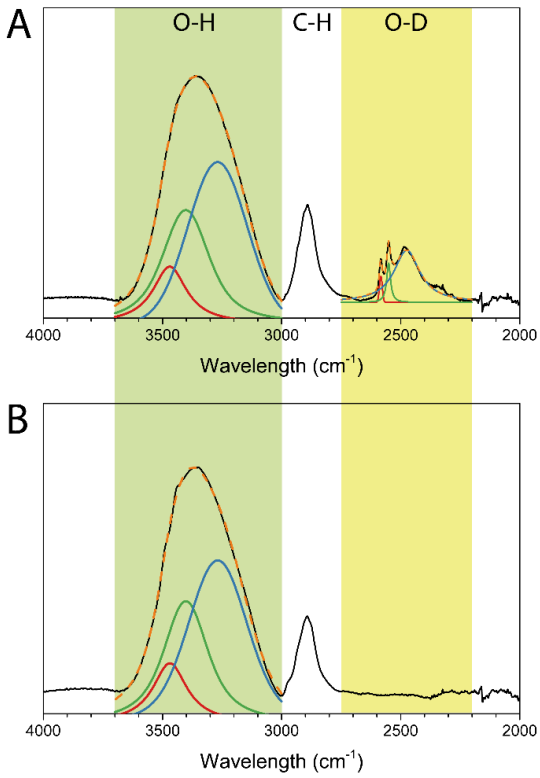

Figure S6.3 FTIR spectra of CHR prepared by mildly acidic lithium bromide trideuterate (A) and mildly acidic lithium bromide trihydrate (B) treatment. Note: The FTIR spectra were baseline corrected and deconvoluted based on the Viogt peak function using Origin 2016 software.

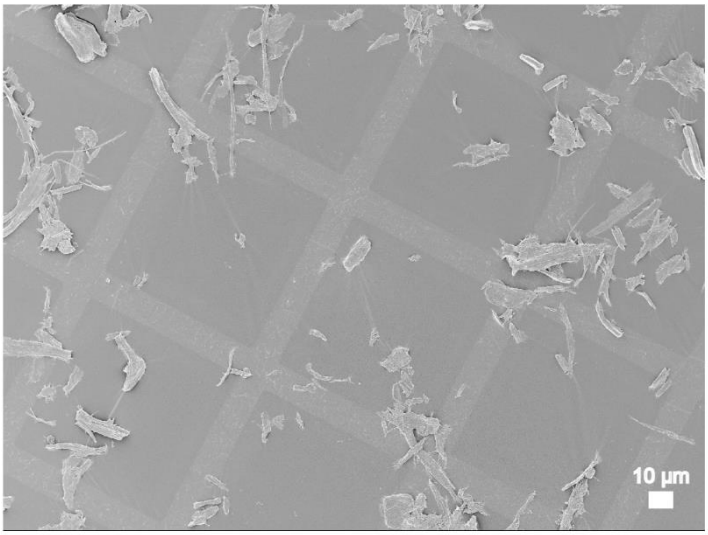

Figure S6.4 The SEM image of precipitated residues collected from the ox-CNC suspension by centrifugation at 4000 rpm for 20 min.

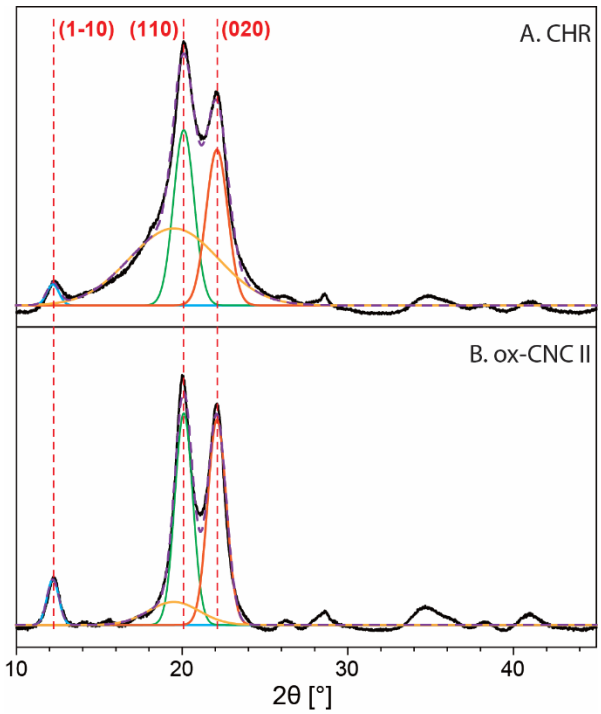

Figure S6.5 No changes of cellulose polymorph during APS oxidation verified by XRD analysis.

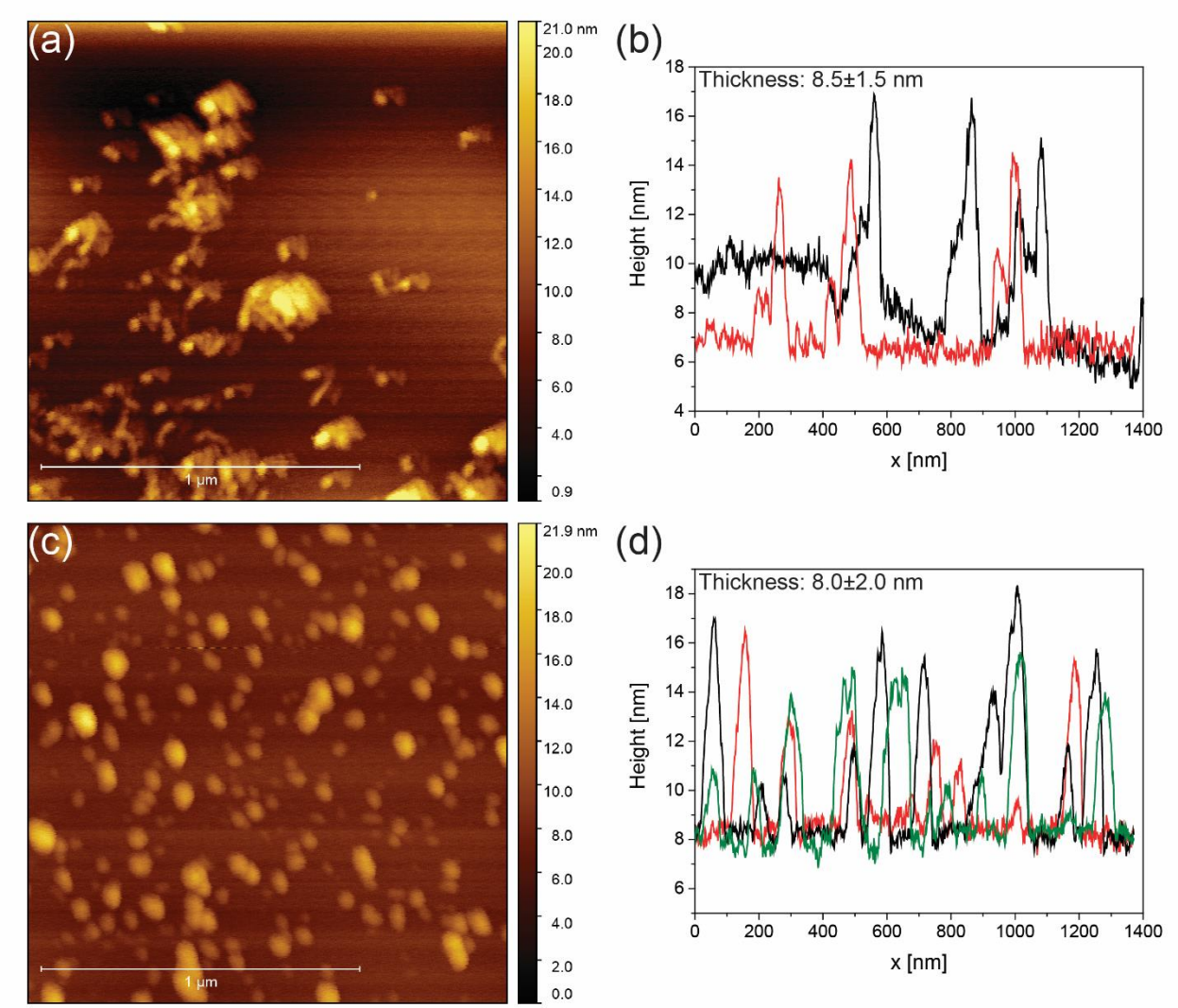

Figure S6.6 AFM height images of ox-CNC from CHR (15 min MALBTH treatment) and thickness distribution at 0.1 M APS (a and b) and 0.6 M APS (c and d).

Figure S6.7 Pictures of ox-CNC suspensions showing the Tyndall effect with laser light passing through (A) and the colloidal stability after 6 month (B).

Reference

(1) Klemm, D.; Heublein, B.; Fink, H. P.; Bohn, A. Cellulose: fascinating biopolymer and sustainable raw material. *Angewandte Chemie* **2005**, *44*, 3358-93.

(2) Zhu, H.; Luo, W.; Ciesielski, P. N.; Fang, Z.; Zhu, J. Y.; Henriksson, G.; Himmel, M. E.; Hu, L. Wood-derived materials for green electronics, biological devices, and energy applications. *Chemical Reviews (Washington, DC)* **2016**, *116*, 9305-74.

(3) Trache, D.; Hussin, M. H.; Haafiz, M. M.; Thakur, V. K. Recent progress in cellulose nanocrystals: sources and production. *Nanoscale* **2017**, *9*, 1763-1786.

(4) Moon, R. J.; Martini, A.; Nairn, J.; Simonsen, J.; Youngblood, J. Cellulose nanomaterials review: structure, properties and nanocomposites. *Chemical Society Reviews* **2011**, *40*, 3941-94.

(5) Lavoine, N.; Desloges, I.; Dufresne, A.; Bras, J. Microfibrillated cellulose - its barrier properties and applications in cellulosic materials: a review. *Carbohydrate Polymers* **2012**,

90, 735-64.

(6) Dufresne, A. Nanocellulose: a new ageless bionanomaterial. *Materials Today* **2013**, *16*, 220-227.

(7) Tardy, B. L.; Yokota, S.; Ago, M.; Xiang, W.; Kondo, T.; Bordes, R.; Rojas, O. J. Nanocellulose–surfactant interactions. *Current Opinion in Colloid & Interface Science* **2017**, *29*, 57-67.

(8) Grishkewich, N.; Mohammed, N.; Tang, J.; Tam, K. C. Recent advances in the application of cellulose nanocrystals. *Current Opinion in Colloid & Interface Science* **2017**, *29*, 32-45.

(9) Wang, X.; Yao, C.; Wang, F.; Li, Z. Cellulose-based nanomaterials for energy applications. *Small* **2017**, *13*, 1702240.

(10) Siqueira, G.; Bras, J.; Dufresne, A. Cellulosic bionanocomposites: A review of preparation, properties and applications. *Polymers* **2010**, *2*, 728-765.

(11) Yu, H.; Qin, Z.; Liang, B.; Liu, N.; Zhou, Z.; Chen, L. Facile extraction of thermally stable cellulose nanocrystals with a high yield of 93% through hydrochloric acid hydrolysis under hydrothermal conditions. *Journal of Materials Chemistry A* **2013**, *1*, 3938-3944.

(12) Camarero Espinosa, S.; Kuhnt, T.; Foster, E. J.; Weder, C. Isolation of thermally stable cellulose nanocrystals by phosphoric acid hydrolysis. *Biomacromolecules* **2013**, *14*, 1223-1230.

(13) Chen, L.; Zhu, J.; Baez, C.; Kitin, P.; Elder, T. Highly thermal-stable and functional cellulose nanocrystals and nanofibrils produced using fully recyclable organic acids. *Green Chemistry* **2016**, *18*, 3835-3843.

(14) Kalashnikova, I.; Bizot, H.; Bertoncini, P.; Cathala, B.; Capron, I. Cellulosic nanorods of various aspect ratios for oil in water Pickering emulsions. *Soft Matter* **2013**, *9*, 952-959.

(15) Capron, I.; Rojas, O. J.; Bordes, R. Behavior of nanocelluloses at interfaces. *Current Opinion in Colloid & Interface Science* **2017**, *29*, 83-95.

(16) Qin, Y.; Qiu, X.; Zhu, J. Understanding longitudinal wood fiber ultra-structure for producing cellulose nanofibrils using disk milling with diluted acid prehydrolysis. *Scientific reports* **2016**, *6*, 35602.

(17) Hirota, M.; Tamura, N.; Saito, T.; Isogai, A. Cellulose II nanoelements prepared from fully mercerized, partially mercerized and regenerated celluloses by 4-acetamido-TEMPO/NaClO/NaClO2 oxidation. *Cellulose* **2012**, *19*, 435-442.

(18) Beaumont, M.; Nypelö, T.; König, J.; Zirbs, R.; Opietnik, M.; Potthast, A.; Rosenau, T. Synthesis of redispersible spherical cellulose II nanoparticles decorated with carboxylate groups. *Greem Chemistry* **2016**, *18*, 1465-1468.

(19) Han, J.; Zhou, C.; French, A. D.; Han, G.; Wu, Q. Characterization of cellulose II nanoparticles regenerated from 1-butyl-3-methylimidazolium chloride. *Carbohydrate Polymers* **2013**, *94*, 773-81.

(20) Langford, J. I.; Wilson, A. Scherrer after sixty years: a survey and some new results in the

determination of crystallite size. *Journal of Applied Crystallography* **1978**, *11*, 102-113.

(21) Macrae, C. F.; Bruno, I. J.; Chisholm, J. A.; Edgington, P. R.; McCabe, P.; Pidcock, E.; Rodriguez-Monge, L.; Taylor, R.; Streek, J. v.; Wood, P. A. Mercury CSD 2.0–new features for the visualization and investigation of crystal structures. *Journal of Applied Crystallography* **2008**, *41*, 466-470.

(22) French, A. D. Idealized powder diffraction patterns for cellulose polymorphs. *Cellulose* **2014**, *21*, 885-896.

(23) Neto, W. P. F.; Putaux, J.-L.; Mariano, M.; Ogawa, Y.; Otaguro, H.; Pasquini, D.; Dufresne, A. Comprehensive morphological and structural investigation of cellulose I and II nanocrystals prepared by sulphuric acid hydrolysis. *RSC Advances* **2016**, *6*, 76017-76027.

(24) Wang, H.; Li, D.; Yano, H.; Abe, K. Preparation of tough cellulose II nanofibers with high thermal stability from wood. *Cellulose* **2014**, *21*, 1505-1515.

(25) Wang, W.; Mozuch, M. D.; Sabo, R. C.; Kersten, P.; Zhu, J.; Jin, Y. Production of cellulose nanofibrils from bleached eucalyptus fibers by hyperthermostable endoglucanase treatment and subsequent microfluidization. *Cellulose* **2015**, *22*, 351-361.

(26) Oun, A. A.; Rhim, J.-W. Isolation of cellulose nanocrystals from grain straws and their use for the preparation of carboxymethyl cellulose-based nanocomposite films. *Carbohydrate Polymers* **2016**, *150*, 187-200.

(27) Zhang, Y.-H. P.; Cui, J.; Lynd, L. R.; Kuang, L. R. A transition from cellulose swelling to cellulose dissolution by o-phosphoric acid: evidence from enzymatic hydrolysis and supramolecular structure. *Biomacromolecules* **2006**, *7*, 644-648.

(28) Lindh, E. L.; Salmén, L. Surface accessibility of cellulose fibrils studied by hydrogen–deuterium exchange with water. *Cellulose* **2017**, *24*, 21-33.

(29) Fan, J.; De Bruyn, M.; Budarin, V. L.; Gronnow, M. J.; Shuttleworth, P. S.; Breeden, S.; Macquarrie, D. J.; Clark, J. H. Direct microwave-assisted hydrothermal depolymerization of cellulose. *Journal of the American Chemical Society* **2013**, *135*, 11728-11731.

(30) Lazko, J.; Sénéchal, T.; Landercy, N.; Dangreau, L.; Raquez, J.-M.; Dubois, P. Well defined thermostable cellulose nanocrystals via two-step ionic liquid swelling-hydrolysis extraction. *Cellulose* **2014**, *21*, 4195-4207.

(31) Chen, L.; Wang, Q.; Hirth, K.; Baez, C.; Agarwal, U. P.; Zhu, J. Tailoring the yield and characteristics of wood cellulose nanocrystals (CNC) using concentrated acid hydrolysis. *Cellulose* **2015**, *22*, 1753-1762.

(32) Carrillo, F.; Colom, X.; Sunol, J.; Saurina, J. Structural FTIR analysis and thermal characterisation of lyocell and viscose-type fibres. *European Polymer Journal* **2004**, *40*, 2229-2234.

(33) Nishiyama, Y.; Langan, P.; Chanzy, H. Crystal structure and hydrogen-bonding system in cellulose Iβ from synchrotron X-ray and neutron fiber diffraction. *Journal of the American Chemical Society* **2002**, *124*, 9074-9082.

(34) Okano, T.; Sarko, A. Mercerization of cellulose. II. Alkali–cellulose intermediates and a possible mercerization mechanism. *Journal of Applied Polymer Science* **1985**, *30*, 325-332.

(35) Lindman, B.; Medronho, B.; Alves, L.; Costa, C.; Edlund, H.; Norgren, M. The relevance of structural features of cellulose and its interactions to dissolution, regeneration, gelation and plasticization phenomena. *Physical Chemistry Chemical Physics* **2017**, *19*, 23704-23718.

(36) Okano, T.; Sarko, A. Mercerization of cellulose. I. X-ray diffraction evidence for intermediate structures. *Journal of Applied Polymer Science* **1984**, *29*, 4175-4182.

(37) Cheng, M.; Qin, Z.; Liu, Y.; Qin, Y.; Li, T.; Chen, L.; Zhu, M. Efficient extraction of carboxylated spherical cellulose nanocrystals with narrow distribution through hydrolysis of lyocell fibers by using ammonium persulfate as an oxidant. *J. Mater. Chem. A* **2014**, *2*, 251-258.

(38) Leung, A. C.; Hrapovic, S.; Lam, E.; Liu, Y.; Male, K. B.; Mahmoud, K. A.; Luong, J. H. Characteristics and properties of carboxylated cellulose nanocrystals prepared from a novel one-step procedure. *Small* **2011**, *7*, 302-5.

(39) Zhang, K.; Sun, P.; Liu, H.; Shang, S.; Song, J.; Wang, D. Extraction and comparison of carboxylated cellulose nanocrystals from bleached sugarcane bagasse pulp using two different oxidation methods. *Carbohydrate Polymers* **2016**, *138*, 237-43.

(40) Nam, S.; French, A. D.; Condon, B. D.; Concha, M. Segal crystallinity index revisited by the simulation of X-ray diffraction patterns of cotton cellulose Ibeta and cellulose II. *Carbohydrate Polymers* **2016**, *135*, 1-9.

(41) Mao, Y.; Liu, K.; Zhan, C.; Geng, L.; Chu, B.; Hsiao, B. S. Characterization of nanocellulose using small-angle neutron, X-ray, and dynamic light scattering techniques. *The Journal of Physical Chemistry B* **2017**, *121*, 1340-1351.

(42) Flauzino Neto, W. P.; Putaux, J.-L.; Mariano, M.; Ogawa, Y.; Otaguro, H.; Pasquini, D.; Dufresne, A. Comprehensive morphological and structural investigation of cellulose I and II nanocrystals prepared by sulphuric acid hydrolysis. *RSC Adv.* **2016**, *6*, 76017-76027.

(43) Yue, Y.; Zhou, C.; French, A. D.; Xia, G.; Han, G.; Wang, Q.; Wu, Q. Comparative properties of cellulose nano-crystals from native and mercerized cotton fibers. *Cellulose* **2012**, *19*, 1173-1187.

Chapter 7 Summary and Recommendations

7.1 General summary

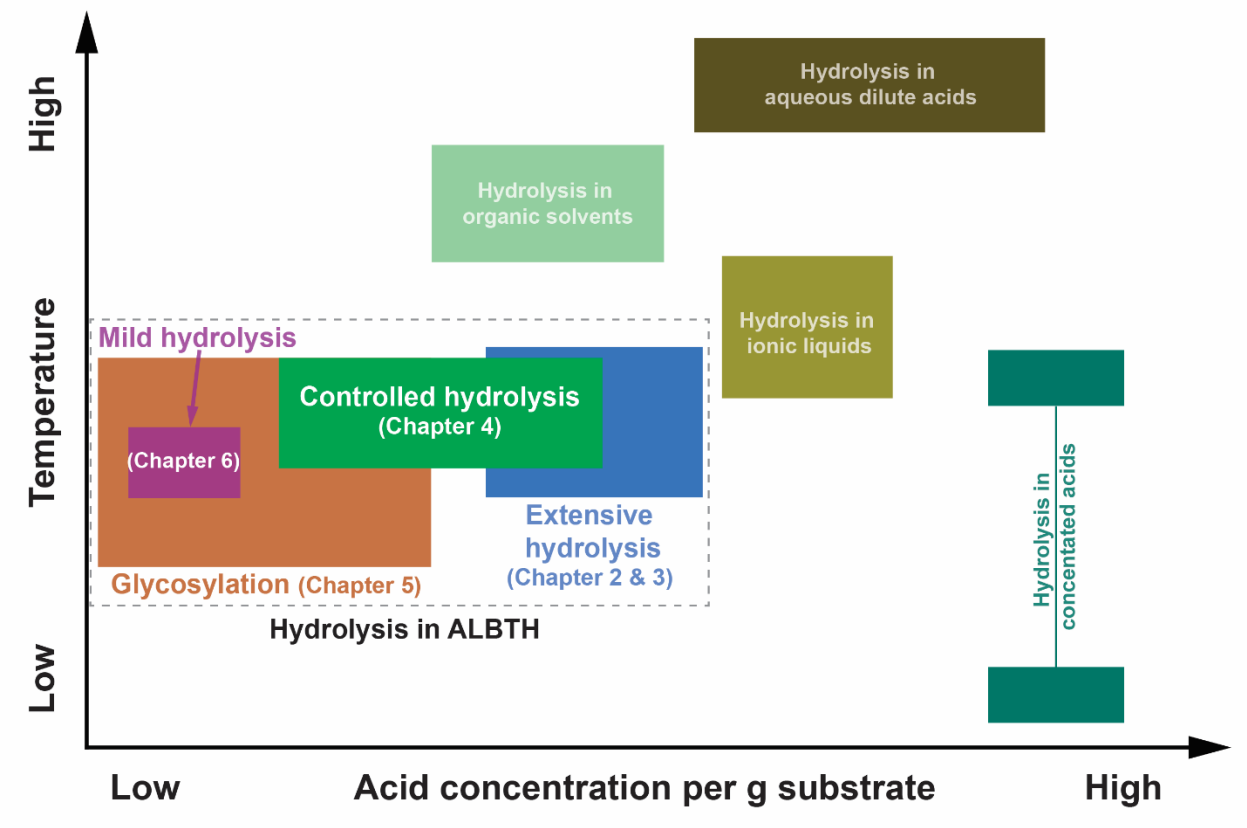

Figure 7.1 The relative severity of cellulose hydrolysis conditions in ALBTH compared to other solvent systems.

As elucidated in this thesis, the acidic lithium bromide trihydrate (ALBTH) system is a promising solvent system for the improved biorefining of lignocellulose. ALBTH hydrolysis allows for: facile quantitation of lignin (Chapter 2), effective fractionation and saccharification of lignocellulose to uncondensed lignin (Chapters 3 and 4), production of concentrated monosaccharides and value-added oligosaccharides (Chapter 4), high-yield synthesis of

oligosaccharides from simple sugars (Chapter 5), and tailored production of cellulose II nanocrystals (Chapter 6).

The varied applications of ALBTH in lignocellulose conversion were dependent on the desired hydrolysis severity, especially for the cellulose fractions (Figure 7.1). Extensive hydrolysis (e.g., 6.7%, w/v biomass loading, 40 mM HCl, 30-120 min reaction) enabled fast and thorough dissolution and hydrolysis of cellulose and hemicelluloses in lignocellulose. The lignin fractions remained primarily as insoluble residue and the minor amounts of soluble lignin could be gravimetrically and spectrophotometrically quantitated. This ALBTH method was applied to different species of biomass including softwood (Douglas fir), hardwood (aspen, poplar, and eucalyptus), and herbage (corn stover and switchgrass). The results indicate that the ALBTH method gave comparable lignin quantitation when compared with the Klason (NREL) method fora given biomass. In addition, the ALBTH method follows a one-step quantitation procedure in short amounts of time (30 min). The ALBTH process can be conducted in a glass vial at atmospheric pressure because of the high boiling point and low vapor pressure of the LiBr solution. It avoids the potential hazards of concentrated sulfuric acid and no autoclave is required. The isolated ALBTH lignin was depolymerized with minimal levels of condensation. The most vulnerable β–*O*–4 aryl ether bonds could be selectively cleaved or converted to uncondensed **HK** and **BD** moieties. Notably, **BD** was identified for the first time in an acid-depolymerized lignin and its appearance suggests the possibility of using simpler routes toward the production of catechol-type monomers, making lignin an increasingly attractive candidate for value-added products. Keeping lignin in a solid state during the ALBTH reaction suppressed condensation due to reduced mobility and thus accessibility of the rigid lignin moieties (α-benzyl carbocations and electron-rich aromatic carbons) to each other. These findings reveal a new strategy for fractionation and depolymerization

of lignin in the solid state to yield less condensed lignin products for downstream valorization.

Controlled hydrolysis in ALBTH was achieved by increasing the biomass loading to 30%-80% (w/v) at 40-240 mM HCl. Cellulose and hemicelluloses in lignocellulose were dissolved and partially hydrolyzed to oligosaccharides together with monosaccharides. In a fed-batch process, saccharification of poplar yielded maximum amounts of soluble mono- and oligosaccharides from glucan (91.0%, oligomer to monomer ratio=1.10) and xylan (90.7%, oligomer to monomer ratio=0.63). The oligosaccharide fraction had a *DP* of 2-10 with inherited β–1,4 glycosidic bond and newly synthesized α/β–1,1, α–1,2, α/β–1,3, α–1,4, and α/β–1,6 glycosidic bonds. The yield of oligosaccharides is due to both controlled hydrolysis of polysaccharides and glycosylation of monomeric sugars during ALBTH. In addition to GlOS production, fractionation and saccharification of lignocellulose by controlled hydrolysis during ALBTH also yielded concentrated monosaccharide solutions (up to 167 g/L) and insoluble lignin fractions (containing abundant β–O–4 aryl ether and uncondensed structures) for upgrading to value-added aromatics.

The acid catalyzed glycosylation reaction in ALBTH was found to be prevalent under a wide range of hydrolysis conditions [e.g., low acid concentration (20 mM HCl), low reaction temperature (70 °C) and high sugar loading concentration (10 g sugars in 1 mL solvent)]. GlOS were synthesized in ALBTH from glucose with high yield (~75%) and selectivity (~99%) and were composed of 2–9 glucose units linked dominantly by α/β–1,6 glycosidic bonds along with a small portion of α/β–1,1, α/β–1,2, α/β–1,3, and α–1,4 glycosidic bonds. Several unique properties of ALBTH contributed to the enhanced glycosylation of glucose including: the water-deficient nature, the ultra-high capacity of dissolving sugars, and the high dissociation of acids in the ALBTH solvent system. The synthesized GlOS were separated from the reaction medium by precipitation in non-solvent (acetone), and the recovered ALBTH could be directly reused for the

next batch of glycosylation, establishing a closed-cycle process for the synthesis of GlOS from glucose in ALBTH. GlOS could be utilized by select lactobacilli and bifidobacteria strains, demonstrating the potential to exploit GlOS as a source of prebiotics. This non-enzymatic glycosylation method provides a new approach for producing high-value, functional, oligosaccharide prebiotics directly from inexpensive and abundant monosaccharides.

Using 2.5 mM H_2SO_4 and decreasing the ALBTH treatment temperature allowed for mild hydrolysis of cellulose under swelling conditions. The application of this MALBTH process involved simultaneous hydrolysis and polymorph transformation of BKP (cellulose I fibers) to yield CHR of cellulose II polymorph with well-organized crystallites. In the hydrogen-deuterium exchange assay, the Li^+ hydrates in MALBTH were proven to penetrate inside the cellulose crystallites under swelling conditions. The proposed inter-plane transition mechanism describes polymorph transformation and enhanced hydrolysis of cellulose under swelling conditions. The APS oxidation of CHR produced ox-CNC (up to 62% yield) at low APS concentrations (0.1-0.6 M) by introducing the surface charges (0.3-1.2 mmol $COOH/g_{cellulose}$). The ox-CNC featured ultra-high crystallinity (above 90%), excellent dispersibility, and good thermal stability. Depending on the conditions of MALBTH hydrolysis and APS oxidation, the length of ox-CNC was tunable (10-200 nm) with relative constant lateral dimensions (8-10 nm). This study provides a new insight into tailoring CNC by simultaneous hydrolysis and polymorph transformation of cellulose I feedstock with emphasis on their interfacial and colloidal properties.

7.2 Recommendations for future research

Although the results in this thesis demonstrates that ALBTH is a promising solvent system for biorefining of lignocellulose, future research is still necessary to optimize the conversion processes

and explore more profound applications using ALBTH or its relevant solvent systems. The following issues listed below should be taken into consideration for any governmental, academic, and industrial institutions who might be interested in this area.

7.2.1 Quantitation of the whole biomass

In Chapter 2, a facile method was developed for quantitation of lignin in lignocellulose using ALBTH. In this process, carbohydrates in lignocellulose were quantitatively converted to aqueous soluble fractions, including not only monosaccharides but sugar degradation productions as well. These degradation products make accurate quantitation of polysaccharides in the current method difficult. Further investigation should be done to modify the ALBTH method for simultaneous quantitation of both lignin and carbohydrates in lignocellulose.

7.2.2 Selective conversion of native lignins from lignocellulose to benzodioxane units

In Chapter 3, a novel lignin structure (benzodioxane) was discovered from the depolymerization of native lignins in ALBTH. This lignin structure was originally discovered in vanilla seed coats which make their lignins entirely from caffeyl alcohol, and could be an ideal moiety to produce valuable 4-propanolcatechol by depolymerization.[1,2] In our current study, however, conversion of β–*O*–4 aryl ether to benzodioxane was less than 30%. Future research should make efforts to improve the benzodioxane yield in the process of isolating lignin from lignocellulose.

7.2.3 Upgrading ALBTH lignin to produce low-molecular weight aromatics

In both Chapters 3 and 4, lignin fractions were isolated from lignocellulose by the ALBTH treatment. In the ALBTH lignin fraction, there were significant amounts of uncondensed lignin structures with minor carbohydrates. Hydrogenation of the ALBTH lignin should be done in the future in efforts to produce value-added low-molecular weight aromatics from lignocellulose. The

choice of different catalysts (such as Ru/C, Pt/C, Pd/C, Raney nickel) and hydrogen sources (such as H_2, isopropanol, methanol) might be taken into consideration in the hydrogenation process.

7.2.4 Investigation of oligosaccharides as prebiotics

In Chapters 4 and 5, high-yield production of oligosaccharides was achieved in ALBTH from lignocellulose, cellulose and glucose following either top-down or bottom-up processes. The GlOS were preliminary tested using probiotic strains for their prebiotic digestibility by *in vitro* fermentation experiments. We were not able to carry out the *in vivo* assessment and pathogen fermentation in our lab, but these experiments are strongly recommended for future research in order to satisfy the criteria for a prebiotic: (1) the ability to resist host digestion; (2) fermentable by intestinal/gut microorganisms; and (3) selective stimulation of beneficial bacteria.[3]

7.2.5 A broad array of glycosylation products

In Chapter 5, the ALBTH catalyzed glycosylation of glucose was extensively studied. Preliminary evaluation of other monosaccharides such as arabinose, xylose, and galactose, was conducted and showed that glycosylation reactions were more favorable among hexoses than pentoses. For future research, comprehensive investigation of various monosaccharides as well as disaccharides (such as sucrose, maltose, and cellobiose) would be recommended. Different sugars can exhibit distinct regio- and stereo-selectivity in glycosylation to form oligosaccharides.

7.2.6 Surface modification of the ox-CNC

In Chapter 6, mild hydrolysis of cellulose in MALBTH under swelling conditions followed by APS oxidation yielded ox-CNC with high surface charges (0.3-1.2 mmol COOH /$g_{cellulose}$), ultra-high crystallinity (above 90%), excellent dispersibility, and good thermal stability. In order to explore and improve its applications as drug delivery carriers or catalyst anchors, further surface modification might be necessary by converting the carboxyl and carboxylic groups to amine,

aldehyde, or thiol groups.[4]

Reference

(1) Chen, F.; Tobimatsu, Y.; Havkin-Frenkel, D.; Dixon, R. A.; Ralph, J. A polymer of caffeyl alcohol in plant seeds. *Proceedings of the National Academy of Sciences* **2012**, *109*, 1772-1777.

(2) Sun, Z.; Fridrich, B. l.; de Santi, A.; Elangovan, S.; Barta, K. Bright side of lignin depolymerization: Toward new platform chemicals. *Chemical Reviews* **2018**, *118*, 614-678.

(3) Gibson, G. R.; Hutkins, R. W.; Sanders, M. E.; Prescott, S. L.; Reimer, R. A.; Salminen, S. J.; Scott, K.; Stanton, C.; Swanson, K. S.; Cani, P. D. The International Scientific Association for Probiotics and Prebiotics (ISAPP) consensus statement on the definition and scope of prebiotics. *Nature Reviews Gastroenterology and Hepatology* **2017**, *14*, 491-502.

(4) Grishkewich, N.; Mohammed, N.; Tang, J.; Tam, K. C. Recent advances in the application of cellulose nanocrystals. *Current Opinion in Colloid & Interface Science* **2017**, *29*, 32-45.

Appendix

List of publications

[1] **Li, N.**, Li, Y.D., Yoo, C.G., Yang, X.H., Lin, X.L., Ralph, J., and Pan, X.J., An uncondensed lignin depolymerized and isolated from lignocellulosic biomass: A mechanistic study, submitted 2018

[2] **Li, N.**, Wang, Z.N., Qu, T.J., Kraft, J., Oh, J.H., van Pijkeren, J.P., Huber G., and Pan, X.J., High-yield synthesis of glucooligosaccharides (GlOS) from glucose via non-enzymatic glycosylation as potential prebiotics, submitted 2018

[3] **Li, N.**, Bian H.Y., Zhu J.Y., Ciesielski P.N., Pan, X.J., Tailorable cellulose II nanocrystal (CNC II) prepared in mildly acidic lithium bromide trihydrate (MALBTH), in preparation 2018

[4] **Li, N.**, Kraft, J., Li, Y.D., and Pan, X.J**.**, Fractionation and controlled hydrolysis of lignocellulose for production of mono-, oligosaccharides and uncondensed lignin, in preparation 2018

[5] Chen, L., Dou, J.; Ma, Q., **Li, N.**, Wu, R., Bian, H., Yelle, D. J., Vuorinen, T., Fu, S., Pan X.J., Rapid and near-complete dissolution of wood lignin at≤ 80° C by a recyclable acid hydrotrope. *Science Advances* 2017, *3*, e1701735.

[6] Yoo, C. G., **Li, N.** (co-first author), Swannell, M., Pan X.J., Isomerization of glucose to fructose catalyzed by lithium bromide in water. *Green Chemistry* 2017, *19*, 4402-4411

[7] Zhang, H., **Li, N.**, Pan X.J., Wu, S., Xie, J., Direct transformation of cellulose to gluconic acid in a concentrated iron (III) chloride solution under mild conditions. *ACS Sustainable Chemistry & Engineering* 2017, *5*, 4066-4072.

[8] Yang, X.H., **Li, N.**, Lin X.L., Pan X.J., and Zhou Y.H., Selective cleavage of the aryl ether bonds in lignin for depolymerization by acidic lithium bromide molten salt hydrate under mild conditions. *Journal of Agricultural Food and Chemistry*, 2016, 44, 8379-8387.

[9] **Li, N.**, Pan X.J., and Alexander J., A facile and fast method for quantitating lignin in lignocellulosic biomass using acidic lithium bromide trihydrate (ALBTH). *Green Chemistry*, 2016, 18, 5367-5376.

[10] Zhang, H.D., **Li N.**, Pan X.J., Wu S.B., and Xie J., Oxidative conversion of glucose to gluconic acid by iron (III) chloride in water under mild conditions. *Green Chemistry*, 2016, 18, 2308-2312.